Coordination between Chromosome Translocation and Peptidoglycan Remodeling during Spore Development

by

Ahmed Mostafa Taha Mohamed

Thesis submitted in fulfilment of the requirements for
the degree of
Doctor of Philosophy

under the supervision of

Dr. Christopher Rodrigues

University of Technology Sydney
Faculty of Science
The iThree Institute

June 2021

Certificate of Original Authorship

I, Ahmed Mohamed, declare that this thesis, is submitted in fulfilment of the requirements for the award of Doctor of Philosophy, in the iThree Institute, Faculty of Science at the University of Technology Sydney.

This thesis is wholly my own work unless otherwise referenced or acknowledged. In addition, I certify that all information sources and literature used are indicated in the thesis. This document has not been submitted for qualifications at any other academic institution.

This research is supported by the Australian Government Research Training Program, Australian Research Council Discovery Project (DP 190100793), the UTS International Research and the UTS President's Scholarships.

Signature: Production Note:
Signature removed prior to publication.

Date: 21/06/2021

Acknowledgements

In the name of Allah, the Most Gracious and the Most Merciful. All praises to Allah for all the strength and courage that have been blessed on me to complete this thesis.

I would like to thank and express my gratitude to everyone who helped and supported me to navigate through the tough times until I reached my goal. First and foremost, I wish to express my sincere appreciation to my supervisor, Chris Rodrigues, whom I consider the best supervisor I could have ever had. Chris trained me to conduct high-quality research, think critically about my data and professionally communicate my work. I am also deeply grateful to the efforts he put into helping me improve and refine my writing skills. Chris's supervision and guidance helped me to become a better scientist. I am grateful for the limitless support I received from him whenever I encountered research or personal problems.

I would like to thank Helena Chan for her much appreciated contributions to this work. Helena's invaluable feedback and proof-reading have helped me refine this thesis. I am very appreciative of the experimental help and support of Johana Luhur, a skillful researcher and a delightful person. I also wish to thank the current and alumni members of the Rodrigues's lab who have been supportive and really fun to work and interact with.

I would like to extend my thanks to our collaborators for their contributions and insightful suggestions. I would like to acknowledge David Rudner, Cécile Morlot, Milena Awad, Dena Lyras, Louise Cole and Christian Evenhuis, who contributed with their expertise to address experimental questions of this thesis. A would like to also acknowledge and thank Cécile Morlot for hosting me in her lab for three months and the valued support she provided during that period.

I extend my gratitude to all the members of the Duggin and Harry laboratories for their useful suggestions and constructive feedback. Moreover, I would like to recognize the assistance I received from the technical staff (Sarah Osvath and Mercedes Ballesteros) while working in the laboratory.

Many thanks to the "too many flies in the office squad" at UTS for all the fun time at the office and the pleasant gatherings we had. I am also grateful to my friends here in Sydney and back home in Cairo for their encouragement throughout my studies.

A special feeling of gratitude to my beloved mother who is an endless source of support, happiness and constant steadfastness throughout my life and education. I am sincerely grateful to my deceased father for his unreplaceable role in my life and the morals and values he instilled in me. I know he would have been proud of me now, and I hope to meet him again in heaven. In addition, huge thanks to my two brothers and only sister for the support they showed and for always standing beside me.

Last but definitely not least, I would like to show express sincere gratitude, deepest appreciation and thankfulness to my wife, sole mate, best friend and soon, the best mother (Dalia). Frankly, without Dalia's unconditional love, endless support, and valuable sacrifices, I would not have been able to be where I am now. I still remember how she encouraged me to pursue my dream to do a PhD and how she never complained about all the long working hours I had; instead she has always been there to cheer me up and motivate me to continue. Simply, I can't put into words to show my profound gratefulness to Dalia; thank you for being in my life.

Abstract

In all cells, including bacteria, coordination between different molecular processes is fundamental for successful growth, division and differentiation. In sporulating bacteria, two fundamental processes, peptidoglycan remodeling and chromosome segregation, occur at the same time and are essential for the early stages of spore development. However, it remains unclear if and how they are coordinated. This thesis addresses this question using the model organism *Bacillus subtilis*.

Upon starvation, some bacteria enter a developmental process called sporulation to produce highly-resistant and dormant cells known as spores. Initially, the starving cell divides asymmetrically in two compartments of different size: the larger one is called the mother cell and the smaller one is called the forespore. Asymmetric division triggers compartment-specific transcription controlled by sigma factors, with σ^F in the forespore and σ^E in the mother cell. Interestingly, the asymmetric septum also traps ~30% of the forespore chromosome in the forespore, while the remaining ~70% resides in the mother cell. Through the septum, A DNA transporter called SpoIIIE translocates the remaining ~70% of the chromosome into the forespore. Concurrently with chromosome translocation, the peptidoglycan within the asymmetric septum undergoes remodeling by hydrolytic and synthetic enzymes, which drive the internalization of the forespore into the mother cell, through a process called engulfment.

During engulfment, two forespore enzymes that function to synthesize a new layer of peptidoglycan are suggested to be functionally redundant, PbpG and PbpF. However, previous observations suggest that PbpG and PbpF could function in separate pathways and thus have specialized roles during sporulation. To investigate this hypothesis, stemming from a genetic screen, this thesis identified SpoIIIM (formerly YqfZ) as being required for efficient sporulation in cells lacking PbpG. Through the phenotypic characterization of cells lacking SpoIIIM and PbpG, multiple lines of evidence led to the conclusion that SpoIIIM, PbpG and SpoIIIE coordinate peptidoglycan remodeling and chromosome translocation at a septal pore. This coordination is required to ensure septal pore stability and its closure upon complete chromosome translocation. Interestingly, other data revealed an important role for the SpoIIIAH-SpoIIQ interaction in the stabilization of the septal pore. Furthermore, the coordination between peptidoglycan remodeling and chromosome translocation was shown to happen through direct interactions between SpoIIIM, PbpG and SpoIIIE. Collectively, this thesis reveals that peptidoglycan remodeling and chromosome translocation are coordinated at

a septal pore, to ensure septal pore stability, successful chromosome translocation and transcriptional compartmentalization during spore development.

Table of contents

Table of Figures and Tables

Figures

Tables

Publications

Journal article

Ahmed Mohamed, Helena Chan, Johana Luhur, Elda Bauda, Benoit Gallet, Cecile Morlot, Louise Cole, Milena Awad, Simon Crawford, Dena Lyras, David Z. Rudner, Christopher D. A. Rodrigues (2021). "Chromosome Segregation and Peptidoglycan Remodeling Are Coordinated at a Highly Stabilized Septal Pore to Maintain Bacterial Spore Development." *Developmental Cell*, 56, 1–16 January 11; https://doi.org/10.1016/j.devcel.2020.12.006

Conferences

Ahmed Mohamed*, Helena Chan, Johana Luhur, Elda Bauda, Benoit Gallet, Cecile Morlot, Louise Cole, Milena Awad, Simon Crawford, Dena Lyras, David Z. Rudner, Christopher D. A. Rodrigues (2020). "Chromosome Segregation and Peptidoglycan Remodeling Are Coordinated at a Highly Stabilized Septal Pore to Maintain Bacterial Spore Development." **Bugs By The Beach**, Newcastle, Australia (virtual oral presentation), 20th November 2020.

*the talk presenter

Abbreviations

α	alpha
A	alanine
amp	ampicillin
β	beta
B.	*Bacillus*
cat	chloramphenicol resistance gene
CFP	cyan fluorescent protein
cfu	colony-forming unit
D	aspartic acid
DNA	deoxyribonucleic acid
DNaseI	deoxyribonuclease I
DSM	Difco Sporulation Medium
DTT	1,4-Dithiothreitol
FM4-64	N-(3-Triethylammoniumpropyl)-4-(6-(4-(Diethylamino) Phenyl) Hexatrienyl) Pyridinium Dibromide
E	Glutamic acid
E.	*Escherichia*
EDTA	ethylenediaminetetraacetic acid
et al.	and others
erm	erythromycin resistance gene
γ	gamma
g	gram (s)
GCW	germ cell wall
GFP	green fluorescent protein
HEPES	4-(2-hydroxyethyl)-1-piperazineethanesulfonic acid
His	histidine
hr	hour

IPTG	isopropyl-1-thio-β-D-galactopyranoside
kan	kanamycin resistance gene
L	litre (s)
LB	Luria-Bertani broth (Lennox)
m	milli (10^{-3})
M	moles per litre
min	minutes
MQW	milli-Q purified water
mypet	monomeric yellow fluorescent protein for energy transfer
n	nano (10^{-9})
neo	neomycin resistance gene
ODx	optical density at (x refers to the wavelength in nm)
opt	optimized
p	probability
$P_{hyperspank}$	IPTG-hyper-inducible promoter
PAGE	polyacrylamide gel electrophoresis
PBS	phosphate buffered saline
PBP	penicillin binding protein
PCR	polymerase chain reaction
pH	power of Hydrogen
phleo	phleomycin resistance gene
PMSF	phenylmethylsulfonyl fluoride
RBS	ribosome binding site
RNase	ribonuclease A
rpm	revolutions per minute
SD	standard deviation
S	serine
SDS	sodium dodecyl sulfate
σ	sigma

spec	spectinomycin resistance gene
tet	tetracycline resistance gene
TMA-DPH	TMA-DPH (1-(4-Trimethylammoniumphenyl)-6-Phenyl-1,3,5-Hexatriene p-Toluenesulfonate)
Tn-seq	transposon sequencing
Tris	tris(hydroxymethyl)methylamine
U	units (enzyme activity)
UV	ultraviolet
V	volt(s)
v/v	volume per volume
W	watt
w/v	weight per volume
X-Gal	5-Bromo-4-Chloro-3-Indolyl β-D-Galactopyranoside
YFP	yellow fluorescent protein
µ	micro (10^{-6})

Chapter 1:

Introduction

1.1 Preface

The depletion of nutrients in the environment triggers a subset of bacteria from the phylum *Firmicutes* to produce metabolically dormant cells called endospores (henceforth spores) through a differentiation process known as sporulation (Errington & Wu, 2017; Morlot & Rodrigues, 2018; Shen *et al*., 2019). Spores are considered among the most resilient cell types on Earth as they can remain viable for thousands of years (Setlow, 2007; Riley *et al*., 2021). Spores can withstand extremely harsh conditions including ultraviolet radiation, space vacuum, toxic chemicals, desiccation, heat and antibiotics (Horneck *et al*., 1994; Setlow, 2006; Errington, 2010; Horneck *et al*., 2012; Cortesão *et al*., 2019). Importantly, some spore-forming bacteria are pathogenic, for instance: *Bacillus anthracis* causes anthrax and is a major bioterrorism concern; *Bacillus cereus* causes food-borne disease, and *Clostridioides difficile* is the cause of infectious diarrhea in hospital settings worldwide (Bauer *et al*., 2011; Paredes-Sabja *et al*., 2014; Swick *et al*., 2016; Shen *et al*., 2019). In the case of *Clostridioides difficile*, it is believed that its spores contribute to high rates of disease recurrence and transmission of new infections (Paredes-Sabja *et al*., 2011; Browne *et al*., 2016; Swick *et al*., 2016; Ramos-Silva *et al*., 2019).

For decades, *Bacillus subtilis* has been the go-to organism to investigate different aspects of prokaryotic differentiation and morphogenesis, including sporulation (Decker & Ramamurthi, 2017; Kovács, 2019). Sporulation is a complex process involving the expression of hundreds of genes, where specialized sigma factors control different stages of spore development (Fawcett *et al*., 2000; Hilbert & Piggot, 2004). Sporulation starts when the starved *B. subtilis* cell divides asymmetrically, resulting in two cellular compartments of different size and fate: the smaller cell is called the forespore and will develop into the mature spore, while the larger cell is called the mother cell, that contributes to the maturation of the spore but then dies once the spore is mature.

After polar division, a central stage in sporulation known as engulfment occurs, where multiple molecular events occur simultaneously to allow the mother cell to engulf the developing spore in a phagocytic-like process. An important aspect of engulfment is cell wall remodeling, which comprises synthesis and hydrolysis of peptidoglycan. Furthermore, concurrently with cell wall remodeling during engulfment, a copy of the chromosome is translocated into the forespore through the septal membranes separating the mother cell and forespore.

Although sporulation has been studied for many years, it is still unclear how peptidoglycan synthesis is regulated during engulfment. Since the discovery of penicillin, peptidoglycan has been the main target of many antibiotics because of its essentiality for bacterial viability (Nikolaidis *et al*., 2014; Sauvage & Terrak, 2016). Since engulfment is yet another important example of how bacteria remodel their cell wall to mediate the growth of a new cell, the spore, it may offer important new insights into how bacteria build one of their most precious assets – the cell wall.

This thesis was initially focused on understanding if two cell wall synthases produced in the forespore function in separate cell wall synthesis pathways. Stemming from this question, this study then led to the discovery of an unappreciated and complex aspect of spore development: how the developing cell coordinates septal cell wall remodeling with chromosome translocation into the developing spore. Since chromosome translocation and cell wall remodeling are likely important aspects of spore formation in all sporulating bacteria, including spore-forming pathogens, ultimately this project could provide new knowledge on factors that might be potential targets for the development of antibiotics against spore-forming pathogens.

1.2 Sporulation in *Bacillus subtilis*

Bacillus subtilis is a Gram-positive, non-pathogenic, spore-forming bacterium used to study fundamental aspects of bacterial biology such as chromosome organization, cell wall remodeling and developmental processes such as biofilm formation and sporulation (Higgins & Dworkin, 2012; Egan *et al*., 2017). Due to its genetic amenability, *B. subtilis* represents the perfect model for studying the sporulation process and has been the go-to organism to study this process for several decades.

Starvation causes *B. subtilis* to enter the sporulation developmental pathway. Under laboratory conditions, upon exhaustion of nutrients at 37ºC, it produces mature spores within a period of 7 hours (Hilbert & Piggot, 2004). During this time, multiple distinct events occur and have been categorized into different stages as detailed below (see also Figure 1.1A).

Stage 0 - Entry to sporulation: at the onset of starvation, the master regulator of sporulation, Spo0A, is activated by phosphorylation through a phosphorelay system involving a set of kinases (Fujita & Losick, 2005; Kovács, 2016). Phophorylated-Spo0A (Spo0A~P) directly controls the transcription of more than one hundred genes (Hoch, 1993; Piggot & Hilbert, 2004; De Jong *et al*., 2010; Higgins & Dworkin, 2012). Importantly, Spo0A~P activates the transcription of genes encoding the sporulation sigma factors (σ^F and σ^E) that control important aspects of sporulation (Haldenwang, 1995; Carniol *et al*., 2004; Dworkin & Losick, 2005; Levine *et al*., 2012).

Stage I - Axial filament formation: during this stage, the two chromosomes of the starving cell are segregated and remodeled into an axial filament with the origin of replication (*oriC*) anchored to cell poles and the termini (*ter*) positioned near the middle of the cell (Figure 1.1A) (Wu & Errington, 1994; Ben-Yehuda *et al*., 2003b; Wang *et al*., 2014). Interestingly, it was demonstrated that a kinetochore-like protein called RacA binds to the centromere-like sites closer to the *oriC*, to tether the chromosome to the cell pole by interacting with the polarly-localized DivIVA protein (Ben-Yehuda *et al*., 2003b, 2005; Schumacher *et al*., 2016). Furthermore, many other players including Soj, Spo0J, SMC, MinD, MinJ and ComN have been found to contribute to the positioning of *oriC* to the cell poles during sporulation (Sharpe & Errington, 1996; Lin & Grossman, 1998; Sullivan *et al*., 2009; Graham *et al*., 2014; Kloosterman *et al*., 2016). Previous work also indicates that the chromosome arms in the axial filament are positioned side-by-side in a linear orientation (Wang *et al*., 2014).

Stage II - Asymmetric division: this stage involves the first morphological event of the sporulation process, which is the formation of the asymmetric septum (Figure 1.1A). The asymmetric septum divides the starving cell into two compartments, different in size and developmental fate; the larger one is called the mother cell, while the smaller one is the forespore that will develop into the mature spore (Hilbert & Piggot, 2004; Errington & Wu, 2017). To initiate asymmetric septation, Spo0A and σ^H increase the expression levels of the cell division protein FtsZ, to switch division from the cell center (midcell) to a near-polar position where the asymmetric septum will develop (Levin & Losick, 1996; Ben-Yehuda & Losick, 2002; Barák & Muchová, 2018). It remains unclear how the asymmetric division site is specifically determined. However, a sporulation protein called RefZ (a regulator of FtsZ) contributes to the polar switch of the Z-ring (Wagner-Herman *et al*., 2012; Miller *et al*., 2016). Furthermore, RefZ together with its cognate binding motifs (RBMs) determine the position of the chromosome arms with respect to the asymmetric septum (Miller *et al*., 2016; Barák & Muchová, 2018).

Another key player during this stage is SpoIIE which is required for various roles, including stabilization of the polar Z-ring and thus formation of the asymmetric septum, and activation of σ^F in the forespore (Barák & Youngman, 1996; Feucht *et al*., 2002; Barák *et al*., 2019). Consistent with its roles in asymmetric septum formation, cells lacking *spoIIE* form a thicker asymmetric septum and are severely defective in spore formation (Barák & Youngman, 1996; Feucht *et al*., 2002).

Once the asymmetric septum is formed, the first sporulation sigma factor, σ^F, becomes activated within the forespore, by a mechanism involving the relief of anti-sigma factors that collectively hold σ^F inactive. SpoIIE dephosphorylates the anti-anti-σ^F factor SpoIIAA~P, which activates SpoIIAA and promotes its interaction with SpoIIAB, an anti-σ^F factor, allowing it to dissociate from σ^F and thus relieving the inhibition on σ^F (Coppolecchia *et al*., 1991; Arigoni *et al*., 1996; Hilbert & Piggot, 2003). The activation of σ^F in turn leads to activation of the mother cell σ^E through a cascade involving two forespore signaling proteins, SpoIIR and SpoIIT, that stimulate the processing of the inactive pro-σ^E into the mother cell σ^E (Figure 1.1B) (Fujita & Losick, 2003; Hilbert & Piggot, 2004; Imamura *et al*., 2008; Diez *et al*., 2012; Meeske *et al*., 2016). The activation of sigma factors, especially σ^E, allows remodeling of the septum and results in curving of the septum and migration of the mother cell membranes around the forespore (Khanna *et al*., 2019; Riley *et al*., 2021). Furthermore, the

trapping of the chromosome in the asymmetric septum triggers the assembly of a specialized DNA translocase called SpoIIIE that "pumps" the chromosome into the forespore (Wu & Errington, 1994, 1997; Ben-Yehuda *et al*., 2003a; Fiche *et al*., 2013).

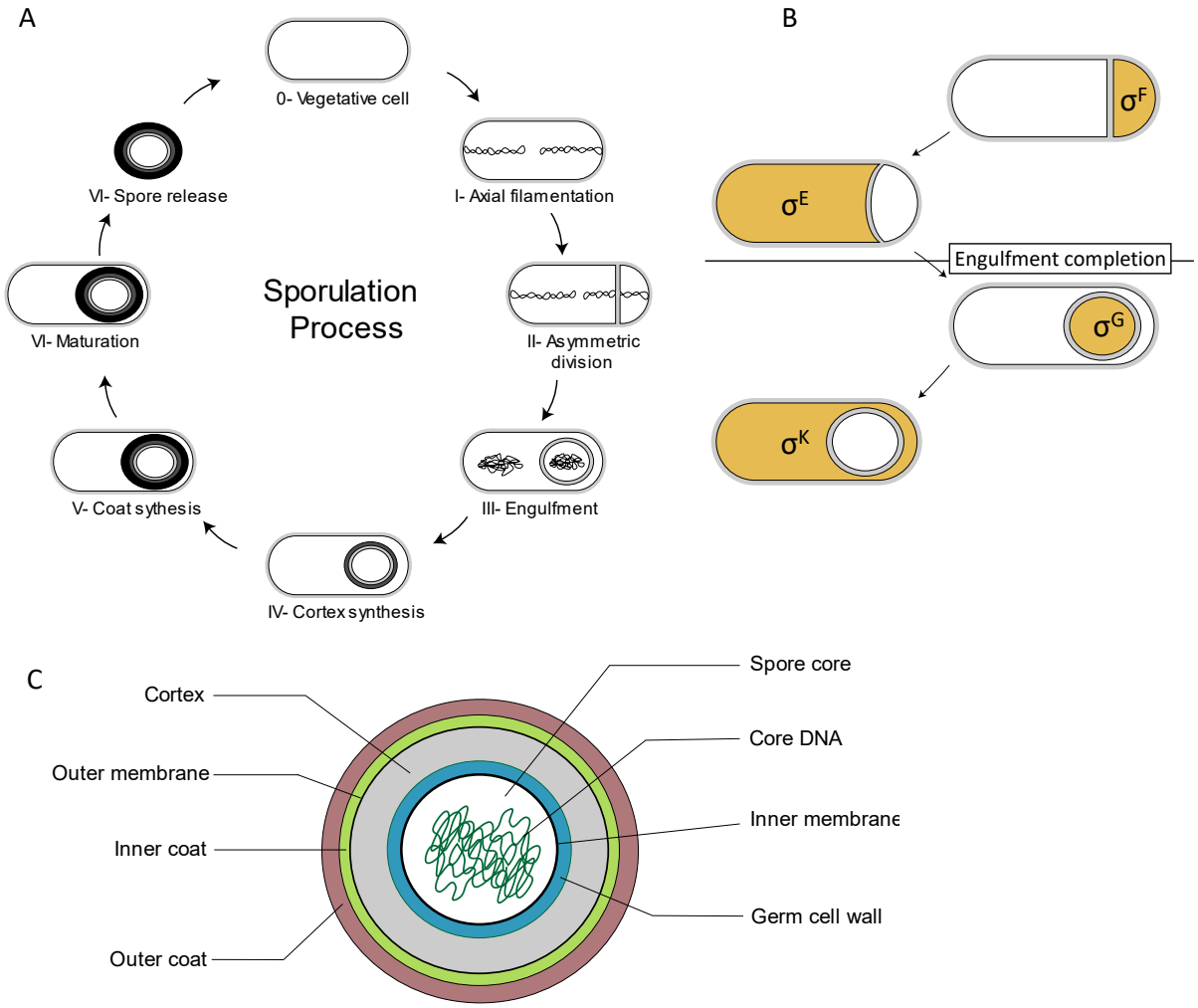

Figure 1.1: The sporulation stages and the spore structure. (A) Schematic illustrations of the sporulation process in *Bacillus subtilis*. Starvation induces the vegetative cell to initiate sporulation by segregating the duplicated chromosome, followed by the formation of an asymmetric septum that divides the cell into a small compartment called the 'forespore' and a larger cell known as the 'mother cell'. Following that, the mother cell engulfs the spore in a phagocytic-like process called engulfment. Later, the spore matures by adding protective layers of cortex and coat and is released into the environment upon mother cell lysis. **(B)** Schematic illustrations of the activation cascade of sporulation sigma factors. After asymmetric division, σ^F becomes active in the forespore and then it activates σ^E in the mother cell. Subsequent to engulfment completion, σ^E activates σ^G in the spore that in turn activates σ^K in the mother cell. **(C)** A schematic illustration of the mature spore structure. The figures are based on others listed in (Errington, 2003; Hilbert & Piggot, 2004; Leggett *et al*., 2012).

Stage III – Engulfment: Upon the activation of σ^E in the mother cell (Figure 1.1B), specific proteins encoded by genes including *spoIIM*, *spoIIP* and *spoIID* form a complex called the DMP complex, which initiates septal PG thinning (Eichenberger *et al*., 2001; Tan &

Ramamurthi, 2014). Remodeling of the septal PG initiates the engulfment process, where the mother cell membranes migrate symmetrically around the forespore and surround it in a phagocytic-like process (Figure 1.1A) (Abanes-De Mello *et al*., 2002; Khanna *et al*., 2019).

During engulfment, a thin layer of peptidoglycan (PG) called Germ Cell Wall (GCW) is formed between the forespore and mother cell membranes by two forespore-produced PG synthases, known as PbpG and PbpF (Figure 1.1C) (Meador-Parton & Popham, 2000; Tocheva *et al*., 2013; Popham & Bernhards, 2015). As a result of engulfment, the forespore ends up with a Gram-negative like envelope, where two membranes encase the engulfed forespore, the inner membrane derived from the forespore and an outer membrane derived from the mother cell (Figure 1.1C) (Higgins & Dworkin, 2013). Successful engulfment entails many processes including PG hydrolysis and synthesis, membrane synthesis and formation of the transenvelope SpoIIIAH-SpoIIQ interaction (discussed later).

Stage IV, V, VI – Cortex synthesis, Coat synthesis and Maturation: After engulfment, the activation of σ^G in the forespore is dependent on the SpoIIIA-SpoIIQ complex (A-Q complex), which is composed of the forespore protein SpoIIQ and the eight proteins encoded in the *spoIIIA* operon (SpoIIIAA, SpoIIIAB, SpoIIIAC, SpoIIIAD, SpoIIIAE, SpoIIIAF, SpoIIIAG and SpoIIIAH) and GerM from the mother cell side (Sun *et al*., 2000; Chary *et al*., 2006; Doan *et al*., 2009; Rodrigues *et al*., 2016a, 2016b; Morlot & Rodrigues, 2018). Camp *et al*. identified a small protein called Fin that facilitates the switch between σ^F to σ^G by deactivating σ^F and promoting σ^G activation (Camp *et al*., 2011; Erickson *et al*., 2017).

Finally, σ^K is activated in the mother cell through proteolytic activation of pro-σ^K, mediated by the metalloprotease SpoIVFB (Haldenwang, 1995; Fimlaid & Shen, 2015; Ramírez-Guadiana *et al*., 2018; Sun *et al*., 2021). Interestingly, the anti-sigma factor CsfB (also called Gin) acts in both compartments where it binds to σ^G to prevent its early activation during σ^F activity in the spore, and binds and inactivates σ^E to promote σ^K activation in the mother cell (Serrano *et al*., 2015; Martínez-Lumbreras *et al*., 2018; Mearls *et al*., 2018). The activation of σ^K in the mother cell drives the expression of several proteins involved in spore maturation and mother cell lysis (Errington, 2003; Vasudevan *et al*., 2007; Mckenney *et al*., 2013; Driks & Eichenberger, 2016).

The protective layers around the forespore include a thick layer of specialized PG called the cortex that is deposited between its double membranes on top of the GCW (Vasudevan *et al*.,

2007; Eichenberger, 2010; Tocheva *et al*., 2013; Popham & Bernhards, 2015). Another important multilayered proteinaceous structure surrounding the spore is called the coat, composed of basement layer, inner coat and outer coat, followed by the most external layer called the crust (Kim *et al*., 2006; Setlow, 2006; Mckenney *et al*., 2013; Tan & Ramamurthi, 2014; Driks & Eichenberger, 2016; Shuster *et al*., 2019).

Forespore maturation involves many events, including the addition of protective layers to fortify the forespore, dehydration and modification of the spore cytoplasm by accumulation of Ca^{++} and dipicolinic acid (DPA) and production of small-acid soluble proteins (SASPs) that protect the DNA (Setlow, 2007; Moeller *et al*., 2009; Driks & Eichenberger, 2016; Ramírez-Guadiana *et al*., 2017). Detailed appreciation of these processes is beyond the scope of this thesis and thus are only briefly mentioned.

Finally, once the spore is fully developed (Figure 1.1C), the mother cell undergoes controlled lysis by CwlB and CwlC produced under σ^K, releasing the mature spore into the environment where it lies dormant until favorable conditions arise (Figure 1.1A) (Smith & Foster, 1995; Nugroho *et al*., 1999; Vermassen *et al*., 2019). Upon suitable growth conditions, the dormant spore germinates, restoring vegetative growth (Figure 1.1A).

1.3 Cell wall structure and the synthesis and hydrolysis of PG

The initial research question of this thesis is centered around GCW synthesis during engulfment. The forespore GCW (PG) resembles that of the vegetative cell (Meador-Parton & Popham, 2000; Tocheva *et al*., 2013; Popham & Bernhards, 2015). Since the assembly of PG is well studied during vegetative growth and many studies have elucidated important mechanistic details surrounding this process, it is important to consider more broadly how the PG layers are remodeled during vegetative growth, as discussed next, as a means to inform how PG synthesis could be regulated and occur during spore development.

The bacterial cell wall can be viewed as an exoskeleton and is a fundamental feature of almost all bacteria (Koch, 2000; Margolin, 2009). The cell wall serves as a shape and size determinant and protects the bacterial cell from external insults and changes in osmotic tension in the environment (Gautam *et al*., 2011; Typas *et al*., 2012; Egan *et al*., 2017). The major component of the cell wall is PG; a mesh-like layer composed of glycan strands connected together by peptide crosslinks (Typas *et al*., 2012). The glycan strands are made of alternating sugars of *N*-acetylglucosamine (GlcNAc) and N-acetylmuramic acid (MurNAc) linked by β-1,4-glycosidic

bonds, while the crosslinks are oligopeptides that vary in length (Figure 2) (Caccamo & Brun, 2017).

Gram-positive bacteria have no outer-membrane, so the cell wall constitutes the exterior layer, is relatively thick (10–40 nm) and is enriched in some anionic polymers, such as teichoic acid or teichuronic acid (Egan *et al*., 2017). Meanwhile, Gram-negative bacteria have a double membrane with a thin layer of PG (3–6 nm) in between (Egan *et al*., 2017). During sporulation, the GCW is sandwiched between two membranes, the forespore and mother cell membranes, similar to Gram-negative bacteria.

1.3.1 PG synthesis

For decades, PG synthesis has been the main target of many antibiotics due to its importance for cell growth and viability and its absence in humans, which makes it a perfect drug target (Gautam *et al*., 2011; Nikolaidis *et al*., 2014). The growth of the PG sacculus involves complexes involved in PG synthesis and hydrolysis that are associated with cytoskeletal elements that serve as a scaffold for the biosynthetic machineries (Margolin, 2009; Cava *et al*., 2013; Egan *et al*., 2020).

PG synthesis can be divided into three processes, taking place in different areas of the cell: the cytoplasm and the inner and outer leaflets of the cytoplasmic membrane (Figure 1.2) (Pinho *et al*., 2013).

In the cytoplasm, precursors of GlcNAc and MurNAc are synthesized and then through a linear set of reactions dependent on the Mur ligases (Mur enzymes), amino acids (L-Ala-D-Glu-L-*meso*-diaminopimelic acid-D-Ala-D-Ala) are added to UDP-MurNAc to form N-acetylmuramic acid-pentapeptide (Morales Angeles *et al*., 2017; Zhao *et al*., 2017). At the inner leaflet of the cytoplasmic membrane, the PG precursors are linked to a membrane-bound lipid molecule (undecaprenyl pyrophosphate) or bactoprenol (Scheffers & Pinho, 2005; Barreteau *et al*., 2008). UDP-MurNAc-pentapeptide is attached by MraY to undecaprenyl pyrophosphate giving Lipid I, undecaprenyl pyrophosphoryl-MurNAc-pentapeptide (Barreteau *et al*., 2008). Consequently, MurG transfers GlcNAc from UDP-GlcNAc to Lipid I, yielding Lipid II (undecaprenyl-pyrophosphoryl MurNAc-pentapeptide-GlcNAc) (Bhavsar & Brown, 2006). Lipid II subunits are then flipped to the outer leaflet of the membrane by MurJ or Amj, both of which act as flippases in *B*. *subtilis* (Meeske *et al*., 2015).

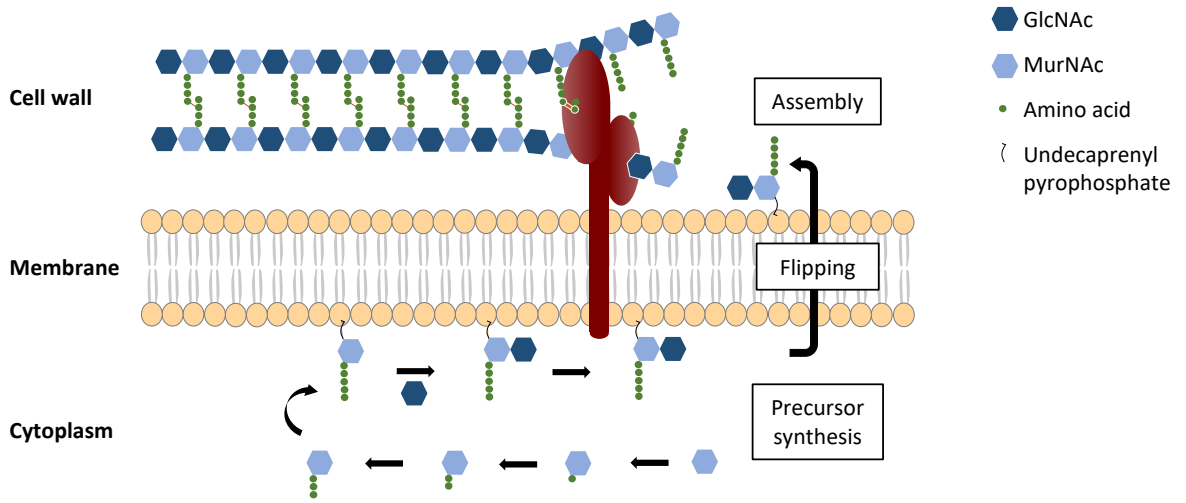

Figure 1.2: Diagram of PG synthesis in Gram-positive bacteria. PG synthesis starts in the cytoplasm where PG units are synthesized in the form of UDP-MurNAc-pentapeptide and UDP-GlcNAc. Next, the PG monomers are attached to inner membrane bound proteins to form Lipid I and then Lipid II. Lipid II is then flipped to the outer leaflet of the cytoplasmic membrane. Finally, PBPs extend the glycan strand by adding new PG units through transglycosylation (TG) and connect the glycan strands by transpeptidation (TP) activity. The figure is based on others listed in (Pinho *et al*., 2013; Caccamo & Brun, 2017).

On the outer leaflet of the membrane, flipped Lipid II is polymerized into the PG matrix by two chemical reactions, transglycosylation (TG) and transpeptidation (TP), that extend the glycan strands and cross-link the peptide chains, respectively (Gautam *et al*., 2011). In *B. subtilis*, during cross-linking by TP, the unlinked terminal amino acid of the pentapeptide – D-alanine – is removed and the chain is modified into tetrapeptide (Atrih *et al*., 1999; Morales Angeles *et al*., 2017).

The TG and TP activities are catalyzed by Penicillin Binding Proteins (PBPs) that are classified into High Molecular Mass (HMM PBPs) and Low Molecular Mass (LMM PBPs) (Sauvage *et al*., 2008). HMM PBPs can be further categorized into class A and B: class A PBPs are bifunctional and exhibit both TG and TP activities, whilst class B PBPs have only the TP function (Typas *et al*., 2012; Egan *et al*., 2015). LMM PBPs usually function as carboxypeptidases that remove the D-Ala residues from stem peptides and endopeptidases that cleave off peptide bonds in the stem peptides (Nelson & Young, 2001; Scheffers & Pinho, 2005; Angeles & Scheffers, 2020).

Apart from PBPs, a relatively new family of proteins called SEDS (shape, elongation, division, and sporulation) has been shown to play an important role in PG synthesis during cell elongation, division and sporulation (Caccamo & Brun, 2017; Egan *et al*., 2020). Members of the SEDS family like RodA and FtsW, which are present in both *B. subtilis* and *E. coli*, have

been shown to possess transglycosylase activity and generate new PG in the absence of the class A PBPs during cell elongation and division (Cho *et al*., 2016; Meeske *et al*., 2016; Emami *et al*., 2017). Interestingly, *B. subtilis* encodes another SEDS protein called SpoVE, which is required for the cortex PG synthesis during spore formation (Vasudevan *et al*., 2007; Fay *et al*., 2010; Leclercq *et al*., 2017; Luhur *et al*., 2020). To synthesize PG, the SEDS transglycosylase requires association with a class B PBP (bPBP) to provide transpeptidase activity (Typas *et al*., 2012; Egan *et al*., 2015; Rohs *et al*., 2018; Taguchi *et al*., 2019). Consistent with this idea, a recent study demonstrating the crystal structure of RodA-PBP2 complex revealed that the transglycosylase activity of RodA is activated by interaction with PBP2 (bPBP) (Sjodt *et al*., 2020). Therefore, the SEDS-bPBP complex provides the cell with another combination of the TG and TP activities which confers robust cell viability (Rohs *et al*., 2018). Similarly, the transglycosylase SpoVE requires the transpeptidase SpoVD to generate the forespore cortex (Fay *et al*., 2010).

In rod-shaped bacteria, two major biosynthetic complexes are thought to add new PG to the cell wall, these are the elongasome and divisome (Zhao *et al*., 2017; Angeles & Scheffers, 2020). The elongasome catalyzes the synthesis and insertion of new PG during cell elongation and the divisome orchestrates this same process during cell division and is required for membrane constriction and cell separation (Yang *et al*., 2011; Randich & Brun, 2015). The elongasome and divisome are composed of cytoskeletal proteins, PG synthases, PG hydrolases and other membrane-associated proteins (Caccamo & Brun, 2017).

1.3.2 PG hydrolysis

The synthesis of new PG is coordinated with PG hydrolysis, that cleaves the pre-existing PG and is believed to make space for insertion of new PG strands into the existing cell wall (Lee & Huang, 2013). PG cleavage or hydrolysis happens by cleaving glycoside and/or amide bonds via specialized autolysins (hydrolases) (Vollmer *et al*., 2008). Autolysins are categorized into various types, among them the amidases that hydrolyze the bond between the MurNAc component of the glycan strands and the stem peptide side chain (Uehara *et al*., 2010). Other types of peptidases such as carboxypeptidases and endopeptidases hydrolyze the internal amide bonds between the amino acids within stem peptides (Vollmer *et al*., 2008; Wyckoff *et al*., 2012). On the other hand, lytic transglycosylases (LTs) do not possess hydrolytic activity but cleave the glycan strands at the β-1,4-glycosidic bonds between GlcNAc and MurNAc (Dik *et al*., 2017). LTs are believed to loosen the PG matrix for many purposes such as incorporating

new PG material, cell division and inserting specialized secretion systems and flagella into the cell envelope (Scheurwater *et al*., 2008).

1.3.3 Cytoskeletal elements

Rod-shaped bacteria such as *B. subtilis* have specialized cytoskeletal elements that help drive PG biosynthetic complexes during cell growth and division (Bhavsar & Brown, 2006; Randich & Brun, 2015). The current thinking is that building new cell wall requires arrangement of the PG synthetic and hydrolytic machineries to follow a definite pattern, which is maintained by actin and tubulin-like proteins that are quite abundant in rod-shaped bacteria (Egan *et al*., 2017). Bacterial actin-like proteins like MreB and its homologous Mbl and MreBH are determinants of rod shape and are structurally similar to actin filaments in eukaryotic cells (Jones *et al*., 2001; Domínguez-Escobar *et al*., 2011). MreB-like proteins form short dynamic filaments that localize on the inner leaflet of the membrane, orienting almost perpendicularly to the long-axis of the cell, where they direct the localization of PG biosynthetic machinery required for cell wall synthesis (Ent *et al*., 2001; Domínguez-Escobar *et al*., 2011; Garner *et al*., 2011; Domínguez-Cuevas *et al*., 2013; Hussain *et al*., 2018).

Another essential cytoskeletal element is the tubulin-like protein FtsZ, which localizes to midcell during cell division and polymerizes at the inner leaflet of the cytoplasmic membrane into a ring-shaped structure called the Z-ring (Ortiz *et al*., 2015; McCausland *et al*., 2019). The Z-ring functions as a dynamic scaffold, allowing for the recruitment and assembly of division proteins into the divisome, which coordinates PG remodeling with membrane constriction at the division site (Uehara & Park, 2008; Randich & Brun, 2015; Yang *et al*., 2017; Bisson-Filho *et al*., 2017). In FtsZ mutants, cell division is blocked but the cells are still able to synthesize lateral PG, resulting in cell elongation without division (Scheffers & Pinho, 2005; Typas *et al*., 2012).

1.3.4 Regulation of PG synthesis and hydrolysis

During cell growth, the PG synthases catalyze the polymerization of new PG strands into the existing PG meshwork in a process that requires PG hydrolases to make a space, allowing the addition of nascent PG and hence elongation (Cava *et al*., 2013). Such coordination of new PG incorporation and old PG loosening necessitates a high level of regulation at both the level of synthesis and hydrolysis, to avoid excessive cleavage of cell wall, which can compromise the stability of the cell wall and lead to cell lysis (Lee & Huang, 2013).

1.3.4.1 Regulation of PG hydrolysis

One well studied example of the regulation of PG hydrolysis during vegetative growth in *B. subtilis* relates to the two autolysins, LytE and CwlO (Lee & Huang, 2013). Both CwlO and LytE, D,L-endopeptidases, are functionally redundant and thus constitute a synthetically lethal pair; cells need at least one of these enzymes to survive (Hashimoto *et al*., 2012). The function of these autolysins is dependent on their regulation. For instance, the regulation of LytE function requires interaction with MreBH – a MreB isoform – to localize to the lateral wall and to the division septum of the cell (Carballido-López *et al*., 2006). *B. subtilis* cells lacking *mreBH* fail to localize LytE to the lateral cell wall and produce long, slender cells similar to the Δ*lytE* mutant, supporting the idea that LytE function is dependent on the interaction with MreBH (Carballido-López *et al*., 2006). The regulation of PG hydrolysis during elongation by CwlO appears to be controlled by FtsEX, an ATP-binding cassette (ABC) transporter-like complex (Domínguez-Cuevas *et al*., 2013; Meisner *et al*., 2013).

1.3.4.2 Regulation of PG synthesis

An important example of the regulation of PG synthesis has been demonstrated in the Gram-negative bacterium *E. coli,* where two functionally redundant class A PBPs, PBP1a and PBP1b, contribute to cell wall synthesis (Typas *et al*., 2010; Egan *et al*., 2015). The functional redundancy between PBP1a and PBP1b led Paradis-Bleau *et al*. to carry out synthetically-lethal transposon insertion screens to identify genes that could function in the PBP1a or PBP1b pathway for PG synthesis (Paradis-Bleau *et al*., 2010). Interestingly, it was demonstrated that LpoA and LpoB are outer-membrane anchored regulators of PBP1a and PBP1b, respectively (Paradis-Bleau *et al*., 2010; Egan *et al*., 2014, 2018; Ranjit *et al*., 2017). Consistent with their roles as regulators of their cognate PBPs, double mutants lacking *lpoA lpoB* are not viable (Paradis-Bleau *et al*., 2010).

1.4 Engulfment

As mentioned earlier, engulfment is a central step during sporulation that is absolutely required for the formation of mature spores and involves PG remodeling orchestrated by PG synthases and PG hydrolases (Higgins & Dworkin, 2012; Khanna *et al*., 2019). Engulfment starts shortly after the formation of the asymmetric septum and is evidenced under the microscope by curving of the septum at the interface between the mother cell and forespore (Figure 1.3). At this stage, from a 2-D standpoint, the curved membranes generate two leading edges, which migrate around the forespore, until they fuse at the pole of the mother cell and result in the forespore

becoming internalized inside the mother cell cytoplasm. From the 3-D standpoint, the leading edge of the engulfing membrane surrounds the forespore circumferentially (Figure 1.3). Upon completion of engulfment, the forespore has a Gram-negative like envelope, surrounded by two membranes that sandwich a thin layer of PG (Figure 1.3).

During engulfment, multiple processes, some essential and some redundant, occur at the same time. These processes include membrane remodeling, the establishment of the AH-Q zipper-like interaction and PG remodeling. The proteins and protein complexes involved in these processes, and the roles they play, are discussed next.

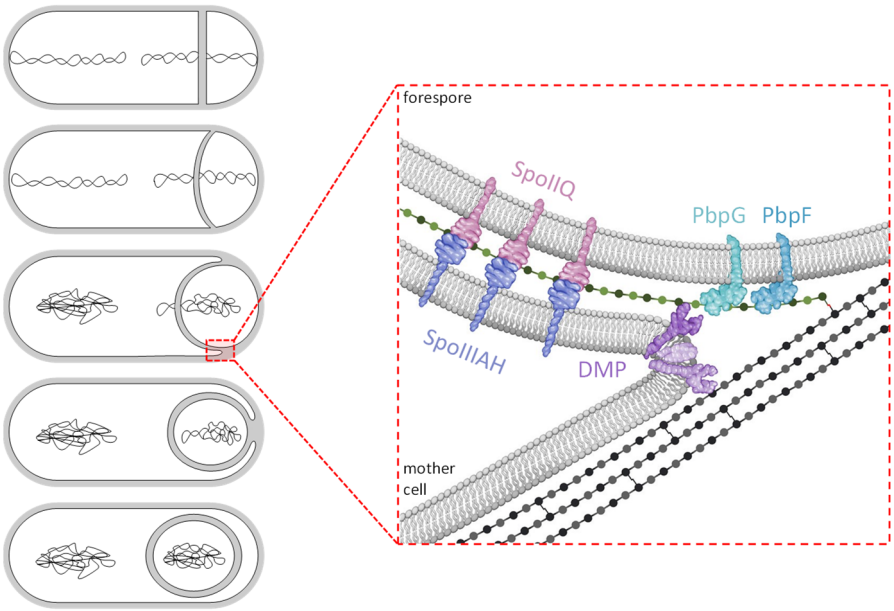

Figure 1.3: Schematic illustrations of engulfment progression and events happening during it. The schematic on the left shows the progression of engulfment that starts after asymmetric septum formation. The mother cell membranes migrate around the forespore and engulf it in a phagocytic-like event. By the end of engulfment, the forespore is internalized within the mother cell cytoplasm, where it undergoes maturation. The zoomed schematic illustrates the leading edges of the engulfing membranes where the SpoIIIAH-SpoIIQ interaction (blue and purple) is formed across the membranes. PbpG (light teal) and PbpF (light blue) drive the synthesis of the forespore PG layer (black line with dark green and black dots) that is sandwiched between the forespore and the mother cell membranes. From the mother cell side, the DMP complex (violet complex) catalyzes PG hydrolysis to allow the leading edge to migrate around the forespore.

1.4.1 Membrane remodeling

Once septal PG thinning begins, the mother membranes start migrating around the forespore until the leading edges of the migrating membranes meet at the forespore apex and undergo membrane fission (Figure 1.4) (Errington, 2003; Doan *et al*., 2013). Notably, Doan *et al*. were the first to identify a protein catalyzing membrane fission, FisB, in bacteria and specifically during sporulation (Doan *et al*., 2013). FisB is produced under the control of the mother cell

σ^E and by the end of engulfment, becomes enriched at the leading edges of the engulfing membranes, where it catalyzes membrane fission through its large extracellular lipid-interacting domain (Doan *et al*., 2013). Consistent with its role in membrane fission, Doan *et al*. used *in vitro* assays to show that FisB interacts closely with liposomes containing cardiolipin, which is enriched in the membrane lipids of sporulating cells (Doan *et al*., 2013; Tan & Ramamurthi, 2013). Furthermore, and consistent with FisB's key role in membrane fission, the majority of cells lacking *fisB* failed to complete engulfment and instead exhibited a defect in membrane fission (Doan *et al*., 2013; Tan & Ramamurthi, 2013). Interestingly, the authors noticed a subset of *fisB* mutant cells that could complete membrane fission at a slower rate (Doan *et al*., 2013). This observation argues that FisB may not be the only protein involved in membrane fission at the end of engulfment.

Several previous reports from the Pogliano laboratory suggested that the DNA translocase SpoIIIE is required for two membrane fission events: one happening at the end of engulfment and one happening during the last stages of asymmetric septum formation (Sharp & Pogliano, 1999, 2003; Liu *et al*., 2006; Fleming *et al*., 2010). However, Doan *et al*., through immunoblotting analysis, demonstrated that FisB protein levels decreased in cells lacking *spoIIIE* (Doan *et al*., 2013). Thus, it is unlikely that SpoIIIE directly mediates membrane fission at the end of engulfment; instead it appears that SpoIIIE contributes to membrane fission by stabilizing FisB.

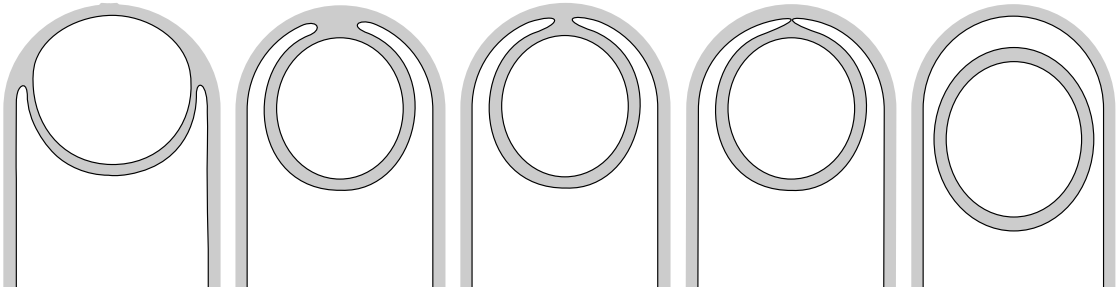

Figure 1.4: Diagram of the progression of membrane movement during engulfment. At the beginning of engulfment, the septum becomes curved. Next, the mother cell membranes migrate around the forespore until the leading edges are at an approximate distance, where FisB starts to act to fuse the membranes at the forespore apex.Upon engulfment, the forespore ends up surrounded by two membranes. The figure is based on that listed in (Doan *et al*., 2013).

With regards to the septal membrane fission event, SpoIIIE was also suggested to promote fission of the septal membranes at the time of asymmetric division (Liu *et al*., 2006; Fleming *et al*., 2010). This septal membrane fission event was thought to ensure forespore and mother cell compartmentalization by generating two distinct membranes (Liu *et al*., 2006).

Importantly, it has been reported recently that membrane synthesis is required for proper forespore growth, which emphasizes the role of membrane synthesis as a spore size determinant (Lopez-Garrido *et al*., 2018). Under a specific condition where engulfment is blocked (*spoIIM* mutant), and the forespore compartment enlarges in size, Lopez-Garrido *et al*. showed that blocking membrane synthesis using an antibiotic, cerulenin, could inhibit forespore growth (Lopez-Garrido *et al*., 2018).

1.4.2 SpoIIIAH-SpoIIQ interaction

The SpoIIIAH-SpoIIQ interaction (henceforth AH-Q interaction) is an integral part of the A-Q complex, a putative specialized secretion system that likely mediates molecular intercellular transport between the mother cell and the forespore (Camp & Losick, 2009; Rodrigues *et al*., 2016b) and acts as an important platform for protein-protein interactions during spore development (Doan *et al*., 2005; Aung *et al*., 2007; Rodrigues *et al*., 2016a). The A-Q complex in *B*. *subtilis* is thought to be composed of nine mother cell proteins, eight encoded in the *spoIIIA* operon (AA, AB, AC, AD, AE, AF, AG and AH) and GerM, and one spore protein SpoIIQ (Camp & Losick, 2008; Doan *et al*., 2009; Rodrigues *et al*., 2016a; Morlot & Rodrigues, 2018). The members of the A-Q complex are essential for the forespore size, shape and transcriptional potential. Engulfed forespores lacking any of these proteins are unable to activate σ^G and sustain forespore gene transcription (Doan *et al*., 2009; Rodrigues *et al*., 2013, 2016a).

The AH-Q interaction is formed across the septal membranes between SpoIIIAH and SpoIIQ (Blaylock *et al*., 2004; Meisner *et al*., 2012; Levdikov *et al*., 2012). Importantly, the AH-Q transenvelope interaction not only functions as an integral part of the A-Q complex (Doan *et al*., 2009; Meisner *et al*., 2012; Morlot & Rodrigues, 2018), but also plays an important role in engulfment progression (Figure 1.4) (Broder & Pogliano, 2006; Doan *et al*., 2009; Levdikov *et al*., 2012). The AH-Q interaction is suggested to act as a ratchet, or a zipper-like complex, to promote forward movement of the engulfing membranes (Blaylock *et al*., 2004; Broder & Pogliano, 2006). Consistent with this idea, the engulfment of lysozyme-protoplasted sporulating cells is mainly dependent on the AH-Q interaction (Broder & Pogliano, 2006). This observation is further supported by biophysical modeling showing that membrane engulfment in protoplasted cells requires a minimum number of AH and Q proteins (Ojkic *et al*., 2014).

1.4.3 PG remodeling during engulfment

An important molecular aspect of engulfment is PG remodeling, which appears to involve proteins in the mother cell and the forespore (Ojkic *et al*., 2016; Khanna *et al*., 2019). PG remodeling during engulfment starts with PG hydrolysis by the DMP complex at the asymmetric septum and then PG synthesis throughout engulfment at places where the PG is hydrolyzed (Aung *et al*., 2007; Tocheva *et al*., 2013). This PG remodeling results in a layer of PG (the GCW) sandwiched between the double membrane of the forespore, that is similar in structure to vegetative PG, except it is thinner (Popham, 2002). The GCW constitutes 5-10% of the total spore PG and is deposited on top of the inner spore membrane. Later after engulfment, the GCW serves as a foundation for deposition of cortex PG (Popham, 2002). Unlike GCW, the cortex PG is modified and contains muramic-δ-lactam residues, which decreases the degree of cross-linking between the glycan strands (Meador-Parton & Popham, 2000; Tan & Ramamurthi, 2014). These processes of PG synthesis and hydrolysis are discussed in more detail next.

1.4.3.1 PG synthesis during engulfment

The process of GCW synthesis during engulfment is carried out by the class A penicillin-binding proteins, PbpG and PbpF produced in the forespore (Figure 1.3) (Scheffers, 2005; Popham & Bernhards, 2015; Ojkic *et al*., 2016; Angeles & Scheffers, 2020). PbpG and PbpF are functionally redundant, and thus at least one of them is required for the synthesis of GCW during sporulation (Meador-Parton & Popham, 2000; McPherson *et al*., 2001). It was suggested that GCW synthesis happens ahead of the leading edge of the engulfing membranes (Tocheva *et al*., 2013; Khanna *et al*., 2019). The layer of GCW seems to act as a substratum for the deposition of layers of cortex PG after engulfment (Figure 8A) (McPherson *et al*., 2001; Popham & Bernhards, 2015). Consistent with this idea, cells lacking both *pbpG* and *pbpF* have severe defects in cortex structure and assembly, and thus fail to produce dormant spores (McPherson *et al*., 2001).

Interestingly, PbpG is exclusively expressed in the forespore mainly under σ^F control and to a lesser extent under σ^G control (Pedersen *et al*., 2000; Popham & Bernhards, 2015), whereas, PbpF is slightly expressed during vegetative growth conditions, but produced extensively during sporulation within the spore compartment under σ^G control, which is activated after engulfment is completed (Popham & Setlow, 1993; McPherson *et al*., 2001). In addition, another difference between PbpG and PbpF is that cells lacking *pbpG* produce spores that have

an abnormal, jellybean-like morphology, whereas cells lacking *pbpF* are wild-type in morphology (Rodrigues *et al*., 2016a). Considering the differences in the transcriptional control of PbpG and PbpF and the morphological defect of *pbpG* mutant forespores, it is difficult to fully grasp their functional redundancy. One hypothesis is that PbpG starts GCW synthesis under σ^F control and then PbpF functions to maintain the PG layers under σ^G control. Therefore, it is possible that PbpG and PbpF could be involved in separate pathways of PG synthesis during engulfment. This idea is consistent with the specialized roles of another two functionally redundant class A PBPs in *E. coli*, PBP1a and PBP1b, with PBP1a believed to be mostly involved in PG synthesis during cell elongation and PBP1b mostly involved in PG synthesis during cell division (Banzhaf *et al*., 2012; Mueller *et al*., 2019; Egan *et al*., 2020; Vigouroux *et al*., 2020).

Interestingly, a double mutant of *pbpG* and *pbpF* does not appear to have engulfment defects (McPherson *et al*., 2001), suggesting that they are dispensable for engulfment. However, more recent work showed that blocking PG synthesis with antibiotics during engulfment disrupts mother cell membrane migration (Meyer *et al*., 2010; Ojkic *et al*., 2014, 2016; Khanna *et al*., 2019). In these reports, the authors used antibiotics to block PG synthesis and this resulted in asymmetric migration of the engulfing membranes and failure to complete membrane fission at the forespore apex (Meyer *et al*., 2010; Ojkic *et al*., 2016). Although antibiotics could affect other aspects of cellular processes (Cho *et al*., 2014; Mitosch & Bollenbach, 2014; Takahashi *et al*., 2017), these observations suggest that other PG synthetic proteins could be involved in PG synthesis during engulfment. Furthermore, Ojkic *et al.* highlighted that blocking PG synthesis using certain antibiotics results in delocalization of the DMP complex at the leading edges (Ojkic *et al*., 2016), suggesting a relationship between PG synthesis and hydrolysis during engulfment.

1.4.3.2 PG hydrolysis during engulfment

A critical event during engulfment is thinning of the septal PG that is thought to begin at the midpoint of the asymmetric septum and then move outwards, toward the edges of the septum, where it then reaches the lateral PG that surrounds the entire sporangium (Figure 1.3) (Hilbert & Piggot, 2004; Khanna *et al*., 2020). Various studies support the idea that degradation of the septal PG is mediated by a protein complex known as the DMP complex (Aung *et al*., 2007; Chastanet & Losick, 2007; Khanna *et al*., 2019). Consistent with this role, sporulating cells

lacking the DMP complex fail to initiate engulfment and have a septum with thick PG (Eichenberger *et al*., 2001; Khanna *et al*., 2019).

The DMP complex is composed of three σ^E-dependent proteins: SpoIID, SpoIIM and SpoIIP (Figure 1.3) (Pogliano *et al*., 1999; Abanes-De Mello *et al*., 2002; Aung *et al*., 2007; Chastanet & Losick, 2007; Morlot *et al*., 2010). SpoIIP is also expressed in the forespore compartment under σ^F control but to a much lesser degree compared to its expression under σ^E control (Dworkin & Losick, 2005). Consistent with their essentiality for engulfment, null mutants of any of *spoIIM*, *spoIIP* or *spoIID* fail to initiate engulfment and show a characteristic phenotype referred to as "bulges" (Figure 1.5) (Eichenberger *et al*., 2001; Abanes-De Mello *et al*., 2002; Gutierrez *et al*., 2010; Meyer *et al*., 2010). The bulges result from incomplete septal thinning and form at the middle of the septum, protruding toward the mother cell cytosol and expanding as a result of membrane synthesis and chromosome-induced turgor pressure as the chromosome is translocated into the forespore (Figure 1.5) (Lopez-Garrido *et al*., 2018). Double mutants of *spoIID* and *spoIIP* fail to degrade septal PG and the asymmetric septum remains flat (Eichenberger *et al*., 2001; Abanes-De Mello *et al*., 2002; Chastanet & Losick, 2007).

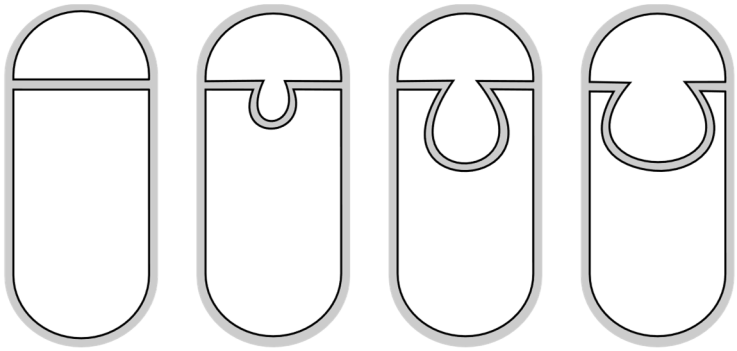

Figure 1.5: Diagram of septal bulge formation and growth. Formation of a bulge in a mutant lacking any of *spoIID*, *spoIIM* or *spoIIP*. The bulges start as membrane invaginations that grow toward the mother cell side and grow over time.

(a) Localization of the DMP complex

Multiple lines of evidence suggest that the DMP complex is localized to the sporulation septum following a protein localization hierarchy. Localization of the DMP complex depends on a protein called SpoIIB, produced at the onset of sporulation under σ^H control (Margolis *et al*., 1993; Perez *et al*., 2000; Aung *et al*., 2007; Dworkin, 2014). SpoIIB localizes to the asymmetric septum in an FtsZ-dependent manner and then recruits SpoIIM (Perez *et al*., 2000; Aung *et al*., 2007). SpoIIM then recruits SpoIIP and finally SpoIIP recruits SpoIID (Aung *et al*., 2007; Chastanet & Losick, 2007). Consistent with this protein localization hierarchy, mutants lacking

spoIIM fail to localize SpoIIP and SpoIID, whilst *spoIIP* null mutants fail to localize SpoIID but do not affect SpoIIM localization (Chastanet & Losick, 2007). Consequently, *spoIID* mutants do not affect the localization of SpoIIM and SpoIIP (Aung *et al*., 2007; Chastanet & Losick, 2007).

Interestingly, *spoIIB* mutant cells are still capable of partially localizing the DMP complex, which suggests an alternative pathway for localization of the DMP complex (Aung *et al*., 2007). Indeed, it was found that cells lacking *spoIIB* and *spoIVFA* fail to initiate engulfment. Thus, SpoIVFA is also required for the localization of the DMP complex (Aung *et al*., 2007). To add to the complexity of how the DMP complex is localized, the localization of SpoIVFA to the septum requires the AH-Q zipper-like interaction, which suggests an indirect role for the AH-Q interaction in the localization of the DMP complex (Aung *et al*., 2007).

(b) Enzymatic activities and coordination between SpoIIP and SpoIID

Previously, it was reported that SpoIIM has no enzymatic activity and acts as a scaffold for recruiting SpoIIP and SpoIID (Aung *et al*., 2007; Chastanet & Losick, 2007). In 2010, Morlot *et al*. used biochemical assays to examine the catalytic activities of purified SpoIIP and SpoIID (Morlot *et al*., 2010). They found that SpoIIP has a dual function as an amidase, degrading the peptide bonds between the MurNAc subunit in the glycan strands and the stem peptide, and as an endopeptidase, hydrolyzing the peptide cross-links (Morlot *et al*., 2010). Interestingly, SpoIID appeared to be the founding member of a new family of lytic transglycosylases, which cleave the glycosidic bonds of denuded glycan strands (Morlot *et al*., 2010; Nocadello *et al*., 2016).

Morlot *et al*. also investigated how the hydrolytic activities of SpoIIP and SpoIID are regulated during engulfment and discovered that these enzymes regulate each other. It was demonstrated that SpoIID activity only occurs when SpoIIP, or another amidase, was added to the reaction. Reciprocally, it was shown that the amidase activity of SpoIIP was enhanced by the addition of SpoIID (Morlot *et al*., 2010). Collectively, this work suggests that SpoIID acts to cleave the glycan strands only after removal of the peptide side chains by SpoIIP and SpoIIP activity is then stimulated by SpoIID. Thus, the activity of SpoIIP and SpoIID are intrinsically regulated during engulfment through a catalytic cycle (Morlot *et al*., 2010).

1.5 Chromosome translocation

Concurrently with engulfment, another critical aspect of spore development is the translocation of a copy of the chromosome into the forespore (Figure 1.6). As mentioned earlier, the asymmetric septum is laid down over the chromosome axial filament, resulting in ~30% of the chromosome being trapped inside the forespore compartment and the remaining ~70% still residing in the mother cell cytoplasm (Wu & Errington, 1994, 1998). Soon after asymmetric septum formation, the DNA translocase SpoIIIE translocates the remaining ~70% of the chromosome into the forespore (Wu & Errington, 1994; Sharpe & Errington, 1995; Sharp & Pogliano, 2002; Burton *et al*., 2007; Fiche *et al*., 2013). SpoIIIE assembly requires trapped DNA in the septum, after which SpoIIIE pumps the chromosome into the forespore (Wu & Errington, 1994, 1997; Ben-Yehuda *et al*., 2003a; Fiche *et al*., 2013). As SpoIIIE is translocating the chromosome, it strips the DNA strands from attached RNA polymerases, transcription factors and other proteins to ensure compartment specific transcription in the forespore (Marquis *et al*., 2008).

During chromosome translocation by SpoIIIE, the two termini regions of the chromosomes are thought to be connected through a cohesive force (Willis *et al*., 2020). Once the *ter* region of the forespore chromosome reaches the septum, the *ter* region of the mother cell becomes separated (Bogush *et al*., 2007; Willis *et al*., 2020). Thus, although SpoIIIE is required for segregating the two termini regions, it is unclear why or how they remain connected during chromosome translocation. Willis *et al*. suggested that termini cohesion could help to prevent midcell septation (Willis *et al*., 2020).

Using a quantitative fluorescence-based assay to examine chromosome translocation in wild-type cells, Burton *et al*. showed that SpoIIIE completes chromosome translocation across the septum and into the forespore in ~20 mins (Bath *et al*., 2000; Burton *et al*., 2007; Liu *et al*., 2015). Burton *et al*. and others also demonstrated that SpoIIIE translocates the two arms of the chromosome axial filament at the same time (Burton *et al*., 2007; Ptacin *et al*., 2008; Fiche *et al*., 2013; Wang *et al*., 2014). Interestingly, a recent report using time-lapse fluorescence microscopy, cryo-electron tomography and biophysical modeling showed that SpoIIIE-mediated chromosome translocation generates turgor pressure within the forespore compartment (Lopez-Garrido *et al*., 2018). The authors suggested that the turgor pressure stretches the forespore septal PG and thus "inflates" the forespore, allowing it to adopt its oblong shape and normal dimensions (Lopez-Garrido *et al*., 2018). Consistent with this idea,

cells lacking *spoIIIE,* which do not translocate the chromosome, fail to inflate the forespore and instead the forespore appears deformed and smaller in size (Lopez-Garrido *et al*., 2018). The next sections examine SpoIIIE and its roles in sporulation in more detail.

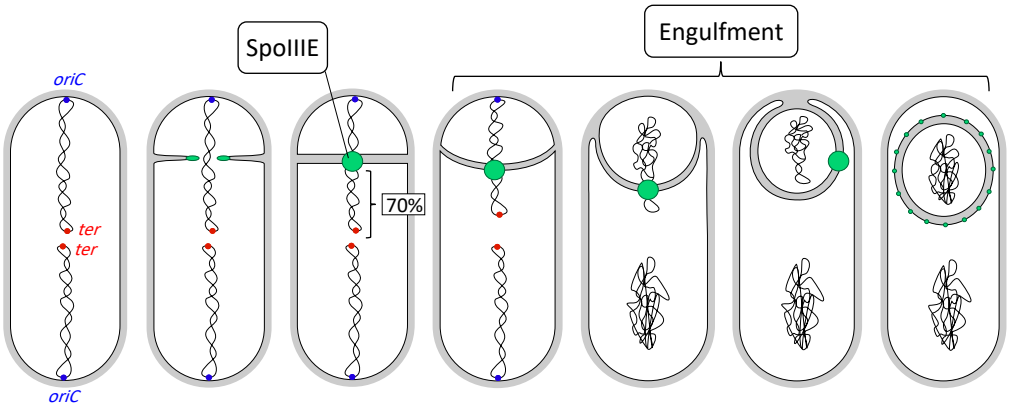

Figure 1.6: Diagram of chromosome translocation concurrent with engulfment. A schematic illustration of chromosome translocation and the different stages of engulfment. Initially, the starved cell duplicates and arranges its chromosomes (black squiggles) in filament-like structures with the *oriC* (blue dots) anchored to cell poles and *ter* (red dots) to midcell, the *ter* cohesion is omitted for clarity. Next, SpoIIIE enriches at the edges of the developing asymmetric septum that divides the cell into a small forespore and a large mother cell. The asymmetric septum traps ~70% of the forespore chromosome outside and this triggers SpoIIIE (green circle) to assemble into a single focus at the middle of the septum. At this stage, SpoIIIE initiates chromosome translocation into the forespore, while the septum curves due to PG remodeling and the mother cell membranes start to wrap around the forespore to engulf it. Chromosome translocation continues concurrently with engulfment progression. Upon completion of chromosome translocation, SpoIIIE moves around the forespore before it disperses in the forespore outer membrane by the time of engulfment completion.

1.5.1 SpoIIIE domain structure and function

SpoIIIE is an ATP-fueled DNA motor that belongs to the FtsK/SpoIIIE family of DNA translocases that hydrolyze an ATP molecule per two nucleotides of DNA to translocate the chromosome (Wu, 2009; Demarre *et al*., 2013; Liu *et al*., 2015). SpoIIIE is a polytropic membrane protein composed of three domains: a transmembrane domain containing four transmembrane helices at the N-terminus that are required for SpoIIIE septal localization, a poorly conserved and unstructured linker region and a C-terminal motor domain to which it is connected (Wu & Errington, 1997; Bath *et al*., 2000; Sharp & Pogliano, 2002). The motor domain itself is made up of three subunits (α, β and γ), where α and β subunits belong to the RecA-like family of ATPases (Bigot *et al*., 2007; Burton & Dubnau, 2010; Demarre *et al*., 2013; Crozat *et al*., 2014). The α and β subunit have been shown to hexamerize into a ring through which a single, double-stranded segment of DNA is threaded by ATP hydrolysis (Bath *et al*., 2000; Crozat & Grainge, 2010; Sherratt *et al*., 2010; Cattoni *et al*., 2014). Based on the above, it has been hypothesized that translocation of the chromosome into the forespore

requires at least two SpoIIIE hexamers, one for each arm of the chromosome (Burton *et al*., 2007).

The γ subunit is believed to scan the translocated chromosome to recognize and bind to specific octameric sequences of (GAGAAGGG) called SRS (SpoIIIE recognition sequence) (Ptacin *et al*., 2008; Cattoni *et al*., 2013). The SRS sequences are distributed on the chromosome and enriched closer to the *ter* region, where ~85% of the SRSs occur on the leading strand (Pease *et al*., 2005; Ptacin *et al*., 2008; Besprozvannaya & Burton, 2014). Interestingly, Nöllmann *et al*. suggested that the linker region acts as a coil, allowing the motor to move along the DNA to search for the SRS regions until the linker is fully stretched, then the linker retracts back, bringing the chromosome with it towards the septal membrane (Fiche *et al*., 2013). Using quantitative atomic force microscopy (AFM) and mathematical modeling, Chara *et al*. showed that the binding of the γ subunit to the SRS sequences is not required to activate DNA translocation by the α, β motor subunit (Chara *et al*., 2018). Consistent with this idea, the α, β motor subunit retains some DNA translocation activity and can translocate DNA lacking the SRS motif (Besprozvannaya *et al*., 2013; Cattoni *et al*., 2013; Chara *et al*., 2018). Thus, a major role for the γ subunit is to bind to SRS and ensure efficient and directional chromosome translocation (Chara *et al*., 2018).

1.5.2 A role for SpoIIIE in maintaining compartmentalization during early spore development

Another critical role of SpoIIIE is to maintain compartmentalization of the mother cell and forespore, allowing for compartment specific activity of σ^F and σ^E during engulfment (Wu & Errington, 1994; Li & Piggot, 2001; Hilbert & Piggot, 2004). It was suggested that SpoIIIE acts a plug or diffusion barrier that prevents molecules from passing through the septum, including the sigma factors (Liu *et al*., 2006; Besprozvannaya *et al*., 2014). Consistent with this idea, the absence of *spoIIIE* not only abolishes chromosome translocation, but also results in cytoplasmic miscompartmentalization (Wu & Errington, 1994; Hilbert & Piggot, 2004). It has been suggested that the absence of SpoIIIE leaves a pore or hole in the septum, through which molecules could diffuse freely between the forespore and the mother cell during engulfment (Wu & Errington, 1997; Hilbert *et al*., 2004).

Interestingly, the cytoplasmic miscompartmentalization defect of cells lacking *spoIIIE* can be suppressed by blocking PG hydrolysis during engulfment (Wu & Errington, 1994; Wu *et al*.,

1995; Hilbert *et al*., 2004). It has been suggested that prior to septal PG hydrolysis, the septal hole or pore left open in the absence *spoIIIE* is too small to allow miscompartmentalization of molecules like GFP (green fluorescent protein), but upon PG hydrolysis, the hole/pore enlarges, allowing GFP and probably σ^F to pass through (Hilbert *et al*., 2004). Interestingly, this suggests a relation between SpoIIIE-mediated compartmentalization and PG remodeling during engulfment and that maintaining compartmentalization depends on the amount of septal PG present within the septum.

1.5.3 A role for SpoIIIE in chromosome segregation during vegetative growth

During vegetative growth, although SpoIIIE is not generally required for chromosome segregation, disrupting DNA replication initiation makes SpoIIIE essential for post-septational partitioning of the chromosomes between sister cells (Sharpe & Errington, 1995; Wu & Errington, 1997; Biller & Burkholder, 2009; Kaimer *et al*., 2009). This suggests that SpoIIIE could be required during stressful or unusual vegetative growth conditions where septation happens before chromosome segregation, similar to what occurs during sporulation (Sharpe & Errington, 1995; Sciochetti & Piggot, 2000). Consistent with this idea, using photo-activated localization microscopy (PALM), SpoIIIE was shown to localize during vegetative growth at future division sites, as dynamic or static clusters (Fiche *et al*., 2013).

Interestingly, *B. subtilis* cells encode another DNA translocase called SftA, that also belongs to the FtsK/SpoIIIE family, however it lacks the transmembrane domain (Biller & Burkholder, 2009; Kaimer *et al*., 2009; Burton & Dubnau, 2010; El Najjar *et al*., 2017). SftA localizes to the division septum in an FtsZ-dependent manner and acts together with SpoIIIE to segregate the chromosome dimers (Biller & Burkholder, 2009; Kaimer *et al*., 2011; El Najjar *et al*., 2018). Consistent with this idea, the absence of both *spoIIIE* and *sftA* is deleterious to cells growing under normal conditions (Kaimer *et al*., 2009). However, during sporulation the absence of *sftA* does not impact chromosome segregation, suggesting that SftA is not required for spore formation (Wu, 2009; Bose *et al*., 2016).

1.5.4 SpoIIIE localization during sporulation

The localization of SpoIIIE has been extensively investigated using different approaches that have provided conflicting insights into how SpoIIIE is organized in the asymmetric septum. SpoIIIE is produced in both vegetative and sporulating cells under the control of σ^A, the primary sigma factor in *B. subtilis* (Foulger & Errington, 1989; Sharpe & Errington, 1995;

Fiche *et al*., 2013). In 1994, Wu & Errington were the first to show that SpoIIIE localizes as a single focus to the asymmetric septum by the use of immunofluorescence microscopy (Figure 1.6) (Wu & Errington, 1994). Furthermore, they characterized two classes of SpoIIIE mutations that affect its stability and functionality: class I mutants localize to the septum, but fail to translocate the chromosome, while class II mutants are unstable (Wu & Errington, 1994, 1997). An interesting and well-characterized mutant that belongs to class I mutants was referred to as *spoIIIE36*, which was later shown to be a translocation-defective allele of SpoIIIE that persists as a septal focus and maintains compartmentalization (Wu & Errington, 1994, 1997, 1998; Harry *et al*., 1995).

In 1999, Sharp & Pogliano also used immunofluorescence microscopy combined with image quantification of different patterns of SpoIIIE localization, to show that SpoIIIE changes localization throughout engulfment (Figure 1.6) (Sharp & Pogliano, 1999). In this report, the authors illustrated that SpoIIIE initially localizes as a discrete focus to the middle of the asymmetric septum that then moves around the forespore before the focus disperses in the forespore membrane (Figure 1.6) (Sharp & Pogliano, 1999; Pogliano *et al*., 2003). Later work by the same authors demonstrated that SpoIIIE fails to form a focus at the septum if expressed from the forespore side, however expressing SpoIIIE under the control of a mother cell promoter allowed wild-type-like localization and activity (Sharp & Pogliano, 2002). They also demonstrated that the transmembrane domain of SpoIIIE is sufficient for its septal localization (Sharp & Pogliano, 2002).

Interestingly, in 2013, using a form of high-resolution microscopy, photo-activated localization microcopy (PALM), the Nöllmann laboratory investigated SpoIIIE's orientation within the septum (Fiche *et al*., 2013). They showed that SpoIIIE is predominately localized as a single focus on the mother cell side of the septal membrane in wild-type cells and assembles into complexes containing 47±20 SpoIIIE molecules (Fiche *et al*., 2013). Consistent with this result, research from the Pogliano laboratory used the same approach and reported similar observations (Shin *et al*., 2015). However, when Shin *et al*. examined SpoIIIE localization using PALM in engulfment-blocked cells lacking either *sigE* or *spoIIP spoIID*, they observed SpoIIIE as dual foci, one on each side of the septum, in 39% and 26% of the cells, respectively (Shin *et al*., 2015). This observation led Shin and co-workers to suggest that the dual foci of SpoIIIE represent two complexes, one in the forespore and another in the mother cell (Shin *et al*., 2015). The authors reasoned that the thicker septum of *sigE* or *spoIIP spoIID* null mutant

cells allowed for separation of the forespore and mother cell SpoIIIE complexes and thus their detection within the resolution of PALM (20-50 nm) (MacDonald *et al*., 2015). The exact significance of SpoIIIE on the forespore side of the septum is controversial, as detailed next.

1.5.5 Models of chromosome translocation

For many years, there has been an on-going debate surrounding the mechanism of how the chromosome is translocated into the forespore (Wu & Errington, 1997; Errington *et al*., 2001; Sharp & Pogliano, 2002; Becker & Pogliano, 2007; Burton *et al*., 2007; Fleming *et al*., 2010; Fiche *et al*., 2013; Shin *et al*., 2015). Two main models, the Aqueous Pore Model and the Membrane Channel Model, have been proposed based on multiple lines of evidence and, in some cases, conflicting data. These models differ in two major points, the nature of the septum at the time of chromosome translocation and the organization of SpoIIIE at the septum, as discussed next.

1.5.5.1 Aqueous Pore Model

In 1997, Errington and colleagues proposed that SpoIIIE localizes from the mother cell side and translocates the chromosome through a pore within the septum (Figure 1.7) (Wu & Errington, 1997). According to this model, the septal membranes are unfused during chromosome translocation to allow for passage of the DNA, and SpoIIIE localizes to the septal pore through its transmembrane segment (Figure 1.7) (Wu & Errington, 1997; Errington *et al*., 2001). Later in 2013, Nöllmann and co-workers generated a more refined version of this model by demonstrating, through the use of PALM, that SpoIIIE localizes mainly from the mother cell side (Fiche *et al*., 2013). In their model, Nöllmann and co-workers suggested that SpoIIIE would function to translocate the chromosome only in one direction, from the mother cell into the forespore through an aqueous pore (Figure 1.7) (Fiche *et al*., 2013). One of the interesting ideas of this model is that SpoIIIE acts as a checkpoint to prevent completion of cytokinesis until the chromosome is fully translocated into the forespore (Fiche *et al*., 2013). This checkpoint is maintained through possible interactions with other proteins localized within the septum that are involved in septal PG remodeling and completion of cytokinesis. Despite many years of research, genetic support for the Aqueous Pore Model remains to be obtained. Furthermore, it is unclear how such a pore would be maintained in the face of septal PG remodeling at the onset of engulfment.

1.5.5.2 Membrane Channel Model

The Membrane Channel Model was first proposed by the Pogliano laboratory in 2006 and later refined by the Rudner laboratory in 2007 (Liu *et al*., 2006; Burton *et al*., 2007). In this model, the septal membranes are predicted to be fused before chromosome translocation is initiated and SpoIIIE mediates the fusion of the septal membranes upon septum formation (Figure 1.7) (Liu *et al*., 2006; Becker & Pogliano, 2007; Burton *et al*., 2007; Fleming *et al*., 2010). Interestingly, to reconcile the need to translocate the chromosome across a fused septal membrane, it was suggested that the transmembrane domain of SpoIIIE assembles into a pair of channels spanning the septal membranes, with one channel translocating an arm of the chromosome (Figure 1.7) (Liu *et al*., 2006; Fleming *et al*., 2010; Shin *et al*., 2015). Although it remains to be shown if the transmembrane segments of SpoIIIE can hexamerize into channels, the transmembrane domain of the SpoIIIE homolog, FtsK, has been shown to form hexamers *in vitro* (Bisicchia *et al*., 2013). Interestingly, other data argue that the transmembrane domain of FtsK is dispensable for chromosome segregation in *E. coli* (Dubarry & Barre, 2010), raising questions about the biological significance, if any, of the *in vitro* hexamerization of the FtsK transmembrane domain.

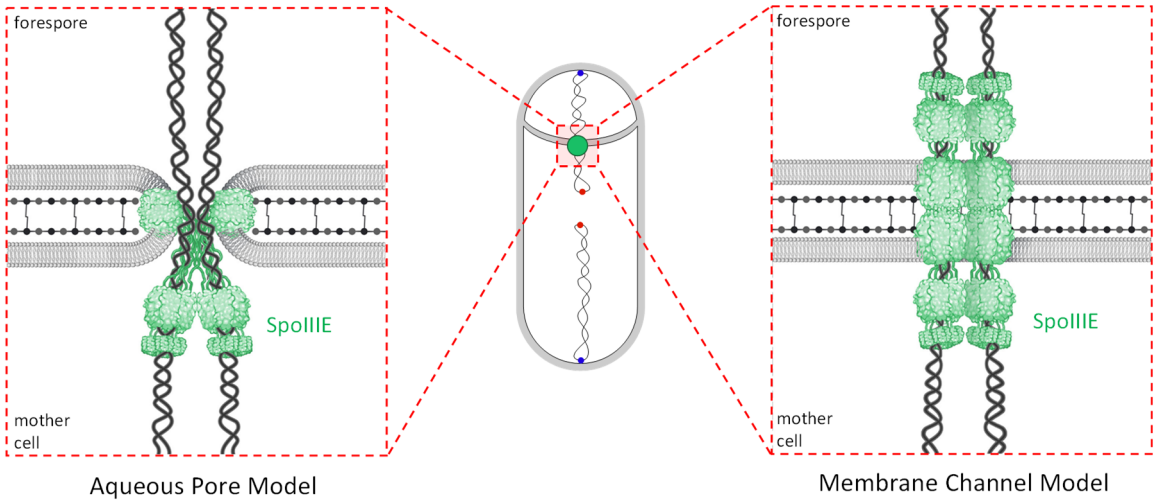

Figure 1.7: Schematic illustrations of the two models of chromosome translocation. The schematic in the middle shows a cell with SpoIIIE (green circle) that assembles as a focus in the septum and translocates the chromosome (black squiggles) into the forespore. The schematic on the left shows the Aqueous Pore Model where SpoIIIE localizes from the mother cell side within unfused septal membranes that form an aqueous pore in the membrane. The schematic on the right shows the Membrane Channel Model where SpoIIIE localizes on both sides of the fused septal membranes and assembles into two co-axial channels.

Another key aspect of the Channel Model is that SpoIIIE functions as a bidirectional motor, as it is thought to exist on both sides of the septum, in the forespore and in the mother cell (Liu *et*

al., 2006; Fleming *et al*., 2010; Shin *et al*., 2015). The most significant piece of data to support this organization of SpoIIIE within the septum is that SpoIIIE is present on both sides of the asymmetric septum, in a subset of cells, when engulfment is blocked (Figure 1.7) (Shin *et al*., 2015). Considering the idea of a dual motor, it has been hypothesized that the mother cell SpoIIIE motor translocates the chromosome into the forespore, whereas the forespore motor translocates the chromosome back into the mother cell (Sharp & Pogliano, 2002; Shin *et al*., 2015; Lopez-Garrido *et al*., 2018). To prevent translocation conflicts between the forespore and mother cell motors, it was suggested that the forespore motor is held inactive, possibly by yet-to-be-defined factors (Lopez-Garrido *et al*., 2018).

More importantly, neither the Channel nor Aqueous Pore models have considered the fact that chromosome translocation happens concomitantly with other critical processes during engulfment, including PG remodeling. As explained earlier, PG remodeling reshapes the forespore and encases it with a double membrane envelope. Therefore, a key point toward understanding how the chromosome is translocated across the septal membranes is to investigate if there is an interplay between chromosome translocation and other molecular events occurring during engulfment.

1.6 Lessons from FtsK: a DNA translocase in *E. coli*

FtsK in *E. coli* is a closely related homolog of SpoIIIE (Sciochetti & Piggot, 2000; Errington *et al*., 2001; Sherratt *et al*., 2010; Burton & Dubnau, 2010). Similar to SpoIIIE, FtsK has three domains, including the N-terminal transmembrane domain ($FtsK_N$), a large linker region ($FtsK_L$) and the C-terminal motor domain ($FtsK_C$) composed of the α, β and γ subunits (Massey *et al*., 2006; Crozat & Grainge, 2010). Interestingly, the α and β subunits of FtsK and of SpoIIIE have 50% sequence identity, whereas the $FtsK^{\gamma}$ subunit has 42% identity to that of SpoIIIE (Barre, 2007). Like SpoIIIE, the α and β subunits form a hexameric ring and also hydrolyze ATP to generate the energy required for chromosome partitioning (Massey *et al*., 2006; Jean *et al*., 2020). The $FtsK^{\gamma}$ subunit binds to FtsK-orienting polar sequences (KOPs) that are enriched close to the *dif* site (deletion-induced filamentation) to ensure directionality of DNA movement (Grainge, 2013; Stouf *et al*., 2013; Crozat *et al*., 2014).

Interestingly, it was found that the purified $FtsK_N$ domain can assemble into hexamers *in vitro* (Bisicchia *et al*., 2013), suggesting that it may form membrane channels in the division septum through which chromosome segregation between sister cells occurs. However, the role of the

transmembrane segments in supporting the actual segregation of chromosomes was debated by transmembrane domain swapping experiments. It was shown that swapping the $FtsK_N$ domain with that of other proteins still allowed efficient chromosome segregation (Dubarry & Barre, 2010).

1.6.1 Roles of FtsK in chromosome partitioning in *E. coli*

FtsK is a multifunctional protein that is involved in cell division, chromosome segregation and chromosome dimer resolution (Crozat & Grainge, 2010; Crozat *et al*., 2014). In *E. coli*, septation starts before complete segregation of the sister chromosomes, but unlike in sporulating *B. subtilis*, about 0.3 megabases of one chromosome is trapped outside the recipient cell (Crozat & Grainge, 2010; Stouf *et al*., 2013; Besprozvannaya & Burton, 2014). In a similar fashion to SpoIIIE, FtsK localizes to the division septum where it segregates the chromosomes of the sister cells (Demarre *et al*., 2013; Crozat *et al*., 2014). Interestingly, FtsK is considered the fastest translocase characterized so far, with a translocation rate of up to 17.5 $kb \cdot s^{-1}$ (Jean *et al*., 2020). To resolve chromosome dimers, the $FtsK^{\gamma}$ subunit interacts with the XerCD recombinase to activate site-specific recombination at the *dif* site (Massey *et al*., 2006; Grainge, 2013; May *et al*., 2015).

1.6.2 FtsK couples chromosome segregation with cytokinesis

Based on its localization at the division septum, and considering that the $FtsK_N$ domain is dispensable for chromosome segregation, it has been suggested that FtsK assembles at a closing pore within the septum, through which the chromosome is being pumped (Errington *et al*., 2001; Bigot *et al*., 2007; Kennedy *et al*., 2008; Crozat & Grainge, 2010; Reyes-Lamothe *et al*., 2012; Fiche *et al*., 2013). Accordingly, FtsK is thought to function as a checkpoint that couples chromosome segregation with cytokinesis, where FtsK could delay cytokinesis until segregation of the sister chromosomes is completed (Grainge, 2010; Demarre *et al*., 2013; Berezuk *et al*., 2014; Männik & Bailey, 2015). Once FtsK clears the chromosome from the closing septal pore, the sister cells can complete cytokinesis and separate.

Several reports suggest that FtsK coordinates chromosome segregation with cell division possibly by stimulating PG synthesis to complete cytokinesis (Reyes-Lamothe *et al*., 2012; Coltharp *et al*., 2016; Männik *et al*., 2017; Du & Lutkenhaus, 2017). Consistent with this suggestion, FtsK has been shown to interact with several proteins involved in PG synthesis including PBP1a, PBP3, PBP5 (or FtsI) and SPOR (sporulation-related repeat) domain-

containing proteins including RlpA, FtsN and DamX (Di Lallo *et al*., 2003; Errington *et al*., 2003; Grenga *et al*., 2008; Berezuk *et al*., 2018). Interestingly, the SPOR-domain containing proteins FtsN and DamX have been shown to stimulate PG synthesis of class A PBPs during cell division (Berezuk *et al*., 2018; Pazos *et al*., 2020). In addition, multiple studies have shown that the transmembrane domain of FtsK is required for cell division and viability (Grenga *et al*., 2008; Demarre *et al*., 2013). It was found that FtsK interacts and recruits different components of the divisome, such FtsZ, FtsQ, FtsL and FtsI (Grenga *et al*., 2008; Dubarry *et al*., 2010; Grainge, 2010; Du & Lutkenhaus, 2017). Therefore, it appears that FtsK is one of the key players in *E. coli* cell division and not limited to DNA translocation. In light of these FtsK roles, it is tempting to speculate that SpoIIIE could perform similar roles during spore development.

1.7 Thesis aims

As mentioned in the Introduction (section 1.3.4.2), some bacteria encode functionally redundant class A PBPs to ensure robust cell wall synthesis and thus secure their viability (Hoskins *et al*., 1999; Paradis-Bleau *et al*., 2010; Typas *et al*., 2010; Sassine *et al*., 2017). However, despite their redundancy, some PBPs also function in separate pathways to ensure PG synthesis during different stages of the cell cycle (Banzhaf *et al*., 2012; Mueller *et al*., 2019; Egan *et al*., 2020; Vigouroux *et al*., 2020). Interestingly, sporulating *B. subtilis* cells produce two functionally redundant class A PBPs known as PbpG and PbpF (Meador-Parton & Popham, 2000; McPherson *et al*., 2001; Popham & Bernhards, 2015). At least one of these PBPs needs to be present to synthesize the GCW during engulfment (Scheffers, 2005; Ojkic *et al*., 2016). Interestingly, PbpG and PbpF differ from each other in that each protein is produced at different times of spore development and the phenotype of their mutants is also different (Popham & Setlow, 1993; Pedersen *et al*., 2000; Rodrigues *et al*., 2016a). Based on these differences, the primary objective of this thesis was to investigate if PbpG and PbpF could function in separate pathways and thus have specialized roles during sporulation. Interestingly, in addressing this question, at least for PbpG, this thesis also revealed a previously uncharacterized and critical coordination between PG remodeling during engulfment and chromosome translocation and provided strong evidence that chromosome translocation occurs through a septal pore.

In Chapter 3, stemming from a transposon-sequencing genetic screen in *pbpF* and *pbpG* mutants, the SpoIIIM protein (formerly YqfZ, a poorly-studied sporulation protein) was identified as being required for efficient sporulation in cells lacking PbpG. Various approaches showed that SpoIIIM and PbpG are required to maintain forespore morphology and cytoplasmatic compartmentalization. Interestingly, the forespores of cells lacking SpoIIIM and PbpG were found to resemble those lacking SpoIIIE with respect to forespore morphology and the degree of compartmentalization. Importantly, it was found that SpoIIIM and PbpG (and SpoIIIE) are only required for compartmentalization if septal PG hydrolysis by the DMP complex is active. These observations led to the primary hypothesis that SpoIIIM and PbpG function to counterbalance the activity of the DMP complex around a septal pore, possibly by contributing to PG synthesis around the pore. Other hypotheses were also raised to explain these observations and were tested in the subsequent chapters.

In Chapter 4, the hypothesis that SpoIIIM and PbpG contribute to compartmentalization by stabilizing SpoIIIE was tested by examining SpoIIIE localization. It was found that SpoIIIM and PbpG are not required for SpoIIIE stability but are instead required for efficient chromosome translocation and retention of the translocated chromosome in the forespore, as demonstrated by chromosome translocation assays using fluorescently labelled LacI bound to different repeats of *lacO* sites on the chromosome. Other data suggested that in cells lacking SpoIIIM and PbpG the forespore chromosome is likely to be effluxed back to the mother cell in a passive and random fashion, rather than actively reverse translocated. Importantly, just like what was reported in Chapter 3, it was found that SpoIIIM and PbpG are only required for efficient chromosome translocation and retention of the translocated chromosome in the forespore, if septal PG hydrolysis by the DMP complex is active. These observations and others led to the hypothesis that SpoIIIM, PbpG and SpoIIIE together coordinate chromosome translocation with PG synthesis at a septal pore to ensure retention of the forespore chromosome in the forespore during PG hydrolysis by the DMP complex.

Chapter 5 provides strong evidence that the septal membranes are unfused during chromosome translocation and reveals an important role for the AH-Q interaction in the stabilization of the septal pore. Using various microscopy-based approaches, in cells lacking SpoIIIM, PbpG, SpoIIIE and the AH-Q transenvelope interaction, an unusual phenotype was observed whereby the septal membranes retract. It was found that this septal retraction phenotype happens shortly after the onset of PG hydrolysis by the DMP complex and depends on the DMP complex. Furthermore, by exploiting the septal retraction phenotype and by manipulating the timing of DMP complex gene expression, data was obtained that suggests SpoIIIE, PbpG and SpoIIIM also function to coordinate timely closure of the septal pore upon completion of chromosome translocation. These observations led to the idea that the chromosome is translocated through a highly-stabilized septal pore.

In Chapter 6, building on the observations in the previous chapters, using fluorescence microscopy to examine protein localization and protein interaction assays, we found evidence that the coordination between PG remodeling and chromosome translocation at the septal pore occurs through direct protein-protein interactions between SpoIIIE, SpoIIM and PbpG. In addition, data in this chapter demonstrates that the catalytic activity of PbpG plays a critical role in maintaining and closing the septal pore. Collectively, these data reinforce the notion

that there is a dedicated mechanism involving SpoIIIE, SpoIIIM and PbpG to maintain balanced PG remodeling during chromosome translocation through a septal pore.

Chapter 2:

Materials and Methods

2.1 Chemicals, reagents and solutions

The chemicals and antibodies used in this study are listed in Table 2.1. The buffers and solutions used throughout this work are listed in Table 2.2.

Table 2.1: Commonly used chemicals and reagents.

Reagents	Source	Identifier
Antibodies		
THE^{TM} His Tag Antibody, mAb, Mouse	GenScript	Cat#A00186
anti-FtsZ	(Hajduk *et al*., 2019)	N/A
anti-SpoIIIAG	(Doan *et al*., 2009)	N/A
Chemicals		
FM4-64	Thermo Fisher Scientific	Cat#T13320
SYTOX® Orange	Thermo Fisher Scientific	Cat#S11368
TMA-DPH	Thermo Fisher Scientific	Cat#T204
X-Gal	Invitrogen Life Technologies	Cat#15520-034

Table 2.2: Buffer and solutions.

Buffer / Solution	Constituents*
PBS	137 mM NaCl, 2.7 mM KCl, 10.1 mM Na_2HPO_4, 1.8 mM KH_2PO_4; pH 7
Lysis buffer (DNA extraction)	20 mM Tris pH 7.5, 50 mM EDTA, 100 mM NaCl
TBE	89 mM Tris-HCl, 89 mM boric acid, 2.5 mM EDTA, pH 8.3
1X SMM	1 M sucrose, 40 mM maleic acid, 40 mM $MgCl_2$·6H2O, pH 6.5
Lysis buffer (SDS-PAGE)	20 mM Tris pH 7.5, 10 mM EDTA, 1 mg/mL lysozyme, 1 mM PMSF, 10 µg/mL DNAse I, 100 µg/mL RNase A
Sample buffer (2X)	4% SDS, 250mM Tris pH 6.8, 20% glycerol, 10mM EDTA, BPB (40 µl of 1% stock)
SDS running buffer (10X)	0.2 M Tris base, 1.5 M Glycine, 35 mM SDS
Western transfer buffer	20 mM tris base, 0.15 M glycine, 3.5 mM SDS, 20% MeOH (v/v)
SDS-PAGE loading buffer	62.5 mM Tris-HCl pH 6.8, 10% (v/v) glycerol, 5% (v/v) 2-mercaptoethanol, 2% (w/v) SDS, 0.1% bromophenol blue; pH 8.5
Hypotonic buffer	20 mM Hepes 8 (Na+), 200 mM NaCl, 1 mM DTT, 1 mM $MgCl_2$, 1 mM $CaCl_2$ 1 mM PMSF, 0.5 µg/mL leupeptin, 0.7 µg/mL pepstatin A; pH 8
G2 buffer	20 % (w/v) glycerol, 20 mM HEPES, 200 mM NaCl, 1 mM DTT, 1 mM PMSF, 0.5 µg/mL leupeptin, 0.7 µg/mL pepstatin A; pH 8
Elution Buffer	2 % (w/v) SDS, 125 mM Tris-HCl; pH 6.8

*the solutions listed here used (1X), unless otherwise specified.

2.2 *Bacillus subtilis* strains

All the *Bacillus subtilis* strains were derived from strain 168 or PY79 (Zeigler *et al*., 2008; Asare *et al*., 2015) and are listed in Table 2.3.

Table 2.3: *Bacillus subtilis* strains.

Strains	Genotype*	Source
bBB042	*spoIIIE-gfp (spec)*	(Burton *et al*., 2007)
bBB069	*spoIIIE36-gfp (kan)*	(Besprozvannaya *et al*., 2014)
bDR2413 (168)	wild-type	(Zeigler *et al*., 2008)
bCR1557	*pbpG::kan*	This study
bCR1558	*pbpF::tet*	This study
bCR1592	*spoIIIM::erm*	This study
bCR1600	*pbpG::kan, spoIIIM::erm*	This study
bCR1602	*pbpF::loxP tet, spoIIIM::erm*	This study
bAT001	*pbpG::kan, pbpF::tet*	This study
bAT007	*ycgO::$P_{spoIIIM}$-spoIIIM (spec), spoIIIM::erm*	This study
bAT010	*ycgO::$P_{spoIIIM}$-spoIIIM (spec), pbpG::kan, spoIIIM::erm*	This study
bAT023	*ycgO::$P_{spoIIIM}$-opt_{RBS}-gfp-spoIIIM (spec), spoIIIM::erm*	This study
bAT024	*ycgO::$P_{spoIIIM}$-opt_{RBS}-gfp-spoIIIM (spec), spoIIIM::erm, pbpG::kan*	This study
bAT057	*ycgO::$P_{spoIIIM}$-opt_{RBS}-gfp (spec)*	This study
bAT058	*ycgO::$P_{spoIIIM}$-opt_{RBS}-gfp (spec), sigE::erm*	This study
bAT087	*amyE::P_{spoIIQ}-cfp(Bs) (cat)*	This study
bAT088	*amyE::P_{spoIIQ}-cfp(Bs) (cat), spoIIIM::erm*	This study
bAT089	*amyE::P_{spoIIQ}-cfp(Bs) (cat), pbpG::kan*	This study
bAT090	*amyE::P_{spoIIQ}-cfp(Bs) (cat), pbpF::tet*	This study
bAT091	*amyE::P_{spoIIQ}-cfp(Bs) (cat), pbpG::kan, spoIIIM::erm*	This study
bAT092	*amyE::P_{spoIIQ}-cfp(Bs) (cat), pbpF::tet, spoIIIM::erm*	This study
bAT121	*ycgO::$P_{spoIIIM}$-spoIIIM-his6 (spec), spoIIIM::erm*	This study
bAT122	*ycgO::$P_{spoIIIM}$-spoIIIM-his6 (spec), pbpG::kan, spoIIIM::erm*	This study
bAT281	*amyE::P_{spoIIQ}-cfp(Bs) (cat), spoIIIAA::lox72*	This study
bAT283	*amyE::P_{spoIIQ}-cfp(Bs) (cat), spoIIIAA::lox72, spoIIIM::erm*	This study
bAT285	*amyE::P_{spoIIQ}-cfp(Bs) (cat), spoIIIAA::lox72, pbpG::kan,*	This study
bAT287	*amyE::P_{spoIIQ}-cfp(Bs) (cat), spoIIIAA::lox72, spoIIIM::erm, pbpG::kan,*	This study
bAT440	*spoIIIE::neo, spoIIIM::erm, ycgO::$P_{spoIIIM}$-opt_{RBS}-gfp-spoIIIM (spec)*	This study
bAT353	*ycgO::P_{spoIID}-opt_{RBS}-gfp-spoIIIM (spec)*	This study
bAT442	*spoIIIE::neo, ycgO::P_{spoIID}-opt_{RBS}-gfp-spoIIIM (spec)*	This study
bAT455	*amyE::P_{spoIIQ}-cfp(Bs) (cat), pbpG::lox72*	This study
bAT456	*amyE::P_{spoIIQ}-cfp(Bs) (cat), spoIIIM::lox72, pbpG::lox72*	This study
bAT457	*spoIIIE::neo, amyE::P_{spoIIQ}-cfp(Bs) (cat)*	This study
bAT458	*spoIIIE::neo, amyE::P_{spoIIQ}-cfp(Bs) (cat), spoIIIM::lox72*	This study
bAT459	*spoIIIE::neo, amyE::P_{spoIIQ}-cfp(Bs) (cat), pbpG::lox72*	This study
bAT460	*spoIIIE::neo, amyE::P_{spoIIQ}-cfp(Bs) (cat), spoIIIM::lox72, pbpG::lox72*	This study
bAT469	*spoIIP::tet, spoIID::spec, amyE::P_{spoIIQ}-cfp(Bs) (cat)*	This study
bAT470	*spoIIP::tet, spoIID::spec, amyE::P_{spoIIQ}-cfp(Bs) (cat), spoIIIM::lox72*	This study
bAT471	*spoIIP::tet, spoIID::spec, amyE::P_{spoIIQ}-cfp(Bs) (cat), pbpG::lox72*	This study

bAT472	*spoIIP::tet, spoIID::spec, amyE::P_{spoIIQ}-cfp(Bs) (cat), spoIIIM::lox72, pbpG::lox72*	This study
bAT475	*spoIIIE::neo, spoIIP::tet, spoIID::spec, amyE::P_{spoIIQ}-cfp(Bs) (cat)*	This study
bAT476	*spoIIQ::erm, spoIIIE::neo, amyE::P_{spoIIQ}-cfp(Bs) (cat)*	This study
bAT478	*spoIIQ::erm, amyE::P_{spoIIQ}-cfp(Bs) (cat)*	This study
bAT479	*spoIIQ::erm, amyE::P_{spoIIQ}-cfp(Bs) (cat), spoIIIM::lox72*	This study
bAT480	*spoIIQ::erm, amyE::P_{spoIIQ}-cfp(Bs) (cat), pbpG::lox72*	This study
bAT481	*spoIIQ::erm, amyE::P_{spoIIQ}-cfp(Bs) (cat), spoIIIM::lox72, pbpG::lox72*	This study
bAT490	*spoIIQ::erm, spoIIP::tet, spoIID::spec, amyE::P_{spoIIQ}-cfp(Bs) (cat)*	This study
bAT491	*spoIIQ::erm, spoIIP::tet, spoIID::spec, amyE::P_{spoIIQ}-cfp(Bs) (cat), spoIIIM::lox72*	This study
bAT492	*spoIIQ::erm, spoIIP::tet, spoIID::spec, amyE::P_{spoIIQ}-cfp(Bs) (cat), pbpG::lox72*	This study
bAT493	*spoIIQ::erm, spoIIP::tet, spoIID::spec, amyE::P_{spoIIQ}-cfp(Bs) (cat), spoIIIM::lox72, pbpG::lox72*	This study
bAT497	*spoIIIE::neo, spoIIQ::erm, spoIIP::tet, spoIID::spec, amyE::P_{spoIIQ}-cfp(Bs) (cat)*	This study
bAT498	*ycgO::$P_{spoIIIE}$-spoIIIE*D584A(phleo), spoIIIE::neo, amyE::P_{spoIIQ}-cfp(Bs) (cat)*	This study
bAT499	*ycgO::$P_{spoIIIE}$-spoIIIE*D584A(phleo), spoIIIE::neo, spoIIIM::lox72, amyE::P_{spoIIQ}-cfp(Bs) (cat)*	This study
bAT500	*ycgO::$P_{spoIIIE}$-spoIIIE*D584A(phleo), spoIIIE::neo, pbpG::lox72, amyE::P_{spoIIQ}-cfp(Bs) (cat)*	This study
bAT501	*ycgO::$P_{spoIIIE}$-spoIIIE*D584A(phleo), spoIIIE::neo, spoIIIM::lox72, pbpG::lox72, amyE::P_{spoIIQ}-cfp(Bs) (cat)*	This study
bAT538	*amyE::P_{spoIIQ}-opt_{RBS}-cfp (kan), sigE::erm, yrvN::$P_{hyperspank}$-opt_{RBS}-spoIIM-lacI (spec), ykoW::$P_{hyperspank}$-opt_{RBS}-spoIIP-lacI (phleo), pelB::$P_{hyperspank}$-opt_{RBS}-spoIID-lacI (cat)*	This study
bAT539	*amyE::P_{spoIIQ}-opt_{RBS}-cfp (kan), spoIIQ::tet, sigE::erm, yrvN::$P_{hyperspank}$-opt_{RBS}-spoIIM-lacI (spec), ykoW::$P_{hyperspank}$-opt_{RBS}-spoIIP-lacI (phleo), pelB::$P_{hyperspank}$-opt_{RBS}-spoIID-lacI (cat)*	This study
bAT540	*amyE::P_{spoIIQ}-opt_{RBS}-cfp (kan), spoIIQ::tet, sigE::erm, yrvN::$P_{hyperspank}$-opt_{RBS}-spoIIM-lacI (spec), ykoW::$P_{hyperspank}$-opt_{RBS}-spoIIP-lacI (phleo), pelB::$P_{hyperspank}$-opt_{RBS}-spoIID-lacI (cat), pbpG::lox72*	This study
bAT552	*pelB::$P_{spoIIIE}$-spoIIIE-gfp (cat), spoIIIE::kan*	This study
bAT553	*pelB::$P_{spoIIIE}$-spoIIIE-gfp (cat), spoIIIE::kan, spoIIIM::lox72*	This study
bAT554	*pelB::$P_{spoIIIE}$-spoIIIE-gfp (cat), spoIIIE::kan, pbpG::lox72*	This study
bAT555	*pelB::$P_{spoIIIE}$-spoIIIE-gfp (cat), spoIIIE::kan, pbpG::lox72, spoIIIM::lox72*	This study
bAT557	*amyE::P_{spoIIQ}-opt_{RBS}-cfp (kan), spoIIQ::tet, spoIIIE::lox72, sigE::erm, yrvN::$P_{hyperspank}$-opt_{RBS}-spoIIM-lacI (spec), ykoW::$P_{hyperspank}$-opt_{RBS}-spoIIP-lacI (phleo), pelB::$P_{hyperspank}$-opt_{RBS}-spoIID-lacI (cat)*	This study
bAT558	*spoIIQ::tet, pelB::$P_{spoIIIE}$-spoIIIE-gfp (cat), spoIIIE::kan*	This study
bAT559	*spoIIQ::tet, pelB::$P_{spoIIIE}$-spoIIIE-gfp (cat), spoIIIE::kan, spoIIIM::lox72*	This study
bAT560	*spoIIQ::tet, pelB::$P_{spoIIIE}$-spoIIIE-gfp (cat), spoIIIE::kan, pbpG::lox72*	This study
bAT561	*spoIIQ::tet, pelB::Ps_{poIIIE}-spoIIIE-gfp (cat), spoIIIE::kan, spoIIIM::lox72, pbpG::lox72*	This study
bAT604	*spoIIB::erm, amyE::P_{spoIIQ}-cfp(Bs) (cat)*	This study
bAT605	*spoIIB::erm, amyE::P_{spoIIQ}-cfp(Bs) (cat), spoIIIM::lox72*	This study
bAT606	*spoIIB::erm, amyE::P_{spoIIQ}-cfp(Bs) (cat), pbpG::lox72*	This study
bAT607	*spoIIB::erm, amyE::P_{spoIIQ}-cfp(Bs) (cat), pbpG::lox72, spoIIIM::lox72*	This study

bAT608	*spoIIB::erm, amyE::P_{spoIIQ}-cfp(Bs) (cat),spoIIIE::neo*	This study
bAT627	*spoIIIM::lox72, amyE::P_{spoIIQ}-spoIVF$_{RBS}$-lacI-gfp (spec), yycR::lacO*48 *(cat)*	This study
bAT628	*pbpG::lox72, amyE::P_{spoIIQ}-spoIVF$_{RBS}$-lacI-gfp (spec), yycR::lacO*48 *(cat)*	This study
bAT629	*spoIIIM::lox72, pbpG::lox72, amyE::P_{spoIIQ}-spoIVF$_{RBS}$-lacI-gfp (spec), yycR::lacO*48 *(cat)*	This study
bAT630	*spoIIIM::lox72, amyE::P_{spoIIQ}-spoIVF$_{RBS}$-lacI-gfp (spec), pelB::lacO*48 *(kan)*	This study
bAT631	*pbpG::lox72, amyE::P_{spoIIQ}-spoIVF$_{RBS}$-lacI-gfp (spec), pelB::lacO*48 *(kan)*	This study
bAT632	*spoIIIM::lox72, pbpG::lox72, amyE::P_{spoIIQ}-spoIVF$_{RBS}$-lacI-gfp (spec), pelB::lacO*48 *(kan)*	This study
bAT633	*spoIIIM::lox72, amyE::P_{spoIIQ}-spoIVF$_{RBS}$-lacI-gfp (spec), yhdG::lacO*48 *(erm)*	This study
bAT634	*pbpG::lox72, amyE::P_{spoIIQ}-spoIVF$_{RBS}$-lacI-gfp (spec), yhdG::lacO*48 *(erm)*	This study
bAT635	*spoIIIM::lox72, pbpG::lox72, amyE::P_{spoIIQ}-spoIVF$_{RBS}$-lacI-gfp (spec), yhdG::lacO*48 *(erm)*	This study
bAT643	*spoIIIM::lox72, amyE::P_{spoIIQ}-spoIVF$_{RBS}$-lacI-gfp (spec), yrvN::lacO*48 *(phleo)*	This study
bAT644	*pbpG::lox72, amyE::P_{spoIIQ}-spoIVF$_{RBS}$-lacI-gfp (spec), yrvN::lacO*48 *(phleo)*	This study
bAT645	*spoIIIM::lox72, pbpG::lox72, amyE::P_{spoIIQ}-spoIVF$_{RBS}$-lacI-gfp (spec), yrvN::lacO*48 *(phleo)*	This study
bAT646	*amyE::P_{spoIIQ}-spoIVF$_{RBS}$-lacI-gfp (spec), pelB::lacO*48 *(kan)*	This study
bAT647	*amyE::P_{spoIIQ}-spoIVF$_{RBS}$-lacI-gfp (spec), yhdG::lacO*48 *(erm)*	This study
bAT648	*amyE::P_{spoIIQ}-spoIVF$_{RBS}$-lacI-gfp (spec), yycR::lacO*48 *(cat)*	This study
bAT649	*amyE::P_{spoIIQ}-spoIVF$_{RBS}$-lacI-gfp (spec), yrvN::lacO*48 *(phleo)*	This study
bAT652	*spoIIIE::neo, amyE::P_{spoIIQ}-cfp(Bs) (cat), ycgO::$P_{spoIIIE}$-spoIIIE36 (spec)*	This study
bAT653	*spoIIIE::neo, amyE::P_{spoIIQ}-cfp(Bs) (cat), spoIIIM::lox72, ycgO::$P_{spoIIIE}$-spoIIIE36 (spec)*	This study
bAT654	*spoIIIE::neo, amyE::P_{spoIIQ}-cfp(Bs) (cat), pbpG::lox72, ycgO::$P_{spoIIIE}$-spoIIIE36 (spec)*	This study
bAT655	*spoIIIE::neo, amyE::P_{spoIIQ}-cfp(Bs) (cat), spoIIIM::lox72, pbpG::lox72, ycgO::$P_{spoIIIE}$-spoIIIE36 (spec)*	This study
bAT668	*spoIIB::erm, amyE::P_{spoIIQ}-spoIVF$_{RBS}$-lacI-gfp (spec), pelB::lacO*48 *(kan)*	This study
bAT669	*spoIIB::erm, spoIIIM::lox72, amyE::P_{spoIIQ}-spoIVF$_{RBS}$-lacI-gfp (spec), pelB::lacO*48 *(kan)*	This study
bAT670	*spoIIB::erm, pbpG::lox72, amyE::P_{spoIIQ}-spoIVF$_{RBS}$-lacI-gfp (spec), pelB::lacO*48 *(kan)*	This study
bAT671	*spoIIB::erm, spoIIIM::lox72, pbpG::lox72, amyE::P_{spoIIQ}-spoIVF$_{RBS}$-lacI-gfp (spec), pelB::lacO*48 *(kan)*	This study
bAT0679	*ycgO::$P_{spoIIIE}$-spoIIIE*D584A(phleo), spoIIIE::neo, amyE::P_{spoIIQ}-cfp(Bs) (cat), spoIIQ::tet*	This study
bAT697	*spoIID::cat, spoIIP::tet, amyE::P_{spoIIQ}-spoIVF$_{RBS}$-lacI-gfp (spec), pelB::lacO*48 *(kan)*	This study
bAT698	*spoIID::cat, spoIIP::tet, spoIIIM::lox72, amyE::P_{spoIIQ}-spoIVF$_{RBS}$-lacI-gfp (spec), pelB::lacO*48 *(kan)*	This study
bAT699	*spoIID::cat, spoIIP::tet, pbpG::lox72, amyE::P_{spoIIQ}-spoIVF$_{RBS}$-lacI-gfp (spec), pelB::lacO*48 *(kan)*	This study
bAT700	*spoIID::cat, spoIIP::tet, spoIIIM::lox72, pbpG::lox72, amyE::P_{spoIIQ}-spoIVF$_{RBS}$-lacI-gfp (spec), pelB::lacO*48 *(kan)*	This study

bAT743	*pelB::$P_{spoIIIE}$-spoIIIE36 (tet), spoIIIE::neo, spoIIIM::erm, ycgO::$P_{spoIIIM}$-opt_{RBS}-gfp-spoIIIM (spec)*	This study
bAT779	*spoIIP::tet, spoIID::spec, pelB::$P_{spoIIIE}$-spoIIIE-gfp (cat), spoIIIE::kan*	This study
bAT810	*yycR(−7°)::tetO*48 *(cat), ycgO::P_{ftsW}-tetR-cfp (spec)* terminators *P_{ftsW}-lacI-mypet, pelB (+174°)::lacO*48 *(kan), spoIIIM::lox72, pbpG::lox72*	This study
bAT811	*spoIIQ::tet, ycgO::$P_{spoIIIM}$-spoIIIM-his6 (spec), spoIIIM::erm*	This study
bAT834	*spoIIIE::kan, ycgO::$P_{spoIIIM}$-spoIIIM-his6 (spec), spoIIIM::erm*	This study
bAT835	*spoIIIE::kan, pelB::$P_{spoIIIE}$-spoIIIE-gfp (cat), ycgO::$P_{spoIIIM}$-spoIIIM-his6 (spec), spoIIIM::erm*	This study
bAT837	*pelB::$P_{spoIIIE}$-spoIIIE36 (tet), spoIIIE::neo, ycgO::P_{spoIID}-opt_{RBS}-gfp-spoIIIM (spec)*	This study
bAT844	*pelB::$P_{spoIIIE}$-spoIIIE36 (tet), spoIIIE::kan, ycgO::$P_{spoIIIM}$-spoIIIM-his6 (spec), spoIIIM::erm*	This study
bAT855	*ycgO::P_{pbpG}-his6-pbpG (erm), amyE::P_{spoIIQ}-cfp(Bs) (cat), pbpG::Kan*	This study
bAT856	*ycgO::P_{pbpG}-his6-pbpG (erm), amyE::P_{spoIIQ}-cfp(Bs) (cat), spoIIIM::lox72, pbpG::kan*	This study
bAT857	*ycgO::P_{pbpG}-his6-pbpG (erm), amyE::P_{spoIIQ}-cfp(Bs) (cat), pbpG::Kan, pbpF::loxP tet*	This study
bAT858	*ycgO::P_{pbpG}-his6-pbpG (E94A, S365A) (erm), amyE::P_{spoIIQ}-cfp(Bs) (cat), pbpG::kan*	This study
bAT859	*ycgO::P_{pbpG}-his6-pbpG (E94A, S365A) (erm), amyE::P_{spoII}Q-cfp(Bs) (cat), spoIIIM::lox72, pbpG::kan*	This study
bAT860	*ycgO::P_{pbpG}-his6-pbpG (E94A, S365A) (erm), amyE::P_{spoIIQ}-cfp(Bs) (cat), pbpG::kan, pbpF::loxP tet*	This study
bAT861	*ycgO::P_{pbpG}-his6-pbpG (erm), spoIIQ::tet, amyE::P_{spoIIQ}-cfp(Bs) (cat), pbpG::lox72*	This study
bAT862	*ycgO::P_{pbpG}-his6-pbpG (erm), spoIIQ::tet, amyE::P_{spoIIQ}-cfp(Bs) (cat), spoIIIM::lox72, pbpG::lox72*	This study
bAT863	*ycgO::P_{pbpG}-his6-pbpG (E94A, S365A) (erm), spoIIQ::tet, amyE::P_{spoIIQ}-cfp(Bs) (cat), pbpG::lox72*	This study
bAT864	*ycgO::P_{pbpG}-his6-pbpG (E94A, S365A) (erm), spoIIQ::tet, amyE::P_{spoIIQ}-cfp(Bs) (cat), spoIIIM::lox72, pbpG::lox72*	This study
bAT865	*ycgO::P_{pbpG}-his6-pbpG (erm), yycR::lacO*48 *(cat), amyE::P_{spoIIQ}-$spoIVF_{RBS}$-lacI-gfp (spec), pbpG::lox72*	This study
bAT866	*ycgO::P_{pbpG}-his6-pbpG (erm), yycR::lacO*48 *(cat), amyE::P_{spoIIQ}-$spoIVF_{RBS}$-lacI-gfp (spec), spoIIIM::lox72, pbpG::lox72*	This study
bAT867	*ycgO::P_{pbpG}-his6-pbpG (E94A, S365A) (erm), yycR::lacO*48 *(cat), amyE::P_{spoIIQ}-$spoIVF_{RBS}$-lacI-gfp (spec), pbpG::lox72*	This study
bAT868	*ycgO::P_{pbpG}-his6-pbpG (E94A, S365A) (erm), yycR::lacO*48 *(cat), amyE::P_{spoIIQ}-$spoIVF_{RBS}$-lacI-gfp (spec), spoIIIM::lox72, pbpG::lox72*	This study
bAT869	*ycgO::P_{pbpG}-his6-pbpG (erm), pelB::$P_{spoIIIE}$-spoIIIE-gfp (cat), spoIIIE::kan, pbpG::lox72*	This study
bAT870	*ycgO::P_{pbpG}-his6-pbpG (erm), pelB::$P_{spoIIIE}$-spoIIIE-gfp (cat), spoIIIE::kan, pbpG::lox72, spoIIIM::lox72*	This study
bAT871	*ycgO::P_{pbpG}-his6-pbpG (E94A, S365A) (erm), pelB::$P_{spoIIIE}$-spoIIIE-gfp (cat), spoIIIE::kan, pbpG::lox72*	This study
bAT872	*ycgO::P_{pbpG}-his6-pbpG (E94A, S365A) (erm), pelB::$P_{spoIIIE}$-spoIIIE-gfp (cat), spoIIIE::kan, pbpG::lox72, spoIIIM::lox72*	This study
bAT873	*ycgO::P_{pbpG}-his6-pbpG (erm), spoIIIE::kan, pbpG::lox72*	This study
bHC035	*ycgO::P_{spoIIQ}-opt_{RBS}-pbpG-his6 (tet), pbpG::kan, spoIIIM::erm*	This study
bHC036	*ycgO::Ps_{poIIQ}-opt_{RBS}-pbpG-his6 (tet), pbpG::lox72*	This study

bHC040	*ycgO::P_{spoIIQ}-opt_{RBS}-pbpG-his6 (E94A, S365A) (tet), pbpG::lox72*	This study
bHC046	*ycgO::P_{spoIIQ}-opt_{RBS}-pbpG-his6 (E94A, S365A) (tet), pbpG::kan, spoIIIM::erm*	This study
bHC050	*spoIIQ::cat, ycgO::P_{spoIIQ}-opt_{RBS}-pbpG-His6 (tet), pbpG::kan, spoIIIM::erm*	This study
bHC051	*spoIIQ::cat, ycgO::P_{spoIIQ}-opt_{RBS}-pbpG-his6 (tet), pbpG::lox72*	This study
bHC052	*spoIIQ::cat, ycgO::P_{spoIIQ}-opt_{RBS}-pbpG-his6 (E94A, S365A) (tet), pbpG::lox72*	This study
bHC053	*spoIIQ::cat, ycgO::P_{spoIIQ}-opt_{RBS}-pbpG-his6 (E94A, S365A) (tet), pbpG::kan, spoIIIM::erm*	This study
bWX1200	*spoIIIE36, yycR(−7°)::tetO*48 *(cat), pelB(+174°)::lacO*48 *(kan), ycgO::P_{ftsW}-tetR-cfp (spec)* terminators *P_{ftsW}-lacI-mypet*	(Wang *et al*., 2014)

*Antibiotic resistance genes are labelled as the following: *erm*, Erythromycin; *cat*, Chloramphenicol; *kan*, Kanamycin; *neo*, neomycin; *phleo*, Phleomycin; *spec*, spectinomycin and *tet*, Tetracycline. The antibiotic cassettes in some strains were looped out using the Cre/*lox* system leaving the *lox72* site (Yan *et al*., 2008).

2.3 *Bacillus subtilis* growth media

Vegetative cells were grown on Luria-Bertani broth (LB) (Lennox) agar plates (1.5% w/v) with antibiotics (except wild-type) to select for the growth of strains harboring antibiotic resistance cassettes. The antibiotics were used for strain selection, as listed in Table 2.4. *B. subtilis* strains were stored as 1.8 mL glycerol stocks (14% v/v) at –80°C.

Sporulation was performed using either exhaustion or resuspension method (see section 2.4). In the exhaustion method, the cells were grown in Difco Sporulation Medium (DSM) that was prepared as detailed previously (Schaeffer *et al*., 1965), whereas the resuspension method involved growing in Resuspension Medium as described previously (Harwood & Cutting, 1990; Nicholson & Setlow, 1990; Smith, 1991).

Table 2.4: Antibiotics used for selecting *Bacillus subtilis*

Antibiotic	Working concentration (µg/mL)*
Ampicillin	100
Chloramphenicol	5
Erythromycin	1
Kanamycin	10
Neomycin	2.5
Phleomycin	2
Spectinomycin	100
Tetracycline	10

*Stock solutions were prepared by dissolving antibiotics either in ethanol or purified, deionised water (Milli-Q water, MQW) and sterilized by filtration (0.2 µm filter). All antibiotics were stored at –20°C.

2.4 Sporulation efficiency

Sporulation was induced via resuspension at 37°C according to the Sterlini-Mandelstam method (Smith, 1991) or through exhaustion of nutrients in supplemented Difco Sporulation Medium (DSM) (Schaeffer *et al*., 1965). A single colony was inoculated into a glass tube containing 2 mL of DSM media and incubated at 37ºC on a roller drum for 24–30 hours (hrs). On the following day, the sporulating cultures were heat-killed by incubating the tubes for 20 minutes (min) in a water bath adjusted to 80ºC, to kill any non-sporulating cells and select for heat-resistant spores. Next, heat-resistant spores were serially-diluted in 1X TBase Medium (Smith, 1991) and then plated on LB (Lennox) agar plates and incubated overnight at 37ºC. The number of heat-resistant spores was quantified by counting the number of colony-forming units per mL (cfu/mL) for each strain. Sporulation efficiency of any mutant strain was determined as the percentage of spores produced relative to the WT strain.

2.5 Transformation and storage of *B. subtilis* strains

B. subtilis strains in this study were generated by transformation to integrate specific genetic material, genomic DNA or plasmid vectors harbouring an antibiotic resistance gene, into the genome via homologous recombination (Anagnostopoulos & Spizizen, 1961). The desired genetic material was selected on Lennox LB agar plates containing the antibiotic of interest. The transformation process involved multiple steps, as follows.

1) A single colony of the recipient strain was resuspended in 1 mL solution of 1X MC medium [900 µL ddH_2O, 100 µL 10X MC medium (Loyo & Burton, 2018), 10 µL tryptophan (2 mg/mL), 3 µL 1 M $MgSO_4$] for 4 hrs on a roller drum at 37°C until early stationary phase to induce competence (Konkol *et al*., 2013).

2) 2 µL of genomic DNA (gDNA) from the donor strain or plasmid DNA were added to 200 µL of the above competent cell culture and then incubated for 2 hrs on a roller drum at 37°C.

3) The 200 µL culture from the step above was plated onto LB (Lennox) agar plates containing the antibiotic used to select the gene of interest and incubated overnight at 37°C.

4) On the following day, the antibiotic-resistant colonies were re-streaked on LB (Lennox) agar plates containing the initial antibiotic marker to confirm successful uptake of the genetic material and screened for pre-existing antibiotic marker(s) of the recipient strain, if any, by streaking on plates containing antibiotics.

5) Finally, a single colony that acquired the resistance to all expected antibiotic markers (donor and recipient) was grown in 2 mL LB (Lennox) for 2.5 hrs on a roller drum at 37°C and stored as 1.8 mL glycerol stocks (14% v/v) at –80°C for further use. The deletion mutant strains were either obtained from the *Bacillus* knock-out collection (Addgene) (Koo *et al*., 2017), or previously existing *B*. *subtilis* strains found within the laboratory collections, using the above transformation approach.

2.6 Genomic DNA extraction

To extract genomic DNA, a standard phenol/chloroform extraction protocol was used. A fresh, single colony of the strain of interest was grown in 2 mL LB broth (Lennox) for 3 hrs on a roller drum at 37°C, until mid-exponential phase. Following that, ~1.5 mL of the culture was pelleted by centrifugation on a bench-top centrifuge (11,000 rpm for 1 min). Next, the cell pellet was resuspended in 500 µL of lysis buffer (Table 2.2), with 50 µL of lysozyme (20 mg/mL) and incubated at 37°C for 15 mins. After incubation, 60 µL of 10% (w/v) sarkosyl detergent was added to complete cell lysis and membrane solubilization. Then, 600 µL of phenol was added, the mixture vigorously vortexed for 10 seconds and then submitted to centrifugation at 11,000 rpm for 5 mins to separate the aqueous and organic phase of the mixture. The top aqueous phase was extracted into a fresh tube and 600 µL of 1:1 phenol-chloroform mixture was added, and vortexed. The mixture was centrifuged as described above and then the top aqueous layer was moved into a fresh tube, to which 60 µL of 3 M NaOAc were added to facilitate DNA precipitation. The gDNA was precipitated into a pellet by adding 1 mL of 100% ethanol and gentle inversion of the tube, followed by centrifugation (11,000 rpm for 1 min). The supernatant was discarded, and the gDNA pellet was re-solubilized in 500 µL of ddH_2O and stored at –20°C for further use.

2.7 General molecular biology methods

In this study, the DNA fragments were cloned into ectopic-integration, double cross-over plasmid vectors using standard molecular biology approaches described below.

2.7.1 Polymerase chain reaction

Polymerase Chain Reaction (PCR) was used to amplify DNA fragments (inserts), utilized for cloning into plasmid vectors, confirmation of *B. subtilis* mutants and isothermal assembly. The final volume of PCR reaction was set to 25 µL and included 10.5 µL of ddH_2O, 1 µL of template DNA (either plasmid or *B. subtilis* genomic DNA), 0.5 µL of each primer (10 µM) (listed in

Table 2.5) and 12.5 µL of 2X PCR mix (previously prepared). The 2X PCR mix contained 2 mM nucleotides (dNTPs), Phusion DNA polymerase (2000 units/mL, New England Biolabs), and Phusion polymerase buffer (2X concentration, New England Biolabs). The PCR reactions were incubated in an Eppendorf Mastercycler Nexus Thermal Cycler and set to 30 cycles with an annealing temperature of 55°C and amplification temperature of 72°C. Based on the size of the amplified DNA fragment, the extension time was adjusted. The PCR products used in cloning or isothermal assembly were purified using the Isolate II PCR and Gel Kit manufactured by Bioline following the manufacturer's protocol. The primers used for the PCR reactions are listed in Table 2.5.

Table 2.5: Primers used for PCR

Primer	Sequence*
oAT001	cgcGAATTCctgtataaaaaccgagcattcgc
oAT002	cgcGGATCCttaagggtagaccgggaattt
oAT005	cgcAAGCTTacataaggaggaactactatgagtaaaggagaagaacttttc
oAT006	cgcCTCGAGgccgcttgagcctccagatgatcctttgtatagttcatccatgccatg
oAT007	cgcCTCGAGatgaagcgtctcaccttagtatg
oAT096	aaagcgacagtggcgattgcagaccagaatttctacgat
oAT097	atcgtagaaattctggtctgcaatcgccactgtcgcttt
oAT137	cgcAAGCTTccaaaaaaagcatgttgccgaact
oAT139	gacgcaatgtcatgttcatacg
oAT147	gcgaagcgccagcctgctgcgacgatcaagccgttgctg
oAT148	cagcaacggcttgatcgtcgcagcaggctggcgcttcgc
oAT160	cgcGGATCCtcaatggtgatggtgatgatgtcgccccagcca
oCR353	cgcGGATCCttatgtaatcccagcagcatttacatactcatgaaggaccatgt
oCR416	ggcAAGCTTacaaaggatgatggcaatgaaaccagtaacgttatacgatg
oCR417	gcgCTCGAGcagctgcattaatgaatcggcca
oCR418	gcgCTCGAGggatcatctggaggctcaagcggcatgggaggcacaagcatgagta
oCR659	ccgGGATCCttaatggtgatggtggtgatgagggtagaccgggaatttata
oCR694	cgcGAATTCgtcggacaggcaatcaataaactg
oCR695	gcgCTCGAGaagagagctcatcatatttctctttg
oCR696	gcgCTCGAGgttcaggcatgagtaaaggagaagaacttttcac
oCR697	cgcGGATCCttatttgtatagttcatccatgccatgtg
oCR704	gcgCTCGAGttaagggtagaccgggaatttatac
oCR716	tcgacTCTAGAgtctggttcaggcatgagtgtggcaaagaaaaaacga
oCR717	acccggGGATCCttaagaagagagctcatcatatttctc
oCR718	tcgacTCTAGAgtctggttcaggcatgaagcgtctcaccttagtatgc
oCR719	ccggGGATCCttaagggtagaccgggaatttatacgc
oCR720	tcgacTCTAGAgtctggttcaggcgtggatgcaatgacaaataaacgg
oCR721	ccggGGATCCtcaatgatgtcgccccagccattt
oHC055	gtggatgcaatgcatcatcaccatcaccatacaaataaacggctgagact
oHC056	ccgtttatttgtatggtgatggtgatgatgcattgcatccacaacgggtt

*capital letters indicate restriction sites

2.7.2 DNA agarose gel electrophoresis

After PCR, confirmation of PCR product size was performed using DNA agarose gel electrophoresis. Agarose gels (Bioline) 1% (w/v) were prepared with 0.5X TBE buffer (Table 2.2) and contained the GelRed DNA stain (1:10,000, Biotium) to visualise DNA bands. A 2 µL volume of the PCR product was added to 8 µL of ddH_2O and 2 µL of 6X loading dye (New England Biolabs) for loading onto the agarose gel. The 2-Log DNA ladder (New England Biolabs) was used to estimate the size of DNA bands. Electrophoresis of the DNA agarose gel occurred inside a Mini-Sub Cell GT chamber (Bio-Rad) at 120 V for 1 hr (Bio-Rad PowerPac Basic). Finally, the resolved gel was analyzed using the Syngene InGenius3 software.

2.7.3 Restriction digest

To digest DNA (plasmid or PCR product), a restriction digest reaction was set to a final volume of 30 µL containing 4 µL of DNA, 3 µL CutSmart buffer (10X concentration, New England Biolabs), 1 µL of each restriction enzyme (100,000 units/mL, New England Biolabs), and 21 µL of ddH_2O. After preparing the mixtures, the digestion reactions were incubated at 37°C for 2 hrs to allow for enzyme activity. After 2 hrs, the digested products were run on an agarose gel as detailed above. Next, the DNA bands were excised from the gel using a scalpel on a UV light panel and the DNA from the gel excision fragments was purified using the Isolate II PCR and Gel Kit (Bioline) according to the manufacturer's protocol.

2.7.4 Molecular cloning of plasmid vectors into *Escherichia coli*

The ligation reaction containing the insert and vector was adjusted to a final volume of 10 µL with 3 µL of insert DNA, 1 µL of vector DNA, 1 µL of T4 DNA ligase (400,000 units/mL, New England Biolabs), 1 µL of 10X T4 DNA ligase buffer (New England Biolabs), and 4 µL of ddH_2O. Also, two control reactions were prepared: a vector only control that contained ddH_2O instead of the insert to check for vector self-ligation, and a vector only without ligase control where the insert and T4 DNA ligase were replaced with ddH_2O to check for undigested vector. The three ligation reactions were incubated at room temperature (RT) for 30 mins and then incubated with 100 µL of chemically-competent *E. coli* cells (rubidium chloride, RbCl) (unpublished Rodrigues laboratory protocol) for 15 mins on ice. Next, the cells were heat-shocked at 42°C for 90 seconds to allow for uptake of ligated plasmids. After the heat-shock, the tubes were kept on ice for 5 mins. Then, 900 µL of LB broth (Lennox) was added to each tube, followed by incubation at 37°C for 20 mins. The cells were then centrifuged (11,000 rpm for 1 min) and 900 µL of the supernatant was removed. The pellet was resuspended in the

remaining 100 µL of the supernatant. Finally, the resuspended cells were plated on LB agar (Lennox) plates containing ampicillin (100 µg/mL), and incubated overnight at 37°C. On the following day, 4 colonies from the plate containing the vector and insert reaction were patched on LB agar (Lennox) plates containing ampicillin (100 µg/mL) and separately inoculated into LB broth (Lennox) with ampicillin (100 µg/mL) for overnight growth on a roller drum at 37°C. The following day, plasmid extraction from the 4 cultures was performed using the Bioline Isolate II Plasmid Mini Kit according to the manufacturer's protocol and the purified plasmids digested as described above to confirm the presence of inserts. Sequencing of plasmid inserts was performed through AGRF (Australian Genome Research Facility Ltd) to ensure that the desired inserts were present and had no mutations. *E. coli* isolates containing the correct insert were stored as 1.8 mL glycerol stocks (14% v/v). The plasmids generated in this study are listed in Table 2.6.

Table 2.6: Plasmids list of the generated constructs.

Plasmid	Description	Source
pAT001	*ycgO::$P_{spoIIIM}$-spoIIIM (spec)*	This study
pAT003	*ycgO::$P_{spoIIIM}$-gfp-spoIIIM (spec)*	This study
pAT024	*ycgO::P_{spoIID}-opt_{RBS}-gfp-spoIIIM (spec)*	This study
pAT032	*ycgO::$P_{spoIIIM}$-spoIIIM-his6 (spec)*	This study
pAT057	*pelB::$P_{spoIIIE}$-spoIIIE-gfp (cat)*	This study
pAT090	*ycgO::$P_{spoIIIE}$-spoIIIE36 (tet)*	This study
pCR204	*amyE::P_{spoIIQ}-$spoIVF_{RBS}$-lacI-gfp (spec)*	This study
pHC3	*ycgO::P_{spoIIQ}-opt_{RBS}-pbpG-his6 (tet)*	This study
pHC23	*ycgO::P_{spoIIQ}-opt_{RBS}-pbpG-his6 (E94A, S365A) (tet)*	This study
pHC28	*P_{lac}::T18-spoIIIE (amp)*	This study
pHC29	*P_{lac}::T18-spoIIIM (amp)*	This study
pHC30	*P_{lac}::T18-pbpG (amp)*	This study
pHC32	*P_{lac}::T25-spoIIIE (kan)*	This study
pHC33	*P_{lac}::T25-spoIIIM (kan)*	This study
pHC34	*P_{lac}::T25-pbpG (kan)*	This study
pHC535	*P_{lac}::T25-slmA (kan)*	(Cho *et al*., 2011)
pHC538	*P_{lac}::T18-slmA (amp)*	(Cho *et al*., 2011)
pJL013a	*pelB::spoIIIE36 (tet)*	This study

2.7.5 Plasmid construction

pAT001a [*ycgO::$P_{spoIIIM}$-spoIIIM (spec)*] was generated in a two-way ligation with *Eco*RI-*Bam*HI PCR product containing the *spoIIIM* gene (oligonucleotide primers oAT001 & oAT002 and 168 genomic DNA as template) and pKM083 cut with *Eco*RI and *Bam*HI. pKM083

(*ycgO::spec*) is an ectopic integration vector for double crossover integration at the non-essential *ycgO* locus.

pAT003a [*ycgO::$P_{spoIIIM}$-opt$_{RBS}$-gfp-spoIIIM (spec)*] was generated in a three-way ligation with a *Hin*dIII-*Xho*I PCR product containing *opt$_{RBS}$-gfp* (oligonucleotide primers oAT005 & oAT006 and pCR227 DNA as template), and an *Xho*I-*Bam*HI PCR product containing the *spoIIIM* gene (oligonucleotide primers oAT007 & oAT002) with pAT002a (*ycgO::$P_{spoIIIM}$*) as template cut with *Hin*dIII and *Bam*HI. pCR227 [*yhdG::P_{gerM}-gerM-gfp* (*cat*)] contains *gfp* (C. Rodrigues - laboratory stock).

pAT024a [*ycgO::P_{spoIID}-opt$_{RBS}$-gfp-spoIIIM (spec)*] was generated in a two-way ligation of an *Eco*RI-*Hin*dIII digest product from pCR113 containing *P_{spoIID}*, into an *Eco*RI-*Hin*dIII digest product of pAT003a (*ycgO::$P_{spoIIIM}$-opt$_{RBS}$-gfp-spoIIIM*). pCR113 [*ycgO::P_{spoIID}-malE (cat)*] contains the P$_{spoIID}$ promoter (C. Rodrigues - laboratory stock).

pAT032a [*ycgO::$P_{spoIIIM}$-spoIIIM-his6 (spec)*] was generated in a two-way ligation with *Eco*RI-*Bam*HI PCR product containing the *spoIIIM* gene with a C-terminal hexahistidine tag (oligonucleotide primers oAT001 & oCR659 and 168 genomic DNA as template) and pKM083 cut with *Eco*RI and *Bam*HI. pKM083 (*ycgO::spec*) is an ectopic integration vector for double crossover integration at the non-essential *ycgO* locus.

pAT057a [*pelB::$P_{spoIIIE}$-spoIIIE-gfp (cat)*] was generated in a three-way ligation with an *Eco*RI-*Xho*I PCR product containing *spoIIIE* (oligonucleotide primers oCR694 & oCR695 and bBB042 DNA as template), and an *Xho*I-*Bam*HI PCR product containing *gfp* (oligonucleotide primers oCR696 & oCR697) with pKM020 (*pelB::tet*) as template cut with *Eco*RI and *Bam*HI.

pAT090 [*ycgO::$P_{spoIIIE}$-spoIIIE36 (tet)*] was generated in a two-way ligation with an *Eco*RI-*Bam*HI PCR product containing *spoIIIE36* (oligonucleotide primers oCR694 & oCR717 and bBB069 DNA as template) with pKM086 (*ycgO::tet*) cut with *Eco*RI and *Bam*HI.

pCR20a [*amyE::P_{spoIIQ}-spoIVF$_{RBS}$-lacI-gfp (spec)*] was generated in a three-way ligation with *Hin*dIII-*Xho*I digest product containing *spoIVF$_{RBS}$-lacI* (oCR416 & oCR417 and bXW1200 DNA as template), *Xho*I-*Bam*HI digest product containing *gfp* (oCR418 and oCR353 and pCR154 as template) and pCR154 (amy*E::P_{spoIIQ}-opt$_{RBS}$-gfp (spec)* (C. Rodrigues - laboratory stock) cut with *Hin*dIII and *Bam*HI.

pJL013 [*pelB::P$_{spoIIIE}$-spoIIIE36 (tet)*] was generated in a two-way ligation with an *Eco*RI-*Bam*HI digest product containing *spoIIIE36* from pAT090 (*ycgO::spoIIIE36*) with pKM033 (*pelB::tet*) as template cut with *Eco*RI and *Bam*HI.

pHC3 [*ycgO::P$_{spoIIQ}$-opt$_{RBS}$-pbpG-his6 (tet)*] was generated in a two-way ligation with *Hin*dIII-*Bam*HI PCR product containing the *pbpG* gene [oligonucleotide primers oAT139 & oAT160 and 168 genomic DNA as template] and pCR008 cut with *Hin*dIII and *Bam*HI. pCR008 [*ycgO::P$_{spoIIQ}$-opt$_{RBS}$-gfp-spoIIQ (tet)*] contains the *P$_{spoIIQ}$* promoter (C. Rodrigues - laboratory stock).

pHC23 [*ycgO::P$_{spoIIQ}$-opt$_{RBS}$-pbpG-his6 (E94A, S365A) (tet)*] was generated by sequential rounds of site-directed mutagenesis of pHC3 using oligonucleotide primers oAT96 & oAT97 to introduce the E94A mutation, followed by oAT147 & oAT148 to introduce the S365A mutation.

pHC28 [*P$_{lac}$::T18-spoIIIE (amp)*] and **pHC32** [*P$_{lac}$::T25-spoIIIE (kan)*] were generated in a two-way ligation with *Xba*I-*Bam*HI PCR product containing the *spoIIIE* gene [oligonucleotide primers oCR716 & oCR717 and 168 genomic DNA as template] and pUT18C and pKNT25 (Karimova *et al*., 1998), respectively, cut with *Xba*I and *Bam*HI.

pHC29 [*P$_{lac}$::T18-spoIIIM (amp)*] and **pHC33** [*P$_{lac}$::T25-spoIIIM (kan)*]were generated in a two-way ligation with *Xba*I-*Bam*HI PCR product containing the *spoIIIM* gene [oligonucleotide primers oCR718 & oCR719 and 168 genomic DNA as template] and pUT18C and pKNT25 (Karimova *et al*., 1998), respectively, cut with *Xba*I and *Bam*HI.

pHC30 [*P$_{lac}$::T18-pbpG (amp)*] and **pHC34** [*P$_{lac}$::T25-pbpG (kan)*] were generated in a two-way ligation with *Xba*I-*Bam*HI PCR product containing the *pbpG* gene [oligonucleotide primers oCR720 & oCR721 and 168 genomic DNA as template] and pUT18C and pKNT25 (Karimova *et al*., 1998), respectively, cut with *Xba*I and *Bam*HI.

Other constructs

[*ycgO::P$_{pbpG}$-his6-pbpG (erm)*] and [*ycgO::P$_{pbpG}$-his6-pbpG^{E94A,S365A} (erm)*]

- *Hin*dIII-*P$_{pbpG}$* was amplified by oAT137 and oHC056 using168 genomic DNA as template.
- *his6-pbpG-Xho*I and *his6-pbpG$^{E94A,\ S365A}$-Xho*I were amplified by oHC055 and oCR704 using pHC3 and pHC23 as templates, respectively.

- *Hin*dIII-P_{pbpG} and *his6-pbpG-Xho*I and similarly *Hin*dIII-P_{pbpG} and *his6-pbpG*^{E94A,S365A}-*Xho*I were ligated by isothermal assembly using oHC055 and oHC056 and then ligated into pKM084 (*ycgO::erm,* David Rudner) as template cut with *Hin*dIII and *Xho*I.
- Finally, after ligation into pKM084, the two constructs were transformed directly into *B. subtilis*.

2.7.6 Enzymatic isothermal assembly

Enzymatic isothermal assembly was used to join two or more DNA sequences (Gibson *et al*., 2009). The DNA pieces were designed to have terminal sequence overlap of ~20-25 base pairs (bp) to allow them to be joined covalently. The final volume of the isothermal assembly reaction was adjusted to 20 µL which included 6 µL of ddH_2O, 2 µL of each DNA piece (plasmid or gDNA), and 10 µL of 2X Isothermal mix (unpublished, Rodrigues Laboratory protocol). The reaction was performed on an Eppendorf Mastercycler Nexus Thermal Cycler at 50°C for 30 mins (Gibson *et al*., 2009). DNA agarose gel electrophoresis was performed to confirm the size of the combined DNA fragments.

2.8 Transposon insertion sequencing

The *magellan6* transposon libraries were constructed as described earlier for WT (bDR2413), Δ*pbpG* (bCR1557) and Δ*pbpF* libraries (bCR1558) (Bodi *et al*., 2009; Johnson & Grossman, 2014; Meeske *et al*., 2016). About 750,000 transformant colonies from each library were harvested, aliquoted, and frozen. The aliquots were thawed on ice, resuspended in DSM, and diluted into 50 mL DSM at an OD_{600} of 0.05. Samples were collected at 24 hrs, after most cells had developed into spores. The sporulating cultures (T24) samples were heat-killed at 80ºC for 20 mins to remove vegetative cells, non-mature spores and mutants that failed to generate heat-resistant spores. After the heat-kill, the spores were plated on LB agar to allow for germination. Approximately 750,000 colonies were harvested and resuspended in LB broth (Lennox). A 30 µL aliquot of this cell suspension was used for genomic DNA extraction. Next, the genomic DNA was digested with *Mme*I enzyme to cut the *Mme*I restriction site inserted at the inverted repeat sequences of the *magellan6* transposon. Barcode adapters were ligated onto the *Mme*I digested DNA and the transposon-chromosome junctions were amplified by PCR using 16 cycles. The amplification products were separated by agarose gel electrophoresis and the band of interest was purified and sent for sequencing on the Illumina HiSeq platform using TruSeq reagents (Tufts University, TUCF Genomics facility). The transposon insertions were mapped

to the chromosome of *B. subtilis* 168 (NCBI NC_000964.3) to identify sites that accepted >1 read at each TA site.

2.9 Microscopy techniques

2.9.1 Fluorescence microscopy

Live-cell fluorescence imaging was performed on cells sporulated by the Resuspension Method as described above (Harwood & Cutting, 1990; Smith, 1991). At specific time points, 200 µL of the sporulating cells were collected and pelleted by centrifugation (11,000 rpm for 30 seconds). The cell pellet was resuspended in 10 µL of the semi-permeable membrane dye TMA-DPH (1-(4-Trimethyammoniumphenyl)-6-Phenyl 1,3,5-Hexatriene p-Toluenesulfonate) (0.05 mM) or FM 4-64 (N-(3-Triethylammoniumpropyl)-4-(6-(4-(Diethylamino) Phenyl) Hexatrienyl) Pyridinium Dibromide) (0.67 µg/µL) prepared in resuspension media. After mixing with the dye, the stained cells were spread on 2% (w/v) agarose gel pads prepared with resuspension medium and set using a Gene Frame (Bio-Rad). Next, a coverslip (0.13-0.16 mm thickness) was used to seal the Gene Frame. Images were acquired using standard epifluorescence microscopy using a Zeiss Axioplan 2 Microscope equipped with 100x objective (N/A 1.4). The DAPI filter was used to excite the TMA-DPH membrane dye with an exposure time of 400 milliseconds. CFP, GFP, mOrange and YFP filters were used with exposure times of 600, 800, 450 and 1000 milliseconds, respectively. To perform 3D-structured illumination microscopy (3D-SIM), we used the DeltaVision OMX SR microscope equipped with Olympus PlanApo N 60x objective lens (N/A 1.42). The 1.515 immersion oil was selected after calculating the refractive index using softWoRx software. The mCherry/A568 and GFP/A488 filters were used with exposure times of 15-20 milliseconds and 10-15% intensity (% T).

2.9.2 Transmission electron microscopy (TEM) imaging

For the images in Figure S3.2 (Appendix I), sporulating cells were pelleted by centrifugation in 1.5 mL Eppendorf tubes at 10,000 rpm for 3 mins and placed into primary fixative, consisting of 2.5% glutaraldehyde in 0.1 M sodium cacodylate buffer, for 2 hrs at room temperature. The cells were rinsed in fresh sodium cacodylate buffer three times for 15 mins each. Secondary fixation was performed using 1% osmium tetroxide and 1.5% potassium ferricyanide in cacodylate buffer for 1 hr at RT. The cells were then rinsed in three washes of Milli-Q water for 15 mins each. The fixed cell pellets were dehydrated by incubating in increasing concentrations of ethanol for 15 mins, consisting of 30, 50, 70, 90 and 100% ethanol.

Dehydrated cell pellets were incubated in a mixture of LR White resin and ethanol at a ratio of 1:1 for 6 hrs at RT, followed by a 2:1 LR White/ethanol mixture overnight. Cell pellets were incubated in 100% LR White resin for 6 hrs, followed by another 100% resin change overnight. The cell pellets were then placed into gelatin capsules in 100% resin and the resin polymerised for 24 hrs in an oven at 60°C. Resin embedded tissue was sectioned with a Diatome diamond knife using a Leica UCS ultramicrotome. Sections of thickness 70-90 nm were collected onto formvar-coated 100 mesh copper grids and stained sequentially with 1% uranyl acetate for 10 mins and lead citrate for 5 mins. The sections were imaged in a JEOL 1400+ transmission electron microscope at 80 kV, and images captured with a digital camera at a resolution of 2K x 2K.

For the images in Figure S5.1 (Appendix III), sporulating cells were harvested by centrifugation at 3,220 rpm for 10 mins. The cell pellet (1.4 µL) was dispensed on the 200 µm side of a type A 3 mm gold platelet (Leica Microsystems), covered with the flat side of a type B 3 mm aluminum platelet (Leica Microsystems), and was vitrified by high-pressure freezing using an HPM100 system (Leica Microsystems). Following freeze-substitution at −90°C for 80 hrs in acetone supplemented with 1% OsO4, the samples were warmed up slowly (1°C/hr) to −60°C (AFS2; Leica Microsystems). After 8 to 12 hrs, the temperature was raised (1°C/hr) to −30°C, and the samples were kept at this temperature for another 8 to 12 hrs before being rinsed 4 times in pure acetone. The samples were then infiltrated with gradually increasing concentrations of resin (Embed812, EMS) in acetone (1:2, 1:1, 2:1 [v/v]) for 3 hrs while raising the temperature until 20°C. Pure resin was added at RT. After polymerization at 60°C, 80 nm thin sections were obtained using an ultramicrotome UC7 (Leica Microsystems) and were collected on formvar-carbon-coated 100-mesh copper grids. The thin sections were post-stained for 5 mins with 5% aqueous uranyl acetate, rinsed, and incubated for 2 mins with lead citrate. The samples were observed using a CM12 (Philips) or Tecnai G2 Spirit BioTwin (FEI) microscope operating at 120 kV with an Orius SC1000B CCD camera (Gatan).

2.10 Immunoblot analysis

Whole-cell lysates from sporulating cells (by resuspension) were prepared as previously described (Doan & Rudner, 2007; Rodrigues *et al*., 2016b). At specific time-points, the sporulating cells were collected and pelleted by centrifugation (4000 rpm for 5 mins). The pellets were lysed by the SDS-Lysis buffer (Table 2.2) and incubated at 37°C for 10 min followed by addition of 50 µL SDS-Sample buffer containing 10% (v/v) 2-mercaptoethanol. Following that, the samples were heated for 15 mins at 50°C prior to loading. Equivalent

loading was based on OD_{600} at the time of harvest. Samples were separated on a 12.5% polyacrylamide gel and transferred to a Polyvinylidene fluoride (PVDF) membrane (BioRad). Membranes were blocked with 5% non-fat milk (Coles) with 0.5% Tween-20 for 1 hr. Blocked membranes were probed with mouse anti-His (1:4000) (Genscript), rabbit anti-SpoIIIAG (1:10000, (Doan *et al*., 2009)) or rabbit anti-FtsZ [1:30000, (Hajduk *et al*., 2019)] primary antibodies diluted in 1X PBS with 5% (w/v) non-fat milk and 0.05% (v/v) Tween-20 at 4°C overnight with gentle rocking. Primary antibodies were detected with horseradish-peroxidase conjugated anti-mouse or anti-rabbit antibodies (BioRad) and detected with Western Lightning ECL reagent (ChemiDoc XRS+ imaging system) (BioRad) as described by the manufacturer.

2.11 Protease accessibility assay

Protease accessibility assays were performed in sporulating cells (by resuspension) lacking the SpoIIQ (Q) protein to ensure that the membrane proteins present in the inner and outer forespore membranes would not be artificially inaccessible because of protoplast engulfment (Broder & Pogliano, 2006; Rodrigues *et al*., 2016a). The cultures were harvested at T2.5 to ensure more abundance of SpoIIIM-His6 in the cells. A volume of 25 mL of sporulating cells were harvested by centrifugation (4000 rpm, for 5 mins) at 2.5 hrs after the onset of sporulation, washed, and resuspended in 2 mL 1X SMM buffer (Table 2.2). The cells were protoplasted by lysozyme (5 mg/mL final concentration) for 10 mins with slow agitation. The protoplasts were harvested by centrifugation and resuspended in 1 mL of 1X SMM. Then, 100 µL of protoplasts were incubated with trypsin (30 µg/mL final concentration) (Worthington), trypsin and Triton X-100 (Sigma-Aldrich, 2% final concentration), or 1X SMM for 30 mins at 30°C. The reactions were terminated by the addition of 100 µL 2X SDS sample buffer and incubation for 5 mins at 95 °C. Five microliters from each reaction were analyzed by immunoblot.

2.12 Bacterial two-hybrid assay

To examine the interaction between SpoIIIE, SpoIIIM and PbpG, the bacterial two-hybrid assay (BACTH) was used, as previously described (Karimova *et al*., 1998). The Δ*cya* mutant *Escherichia coli* (BTH101) strain was used. The constructs were built using the pKNT25 or pUT18 plasmids harbouring the catalytic moieties of the *Bordetella pertussis* adenylate cyclase to generate T25 or T18 fusions of SpoIIIE, SpoIIIM or PbpG (see plasmid construction section 2.7.5) (Karimova *et al*., 1998). Next, the BTH101 cells were co-transformed with the constructed pKNT25 and pUT18 plasmids, selecting for colonies that were both kanamycin and ampicillin resistant, that had different combinations of the SpoIIIE, SpoIIIM or PbpG

fusions to T25 and T18 (see the BACTH strains listed in Table 2.7). The strains were grown in 5 mL of LB broth (Lennox) with ampicillin (50 µg/mL) and kanamycin (20 µg/mL) at 30°C overnight. Next, 5 µL of the overnight culture was spotted onto M9 minimal agar containing 40 µg/mL 5-bromo-4-chloro-3-indolyl-β-D-galactopyranoside (X-Gal) (Sigma-Aldrich), kanamycin (20 µg/mL) and ampicillin (50 µg/mL) and incubated at 30°C for 34 hrs. After incubation, the agar plates were photographed.

Table 2.7: *E. coli* stains list used for bacterial two-hybrid assay

Strains	Genotype	Source
cHC001	*T18-spoIIIE + T25-spoIIIE*	This study
cHC002	*T18-spoIIE + T25-spoIIIM*	This study
cHC003	*T18-spoIIIE + T25 (pKT25)*	This study
cHC004	*T18-spoIIIM + T25-spoIIIE*	This study
cHC005	*T18-spoIIIM + T25-spoIIIM*	This study
cHC006	*T18-spoIIIM + T25 (pKT25)*	This study
cHC007	*T18 (pUT18C) + T25-spoIIIE*	This study
cHC008	*T18 (pUT18C) + T25-spoIIIM*	This study
cHC009	*T18 (pUT18C) + T25 (pKT25)*	This study
cHC010	*T18-spoIIIE + T25-pbpG*	This study
cHC012	*T18-spoIIIM + T25-pbpG*	This study
cHC014	*T18-pbpG + T25-spoIIIE*	This study
cHC015	*T18-pbpG + T25-spoIIIM*	This study
cHC016	*T18-pbpG + T25-pbpG*	This study
cHC018	*T18-pbpG + T25 (pKT25)*	This study
cHC024	*T18 (pUT18C) + T25-pbpG*	This study
cAT083	*T18-slmA + T25-slmA*	(Cho *et al*., 2011)

2.13 Co-Immunoprecipitation (co-IP)

To examine the interaction between SpoIIIE and SpoIIIM, a co-immunoprecipitation (co-IP) assay was performed as described previously (Doan *et al,* 2009). Sporulating cells expressing SpoIIIM-His6 and SpoIIIE-GFP as sole sources of SpoIIIM and SpoIIIE, respectively, were used. A volume of 100 mL of cells from sporulating cultures (2 hours after transfer to resuspension medium) was harvested by centrifugation (3,900 rpm, 5 minutes, room-temperature (RT)) and washed twice with 1X SMM. Cells were resuspended in 10 mL of 1X SMM and protoplasts were generated by treating cells with 2 mg/mL lysozyme for 20 minutes at RT with gentle rotation. Protoplasts were then harvested by centrifugation (3,900 rpm, 5 minutes, RT) and lysed in 3 mL of cold Hypotonic buffer (Table 2.2) containing 60 U DNaseI and 40 µg/mL RNaseA, on ice for 1 hour, with vortexing every 15 minutes. Membranes were separated from the cytoplasmic contents by ultracentrifugation (100,000 rpm, 1 hour, 4°C,

Beckman Optima MAX-XP, TLA-55 rotor) and then resuspended in 200 µL of Buffer G2. Crude membranes were solubilized in 1 mL of Buffer G2 (Table 2.2) containing 100 µg/mL lysozyme and 2% (v/v) Triton X-100 with rotation at 4°C for 1 hour. Solubilized membrane proteins were separated by centrifugation (100,000 rpm, 1 hour, 4°C, Beckman Optima MAX-XP, TLA-55 rotor) and then incubated with 25 µL of pre-equilibrated GFP-Trap agarose beads (ChromoTek) for 4 hours at 4 °C with rotation. Beads were washed four times with 400 µL of Buffer G2 containing 0.1% (v/v) Triton X-100, and proteins were eluted from the beads in 25 µL of Elution Buffer (Table 2.2) at 50°C for 15 minutes. Solubilized membrane proteins (Load), flow-through (FT) and immunoprecipitate (IP) were analyzed by SDS-PAGE and immunoblotting as described in section 2.10.

2.14 Quantification and statistical analysis

2.14.1.1 Sporulation Efficiency Analysis

All the sporulation efficiency data are average (± SD) of 3 biological replicates.

2.14.1.2 Tn-seq analysis

Mapped genes in which reads were statistically underrepresented were identified using the Mann Whitney U test, as described previously (Meeske *et al*., 2016). Visual inspection of transposon insertion profiles was performed with the Sanger Artemis Genome Browser and annotation tool therein.

2.14.1.3 Image analysis

Microscopy images were processed by adjusting the brightness and contrast using the Fiji software (Schindelin *et al*., 2012). All quantifications were performed using the manual counting tool of the Fiji software, and the raw data was then exported into Excel for data collation and graph generation. The criteria described below, or in results and legends, was used to quantify each phenotype.

(a) Quantification of forespore morphological phenotypes (Figure 1.4B):

based on membrane staining, any forespore with a normal oblong shape, smaller and circular shape, no specific shape or smaller but localized to mid-cell was classified as WT-looking, Dwarf, Abnormal or Mislocalized, respectively. The percentage of each phenotype (average frequency ± SD of 3 biological replicates) was calculated based on the total number of engulfed forespores counted at T3. n>200 per time-course, per strain, per replicate.

(b) Quantification of forespore miscompartmentalization (Figures 3.5C, 3.8A and 6.2B): any cell with forespore-expressed CFP signal in the mother cell was classified as miscompartmentalized. The percentage of miscompartmentalized cells (average frequency ± SD of 3 biological replicates) was calculated based on the total number of sporulating cells that had progressed into the asymmetric division stage of development and contained CFP signal. n>750 per time-course, per strain, per replicate.

(c) Quantification of chromosome translocation using the LacI-GFP/*lacO* system (Figures 4.4A, 4.6A & B, S4.1A, B & C, and 6.2C):

we followed the criteria described in Figure 4.4A and the percentage of cells (average frequency ± SD of 3 biological replicates) was calculated based on the total number of sporulating cells that contained a GFP focus and had progressed into or beyond asymmetric division. *n*>600 per time-course, per strain, per replicate.

(d) Quantification of chromosome translocation using the dual reporter system (TetR-CFP/*tetO* & LacI-YFP/*lacO*):

we followed the criteria described in Figure 4.5B and the percentage of cells (average frequency ± SD of 3 biological replicates) was calculated relative to the total number of sporulating cells that contained four foci, two CFP foci and two YFP foci. Not all cells contained four visible foci within the plane of view during development: the four foci were clearly visible in approximately 25%, 30% and 47% of the sporulating cells, at T2, T2.5 and T3 respectively. *n*>30 per time-point, per replicate.

(e) Quantification of cells with a SpoIIIE-GFP focus (Figures 4.2D, 5.4C and 6.2D):

the percentage of cells with a SpoIIIE-GFP focus (average frequency ± SD of of 3 biological replicates) was calculated based on the number of sporulating cells that contained a GFP focus, relative to the total number of sporulating cells that contained SpoIIIE-GFP signal (foci or diffuse) in the membranes of the forespore. *n*>950 per time-course, per strain, per replicate.

(f) Quantification of septal retraction (Figures 5.1E and 6.2E):

any cell with forespore-expressed CFP signal in the mother cell and a non-continuous asymmetric septum, or vestiges of an asymmetric septum (based on the membrane signal), was classified as having a retracted septum. The percentage of cells with retracted septa (average frequency ± SD of of 3 biological replicates) was calculated based on the total number of sporulating cells that had progressed into or beyond asymmetric division. *n*>600 per time-point, per strain, per replicate.

(g) Quantification of septal retraction using the DNA staining by SYTOX Orange (Figure 5.6B):

any cell with forespore-expressed CFP signal and two asymmetric septa, one asymmetric septum or vestiges of an asymmetric septum (based on the membrane signal), was classified as 2 septa, 1 septum or No septa, respectively. The percentage of cells with these phenotypes (average frequency ± SD of of 3 biological replicates) was calculated based on the total number of sporulating cells that had progressed into asymmetric division. *n*>600 per time-point, per strain, per replicate.

(h) Quantification of chromosome translocation (Figures 5.7B & D):

any cell with forespore-expressed CFP signal with two asymmetric septa and DNA-stained signal accumulated inside two forespore compartments, one forespore compartment or no accumulated signal, was classified as two translocated, one translocated or not translocated, respectively. The percentage of cells with these phenotypes (average frequency ± SD of of 3 biological replicates) was calculated based on the total number of sporulating cells that had progressed into asymmetric division. n>600 per time-point, per strain, per replicate.

(i) Quantification of GFP-SpoIIIM (Figure 6.3B):

the percentage of cells with a GFP-SpoIIIM focus (average frequency ± SD of 3 biological replicates) was calculated based on the number of sporulating cells that contained GFP signal (focus or band), relative to the total number of sporulating cells that had progressed into or beyond asymmetric division. *n*>750 per time-course, per strain, per replicate.

(j) Analysis of SpoIIIE-GFP foci signal intensity:

The MicrobeJ plugin designed for the Fiji software was used to detect the signal intensity of SpoIIIE-GFP foci (Figure 4.2E), on background subtracted images (Process > Subtract Background) to avoid false positive detections of the fluorescent signal. To determine the signal intensity of SpoIIIE-GFP foci, the brightfield image was set to Channel 1 and the image with the GFP signal to Channel 2. These channels were then merged into one image. For Channel 1 of the image with "Bright" background, the "Bacteria" tab was set to "Fit Shape" and "Rod-Shaped" to detect the bacteria in the brightfield image. Five parameters: "Exclude on Edges", "Shape descriptors", "Segmentation", "Intensity", and "Feature" were checked on. To refine the generated bacteria outlines, the shape descriptors (area, length, and width) were set differently for each time-point corresponding to the contours of individual cell. To resolve unprocessed cells, the manual editing tool was also used. For Channel 2 of the image with

"Dark" background, the "Maxima" tab was set to "Point" and "Basic". The tolerance was set to 15, and the intensity was set from 15-max to ensure detection of the GFP foci with a minimum signal intensity of 15. Three parameters: "Exclude on Edges", "Shape descriptors", and "Associations" were checked on. The raw data were displayed on a MicrobeJ results table, which was then exported into Excel for data collation and graph generation.

Chapter 3:

SpoIIIM and PbpG are required for the forespore morphology and compartmentalization

3.1 Disclaimer

This is to acknowledge that Ms Johana Luhur has contributed to the work presented in this chapter, in relation to quantifying the miscompartmentalization in section 3.3.7. In addtion, Dr. Milena Awad, Dr. Simon Crawford and Prof. Dena Lyras also contributed to the work presented in this chapter through helping with the transmission electron microscopy of the forespore phenotypes presented in Figure S3.2 (Appendix I).

3.2 Introduction

During engulfment, two class A PBPs, known as PbpG and PbpF, are produced in the forespore to synthesize a thin layer of PG (GCW) in the intermembrane space between the forespore and the mother cell (Figure 3.1A) (Scheffers, 2005; Popham & Bernhards, 2015; Ojkic *et al*., 2016). It has been reported that PbpG and PbpF are functionally redundant, where at least one of them is required to generate the GCW (Meador-Parton & Popham, 2000; McPherson *et al*., 2001). In cells lacking both PbpG and PbpF, the GCW is not synthesized and sporulation efficiency is severely reduced (McPherson *et al*., 2001).

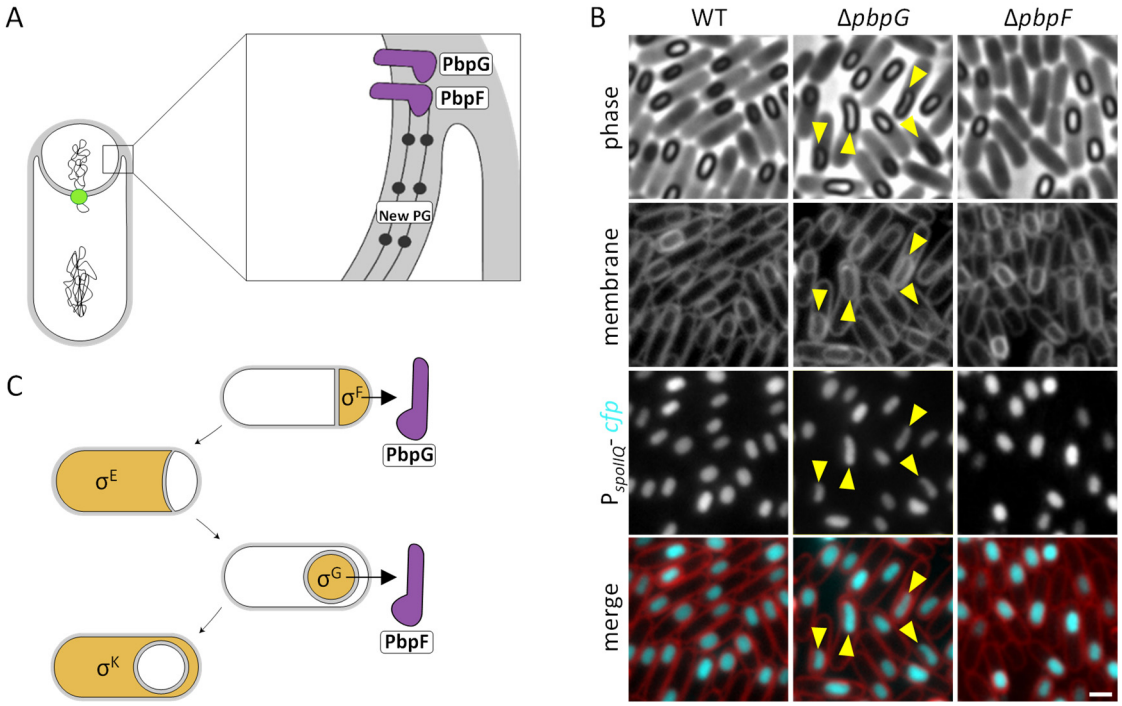

Figure 3.1: Phenotypic and transcriptional differences between PbpG and PbpF. (A) PbpG and PbpF (violet) are expressed in the forespore to synthesize a thin layer of PG (black dotted lines). **(B)** Comparison between the WT, Δ*pbpG* and Δ*pbpF* cells with CFP expressed in the forespore at T5. The Δ*pbpG* forespores (yellow arrows) have a jelly-bean shape, whereas the WT and Δ*pbpF* forespores do not. Scale bar, 1 µm. **(C)** PbpG is mainly expressed under σ^F control during the engulfment process and PbpF is mostly expressed after engulfment completion under σ^G control.

Interestingly, two observations suggest that PbpF and PbpG may also participate in separate genetic pathways involving PG synthesis. Firstly, forespores lacking *pbpG* display an abnormal jellybean-like morphology, whereas most of *pbpF* mutant cells produce wild-type-looking, oblong forespores (Figure 3.1B) (McPherson *et al*., 2001; Rodrigues *et al*., 2016a). Secondly, the timing of *pbpG* and *pbpF* expression is different, despite both genes being expressed in the same compartment. *pbpG* is predominantly expressed under σ^F control during engulfment and slightly expressed under σ^G control, which is active after engulfment completion (Figure 3.1C)

(Pedersen *et al*., 2000). In contrast, the expression of *pbpF* occurs to a lesser extent under σ^F control and then mainly under σ^G control (Figure 1C) (Popham & Setlow, 1993). Based on these differences, we hypothesized that PbpG and PbpF could have specialized roles in PG synthesis during sporulation. This hypothesis is in keeping with a well-studied example from *E. coli*, where two class A PBPs, known as PBP1a and PBP1b, are also functionally redundant (Paradis-Bleau *et al*., 2010; Typas *et al*., 2010). In spite of their functional redundancy, each protein has a specific role during vegetative growth: PBP1a mainly promotes cell elongation, while PBP1b plays a role in cell division and supports PG integrity (Bertsche *et al*., 2006; Banzhaf *et al*., 2012; Vigouroux *et al*., 2020).

In this chapter, stemming from transposon-sequencing data obtained by C. Rodrigues, we investigated the role of a poorly-characterized gene renamed as *spoIIIM* (previously known as *yqfZ*) during sporulation. We found that SpoIIIM is required for spore formation in cells lacking PbpG. Furthermore, we found that SpoIIIM and PbpG are also required for maintaining forespore morphology and cytoplasmatic compartmentalization during engulfment. Importantly, we observed that cells lacking both SpoIIIM and PbpG produce forespores that are phenotypically similar to forespores lacking the DNA translocase SpoIIIE. We hypothesize that SpoIIIM and PbpG could impact successful chromosome translocation by SpoIIIE.

3.3 Results

3.3.1 Tn-seq rationale and identifying *spoIIIM*

To test the hypothesis that PbpG and PbpF could function in separate genetic pathways, we conducted transposon-sequencing (Tn-seq) (see Chapter 2, Materials and Methods, section 2.8) in sporulating cells of WT, Δ*pbpG* and Δ*pbpF* (Meeske *et al*., 2016). The analysis of the Tn-seq data identified a set of potential genes that appear to be required for sporulation specifically in the absence of *pbpG* or *pbpF* (Appendix; Table 3.1 & 3.2). As expected, and validating the Tn-seq screen, *pbpG* gene did not tolerate any transposon insertions in the Δ*pbpF* screen and very few transposon insertions were observed in the *pbpF* gene in the Δ*pbpG* screen (Figure 2.1A & B). This data is consistent with the essentiality of *pbpF* in cells lacking *pbpG* and *vice versa* (McPherson *et al*., 2001). In this thesis, we focused on *yqfZ* (renamed *spoIIIM*), a poorly-characterized gene that was a top hit in the Δ*pbpG* screen (Appendix; Table A1). Consistent with previous work, we validated that *spoIIIM* is transcribed under the control of σ^E during engulfment (Appendix I; Figure S3.1) (Eichenberger *et al*., 2003).

SpoIIIM is a 99 amino acid protein that contains a C-terminal LysM domain and N-terminal single transmembrane segment (Bateman, 2019). Bacterial LysM domains have been implicated in binding to PG or in protein-protein interactions (Buist *et al*., 2008; Mesnage *et al*., 2014; Pereira *et al*., 2019). While WT and Δ*pbpF* sporulating cells accepted many transposon insertions in *spoIIIM*, this was not the case for cells lacking *pbpG* (Figure 3.2C). This suggests that *spoIIIM* is required for sporulation only in the absence of *pbpG*.

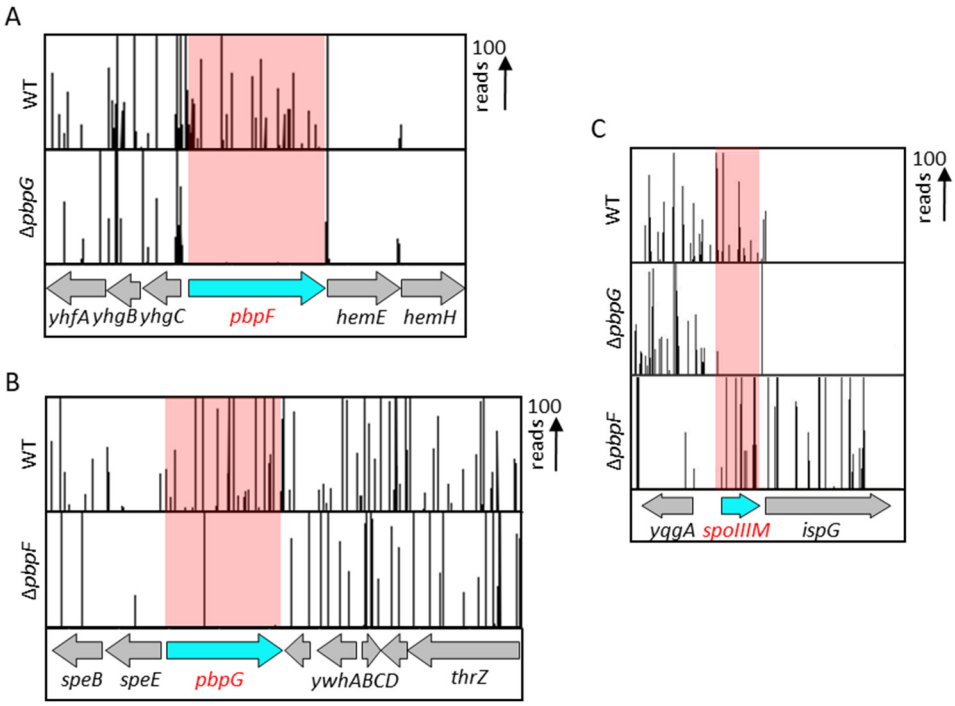

Figure 3.2: Transposon insertion profiles highlight the specific essentiality of genes. (A) Tn-seq profile of *pbpF* (red box) shows many transposon insertions in WT (bDR2413) and none in *pbpG* mutant (bCR1557). **(B)** Tn-seq profile of *pbpG* (red box) shows that it tolerates many transposon insertions in WT (bDR2413) but tolerates fewer insertions in the *pbpF* mutant (bCR1558). **(C)** Tn-seq profile of *spoIIIM* (red box) shows intolerance to any transposon insertions in the *pbpG* mutant (bCR1557), unlike both WT (bDR2413) and the *pbpF* mutant (bCR1558). Tn-seq profiles were prepared using the genome browser and annotation tool (Artemis) for all libraries after 24 hrs growth and sporulation in exhaustion medium. The height of each line reflects the number of sequencing reads at this position.

3.3.2 *spoIIIM* and *pbpG* are a synthetic lethal pair during sporulation

The Tn-seq data suggest that *spoIIIM* is required for sporulation in cells lacking *pbpG*. To test this idea, the sporulation efficiency of cells lacking *spoIIIM*, *pbpG* or *spoIIIM* together with *pbpG* was examined relative to that of the WT. Sporulation efficiency (percentage of spores produced relative to the WT) was determined using the heat-kill assay (see Chapter 2, Materials and Methods, section 2.4).

As previously reported, the Δ*spoIIIM* mutant strain showed a mild sporulation defect (76.6%, relative to WT levels of spores) (Eichenberger *et al*., 2003) and the Δ*pbpG* mutant strain

produced near-WT levels of spores (87.3%) (Figure 3.3A) (McPherson *et al*., 2001). In accordance with the Tn-seq data, the Δ*spoIIIM* Δ*pbpG* double mutant produced fewer spores than either of the single mutants (8.8%, Figure 3.3A).

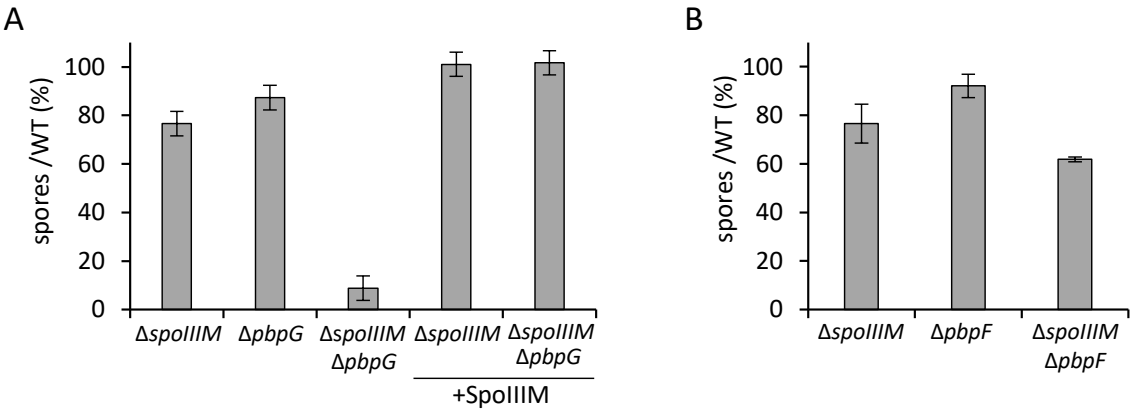

Figure 3.3: Δ*spoIIIM* causes a severe sporulation defect only in cells lacking Δ*pbpG*. (A) Sporulation efficiency relative to WT (bDR2413) of Δ*spoIIIM* (bCR1592), Δ*pbpG* (bCR1557), Δ*spoIIIM* Δ*pbpG* (bCR1600) and the respective *spoIIIM* complementation strains in Δ*spoIIIM* (bAT007) and Δ*pbpG* Δ*spoIIIM* (bAT010) backgrounds in DSM medium. Δ*spoIIIM* (bCR1592) has a slight sporulation defect that is exacerbated when combined with Δ*pbpG* (bCR1600). Complementation of *spoIIIM* recovered the sporulation efficiency in the Δ*spoIIIM* (bAT007) and Δ*pbpG* Δ*spoIIIM* (bAT010) backgrounds. **(B)** Sporulation efficiency relative to WT of Δ*pbpF* (bCR1558), Δ*spoIIIM* (bCR1592) and Δ*pbpF* Δ*spoIIIM* (bCR1602) strains in exhaustion medium. The double mutant of Δ*pbpF* Δ*spoIIIM* (bCR1602) had a mild sporulation defect similar to Δ*spoIIIM* (bCR1592) alone. The sporulation efficiency data are average (± SD) of 3 biological replicates.

To confirm that these sporulation defects were caused by the *spoIIIM* deletion, SpoIIIM was re-introduced into the Δ*spoIIIM* and Δ*spoIIIM* Δ*pbpG* strains and the sporulation efficiency of the resulting strains was determined using the heat-kill assay. *spoIIIM* was integrated ectopically at the non-essential *ycgO* locus. Complementation by SpoIIIM restored sporulation efficiency to WT level in the Δ*spoIIIM* mutant and to the Δ*pbpG* level in the Δ*spoIIIM* Δ*pbpG* double mutant (Figure 3.3A).

As a control experiment, and to validate that *spoIIIM* is not required for sporulation in cells lacking *pbpF*, we compared the sporulation efficiency of the Δ*pbpF* and Δ*spoIIIM* Δ*pbpF* mutants. Consistent with previous results, the Δ*pbpF* mutant had a relatively mild sporulation defect (92.1%, Figure 3.3B) (McPherson *et al*., 2001). Importantly, the Δ*spoIIIM* Δ*pbpF* double mutant had a sporulation defect similar to Δ*spoIIIM* single mutant strain (Figure 3.3B).

These results suggest that SpoIIIM is specifically required for sporulation in cells lacking PbpG. In other words, *spoIIIM* and *pbpG* are a synthetically-lethal pair during the sporulation process.

3.3.3 SpoIIIM and PbpG are required for forespore morphology

To start to understand how SpoIIIM contributes to sporulation and why it becomes more important for this process in the absence of PbpG, we compared WT, Δ*spoIIIM*, Δ*pbpG* and Δ*spoIIIM* Δ*pbpG* mutant sporulating cells using fluorescence microscopy. To this end, we induced these strains to sporulate by the resuspension method (see Chapter 2, Materials and Methods, section 2.4). Using the membrane dye TMA-DPH, we examined the morphological events of forespore development every 30 mins after the onset of asymmetric division (starting at T1.5) (Figure 3.4A).

In the WT cells, after 1.5 hrs from the onset of sporulation (T1.5), the asymmetric septum could be observed in a subset of cells, and at subsequent time-points, engulfment proceeded normally (Figure 3.4A). At T3, the majority of cells had completed engulfment, and the forespores were large, oblong in shape and localized to one pole of the mother cell (Figure 3.4A).

In the Δ*spoIIIM* mutant, at early stages of development, the sporulating cells looked similar to the WT (Figure 3.4A). But as engulfment progressed, at T2 and T2.5 the Δ*spoIIIM* cells had some small-looking forespores that were distinct from the WT (Figure 3.4A). Interestingly, at T3 the Δ*spoIIIM* mutant showed a mixed population of forespores with different morphology, size and position with the sporangium (Figure 3.4A & B). To better assess this phenotype, we categorized the forespores into 4 types; 1) WT-looking forespores that were large and oblong in shape, 2) dwarf forespores that were smaller and more circular in shape, 3) abnormal-looking forespores which appeared deformed with membrane distortions and 4) mislocalized forespores that were similar to dwarf forespores but positioned closer to the mid-cell of the mother cell (Figure 3.4A & B). In Δ*spoIIIM* mutant cells, the quantification of these forespore types revealed that 59.1% were WT-looking, 23.8% dwarf, 13.7% abnormal-looking and 3.2% mislocalized (Figure 3.4B).

In the Δ*pbpG* mutant, the vast majority of sporulating cells produced forespores that were comparable to the WT. However, careful inspection revealed that 2.5% of the forespores population were of the dwarf phenotype at T3 (Figure 3.4A & B).

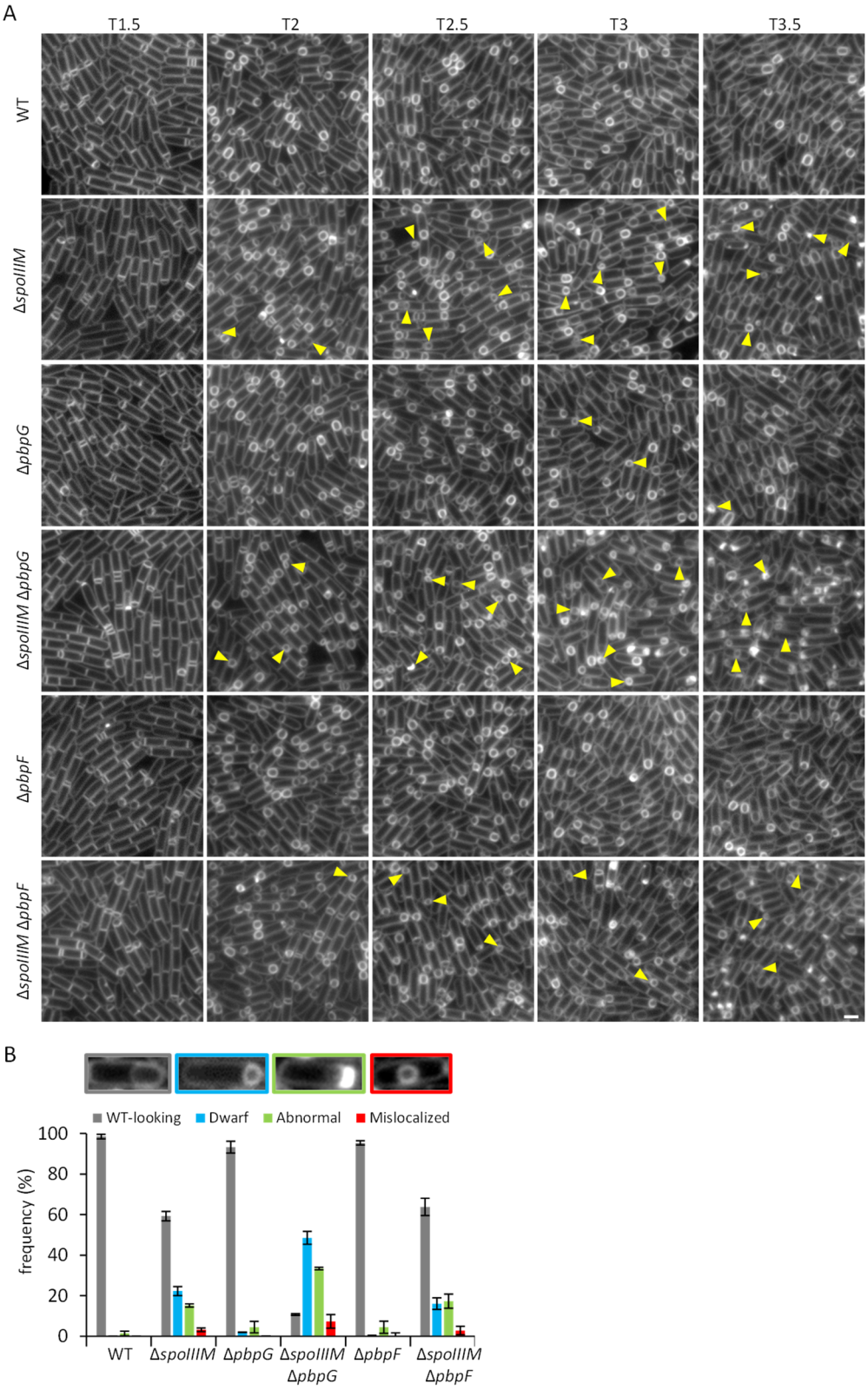

Figure 3.4: SpoIIIM and PbpG are required for spore morphology. (A) Time-course imaging of WT (bAT087), Δ*spoIIIM* (bAT088), Δ*pbpG* (bAT089), Δ*spoIIIM* Δ*pbpG* (bAT091), Δ*pbpF* (bAT090) and Δ*spoIIIM* Δ*pbpF* (bAT092) strains. The yellow arrowheads point to forespores with morphological defects that increased dramatically in cells lacking both *spoIIIM* and *pbpG* (bAT091). Cell membranes were visualized with TMA-DPH fluorescent dye. Scale bar, 2 µm. **(B)** Quantification at T3 of the forespore phenotypes; WT-looking (grey), dwarf (blue), abnormal (green) and mislocalized (red) forespores in all the backgrounds. The data is average frequency (± SD) of 3 biological replicates. (n>200 per strain, per replicate).

In the Δ*spoIIIM* Δ*pbpG* double mutant no obvious differences were observed early in development (Figure 3.4A). However, at T2 and T2.5, cells with many deformed forespores were observed (Figure 3.4A). Surprisingly, by T3 the majority of forespores were deformed and different from the WT. Quantification of the Δ*spoIIIM* Δ*pbpG* forespores at T3 showed that very few were WT-looking (10%), and the majority of them were either dwarf (49%), abnormal (31%) or mislocalized (8%) (Figure 3.4A & B).

To further confirm that Δ*spoIIIM* does not synergize with Δ*pbpF*, we also examined the forespores of the Δ*pbpF* and Δ*spoIIIM* Δ*pbpF* mutants (Figure 3.4A & B). The Δ*pbpF* mutant did not cause morphological defects and the quantification of forespore morphology phenotypes in the Δ*spoIIIM* Δ*pbpF* double mutant were similar to those of the Δ*spoIIIM* mutant alone (Figure 3.4A & B).

To investigate the morphological defects exhibited by Δ*spoIIIM* and Δ*spoIIIM* Δ*pbpG* at a more detailed level, we visualized these mutants by transmission electron microscopy (TEM) at T3.5 (Appendix I; Figure S3.2). Consistent with the fluorescence microscopy images, the WT forespores were oblong in shape and the Δ*pbpG* forespores had a jelly-bean like appearance (Appendix I; Figure S3.2). Interestingly, in sporulating cells lacking *spoIIIM*, the dwarf spores appeared to be deformed in shape with wrinkled membranes. Similarly, the Δ*spoIIIM* Δ*pbpG* dwarf forespores had wrinkled membranes (Appendix I; Figure S3.2).

To conclude, these results suggest that cells lacking both Δ*spoIIIM* and Δ*pbpG* exhibit a severe morphological defect in developing spores. Thus, SpoIIIM and PbpG together play a critical role in maintaining forespore morphology.

3.3.4 SpoIIIM and PbpG are required for forespore compartmentalization

The fluorescence microscopy data indicate that sporulating cells lacking PbpG and SpoIIIM produce forespores with severe morphological defects. In addition, the TEM images highlighted the presence of abnormal forespore membranes in the Δ*spoIIIM* and Δ*spoIIIM* Δ*pbpG* mutants. These data raised the hypothesis that PbpG and SpoIIIM may contribute to integrity of the forespore envelope. If so, then sporulating cells lacking PbpG and SpoIIIM might also exhibit defects in forespore cytoplasmatic compartmentalization. To test if sporulating cells lacking SpoIIIM and PbpG are defective in forespore compartmentalization, we engineered the forespores to express cytoplasmatic CFP under a well-established σ^F-dependent promotor (P_{spoIIQ}) (Hilbert *et al*., 2004). If SpoIIIM and PbpG are required for forespore compartmentalization, we would expect the forespore CFP signal to "leak" into the

mother cell. We used fluorescence microscopy to examine the accumulation of the CFP signal in the forespores over a time-course (Figure 3.5A & B).

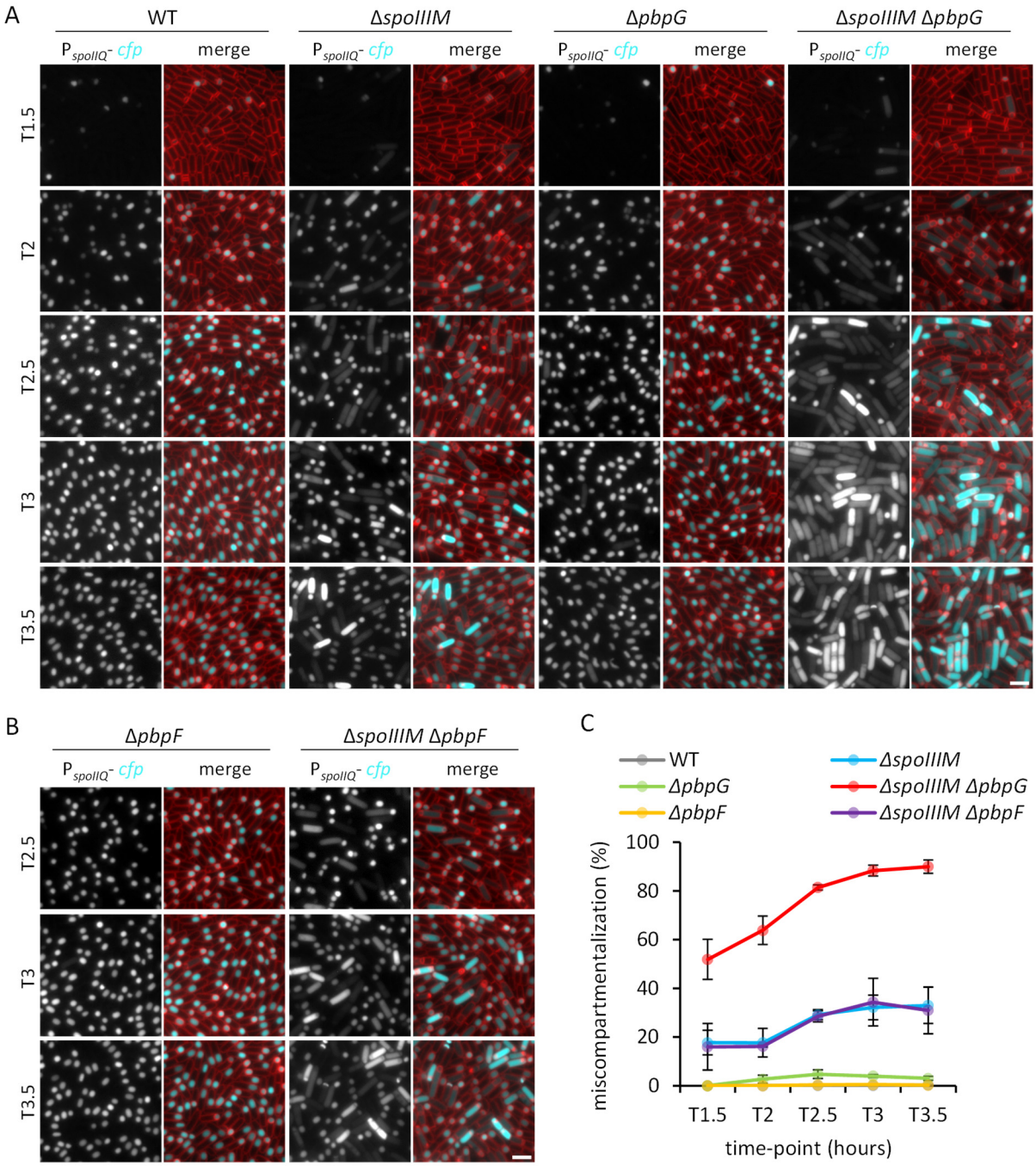

Figure 3.5: Miscompartmentalization of σ^F in Δ*spoIIIM* Δ*pbpG* cells. (A) Time-course imaging of WT (bAT087), Δ*spoIIIM* (bAT088), Δ*pbpG* (bAT089) and Δ*spoIIIM* Δ*pbpG* (bAT091) strains expressing CFP in the forespore. The WT forespores always had the CFP signal within the forespore. Cells lacking *spoIIIM* leaked the forespore CFP into the mother cell from T2 and increased over time. Cells lacking *pbpG* showed slight miscompartmentalization. The double mutant of *spoIIIM pbpG* had severe miscompartmentalization of σ^F. Scale bar is 2 µm. **(B)** Representative images of the time-course imaging of Δ*pbpF* (bAT090) and Δ*spoIIIM* Δ*pbpF* (bAT092) cells expressing CFP in the forespore. The Δ*pbpF* forespores were compartmentalized like the WT. The forespores of Δ*spoIIIM* Δ*pbpF* cells showed miscompartmentalization similar to the Δ*spoIIIM* cells. Scale bar is 2 µm. **(C)** Quantification of miscompartmentalized forespores during a sporulation time-course of WT

(bAT087, grey), Δ*spoIIIM* (bAT088, blue), Δ*pbpG* (bAT089, green), Δ*spoIIIM* Δ*pbpG* (bAT091, red) Δ*pbpF* (bAT090, yellow) and Δ*spoIIIM* Δ*pbpF* (bAT092, violet). Error bars for each time-point are standard deviation of 3 biological replicates (n>950 per time-course, per strain).

Throughout the entire time course, WT forespores were compartmentalized and the CFP signal remained within the forespore (Figure 3.5A). In the Δ*spoIIIM* mutant, the CFP signal was initially (T1.5) confined to the forespores but starting from T2, we observed some Δ*spoIIIM* sporulating cells with the CFP signal in the entire sporangia. To characterize this phenotype more carefully, we quantified the number of forespores that had leaked their CFP signal over the time-course (Figure 3.5C). Our quantification showed that miscompartmentalization of the CFP signal increased over time (Figure 3.5C) and by T3, 34% of the Δ*spoIIIM* sporulating cells were miscompartmentalized (Figure 3.5A & C).

In the Δ*pbpG* mutant, although the vast majority of sporulating cells were compartmentalized, a small fraction exhibited miscompartmentalization, and at T3, miscompartmentalized sporulating cells accounted for 4% of the population (Figure 3.5A & C).

Consistent with the severe forespore morphological defect exhibited by the Δ*spoIIIM* Δ*pbpG* double mutant, we observed a high frequency of miscompartmentalization in the double mutant at all time-points. At T1.5, more than 50% of Δ*spoIIIM* Δ*pbpG* double mutant sporulating cells exhibited miscompartmentalization (Figure 3.5A & C). This pattern of CFP miscompartmentalization increased over time and by T3.5 90% of the sporulating cells were miscompartmentalized (Figure 3.5A & C).

As a further validation of the specific genetic relationship between *pbpG* and *spoIIIM*, the degree of miscompartmentalization in the Δ*spoIIIM* Δ*pbpF* double mutant cells was similar to that of the Δ*spoIIIM* mutant throughout the time-course (Figure 3.5 A, B & C).

Taken together, these data show that Δ*spoIIIM* Δ*pbpG* mutant forespores lack the ability to confine their cytoplasmic contents and indicate that SpoIIIM and PbpG are also required for maintaining forespore compartmentalization during engulfment.

3.3.5 Δ*spoIIIM* Δ*pbpG* forespores are similar to Δ*spoIIIE* forespores

It has been reported previously that the absence of the DNA translocase SpoIIIE results in small deformed forespores (Lopez-Garrido *et al*., 2018). Recent work suggests that the deformed forespores of the Δ*spoIIIE* mutant arise due to the absence of chromosome translocation into the forespore. Based on this result, it has been proposed that translocation of the chromosome into the forespore contributes to its size and morphology (Lopez-Garrido *et al*., 2018) (Figure

3.6A). In addition, it has been shown that sporulating cells lacking *spoIIIE* produce forespores that are miscompartmentalized (Wu & Errington, 1994; Pogliano *et al*., 1997) (Figure 3.6A). These Δ*spoIIIE* mutant phenotypes are similar to those of the Δ*spoIIIM* mutant and Δ*spoIIIM* Δ*pbpG* double mutant. To better compare the phenotypes between these mutants, we examined Δ*spoIIIM* Δ*pbpG* and Δ*spoIIIE* cells side-by-side (Figure 3.6A). Interestingly, we observed a high degree of similarity at the level of forespore morphology and miscompartmentalization (Figure 3.6A). Although, in cells lacking *spoIIIE*, the intensity of the miscompartmentalized CFP signal was always brighter, and we did not observe mislocalized forespores. The similar phenotypes of these mutants suggest that SpoIIIM, PbpG and SpoIIIE participate in a genetic pathway that maintains forespore morphology and compartmentalization. Because the phenotype of the Δ*spoIIIE* mutant appears to be worse than the Δ*spoIIIM* Δ*pbpG* double mutant, we predicted that the Δ*spoIIIE* phenotype will be dominant over the phenotype of the Δ*spoIIIM* and Δ*pbpG* mutants. To test our hypothesis that SpoIIIM and PbpG could function in the same genetic pathway as SpoIIIE, we introduced deletions of *spoIIIM* and/or *pbpG* into cells lacking *spoIIIE* and examined forespore morphology and compartmentalization in the resulting strains.

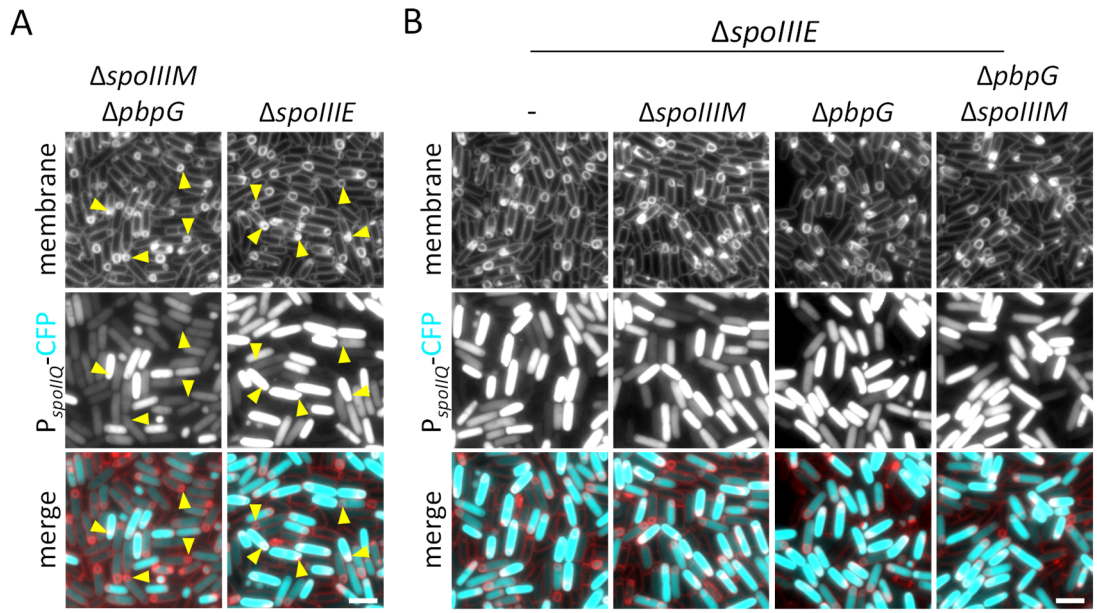

Figure 3.6: Phenotypic similarity between cells lacking *spoIIIM* and *pbpG* or *spoIIIE*. (A) Representative images of miscompartmentalization in Δ*spoIIIM* Δ*pbpG* (bAT091) and Δ*spoIIIE* (bAT457) strains at T3. Scale bar is 2 µm. Yellow arrows refer to small deformed forespores that are comparable between Δ*spoIIIM* Δ*pbpG* and Δ*spoIIIE* cells. **(B)** Representative images of Δ*spoIIIE* (bAT457), Δ*spoIIIE* Δ*spoIIIM* (bAT458), Δ*spoIIIE* Δ*pbpG* (bAT459) and Δ*spoIIIE* Δ*spoIIIM* Δ*pbpG* (bAT460) showing the dominant effect of *spoIIIE* deletion. Scale bar is 2 µm.

As shown in Figure 3.6, cells lacking *spoIIIE* failed to maintain forespore morphology and compartmentalization. Consistent with the idea that the Δ*spoIIIE* phenotype is dominant over

Δ*spoIIIM* and Δ*pbpG*, we observed deformed, small forespores and miscompartmentalization in all cells when Δ*spoIIIE* was combined with Δ*spoIIIM,* Δ*pbpG* or both Δ*spoIIIM* Δ*pbpG* (Figure 3.6B).

In conclusion, these data suggest that SpoIIIM and PbpG may function in a genetic pathway with SpoIIIE, that maintains forespore morphology and compartmentalization. Furthermore, these data suggest that SpoIIIE is the most essential component of this pathway, with SpoIIIM and PbpG acting downstream of SpoIIIE.

3.3.6 Impairing engulfment PG hydrolysis suppresses miscompartmentalization in cells lacking SpoIIIM and PbpG

Previous work shows that the miscompartmentalization of sporulating cells lacking *spoIIIE* can be suppressed by disrupting the engulfment hydrolytic machinery (i.e. DMP complex) (Wu & Errington, 1994; Wu *et al*., 1995; Hilbert *et al*., 2004). As mentioned in the Introduction (section 1.5.3.2), the DMP complex is composed of three σ^E-dependent proteins SpoIID, SpoIIM and SpoIIP and is essential for thinning of septal PG at the onset of engulfment. Deletion of both *spoIID* and *spoIIP* results in cells with a single or two flat septa. It had been shown that Δ*spoIIIE* forespore miscompartmentalization is almost completely suppressed in a Δ*spoIID* Δ*spoIIP* mutant (Figure 3.7A). Since the degree of miscompartmentalization in Δ*spoIIIM* Δ*pbpG* is similar to that of the Δ*spoIIIE* mutant (Figure 3.6), we tested whether disruption of the DMP machinery would also suppress the miscompartmentalization defect in Δ*spoIIIM* Δ*pbpG* cells. To test this, we introduced deletions of both *spoIID* and *spoIIP* into Δ*spoIIIM* and Δ*spoIIIM* Δ*pbpG* mutant strains containing a forespore-expressed CFP reporter (P_{spoIIQ}-*cfp*). We examined the accumulation of the CFP signal by fluorescence microscopy at T3.5, the time point at which we observed the highest degree of miscompartmentalization in these mutants (Figure 3.5A & C).

Interestingly, we observed that deletion of *spoIID* and *spoIIP* suppressed miscompartmentalization of sporulating cells lacking either *pbpG, spoIIIM* or both *spoIIIM* and *pbpG* (Figure 3.7A). Furthermore, the degree of miscompartmentalization suppression in the Δ*spoIIIM* Δ*pbpG* mutant background is similar to that of the Δ*spoIIIE* mutant background. These data suggest that the hydrolytic activity of the DMP complex during engulfment leads to forespore miscompartmentalization if cells lack either *spoIIIE*, *pbpG*, *spoIIIM* or both *spoIIIM* and *pbpG.*

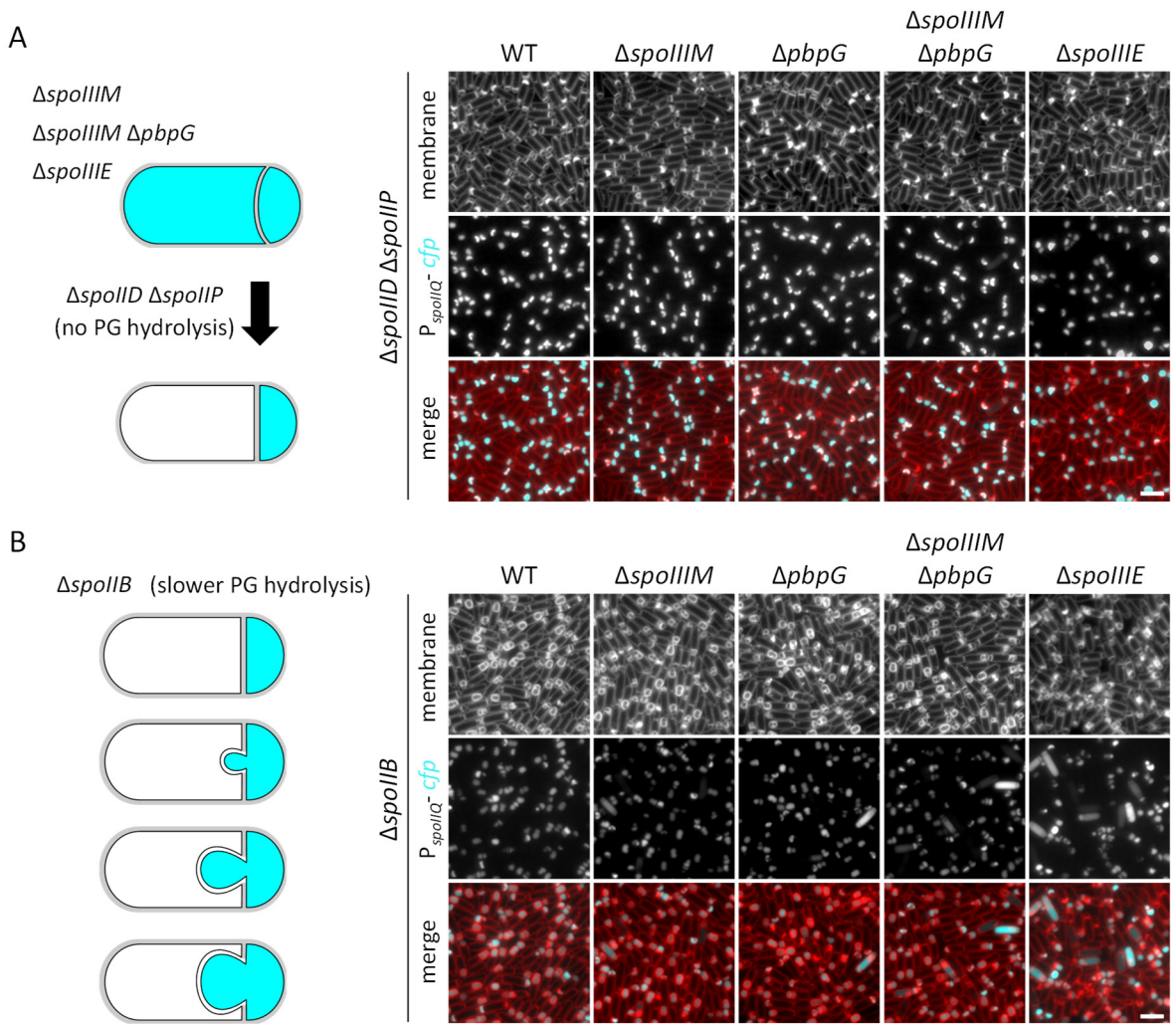

Figure 3.7: Miscompartmentalization suppression by blocking/impairing the DMP complex. (A) Representative images of miscompartmentalization suppression in Δ*spoIID* Δ*spoIIP* double mutant strains at T3: WT (bAT469), Δ*spoIIIM* (bAT470), Δ*pbpG* (bAT471), Δ*spoIIIM* Δ*pbpG* (bAT472) and Δ*spoIIIE* (bAT475). The schematic shows that deletion of *spoIID* and *spoIIP* suppresses miscompartmentalization in Δ*spoIIIM*, Δ*spoIIIM* Δ*pbpG* or Δ*spoIIIE* cells. Scale bar is 2 µm. **(B)** Representative images of miscompartmentalization suppression in Δ*spoIIB* mutant strains at T3; WT (bAT604), Δ*spoIIIM* (bAT605), Δ*pbpG* (bAT606), Δ*spoIIIM* Δ*pbpG* (bAT607) and Δ*spoIIIE* (bAT608). The schematic shows that deletion of *spoIIB* results in bulge formation and also suppresses miscompartmentalization. Scale bar is 2 µm.

To further investigate the effect of PG hydrolysis on forespore compartmentalization in cells lacking either *spoIIIE*, *spoIIIM* or *spoIIIM* and *pbpG*, we employed a different strategy to compromise DMP activity without deleting the DMP proteins. To do this, we compromised the localization of the DMP complex by deleting a gene called *spoIIB*. SpoIIB plays a semi-redundant role in recruiting the DMP complex to the sporulation septum (Perez *et al*., 2000; Aung *et al*., 2007). Cells lacking *spoIIB* partially localize the DMP complex to the septum, resulting in a slower rate of PG hydrolysis (Perez *et al*., 2000). This results in abnormal membrane migration during engulfment and large septal bulges that protrude into the mother

cell. Using fluorescence microscopy, we observed that deletion of *spoIIB* in Δ*spoIIIM* cells markedly reduced forespore miscompartmentalization (Figure 3.7B). Similarly, combining the Δ*spoIIB* mutant with the Δ*spoIIIM* Δ*pbpG* or Δ*spoIIIE* mutants resulted in dramatic reduction in the proportion of miscompartmentalized cells (Figure 3.7B). These data suggest that slowing down the rate of PG hydrolysis also suppresses miscompartmentalization in the Δ*spoIIIM* Δ*pbpG* mutant. Altogether, these data indicate that the miscompartmentalization defect of Δ*spoIIIM* Δ*pbpG* sporulating forespores occurs due to activity of the DMP complex.

3.3.7 Absence of SpoIIIM or PbpG exacerbates miscompartmentalization of a *spoIIIE* hypomorph

The above data suggest that sporulating cells lacking either *spoIIIE* or both *spoIIIM* and *pbpG* produce similar phenotypes in forespore morphology, forespore miscompartmentalization and suppression of miscompartmentalization. These data support the hypothesis that SpoIIIM and PbpG, together with SpoIIIE, function in a mechanism that maintains forespore morphology and compartmentalization during engulfment. To test this idea further, we took advantage of a hypomorphic allele of *spoIIIE* (SpoIIIE^{D584A}) that pumps the chromosome into the forespore slowly and exhibits miscompartmentalization in a small fraction of sporulating cells (Burton *et al*., 2007). If SpoIIIE, SpoIIIM and PbpG contribute to the same mechanism, deletion of *spoIIIM* and *pbpG* will aggravate the defects of the SpoIIIE^{D584A} allele, resulting in severe miscompartmentalization. To test this, we introduced the SpoIIIE^{D584A} allele, as a sole source of SpoIIIE, into cells lacking *spoIIIM* and/or *pbpG*. We used fluorescence microscopy to follow the accumulation of the CFP signal within the forespore throughout a sporulation time-course.

As previously reported, SpoIIIE^{D584A} (otherwise-WT) was able to maintain compartmentalization in most cells (Figure 3.8A & C). In support of our hypothesis, introducing the SpoIIIE^{D584A} allele into the Δ*spoIIIM* or Δ*pbpG* mutants resulted in a dramatic increase in miscompartmentalization. Quantification of miscompartmentalization over the time-course revealed that this phenotype increased over time and reached 94% and 86% in the Δ*spoIIIM* and Δ*pbpG* single mutants, respectively, by T3. (Figure 3.8A & C).

Importantly, in the SpoIIIE^{D584A} background, although cells lacking both Δ*spoIIIM* and Δ*pbpG* reached similar levels of miscompartmentalization compared to the single mutants at T3, we observed miscompartmentalization in virtually all Δ*spoIIIM* Δ*pbpG* sporulating cells from much earlier time-points (T1.5, 92%) (Figure 3.8A & C).

In this particular experiment, to examine chromosome translocation, we also stained the cells with the DNA dye, SYTOX Orange. Incubating this dye with WT sporulating cells results in an accumulated bright signal in the forespore upon chromosome translocation (Figure 3.8B). Whereas, when chromosome translocation is abolished in cells lacking *spoIIIE*, no bright signal appears in the forespore (Figure 3.8B).

Cells having SpoIIIE^{D584A} (otherwise-WT) showed accumulation of the DNA dye in most of the forespores, indicating chromosome translocation in a large proportion of cells (Figure 3.8C). Interestingly, in the Δ*spoIIIM* or Δ*pbpG* single mutants harboring the SpoIIIE^{D584A} allele, fewer cells showed bright DNA staining in their forespores (Figure 3.8C).

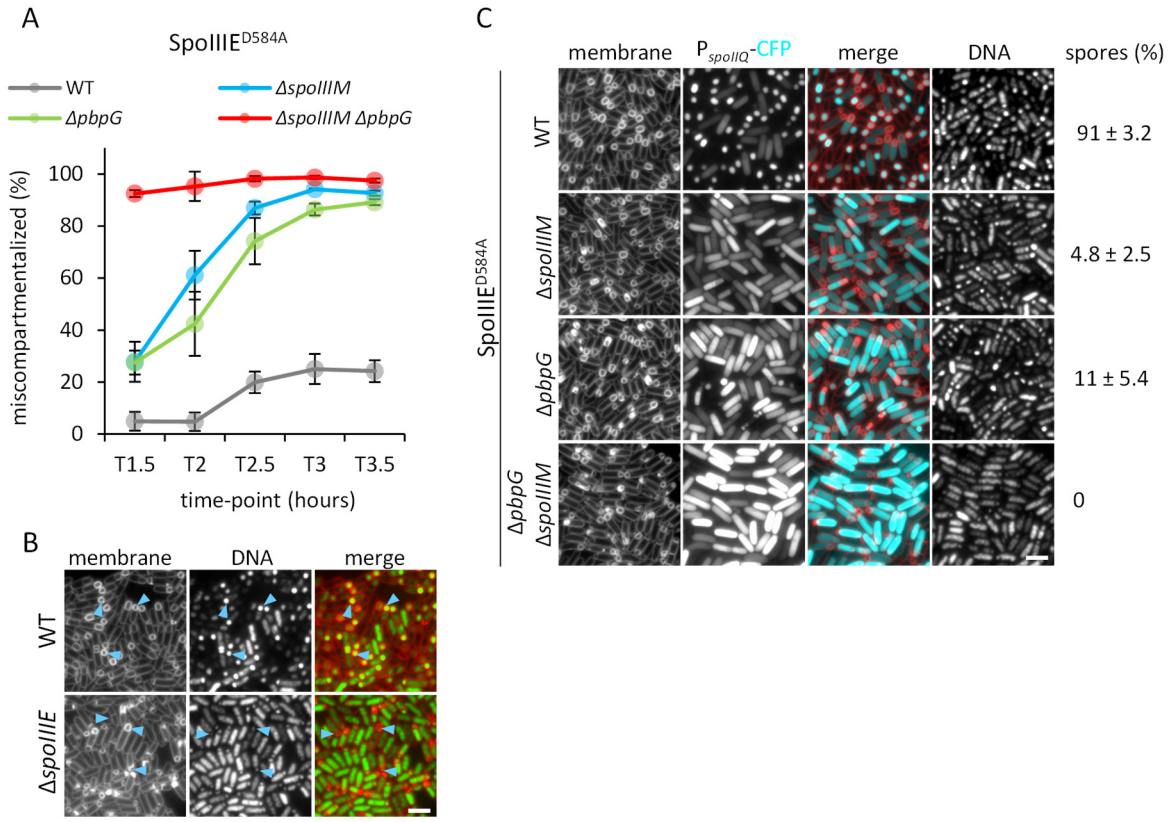

Figure 3.8: Genetic relationship between both SpoIIIM and PbpG, and SpoIIIE. (A) Average frequency of miscompartmentalized cells during a sporulation time-course in the SpoIIIE^{D584A} mutant in otherwise-WT (bAT498, grey), Δ*spoIIIM* (bAT499, blue), Δ*pbpG* (bAT500, green) and Δ*spoIIIM* Δ*pbpG* (bAT501, red) strains. Error bars for each time-point are standard deviation of the population of 3 biological replicates (n>800 per time-course, per strain, per biological replicate). **(B)** Representative images of WT (bAT87) and Δ*spoIIIE* (bAT457) showing chromosome translocation after incubation for 1 hr with the DNA dye, SYTOX Orange. In the WT, the blue arrowheads refer to the bright signal accumulation in the forespores upon chromosome translocation, while the Δ*spoIIIE* mutant fails to show the same degree of signal accumulation in the forespores. Scale bar is 2 µm. **(C)** Representative images of miscompartmentalization in the SpoIIIE^{D584A} mutant in otherwise-WT (bAT498), Δ*spoIIIM* (bAT499), Δ*pbpG* (bAT500) and Δ*spoIIIM* Δ*pbpG* (bAT501) strains at T3.5. DNA is visualized by SYTOX Orange staining. Scale bar is 2 µm. Sporulation efficiency using exhaustion method of otherwise-WT (bAT498), Δ*spoIIIM* (bAT499), Δ*pbpG* (bAT500) and Δ*spoIIIM* Δ*pbpG* (bAT501) strains. The sporulation efficiency data are average (± SD) of 3 biological replicates.

Furthermore, in the Δ*spoIIIM* Δ*pbpG* double mutant harboring the SpoIIIE^{D584A} allele, even fewer cells displayed bright DNA staining in the forespore (Figure 3.8C). This suggests that combining the SpoIIIE^{D584A} allele with the Δ*spoIIIM* or Δ*pbpG* mutant, or both, results in failure to translocate the chromosome in a large proportion of cells.

Finally, we also examined the sporulation efficiency of the different mutants harboring the SpoIIIE^{D584A} allele, using the heat-kill assay. As expected, cells with SpoIIIE^{D584A} alone sporulated with 91% sporulation efficiency relative to WT (Figure 3.8C). Addition of the Δ*spoIIIM* and Δ*pbpG* mutants to this background showed sporulation efficiencies of 4.8% and 11%, respectively, relative to WT. Furthermore, consistent with the microscopy images, the Δ*spoIIIM* Δ*pbpG* mutant combined with the SpoIIIE^{D584A} allele failed to produce viable mature spores (Figure 3.8C).

These results show that combining the SpoIIIE^{D584A} mutant with either Δ*spoIIIM,* Δ*pbpG* or both Δ*spoIIIM* and Δ*pbpG* causes an exacerbation in their miscompartmentalization and sporulation phenotype and appears to also lead to a defect in chromosome translocation into the forespore. These data suggest that SpoIIIM and PbpG may function directly or indirectly with SpoIIIE in maintaining forespore shape, compartmentalization and chromosome translocation.

3.4 Discussion

In this chapter, we identified *spoIIIM*, a gene of previously unknown function, as an important factor in the maintenance of forespore cytoplasmic compartmentalization during engulfment. Our data indicate that SpoIIIM plays a more important role in spore development in cells lacking the forespore class A PG synthase PbpG, and together these proteins are critical in maintaining forespore morphology and cytoplasmic compartmentalization. Importantly, our data further suggest that the Δ*spoIIIM* Δ*pbpG* double mutant phenotype is similar to that of the Δ*spoIIIE* mutant. Furthermore, just like what has been observed in the Δ*spoIIIE* mutant (Hilbert *et al*., 2004), we found that PG hydrolysis is what causes forespore miscompartmentalization in the Δ*spoIIIM* Δ*pbpG* double mutant. The significance of the phenotypes exhibited by the Δ*spoIIIM* Δ*pbpG* double mutant and how they may relate to SpoIIIE function or other developmental processes is discussed.

3.4.1 Possible models for how SpoIIIM and PbpG might contribute to the early stages of spore development

Our data suggest that SpoIIIM and PbpG contribute to forespore size, morphology, and compartmentalization. Although the phenotypes reported in this chapter for the Δ*spoIIIM* Δ*pbpG* double mutant are very similar to those of the Δ*spoIIIE* mutant, somewhat similar phenotypes have also been reported previously for mutants of genes encoding the A-Q complex and genes required for engulfment. Thus, it is important to consider possible working models, and their likelihood, for how SpoIIIM and PbpG might contribute to these processes.

Model 1: SpoIIIM and PbpG participate in the A-Q complex

One model is that SpoIIIM and PbpG contribute to the role of the A-Q complex in maintaining forespore size. The A-Q complex is essential for forespore size and transcriptional potential. (Broder & Pogliano, 2006; Doan *et al*., 2009; Ojkic *et al*., 2014). Previously, small forespores were reported in cells lacking any of the A-Q complex genes (Doan *et al*., 2009; Rodrigues *et al*., 2013, 2016b). Although the small deformed forespores of Δ*spoIIIM* Δ*pbpG* cells are somewhat similar in size to forespores of A-Q complex mutants, the A-Q complex mutants do not exhibit miscompartmentalization (Doan *et al*., 2009; Rodrigues *et al*., 2016b). Furthermore, cells lacking both *spoIIIM* and *pbpG* produce various forespore morphologies (e.g. mislocalized forespores, Figure 3.3A) that have not been observed in any mutants of the A-Q complex. Based on these observations, it seems unlikely that SpoIIIM and PbpG function to maintain forespore morphology through the A-Q complex pathway.

Model 2: SpoIIIM localizes the DMP complex to the leading edges during engulfment

An alternative model is that SpoIIIM, through its LysM domain, could potentially function to localize the DMP complex during engulfment. The mislocalization of the DMP complex in the absence of SpoIIIM could potentially result in hydrolysis of the germ cell wall built around the forespore, thereby compromising its integrity, and leading to shape defects and miscompartmentalization. In favour of this model, we found that reducing or blocking PG hydrolysis suppresses miscompartmentalization in cells lacking *spoIIIM* and both *spoIIIM* and *pbpG* (see Figure 3.7A & B). This hypothesis is based on published observations demonstrating that unregulated or mislocalized PG hydrolysis can compromise the integrity of the cell envelope during vegetative growth, leading to cell lysis and death (Vollmer *et al*., 2008; Uehara & Bernhardt, 2011).

It is possible that the LysM domain of SpoIIIM aids in the localization of the DMP complex by interacting with proteins in this complex. Indeed, bacterial LysM domains have been widely implicated in the localization and regulation of many PG hydrolytic enzymes (Frankel & Schneewind, 2012; Hashimoto *et al*., 2012; Bobrovskyy *et al*., 2018). While LysM domains that localize PG hydrolases are generally present as accessory domains of these enzymes (Buist *et al*., 2008; Frankel & Schneewind, 2012; Mesnage *et al*., 2014), in the case of SpoIIIM it might act separately to localize the DMP complex.

Importantly however, it seems unlikely that SpoIIIM functions as a major localization determinant of the DMP complex, since disrupting the localization of the DMP complex would likely lead to defects in septal PG hydrolysis and result in membrane bulges protruding toward the mother cell during engulfment – a characteristic phenotype arising when DMP complex proteins are mislocalized (Perez *et al*., 2000). Since cells lacking *spoIIIM* are able to undergo engulfment and do not form septal membrane bulges (Figure 3.3A), it is unlikely that it functions in this capacity. It is possible, however, that SpoIIIM, through its LysM domain, could ensure the precise localization of the DMP complex to the leading edges of the migrating membrane during engulfment. Consequently, the absence of *spoIIIM* could cause the DMP complex to become more distributed around the forespore, rather than enriched at the leading edges of the engulfing membranes. If so, a mislocalized DMP complex would non-specifically hydrolyze the forespore germ cell wall and potentially create gaps in the PG, causing defects in forespore envelope integrity and miscompartmentalization. Since PbpG is thought to synthesize the germ cell PG around the forespore, in the absence of *pbpG*, it is possible that a

reduction in PG around the forespore would exacerbate the defects caused by the non-specific activity of the mislocalized DMP complex in the absence of SpoIIIM.

Model 3: SpoIIIM and PbpG contribute to chromosome translocation

The effect of SpoIIIM and PbpG on chromosome translocation could be considered as three possible sub-models.

(a) SpoIIIM and PbpG are required for SpoIIIE stability

The first model is that SpoIIIM and PbpG function to maintain forespore morphology and compartmentalization through stabilization of SpoIIIE. This hypothesis is based on previous work, which showed that compromising SpoIIIE stability results in failure to translocate the chromosome and miscompartmentalization (Wu & Errington, 1994; Liu *et al*., 2006; Fleming *et al*., 2010; Lopez-Garrido *et al*., 2018). In favor of this model, we observed striking phenotypic similarities between the forespore phenotypes of cells lacking either *spoIIIE* or *spoIIIM*, *pbpG* and *spoIIIE* (Figure 3.6B). In support of the stability role, the absence of SpoIIIM and PbpG exacerbated the miscompartmentalization and chromosome translocation defects of cells expressing the partially defective SpoIIIE^{D584A} allele (see Figure 3.8A & C). It is possible that in the absence of *spoIIIM* and *pbpG*, SpoIIIE^{D584A} becomes unstable, resulting in a hole/pore in the septum, due to lack of the possible membrane-fusion function of SpoIIIE (Fleming *et al*., 2010), leading to failure to translocate the chromosome and miscompartmentalization. This hypothesis is in keeping with the previous suggestion that the septal hole/pore in cells lacking SpoIIIE enlarges due to the activity of the DMP complex and hence blocking PG hydrolysis should suppress miscompartmentalization (Hilbert *et al*., 2004).

(b) SpoIIIM and PbpG are required for septal membrane fusion

In light of the Membrane Channel Model (Chapter 1, section 1.6.5.2), SpoIIIM and PbpG may be required for efficient fusion of the septal membranes. Previously, it was suggested that SpoIIIE is essential for membrane fusion, and cells lacking *spoIIIE* fail to fuse the septal membranes and hence undergo miscompartmentalization (Liu *et al*., 2006; Fleming *et al*., 2010; Shin *et al*., 2015). Accordingly, it is possible that SpoIIIM and PbpG directly function to fuse the septal membrane or indirectly contribute to SpoIIIE's role in septal membrane fusion. Thus, in the absence of *spoIIIM* and *pbpG*, membrane fusion does not occur efficiently, leaving a hole/pore in the septum through which molecules could diffuse through, giving rise to the miscompartmentalization phenotype. As above, blocking PG hydrolysis would prevent septal hole/pore enlargement and thus allow for more efficient membrane fusion. Importantly,

SpoIIIM and PbpG do not appear to have functional domains that are involved in membrane fusion, with PbpG being involved in PG synthesis. This suggests that SpoIIIM and PbpG are unlikely to exert their effect on chromosome translocation and compartmentalization by directly participating in septal membrane fusion.

(c) SpoIIIM and PbpG contribute to PG synthesis to maintain aqueous pore stability

According to the Aqueous Pore Model (Chapter 1, section 1.6.5.1), it is possible that SpoIIIM and PbpG contribute to septal PG synthesis around the pore to maintain its stability during chromosome translocation. Previous work hypothesized that SpoIIIE could interact with PG remodelling machinery to prevent cytokinesis over the translocating chromosome (Fiche *et al*., 2013). Perhaps SpoIIIM and PbpG interact with SpoIIIE and help to remodel PG around the septal pore. Indeed, PbpG is well known to function as a PG synthase that generates the germ cell wall around the forespore (McPherson *et al*., 2001; Scheffers, 2005; Ojkic *et al*., 2016). Interestingly, PG-binding LysM domains have been found to be associated with PG synthesizing proteins or involved in protein-protein interactions (Schanda *et al*., 2014; Caveney *et al*., 2019; Pereira *et al*., 2019). Thus, it is possible that SpoIIIM, via its LysM domain, could promote septal PG synthesis by activating another PG synthase and/or bridge SpoIIIE to the PG to provide more stability to the aqueous pore. This stabilized pore will be tight enough to prevent molecules from diffusing through, and importantly, will accommodate the growing turgor pressure resulting from chromosome translocation into the forespore (Lopez-Garrido *et al*., 2018).

According to this model, the absence of *spoIIIM* and *pbpG* would result in less septal PG, and in the presence of active PG hydrolysis, the pore expands and becomes unstable. This unstable pore would fail to maintain compartmentalization and potentially lead to chromosome translocation defects. Consequently, blocking PG hydrolysis would keep the thick septal PG around the pore and thus maintain pore stability and prevent miscompartmentalization.

The following chapters are aimed at distinguishing between these models.

Chapter 4:

SpoIIIM and PbpG are required for efficient chromosome translocation and chromosome retention within the forespore

4.1 Disclaimer

This is to acknowledge that Ms Johana Luhur has contributed to the work presented in this chapter, in relation to examining and quantifying the chromosome translocation in section 4.3.3 and 4.3.6. Ms Luhur also performed the signal intensity analysis of SpoIIIE-GFP in section 4.3.2.

4.2 Introduction

In the previous chapter, we proposed that SpoIIIM and PbpG could maintain forespore morphology and compartmentalization by contributing to either PG hydrolysis or chromosome translocation through SpoIIIE. Our first model is that SpoIIIM functions to localize the DMP complex to the leading edges of the migrating membranes, thus ensuring specific hydrolysis of PG at this site. In this model, the absence of *spoIIIM* would alter the localization of the DMP complex, resulting in uniform localization around the forespore and degradation of newly-made forespore PG, affecting forespore shape and compartmentalization. These defects are exacerbated when forespore PG synthesis is compromised in the absence of *pbpG*.

The second model is that SpoIIIM and PbpG are involved in forespore compartmentalization and chromosome translocation, through a direct or indirect relationship with SpoIIIE. This model can be subdivided into three separate models:

a) SpoIIIM and PbpG are required for SpoIIIE stability, and in the absence of *spoIIIM pbpG*, SpoIIIE becomes unstable, leaving a hole in the septum through which miscompartmentalization happens.

b) SpoIIIM, PbpG and SpoIIIE contribute to PG synthesis around an aqueous pore, to maintain the integrity and stability of this pore; in this model, the absence of *spoIIIM* and *pbpG* would cause the aqueous pore to expand, disrupting chromosome translocation and resulting in miscompartmentalization.

c) SpoIIIM and PbpG fuse the septal membranes or stimulate the proposed membrane fusion activity by SpoIIIE at the septal membrane. Based on this model, membrane fusion would not occur efficiently in the absence of *spoIIIM pbpG*, resulting in a hole that leads to miscompartmentalization.

In this chapter, we start to distinguish between these models. We demonstrate that SpoIIIM is not required for localizing SpoIID or SpoIIP - the hydrolases of the DMP complex - to the leading edges of the engulfing membranes. Furthermore, we show that SpoIIIM and PbpG are not required for SpoIIIE stability but are instead required for its dispersal around the forespore. Interestingly, we found that SpoIIIM and PbpG are required for efficient chromosome translocation and retention of the chromosome in the forespore. We also observed that cells lacking *spoIIIM pbpG* efflux the chromosome from the forespore in a random fashion.

Importantly, we demonstrate that the chromosome translocation defects of cells lacking *spoIIIM pbpG* could be suppressed by reducing or abolishing the rate of DMP complex activity.

4.3 Results

4.3.1 SpoIIIM and PbpG are not required for localization of either SpoIIP or SpoIID

In Chapter 3, we hypothesized that SpoIIIM maintains forespore morphology and compartmentalization by localizing the DMP complex at the leading edge of the engulfing membrane. According to this hypothesis, SpoIIIM, through its LysM domain, would localize the DMP complex precisely to the leading edge of the migrating membrane. This specific localization is critical to restrict hydrolysis activity to the old mother PG and protect the forespore germ cell wall. Thus, in the context of this model, in the absence of *spoIIIM* the DMP complex would fail to localize to the leading edges of the engulfing membranes and instead digest the newly-made forespore PG, resulting in forespore lysis and miscompartmentalization. In this model, the *spoIIIM* phenotype is exacerbated by the *pbpG* mutant, because in the absence of PbpG there would be less PG behind the engulfing membranes to protect forespore integrity.

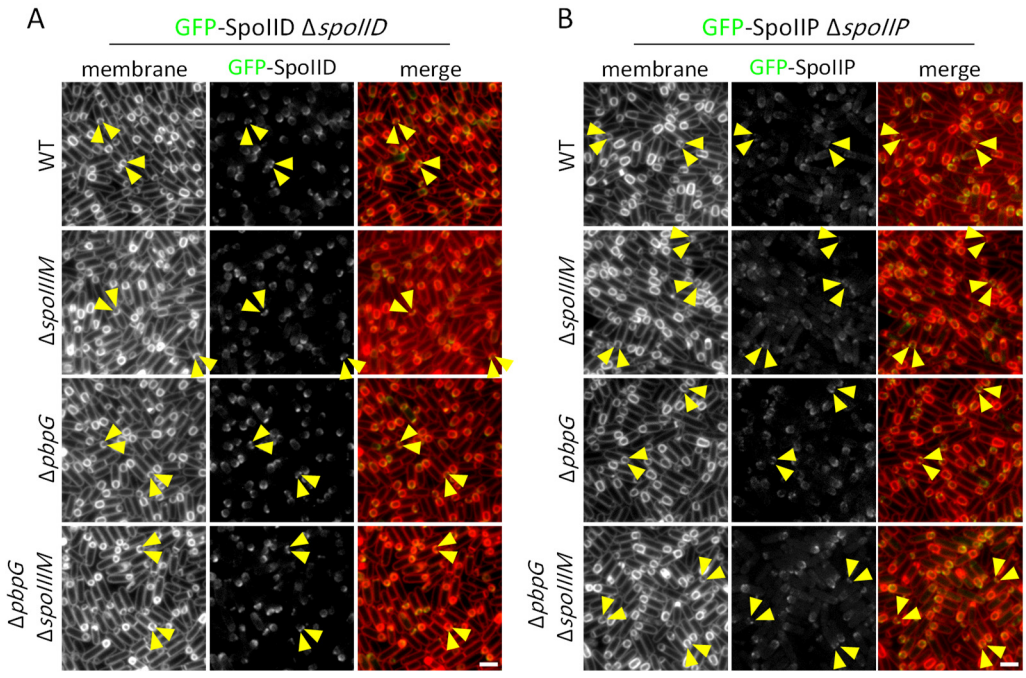

Figure 4.1: SpoIID and SpoIIP localization do not depend on SpoIIIM. (A) Representative images of GFP-SpoIID localization at T2.5 in Δ*spoIID* (bAT200), Δ*spoIID* Δ*spoIIIM* (bAT201), Δ*spoIID* Δ*pbpG* (bAT202) and Δ*spoIID* Δ*spoIIIM* Δ*pbpG* (bAT203) strains. The yellow arrowheads point to GFP-SpoIID that appeared similar in all the genetic backgrounds. Scale bar, 2 μm. **(B)** Representative images of GFP-SpoIIP localization at T2.5 in Δ*spoIIP* (bAT204), Δ*spoIIP* Δ*spoIIIM* (bAT205), Δ*spoIIP* Δ*pbpG* (bAT206) and Δ*spoIIP* Δ*spoIIIM* Δ*pbpG*

(bAT207) strains. The yellow arrowheads point to GFP-SpoIIP that appeared similar in all the genetic backgrounds. Scale bar, 2 μm.

To test our hypothesis, we separately examined the localization of functional GFP-SpoIID and GFP-SpoIIP fluorescent fusions (Aung *et al*., 2007; Chastanet & Losick, 2007), in sporulating cells of WT, Δ*spoIIIM*, Δ*pbpG* and Δ*spoIIIM* Δ*pbpG*. Thus, if SpoIIIM is required for SpoIID and/or SpoIIP enrichment at the leading edges, we would expect the *spoIIIM* mutant to show more localization of GFP-SpoIID or GFP-SpoIIP lagging behind the leading edges of the engulfing membrane and less enrichment at the leading edge.

Consistent with previous work (Aung *et al*., 2007; Chastanet & Losick, 2007), GFP-SpoIID was enriched at the leading edges of the engulfing membrane in WT cells (Figure 4.1A). In the absence of *spoIIIM* or *pbpG*, we did not observe major changes in localization of GFP-SpoIID (Figure 4.1A). Furthermore, GFP-SpoIID localized to the leading edges of engulfing membranes even in the *spoIIIM pbpG* double mutant (Figure 4.1A). Similarly, GFP-SpoIIP localized to the leading edges of engulfing membranes in all genetic backgrounds (Figure 4.1B). Based on these data, and the data presented next, it is unlikely that SpoIIIM contributes to localization of the DMP complex.

4.3.2 SpoIIIM and PbpG are required for the dynamic localization of SpoIIIE

An alternative model proposed in Chapter 3 was that SpoIIIM and PbpG maintain forespore morphology and compartmentalization by contributing to SpoIIIE stability. Thus, in the context of this model, in the absence of *spoIIIM* and *pbpG*, SpoIIIE becomes unstable leaving a hole in the septum through which forespore cytoplasmic contents leak through. This model is based on previous work demonstrating that some SpoIIIE mutant alleles result in unstable SpoIIIE that fail to localize efficiently to the middle of the septum, resulting in opening of the septal pore and miscompartmentalization (Wu & Errington, 1997; Sharp & Pogliano, 1999; Liu *et al*., 2006). To test this hypothesis, we used fluorescence microscopy to monitor the localization of a previously-used and functional SpoIIIE-GFP fluorescent fusion (Burton *et al*., 2007) in WT, Δ*spoIIIM*, Δ*pbpG* and Δ*spoIIIM* Δ*pbpG* strains throughout a sporulation time-course.

In WT cells, SpoIIIE-GFP formed a distinct focus in the middle of the asymmetric septum at T1.5 (Figure 4.2A). This SpoIIIE-GFP focus then moved away from the middle of the septum as engulfment progressed (Figure 4.2A & B). By T3, and when most cells have completed engulfment, the SpoIIIE-GFP focus dissociated in the forespore membrane, with SpoIIIE-GFP

appearing as a dispersed signal (Figure 4.2A, B & C). This pattern of SpoIIIE-GFP localization is consistent with previous observations (Wu & Errington, 1997; Pogliano *et al*., 2003; Liu *et al*., 2006; Burton *et al*., 2007).

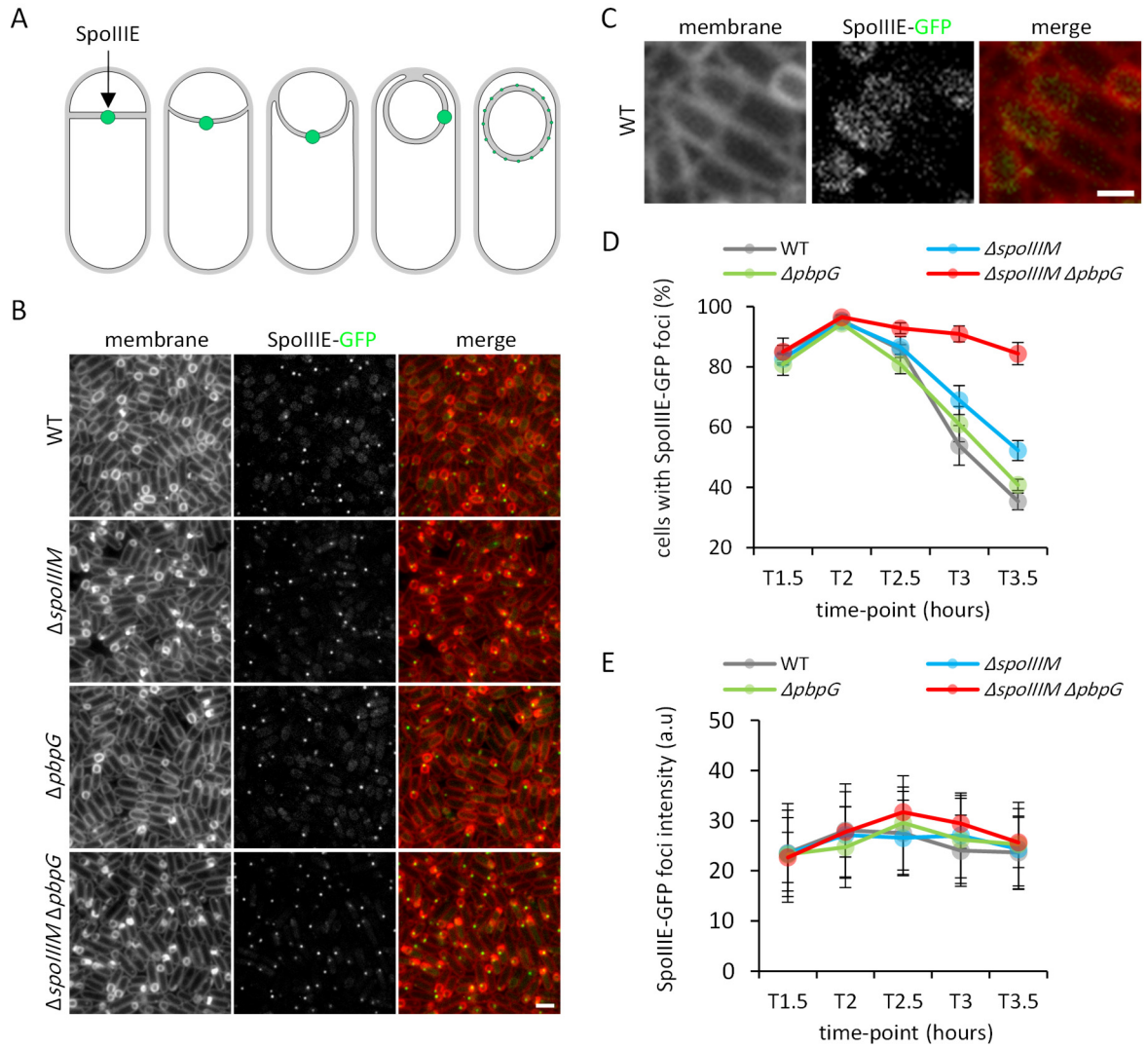

Figure 4.2: SpoIIIE dispersal requires SpoIIIM and PbpG. (A) Schematic illustration of SpoIIIE localization during engulfment. **(B)** Representative images of SpoIIIE-GFP localization in WT (bAT552), Δ*spoIIIM* (bAT553), Δ*pbpG* (bAT554) and Δ*spoIIIM* Δ*pbpG* (bAT555) strains at T3.5. Scale bar is 2 µm. **(C)** Representative image of SpoIIIE foci dispersal in WT (bAT552) cells that have completed engulfment. Scale bar is 1 µm. **(D)** Average frequency of cells with SpoIIIE-GFP foci in WT (bAT552, grey), Δ*spoIIIM* (bAT553, blue), Δ*pbpG* (bAT554, green) and Δ*spoIIIM* Δ*pbpG* (bAT555, red) strains during a sporulation time-course. Error bars for each time-point are standard deviation of 3 biological replicates (n>1000 per time-course, per strain). **(E)** Average fluorescence intensity of SpoIIIE-GFP foci in WT (bAT552, grey), Δ*spoIIIM* (bAT553, blue), Δ*pbpG* (bAT554, green) and Δ*spoIIIM* Δ*pbpG* (bAT555, red) strains during a sporulation time-course. Error bars for each time-point are standard deviation of the population (n>400, per time-point, per strain).

In cells lacking *spoIIIM*, SpoIIIE-GFP initially localized in a similar fashion as WT cells (Figure 4.2A). However, upon engulfment completion, we observed that more cells appeared to still have SpoIIIE-GFP foci, rather than the typical membrane-dispersed SpoIIIE-GFP signal

observed in WT cells (Figure 4.2A& C). To better investigate this observation, we quantified the number of SpoIIIE-GFP foci over the sporulation time-course (Figure 4.2D). While the WT cells showed a decline in the number of cells with SpoIIIE-GFP foci over time, with 35% of the sporulating cells containing SpoIIIE-GFP foci at T3.5, 52% of Δ*spoIIIM* cells still had SpoIIIE-GFP foci at the same time-point (Figure 4.2D). Cells lacking *pbpG* behaved similarly to WT cells, with 40% of the cells having SpoIIIE-GFP foci at T3.5 (Figure 4.2D). Although the Δ*spoIIIM* Δ*pbpG* double mutant cells had almost the same number of SpoIIIE-GFP foci as the WT at the beginning of engulfment (T1.5, T2 and T2.5) (Figure 4.2D), at T3.5 the majority of double mutant cells still had SpoIIIE-GFP foci (84%) (Figure 4.2B & D). These data suggest that SpoIIIM and PbpG are not required for stability of SpoIIIE foci, but are instead required for SpoIIIE foci dispersal, as engulfment nears completion.

To more convincingly demonstrate that SpoIIIE-GFP foci in the Δ*spoIIIM* Δ*pbpG* double mutant are as stable as WT foci, we analyzed the signal intensity of SpoIIIE-GFP foci over a time-course experiment, using unbiased image-segmentation tools (MicrobeJ, Ducret *et al*., 2016) (see Materials and Methods). This quantification showed that SpoIIIE-GFP focus signal intensity is similar in all strains throughout the entire sporulation time-course (Figure 4.2E). This indicates that SpoIIIE-GFP foci in the WT, Δ*spoIIIM,* Δ*pbpG* and Δ*spoIIIM* Δ*pbpG* strains have the same intensity. This further suggests SpoIIIM and PbpG are not required for SpoIIIE stability.

These data indicate that the miscompartmentalization observed in cells lacking *spoIIIM* and/or *pbpG* happens in the presence of stable SpoIIIE, suggesting that SpoIIIM and PbpG play a more direct role in maintaining compartmentalization during spore development.

4.3.3 SpoIIIM and PbpG impact chromosome translocation

The above data demonstrate that SpoIIIM and PbpG do not affect SpoIIIE stability, so we wondered if SpoIIIM and PbpG affect SpoIIIE's activity in forespore chromosome translocation. This possibility seemed likely since we observed in Chapter 3 that the chromosome translocation defect of the SpoIIIE^{D584A} mutant is exacerbated when combined with the *spoIIIM* or *pbpG* mutants (Figure 3.8A). To test this, we stained sporulating cells of WT, Δ*spoIIIM*, Δ*pbpG* and Δ*spoIIIM* Δ*pbpG* with the DNA dye, SYTOX Orange, to examine bulk chromosome translocation (see Chapter 3, section 3.2.7). If SpoIIIM and PbpG affect SpoIIIE-dependent chromosome translocation, we would expect that the mutant strains show fewer forespores containing bright DNA-dye signal. To this end, we examined forespores in

all genetic backgrounds at T3, a time point at which most of the cells would have completed chromosome translocation into the forespore (Burton *et al*., 2007).

As previously shown, the majority of WT sporulating cells displayed bright DNA-staining in the forespore, suggesting efficient chromosome translocation (Figure 4.3). Like the WT cells, the majority of Δ*pbpG* forespores displayed bright DNA-staining (Figure 4.3). Interestingly, some cells of the *spoIIIM* mutant did not show bright DNA-staining in the forespore (Figure 4.3). Strikingly, in the *spoIIIM pbpG* double mutant cells, we observed many forespores without bright DNA signal (Figure 4.3). Qualitatively, these data suggest that SpoIIIM and PbpG together contribute to chromosome translocation.

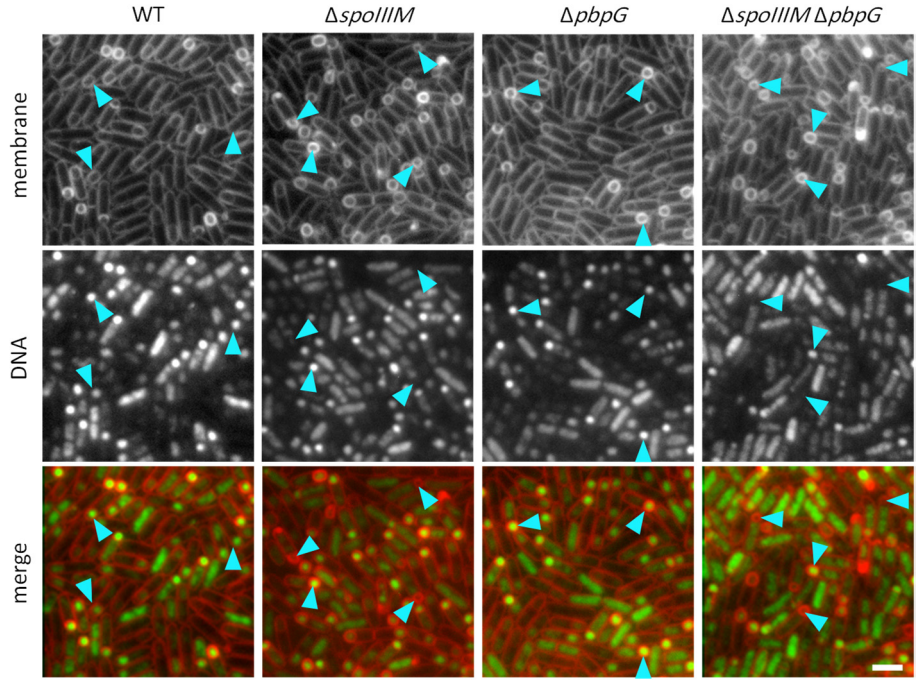

Figure 4.3: SpoIIIM and PbpG affect chromosome translocation into the forespore. Representative images of chromosome translocation in the WT (bDR2413), Δ*spoIIIM* (bCR1592), Δ*pbpG* (bCR1557) and Δ*spoIIIM* Δ*pbpG* (bCR1600) strains, showing chromosome translocation after incubation for 1 hr with the DNA dye, SYTOX Orange. The cyan arrowheads refer to the bright signal accumulation in the forespores upon chromosome translocation, and also point to forespore that do not have the bright signal in the mutant strains. Scale bar is 2 μm.

4.3.4 SpoIIIM and PbpG are required for efficient chromosome translocation and retention of the chromosome in the forespore

Although the DNA staining experiment above suggests that SpoIIIM and PbpG are required for chromosome translocation into the forespore, it was unclear whether SpoIIIE failed to translocate the whole chromosome or parts of it. To quantitatively examine the effect of SpoIIIM and PbpG on chromosome translocation, we used the LacI/*lacO* system, which has

been used previously to examine chromosome translocation during sporulation (Webb *et al*., 1997; Becker & Pogliano, 2007; Kaimer *et al*., 2011; Wang *et al*., 2014). In this system, the DNA-binding repressor fusion, LacI-GFP, binds to the operator sequence, *lacO.* Cells were engineered to express the LacI-GFP fluorescent fusion under the control of a forespore promoter (P_{spoIIQ}; P_{spoIIQ}-*lacI-gfp*) at the *amyE* locus (27.9°) that gets "trapped" in the forespore after asymmetric division (Figure 4.4A) (Khvorova *et al*., 2000; Marquis *et al*., 2008). In addition, the cells also harbor an array of 48 *lacO* repeats inserted at the *pelB* locus (174°) close to the terminus (Figure 4.4A). If the chromosome is successfully translocated into the forespore, LacI-GFP in the forespore would bind to the *lacO*48 sequences near the terminus, resulting in a GFP focus in the forespore (Figure 4.4A). Conversely, cells that fail to translocate the chromosome would fail to produce a GFP focus in the forespore (Figure 4.4A). Using this approach, we examined chromosome translocation in the WT, Δ*spoIIIM*, Δ*pbpG* and Δ*spoIIIM* Δ*pbpG* cells using fluorescence microscopy over a sporulation time-course and quantified the number of forespores with a GFP focus inside (Figure 4.4B). Taking into consideration the forespore miscompartmentalization defect of the Δ*spoIIIM* and Δ*spoIIIM* Δ*pbpG* strains, we would also expect to observe a second GFP focus in the mother cell (Figure 4.4A). Furthermore, if the miscompartmentalized cells fail to translocate the chromosome, we would also expect to observe two GFP foci within the mother cell (Figure 4.4A & D). No GFP foci were observed in most of the cells examined at T1.5, suggesting that chromosome translocation had not yet been completed. Thus, we examined all the stains at T2, T2.5 and T3.

In WT cells, we observed a GFP focus in all forespores by T2, indicating successful chromosome translocation of the *pelB* locus into the forespore (Figure 4.4B). Similar observations were made at the T2.5 and T3 time points (Figure 4.4B & C), suggesting that chromosome translocation happened efficiently, and that no chromosome then leaked back out.

In cells lacking *spoIIIM,* at T2, 97% of the forespores had a GFP focus and only 3% of the population had two GFP foci in the mother cell (Figure 4.4B). These data suggest that most *spoIIIM* mutant cells could complete chromosome translocation, whereas a small subset failed to do so. At T2.5 and at T3, the number of forespores with a GFP focus decreased to 90% and 87%, respectively (Figure 4.4B & C), and the number of cells with two mother cell foci increased to 10% and 13%, respectively. (Figure 4.4B & C). The increase in cells with two mother cell foci indicates that some Δ*spoIIIM* forespores were unable to retain the chromosome inside the forespore, with the chromosome ending back in the mother cell. The failure of some *spoIIIM* mutant cells to retain the chromosome in the forespore could suggest either passive

efflux or reverse translocation of the chromosome back into the mother cell (see next, section 4.3.5).

In cells lacking *pbpG*, throughout the three time-points, most cells had successfully translocated their chromosome into the forespore (Figure 4.4B & C). However, we observed a subset of cells (2%) that failed to retain their chromosome at T3 (Figure 4.4B & C).

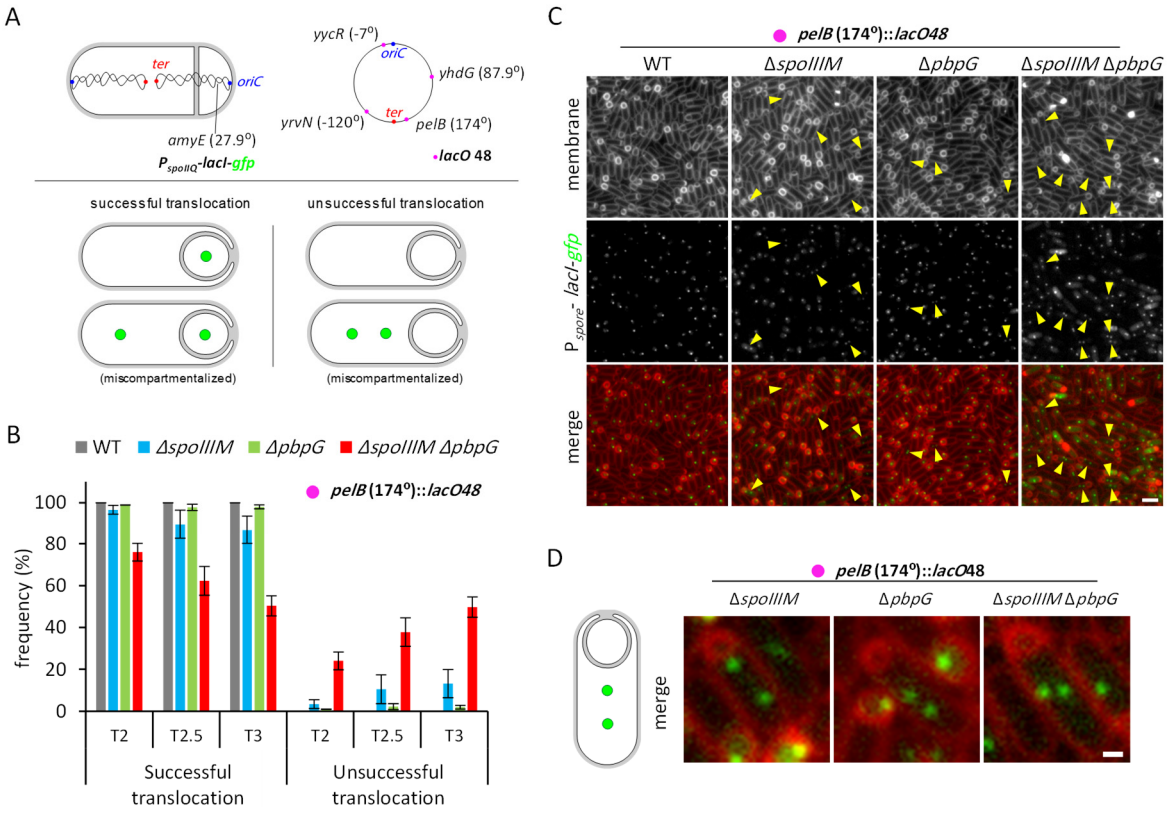

Figure 4.4: Successful chromosome translocation requires SpoIIIM and PbpG. (A) Schematic illustration of experimental rationale using the LacI/*lacO* system for visualizing chromosome translocation. LacI-GFP (green dots), expressed in the forespore (P_{spoIIQ}) from the *amyE* locus, binds to *lacO*48 sites (pink dots) inserted at the *yhdG*, *pelB*, *yrvN* or *yycR* chromosomal locus. The origin (*oriC*) and terminus (*ter*) loci are shown in blue and red, respectively. Successful chromosome translocation is indicated by a LacI-GFP focus in the forespore, with an additional focus in the mother cell compartment in the event of miscompartmentalization. Unsuccessful chromosome translocation is indicated by an absence of LacI-GFP foci, or by two LacI-GFP foci in the mother cell compartment in the event of miscompartmentalization. **(B)** Average frequency of cells with a LacI-GFP focus in the forespore (successful translocation) or with no or two LacI-GFP foci in the mother cell (unsuccessful translocation, expulsion) during a sporulation time-course, with *lacO*48 integrated at the *pelB* locus (174°). **(C)** Representative images of LacI-GFP foci at T3 in WT (bAT646), Δ*spoIIIM* (bAT630), Δ*pbpG* (bAT631) and Δ*spoIIIM* Δ*pbpG* (bAT632) strains containing *lacO*48 inserted at the *pelB* locus (174°). Yellow arrowheads point to cells with two mother cell foci. Scale bar is 2 µm. **(D)** Representative images of cells at T3 with two LacI-GFP foci in the mother cell of Δ*spoIIIM* (bAT630), Δ*pbpG* (bAT631) and Δ*spoIIIM* Δ*pbpG* (bAT632) strains containing *lacO*48 inserted at the *pelB* locus (174°). Scale bar is 1 µm.

Interestingly, in the Δ*spoIIIM* Δ*pbpG* cells, a more dramatic trend was observed: at T2, 76% of the forespores had a GFP focus and 24% showed two GFP foci in the mother cell (Figure 4.4B). This suggests that while many Δ*spoIIIM* Δ*pbpG* cells can translocate the forespore

chromosome, some fail to do so. Importantly, the number of cells with a GFP focus in the forespore dropped to 62% and 50%, at T2.5 and T3, respectively (Figure 4.4B & C). This decrease in the number of cells with forespore GFP foci was accompanied by an increase in the number of cells with two mother GFP foci, 38% and 50% at T2.5 and T3, respectively (Figure 4.4B, C & D). Thus, although many Δ*spoIIIM* Δ*pbpG* sporulating cells initially translocated their chromosome into the forespore, many failed to retain the chromosome there.

The failure of the Δ*spoIIIM* and Δ*spoIIIM* Δ*pbpG* mutants to retain the forespore chromosome led us to wonder if the entire chromosome was being effluxed back into the mother cell. To test this, we engineered the cells to contain *lacO*48 arrays at different positions on the chromosome, *yycR*::-7°, *yhdG*::87° and *yrvN*::-120° (Figure 4.4A). Interestingly, all the strains showed comparable results to what was obtained with *lacO*48 at the *pelB* locus near the terminus (Appendix II; Figure S4.1A, B & C). These findings suggest that the entire chromosome is effluxed or reversely translocated back into the mother cell.

Collectively, these results suggest that SpoIIIE requires SpoIIIM and PbpG to efficiently translocate the chromosome into the forespore. Furthermore, these data raise the possibility that SpoIIIM and PbpG either function to prevent passive chromosome efflux or reverse translocation by SpoIIIE back into the mother cell.

4.3.5 Chromosome translocation defects in Δ*spoIIIM* Δ*pbpG* suggests efflux of the chromosome rather than reverse translocation

The above data suggest that cells lacking *spoIIIM* and *pbpG* fail to retain the entire chromosome in the forespore after chromosome translocation is completed. A similar observation was reported recently in cells where SpoIIIE is degraded shortly after the start of chromosome translocation (Lopez-Garrido *et al*., 2018), with the authors noting two phenotypes. One phenotype is the chromosome being slowly translocated back into the mother cell, at similar rates as forward translocation, referred to as “reverse translocation”; in this instance reverse translocation is mediated by SpoIIIE. The second phenotype is the chromosome being more abruptly expelled out of the forespore, referred to as “chromosome efflux” (Lopez-Garrido *et al*., 2018). In light of this data, we wanted to obtain insight into whether failure to retain the chromosome in the forespore in the absence of SpoIIIM and PbpG was due to reverse chromosome translocation or passive efflux. To test this, we took advantage of a previously characterized strain that contains two different fluorescently-labeled DNA-binding proteins (TetR-CFP and LacI-YFP) produced under the control of a vegetative

promoter (P_{ftsW}) (Wang *et al*., 2014). This strain harbors an array of TetR DNA-binding sequences (*tetO*48) close to the *oriC* (*yycR*::-7°), and an array of LacI DNA-binding sequences (*lacO*48) close the terminus (*pelB*::174°) (Figure 4.5A). Since the expression of TetR-CFP and LacI-YFP is vegetatively-controlled by P_{ftsW}, each of the chromosomes in the sporangium will harbor a CFP focus close to *oriC* and a YFP focus close to the terminus (Figure 4.5A). Using fluorescence microscopy, we imaged the Δ*spoIIIM* Δ*pbpG* cells at T3, the time-point at which we had observed the highest frequency of cells with chromosome retention defects in the Δ*spoIIIM* Δ*pbpG* double mutant (see Figure 4.4). To accurately analyze the foci positions, we only examined cells with four foci (represented by 25%, 30% and 47% of the sporulating cells at T2, T2.5 and T3, respectively).

Interestingly, in the Δ*spoIIIM* Δ*pbpG* cells, we observed different combinations of the CFP and YFP foci positions within the forespore and mother cell; thus we quantified the foci patterns and categorized them as the following, with respect to the forespore:

1) "*oriC* and *ter* inside", representing cells with a CFP and a YFP focus in the forespore, which indicates successful chromosome translocation (Figure 4.5B); 2) "*oriC* and *ter* outside", representing cells with no CFP (*oriC*) or YFP (*ter*) foci in the forespore (i.e. all four foci were observed in the mother cell) (Figure 4.5B), indicating a failure to retain the entire chromosome in the forespore; 3) "*oriC* inside and *ter* outside", representing cells with a single CFP focus (*oriC*) in the forespore, and two YFP foci (*ter*) and a CFP focus (*oriC*) in the mother cell (Figure 4.5B), indicating that the forespore trapped the origin of replication, but failed to translocate or retain the terminus region of the chromosome; and finally 4) "*ter* inside and *oriC* outside", where the YFP focus (*ter*) was inside in forespore and the mother cell had two CFP foci (*oriC*) and one YFP focus (*ter*) (Figure 4.5B). This last phenotype suggests that the forespores could trap the terminus, however, the origin of replication was effluxed to the mother cell, an event that is inconsistent with reverse translocation of the chromosome and more consistent with passive, random efflux of the chromosome.

We observed that 15% of the Δ*spoIIIM* Δ*pbpG* double mutant forespores had both *oriC* and *ter* inside. In contrast, 42% of the double mutant forespores had *oriC* and *ter* outside, as all four foci existed in the mother cell (Figure 4.5B). Furthermore, about 28% of the double mutant forespores contained *oriC* inside and *ter* outside. Interestingly, we found that 15% of the forespores had *ter* inside and *oriC* outside (Figure 4.5B).

These data suggest that in the absence of *spoIIIM pbpG*, the chromosome is likely expelled back into the mother cell in a random fashion rather than reversely translocated out of the forespore.

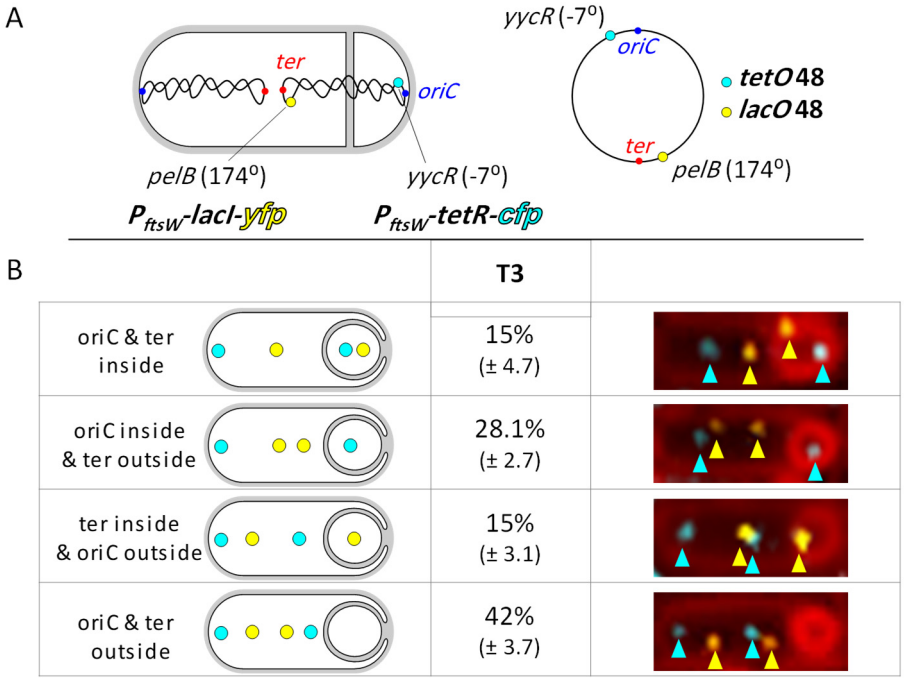

Figure 4.5: The forespore chromosome is effluxed back to the mother cell in the absence of SpoIIIM and PbpG. (A) Schematic illustration of experimental rationale using the LacI/*lacO* and TetR/*tetO* systems for visualizing chromosome translocation and expulsion. Both the LacI-YFP and TetR-CFP are expressed under the vegetative promoter of P_{ftsW}. LacI-YFP binds to *lacO*48 sites (yellow dots) inserted at the *pelB* (174°) locus as a proxy for the chromosomal terminus (*ter*, red). While TetR-CFP binds to *tetO*48 sites (cyan dots) inserted at the *yycR* (-7°) locus as a proxy for the chromosomal origin (*oriC*, blue). **(B)** Quantification of the YFP/CFP foci position patterns in the Δ*spoIIIM* Δ*pbpG* (bAT810) sporangium. The table shows quantification, representative images and schematics of cells containing both *oriC* and *ter* inside the forespore; *oriC* inside and *ter* outside the forespore; *ter* inside and *oriC* outside the forespore; both *oriC* and *ter* outside the forespore, during a sporulation time-course Error bars for each time-point are standard deviation of 3 biological replicates (n>30 per time-point, per biological replicate).

4.3.6 Disrupting PG hydrolysis during engulfment rescues the chromosome translocation defect of cells lacking SpoIIIM and PbpG

In the previous chapter, we demonstrated that PG hydrolysis by the DMP complex in cells lacking either *spoIIIM* or *spoIIIM pbpG* is what causes forespore miscompartmentalization (Chapter 3, section 3.2.6). Thus, we wondered if the activity of the DMP complex is also what leads to the chromosome translocation defect of these mutants. To this end, we employed the same LacI-GFP/*lacO* strategy (described in section 4.2.4) to examine chromosome translocation of the *pelB* locus in cells lacking *spoIIIM, pbpG* and *spoIIIM pbpG* that also lack both *spoIIP* and *spoIID*, during a sporulation time-course.

During the time-course experiment, we observed that virtually all forespores, in all genetic backgrounds, contained a LacI-GFP focus, indicating successful chromosome translocation (Figure 4.6A). Quantification of the number of forespores with a GFP focus over time indicated almost complete suppression of chromosome efflux, in all mutant strains examined (Figure 4.6A). Thus, chromosome translocation happens efficiently in the Δ*spoIIIM* and Δ*spoIIIM* Δ*pbpG* strains when PG hydrolysis is blocked.

Since we were able to suppress the miscompartmentalization defect of the Δ*spoIIIM* and Δ*spoIIIM* Δ*pbpG* strains by slowing down the rate of PG hydrolysis by deleting *spoIIB* (Chapter 3, section 3.2.6), we tested if the *spoIIB* null mutant would also suppress their chromosome translocation defect. To this end, we also used the *lacO*/LacI-GFP system to examine chromosome translocation of the *pelB* locus in cells lacking *spoIIIM, pbpG* and *spoIIIM pbpG* that also lack *spoIIB*. Similar to when *spoIIP* and *spoIID* are deleted, deletion of *spoIIB* almost fully restored successful chromosome translocation in all mutant strains examined (Figure 4.6B).

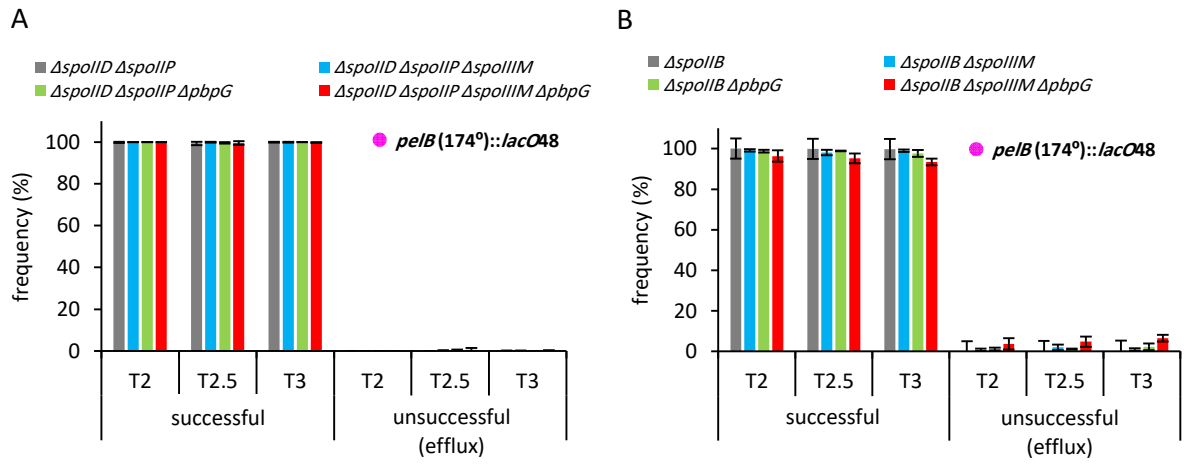

Figure 4.6: Blocking or reducing the rate of PG hydrolysis restores efficient chromosome translocation in the absence of SpoIIIM and PbpG. (A) Average frequency of cells with a LacI-GFP focus in the forespore or with two LacI-GFP foci in the mother cell during a sporulation time-course, with *lacO*48 integrated at the *pelB* locus (174°) in the Δ*spoIID* Δ*spoIIP* double mutant alone (bAT697) or combined with the Δ*spoIIIM* mutant (bAT698), Δ*pbpG* mutant (bAT699) and Δ*pbpG* Δ*spoIIIM* double mutant (bAT700). Error bars for each time-point are standard deviation of 3 biological replicates (n>600 per time-course, per strain, per biological replicate). **(B)** Average frequency of cells with a LacI-GFP focus in the forespore or with two LacI-GFP foci in the mother cell during a sporulation time-course, with *lacO*48 integrated at the *pelB* locus (174°) in the Δ*spoIIB* (bAT668), or Δ*spoIIB* Δ*spoIIIM* mutant (bAT669), Δ*spoIIB* Δ*pbpG* mutant (bAT670) and Δ*spoIIB* Δ*spoIIIM* Δ*pbpG* double mutant (bAT671). Error bars for each time-point are standard deviation of 3 biological replicates (n>600 per time-course, per strain, per biological replicate).

These data suggest that abolishing septal PG hydrolysis, or slowing down its rate, restores chromosome translocation and prevents forespore chromosome efflux into the mother cell in Δ*spoIIIM* and Δ*spoIIIM* Δ*pbpG* cells. Thus, PG hydrolysis by the DMP complex in the absence

of SpoIIIM and PbpG is what leads to chromosome translocation defects. Collectively, these data suggest that SpoIIIM and PbpG are together required for efficient chromosome translocation by counterbalancing the effects of the DMP complex.

4.3.7 SpoIIIM and PbpG counterbalance forespore turgor pressure during active chromosome translocation

Our data so far suggest that SpoIIIM and PbpG are part of a mechanism that counterbalances the effect PG hydrolysis has on forespore compartmentalization and chromosome translocation. This indicates that PG hydrolysis could be detrimental to spore development if not counterbalanced with another pathway that involves both SpoIIIM and PbpG. Several reports suggest that a tight balance between PG hydrolysis and synthesis is required for successful bacterial growth and division (Vollmer *et al*., 2008; Dajkovic *et al*., 2017; Vermassen *et al*., 2019; Sassine *et al*., 2020). Consequently, we hypothesize that SpoIIIM and PbpG function in PG synthesis to maintain the balance with PG hydrolysis during engulfment. This balance becomes more critical as the chromosome is translocated into the forespore, creating turgor pressure on the septal PG. Based on this hypothesis, we reasoned that blocking chromosome translocation would decrease the turgor pressure on septal PG and allow sporulating cells to maintain compartmentalization.

To test this hypothesis, we used a previously characterized SpoIIIE ATPase deficient allele (*spoIIIE36*) that produces a stable SpoIIIE focus, but fails to translocate the chromosome and hence does not generate turgor pressure in the forespore compartment (Wu & Errington, 1994; Sharp & Pogliano, 1999; Besprozvannaya & Burton, 2014). If SpoIIIM and PbpG are required for septal PG synthesis that bears the turgor pressure exerted by the chromosome as it is being translocated into the forespore, we would expect the *spoIIIE36* mutant to suppress, or at least reduce, the miscompartmentalization defect of cells lacking *spoIIIM* and *pbpG*. Using fluorescence microscopy, we examined miscompartmentalization in Δ*spoIIIM*, Δ*pbpG* and Δ*spoIIIM* Δ*pbpG* cells containing the *spoIIIE36* allele.

Consistent with previous reports, *spoIIIE36* (otherwise-WT) was able to maintain compartmentalization throughout the sporulation time-course (Figure 4.7A & B). In Δ*spoIIIM* cells, *spoIIIE36* suppressed miscompartmentalization, with only 14% of the cells exhibiting miscompartmentalization at T3.5 (Figure 4.7A & B, compare to Figure 3.5C, Chapter 3). Interestingly, *spoIIIE36* partially ameliorated the miscompartmentalization defect observed in

Δ*spoIIIM* Δ*pbpG* cells, with only 60% of cells exhibiting miscompartmentalization at T3.5 (Figure 4.7A & B).

Our data here suggest that SpoIIIM and PbpG are required to maintain compartmentalization in the face of turgor pressure resulting from chromosome translocation.

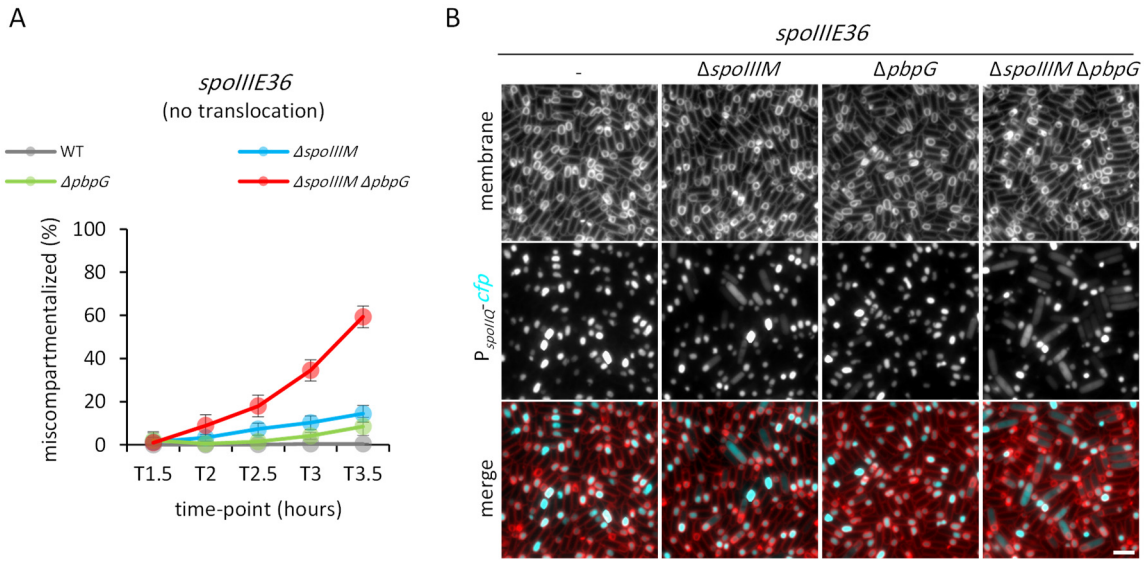

Figure 4.7: Blocking chromosome translocation partially suppresses miscompartmentalization in cells lacking SpoIIIM and PbpG. (A) Average frequency of miscompartmentalized cells during a sporulation time-course in the *spoIIIE36* mutant in otherwise-WT (bAT652, grey), Δ*spoIIIM* (bAT653, blue), Δ*pbpG* (bAT654, green) and Δ*spoIIIM* Δ*pbpG* (bAT655, red*)* strains. Error bars for each time-point are standard deviation of 3 biological replicates (*n*>750 per time-course, per strain). **(B)** Representative images of miscompartmentalization in the *spoIIIE36* mutant in otherwise-WT (bAT652), Δ*spoIIIM* (bAT653), Δ*pbpG* (bAT654) and Δ*spoIIIM* Δ*pbpG* (bAT655*)* strains at T3.5. Scale bar is 2 μm.

4.4 Discussion

In this chapter, we demonstrated that SpoIIIE remains stable in the absence of SpoIIIM and PbpG, suggesting that the forespore miscompartmentalization observed in their absence is not due to SpoIIIE instability, as had been hypothesized in Chapter 3. This important result establishes that forespore miscompartmentalization can occur in the presence of SpoIIIE and that SpoIIIM and PbpG play a more direct role in maintaining compartmentalization. Importantly, we showed that SpoIIIM and PbpG contribute to efficient chromosome translocation into the forespore and retention of the chromosome in the forespore. Furthermore, in cells lacking SpoIIIM and PbpG, we found that the forespore chromosome appears to be effluxed back into the mother cell in a random fashion. Remarkably, our data suggest that the chromosome retention defect observed in the absence of SpoIIIM and PbpG can be suppressed by blocking septal PG hydrolysis. These data point to the possibility that SpoIIIM and PbpG function to counterbalance the effect PG hydrolysis has on a septal pore, through which the chromosome is being translocated into the forespore by SpoIIIE. These observations lead us to propose a model whereby SpoIIIM and PbpG function with SpoIIIE to coordinate chromosome translocation with septal PG remodeling at a septal pore.

4.4.1 How do SpoIIIM and PbpG maintain forespore compartmentalization?

In the previous chapter, we hypothesized that SpoIIIM and PbpG are required for the stability of SpoIIIE (see Discussion 3.3). According to this hypothesis, the absence of SpoIIIM and PbpG would compromise SpoIIIE stability, thereby impacting SpoIIIE's hypothetical role in membrane fission and resulting in a pore in the membrane, leading to miscompartmentalization. In this chapter, our data showed that in cells lacking SpoIIIM and PbpG, SpoIIIE is not degraded but rather appears to reside in active, stable complexes. Thus, the absence of SpoIIIM and PbpG leads to the miscompartmentalization defect independently of SpoIIIE, indicating that SpoIIIM and PbpG likely play a more direct role in maintaining compartmentalization at a septal pore.

Considering the Aqueous Pore model, whereby it was hypothesized that PG remodeling machinery could stabilize the septal pore architecture (Fiche *et al*., 2013), we propose that SpoIIIM and PbpG could function in this capacity by promoting septal PG synthesis around the septal pore during chromosome translocation. The role of PbpG in germ cell PG synthesis is consistent with this idea (McPherson *et al*., 2001; Scheffers, 2005; Ojkic *et al*., 2016). This suggested role of PbpG could be investigated by abolishing its catalytic activity and examining how the lack of PG synthesis by PbpG might impact compartmentalization and chromosome

translocation (see Chapter 6). On the other hand, SpoIIIM could for example, function to regulate or activate PG synthesis through a yet-to-be-defined PBP or stabilize and constrain the septal pore by establishing protein-PG interactions through its PG-binding LysM domain. In support of this role for SpoIIIM, some LysM-containing proteins have been implicated in PG synthesis or protein-PG interactions (Schanda *et al*., 2014; Caveney *et al*., 2019; Pereira *et al*., 2019). Interestingly, it was recently demonstrated that the small proteins, FtsN, DedD and DamX, containing another type of PG binding domain (SPOR domain), stimulate PG synthesis of class A PBPs in *E. coli* (Pazos *et al*., 2020). Thus, it is possible that SpoIIIM functions to promote PG synthesis around the septal pore through its LysM domain. Future investigations using transposon sequencing (Tn-seq) could help to identify the putative PBP that SpoIIIM stimulates.

The data presented in this chapter lead us to propose that SpoIIIM and PbpG are required for maintaining a balance between PG hydrolysis and PG synthesis at a septal pore. In many bacteria, maintaining an optimal balance between PG synthesis and hydrolysis is essential for proper cell growth and division (Hashimoto *et al*., 2012; Lee & Huang, 2013; Sassine *et al*., 2020). Disruption of this delicate balance can result in severe shape defects and cell lysis (Vollmer *et al*., 2008; Uehara *et al*., 2009; Cho *et al*., 2014; Vermassen *et al*., 2019). Considering this well-established concept of a need for balanced PG remodeling to maintain the integrity of the bacterial cell, we propose that the absence of SpoIIIM and PbpG would result in less PG synthesis around the septal pore, resulting in expansion of the septal pore at the onset of septal PG hydrolysis by the DMP complex. This model is supported by our data showing that deletion of SpoIID and SpoIIP to block PG hydrolysis suppresses the miscompartmentalization defect of cells lacking SpoIIIM and PbpG. Recently, cryo-electron tomography data showed that blocking PG hydrolysis retains the thick septal PG (Khanna *et al*., 2019). Consistent with this report, it is possible that blocking or reducing the efficiency of PG hydrolysis in the absence of SpoIIIM, PbpG and SpoIIIE allows the septal PG to remain thick and stable, thereby constraining the septal pore, making it tight enough to prevent miscompartmentalization of proteins the size of CFP.

4.4.2 How do SpoIIIM and PbpG contribute to efficient chromosome translocation and chromosome retention in the forespore?

In this chapter, we found that SpoIIIE is still able to translocate the chromosome into the forespore in the majority of sporulating cells when SpoIIIM and PbpG are absent. Interestingly, ~50% of the forespores failed to retain the chromosome and the entire chromosome was lost

back to the mother cell (Figure 4.4). One interpretation of this observation is that SpoIIIM and PbpG are required to prevent reverse translocation of the chromosome. Reverse translocation is an aspect of the Membrane Channel Model where SpoIIIE functions as a bidirectional motor (Shin *et al*., 2015; Lopez-Garrido *et al*., 2018). In this model, the mother cell SpoIIIE motor ($SpoIIIE^{mc}$) translocates the chromosome into the forespore, whereas the forespore SpoIIIE motor ($SpoIIIE^{fs}$) reversely translocates the chromosome out of the forespore and back into the mother cell (Sharp & Pogliano, 2002; Shin *et al*., 2015; Lopez-Garrido *et al*., 2018). It was suggested that $SpoIIIE^{fs}$ is held inactive by other proteins to prevent reverse translocation of the chromosome out of the forespore (Lopez-Garrido *et al*., 2018). As pointed out in the Introduction, there are conflicting data as to whether SpoIIIE exists on one or both sides of a fused septal membrane (section 1.6.4), if the septal membranes are at all fused during chromosome translocation, as our data otherwise suggest. Nonetheless, if we entertain the Membrane Channel Model and consider the results presented in this chapter in the context of this model, it is tempting to propose that PbpG from the forespore side functions to keep $SpoIIIE^{fs}$ inactive.

Based on the following points, however, we think it is unlikely that PbpG functions to prevent reverse chromosome translocation. Firstly, only a small subset of Δ*pbpG* cells exhibited the forespore chromosome retention defect, which suggests that PbpG is unlikely to function as an inhibitor of $SpoIIIE^{fs}$. Secondly, we observed that chromosome translocation happened successfully in many of the Δ*spoIIIM* Δ*pbpG* forespores at the beginning of engulfment and only afterwards did we observe the chromosome retention defect (Figure 4.4). Thus, it is hard to reconcile these observations with reverse translocation; i.e. if reverse translocation was occurring in this genetic background we would have expected a larger fraction of cells to fail to translocate the chromosome right from the beginning of engulfment. Third, the examination of *oriC*- and *ter*-labelled chromosomes in the *spoIIIM pbpG* double mutant showed that in some cells the *ter* region of the chromosome was retained inside the forespore, while the *oriC* region ended up back in the mother cell (Figure 4.5). This pattern of chromosome loss to the mother cell is inconsistent with a reverse translocation process, unless reverse translocation occurs by a different mechanism that initiates reverse translocation of the origin first and then the terminus. Thus, based on our data, we suggest a simpler model, that the forespore chromosome is effluxed back into the mother cell through a septal pore in a passive manner, that results in random expulsion of different parts of the chromosome.

As with miscompartmentalization data discussed above, we propose that the chromosome is effluxed back into the mother cell in the absence of SpoIIIM and PbpG in a passive manner, through an enlarged septal pore. Chromosome efflux through an enlarged septal pore possibly happens as a result of the build-up of turgor pressure inside the forespore, due to chromosome translocation into the forespore. Indeed, Pogliano and co-workers, based on *in vivo* data and using biophysical modelling (Lopez-Garrido *et al*., 2018), suggested that chromosome translocation into the forespore stretches the septal PG. Thus, the likely reduction of septal PG synthesis due to the absence of SpoIIIM and PbpG makes the forespore unable to sustain this turgor pressure. To redistribute the build-up of pressure occurring in the forespore as a result of chromosome translocation, the forespore loses its chromosome back to the mother cell through the unstable expanding pore. In other words, in the presence of an unstable pore, the forespore cannot sustain the turgor pressure associated with chromosome translocation. Consistent with this hypothesis, we reported that reducing or abolishing the turgor pressure by using the SpoIIIE translocation dead allele, *spoIIIE36*, in cells lacking SpoIIIM and PbpG, partially suppresses the miscompartmentalization defect (Figure 3.8, Chapter 3). Thus, SpoIIIM and PbpG are required to maintain septal pore stability in the face of PG hydrolysis and the turgor pressure resulting from chromosome translocation into the forespore.

4.4.3 A new model: PG remodeling is coordinated with chromosome translocation

Based on the data presented thus far, and the discussion points above, we propose a model where SpoIIIE, SpoIIIM and PbpG coordinate PG remodeling with chromosome translocation at a septal pore (Figure 4.8). In this model, this coordination process possibly occurs through direct interactions between these proteins. We hypothesize that PG synthesis by SpoIIIM and PbpG acts to stabilize the pore at the onset of septal PG hydrolysis by the DMP complex and during translocation of the chromosome. Finally, we also hypothesize that PG synthesis also promotes septal pore closure upon completion of chromosome translocation (Figure 4.8). Interestingly, it was reported in *E. coli* that septal PG synthesis during cell division completes the final steps of constriction and closes the septum in coordination with chromosome segregation by FtsK (Dubarry *et al*., 2010; Coltharp *et al*., 2016; Erickson & Osawa, 2017). Thus, coordination between chromosome translocation and PG synthesis is critical for maintaining balanced PG remodeling in the face of PG hydrolysis at the septum and thus achieves tight compartmentalization, efficient chromosome translocation and chromosome retention in the forespore (Figure 4.8). When SpoIIIM and PbpG are absent, the coordination

between chromosome translocation and PG synthesis is now abolished and leads to unbalanced PG remodeling. Consequently, septal PG hydrolysis leads to septal pore expansion though which miscompartmentalization and chromosome efflux happen (Figure 4.8). Furthermore, in this model SpoIIIM and PbpG also function to maintain pore stability in the face of the chromosome-induced turgor pressure on the forespore PG. To sustain such pressure in the forespore, the septal pore must close immediately upon full chromosome translocation. If not, the septal pore will expand, resulting in chromosome efflux from the forespore and miscompartmentalization of cytoplasmic proteins (Figure 4.5 & Figure 3.5, Chapter 3).

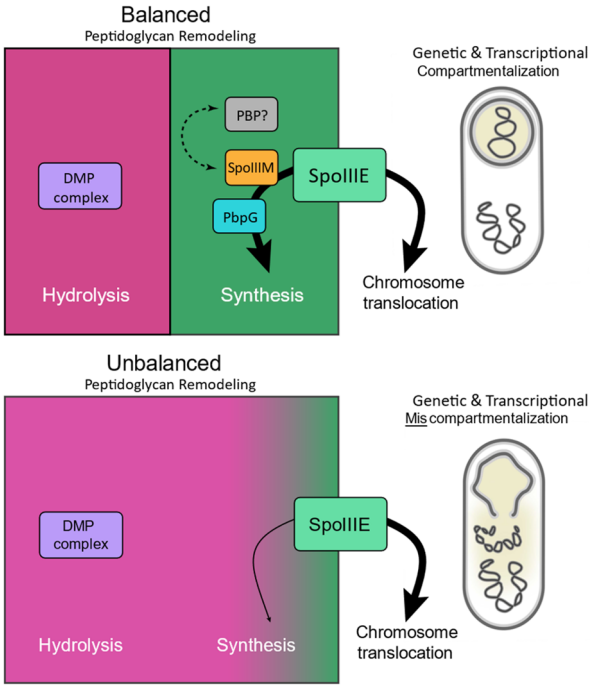

Figure 4.8: Coordination between chromosome translocation and PG synthesis is required for efficient spore development. The top panel shows that SpoIIIE coordinates PG synthesis through SpoIIIM and PbpG, to maintain the balance with PG hydrolysis conducted by the DMP complex. This balanced PG remodeling allows efficient genetic and transcriptional compartmentalization. In the bottom panel, disruption of this coordination in the absence of SpoIIIM and PbpG leads to unbalanced PG remodeling. The hydrolytic activity of the DMP complex leads to miscompartmentalization and chromosome efflux.

4.4.4 Why do SpoIIIE complexes fail to disperse in the absence of SpoIIIM and PbpG?

An intriguing observation we made in this chapter is that SpoIIIE fails to disperse in the forespore membranes when SpoIIIM and PbpG are absent (Figure 4.2). Early during sporulation, SpoIIIE-GFP forms a bright focus in the middle of the asymmetric septum, where the chromosome is trapped (Ben-Yehuda *et al*., 2003a). The SpoIIIE-GFP focus is thought to represent SpoIIIE complexes that are bound to the chromosome (Ben-Yehuda *et al*., 2003a) . Consistent with this idea, if the chromosome is not trapped in the septum (when RacA is absent;

RacA anchors the chromosome to cell poles), SpoIIIE-GFP would fail to assemble into a focus (Ben-Yehuda *et al*., 2003a). As engulfment nears completion, in WT cells, the SpoIIIE-GFP focus disperses (Figure 4.2) (Liu *et al*., 2006), suggesting that SpoIIIE is no longer bound to the chromosome. Since our data showed that SpoIIIE foci failed to disperse in the absence of SpoIIIM and PbpG (Figure 4.2), it is possible that SpoIIIM and PbpG are required for SpoIIIE dispersal (i.e. disassembly from the DNA). It is unclear how SpoIIIM and PbpG could function in this capacity. One possibility is that SpoIIIE somehow senses the septal pore closure and then it disengages from the chromosome and disperses. In the absence of SpoIIIM and PbpG, the septal pore remains open and thus SpoIIIE remains engaged with chromosome, and SpoIIIE complexes fail to disassemble. This possibility requires further investigation to clarify the relationship between SpoIIIM and PbpG with the dispersal of SpoIIIE complexes. One possible experiment is to incubate SpoIIIM and PbpG with the SpoIIIE-DNA complex in an *in vitro* setup to examine if they would stimulate SpoIIIE disassembly from the DNA.

Chapter 5:

Evidence that chromosome translocation occurs through an unfused septal membrane

5.1 Disclaimer

This is to acknowledge that Dr Cécile Morlot, Dr Benoit Gallet and Ms Elda Bauda have contributed to the work presented in this chapter. They helped with transmission electron microscopy of the septal retraction phenotype presented in Figure S5.1 (Appendix III).

5.2 Introduction

The data presented in the previous chapters have led to a model whereby chromosome translocation is coordinated with PG remodelling at a septal pore, to ensure maintenance of cytoplasmic compartmentalization between the mother cell and forespore and to ensure chromosome retention in the forespore. In this model, the septal membrane is not fused during chromosome translocation and the integrity of the septal pore through which the chromosome is translocated is maintained by PG synthesis around the pore and/or protein-PG interactions. Furthermore, in this model SpoIIIE does not function in septal membrane fusion but rather in the recruitment of SpoIIIM and PbpG, which then act to maintain the septal pore by counterbalancing the PG hydrolytic activity of the DMP complex at the septal membrane.

In this chapter, while investigating the role of the SpoIIIAH-SpoIIQ (AH-Q) interaction in compartmentalization, we serendipitously discovered additional evidence that chromosome translocation happens through a pore resulting from an unfused septal membrane. Our data demonstrate that the stability of the unfused septal membrane requires multiple factors including SpoIIIE, SpoIIIM and PbpG, and the AH-Q zipper-like interaction. Remarkably, the absence of SpoIIQ in cells that also lack SpoIIIM, PbpG or SpoIIIE resulted in a phenotype that we denominated septal retraction. Importantly, the septal retraction phenotype is driven by the PG hydrolytic activity of the DMP complex.

Taking advantage of the septal retraction phenotype, and its dependency on PG hydrolysis, we then developed an elegant approach to demonstrate that septal pore closure depends on SpoIIIM and PbpG and that these proteins ensure timely closure of the septal pore upon completion of chromosome translocation. Importantly, using this approach we found that SpoIIIE is not absolutely required for septal pore closure and that cells lacking SpoIIIE complete pore closure over untranslocated DNA. Collectively, these observations support the existence of a septal pore, at which septal PG remodelling is coordinated with chromosome segregation during spore development.

5.3 Results

5.3.1 SpoIIQ is required for septal pore stability in cells lacking PbpG, SpoIIIM or SpoIIIE

In the previous chapters, we showed that reducing the rate of PG hydrolysis (i.e. efficiency of engulfment) by deleting *spoIIB* (a localizer of the DMP complex), could suppress the miscompartmentalization and chromosome translocation defects of sporulating cells lacking

spoIIIM and *pbpG*. To determine if other conditions that reduce engulfment efficiency also suppress the abovementioned defects, we abolished the transenvelope, zipper-like interaction between SpoIIQ and SpoIIIAH, which contributes to the efficiency of engulfment by a ratchet-like mechanism (Blaylock *et al*., 2004; Broder & Pogliano, 2006; Morlot & Rodrigues, 2018) (see Introduction, section 1.5.2). To end this, we examined if deletion of *spoIIQ* could suppress the miscompartmentalization defect observed when SpoIIIM and/or PbpG are absent. We employed fluorescence microscopy to examine miscompartmentalization of the forespore, in cells expressing the CFP reporter (under P_{spoIIQ} control) that harboured the following mutations, during a sporulation time-course: Δ*spoIIQ*, Δ*spoIIQ* Δ*spoIIIM*, Δ*spoIIQ* Δ*pbpG* and Δ*spoIIQ* Δ*spoIIIM* Δ*pbpG*.

As previously reported, in cells lacking *spoIIQ* (otherwise-WT), all forespores were compartmentalized and had a smaller, rounder appearance (Figure 5.1B) (Doan *et al*., 2009; Rodrigues *et al*., 2013, 2016b). In cells lacking both *spoIIQ* and *spoIIIM* we observed a higher frequency of miscompartmentalization compared to cells lacking *spoIIIM* alone (compare to Figure 3.5, Chapter 3). Although the Δ*spoIIQ* Δ*spoIIIM* miscompartmentalized cells expressed the σ^F-dependent CFP signal, the forespore compartment, where σ^F activity occurs and the CFP is transcribed, appeared to be absent in some sporulating cells (Figure 5.1B). Careful inspection of the images revealed remnants of the asymmetric septum in these miscompartmentalized cells, suggesting that these cells initially formed the asymmetric septum and activated σ^F in the forespore compartment but then later the asymmetric septum retracted (Figure 5.1C & D) - we defined this phenotype as “septal retraction” (Figure 5.1C).

To better assess this phenotype, we quantified the number of cells with septal retraction over a sporulation time-course (Figure 5.1E). We found that almost 50% of the Δ*spoIIQ* Δ*spoIIIM* cells had septal retraction by T3 (Figure 5.1B & E). Similarly, the Δ*spoIIQ* Δ*pbpG* cells showed septal retraction in 33% of the cells by T3 (Figure 5.1B & E). Remarkably, the vast majority (98%) of Δ*spoIIQ* Δ*spoIIIM* Δ*pbpG* triple mutant cells exhibited septal retraction at T3 (Figure 5.1B & E). These data suggest that cells lacking SpoIIQ and either SpoIIIM, PbpG or both SpoIIIM and PbpG exhibit defects in septum stability. Since septal retraction is only possible if the septal membrane is not fused, these data importantly point to the possibility that the septum is unfused during chromosome translocation.

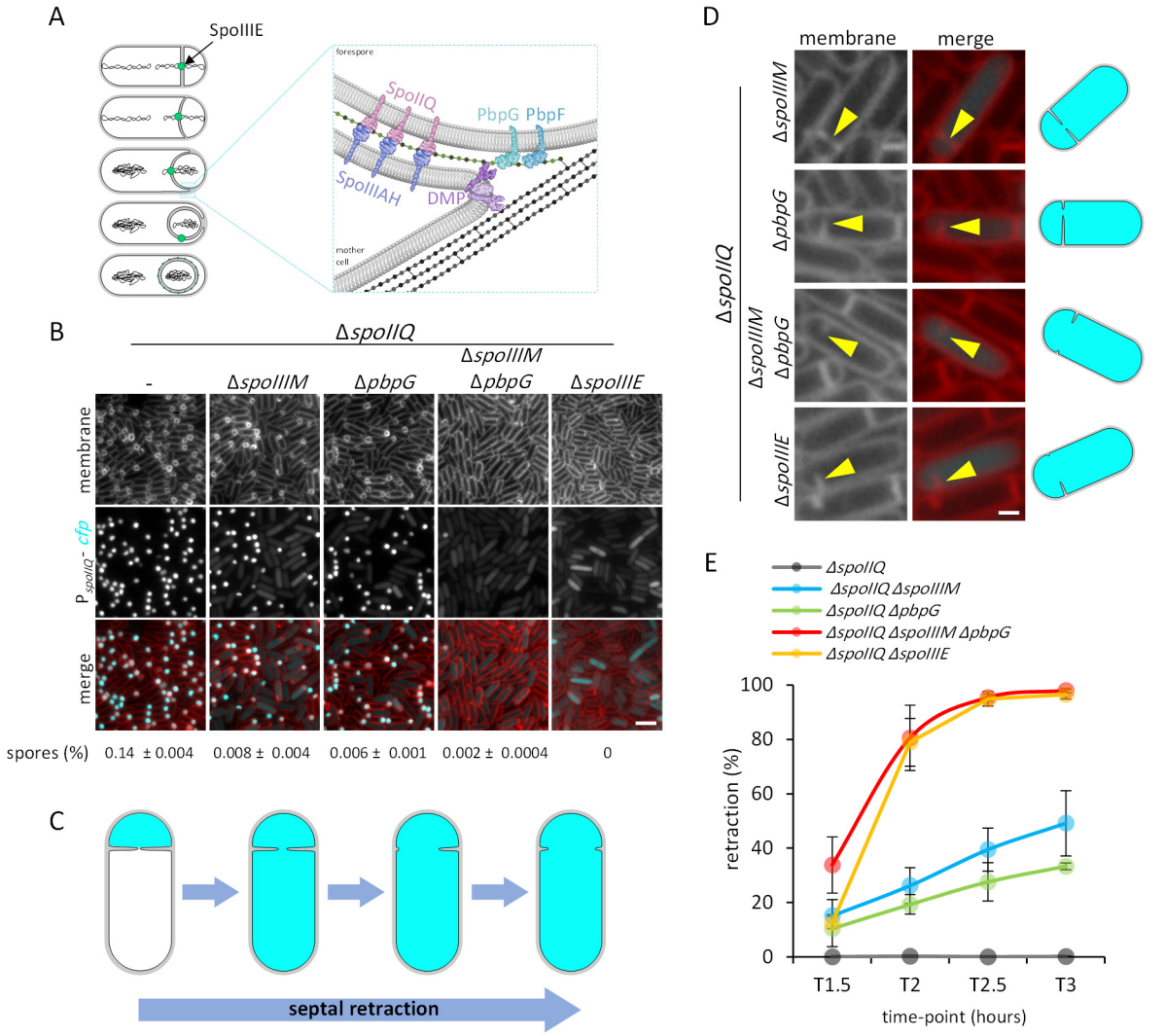

Figure 5.1: Septal stability during engulfment depends on multiple factors. (A) Schematic representation of chromosome translocation and the different stages of engulfment, showing chromosome (black squiggles) and SpoIIIE (green). The zoomed panel shows the processes happening during engulfment at the leading edges, including PG synthesis (green dots and lines) by PbpG (light teal) and PbpF (dark teal) in the forespore membrane, PG hydrolysis by the DMP complex (purple) and the AH-Q interaction across the engulfing membranes. **(B)** Representative images of septal retraction in WT (bAT478), Δ*spoIIIM* (bAT479), Δ*pbpG* (bAT480), Δ*spoIIIM* Δ*pbpG* (bAT481) and Δ*spoIIIE* (bAT476) strains in a Δ*spoIIQ* background at T3. Scale bar is 2 µm. Sporulation efficiency (%, average ± STDEV) is shown below the respective strains. Data are from 3 biological replicates. **(C)** Schematic representation of septal retraction, illustrating that as septal retraction progresses, CFP fluorescence (cyan) leaks from the forespore to fill the entire cell. **(D)** Zoomed-in images showing septal retraction in Δ*spoIIQ* Δ*spoIIIM* (bAT491), Δ*spoIIQ* Δ*pbpG* (bAT492), Δ*spoIIQ* Δ*spoIIIM* Δ*pbpG* (bAT493) and Δ*spoIIQ* Δ*spoIIIE* (bAT497) strains at T3. Yellow arrowheads point to retracting septa. Scale bar is 1 µm. Schematic illustrations of cells are shown on the right. **(E)** Average frequency of cells exhibiting septal retraction in Δ*spoIIQ* (bAT490, black), Δ*spoIIQ* Δ*spoIIIM* (bAT491, blue), Δ*spoIIQ* Δ*pbpG* (bAT492, green), Δ*spoIIQ* Δ*spoIIIM* Δ*pbpG* (bAT493, red) and Δ*spoIIQ* Δ*spoIIIE* (bAT497, yellow) strains during a sporulation time-course. Error bars for each time-point are standard deviation of 3 biological replicates (n>600 per time-point, per strain, per biological replicate).

Based on the phenotypic similarity between cells lacking *spoIIIM pbpG* and cells lacking *spoIIIE*, we wondered if the double mutant of *spoIIQ spoIIIE* would also result in septal retraction like Δ*spoIIQ* Δ*spoIIIM* Δ*pbpG* triple mutant cells. To address this, we expressed

CFP under the control of a forespore promoter (P_{spoIIQ}) in Δ*spoIIQ* Δ*spoIIIE* sporulating cells and examined the cells using fluorescence microscopy during a sporulation time-course. Interestingly, we observed that just like the Δ*spoIIQ* Δ*spoIIIM* Δ*pbpG* cells, the vast majority of the Δ*spoIIQ* Δ*spoIIIE* cells (97%) underwent septal retraction by T3 and had remnants of retracted septa (Figure 5.1B & E).

To visualize the septal retraction phenotype in more detail, we employed transmission electron microscopy (TEM) to examine the Δ*spoIIQ*, Δ*spoIIQ* Δ*spoIIIM* Δ*pbpG* and Δ*spoIIQ* Δ*spoIIIE* strains at T3, when most cells exhibit septal retraction. Consistent with the fluorescence microscopy images, we observed septal retraction within the cells of Δ*spoIIQ* Δ*spoIIIM* Δ*pbpG* or Δ*spoIIQ* Δ*spoIIIE* (Appendix III, Figure S5.1). The TEM images in the Δ*spoIIQ* Δ*spoIIIM* Δ*pbpG* or Δ*spoIIQ* Δ*spoIIIE* cells showed that the retracted membranes had a distorted appearance or resembled the incomplete septa observed in the *spoIIQ* mutant cells, which do not exhibit the septal retraction phenotype (Appendix III, Figure S5.1).

Finally, to determine the effect of septal retraction on spore formation, we tested the sporulation efficiency of the above examined mutants. We found that the triple mutant strain of Δ*spoIIQ* Δ*spoIIIM* Δ*pbpG* formed very few heat-resistant spores (0.002% relative to the WT) (Figure 5.1B), whereas the Δ*spoIIQ* Δ*spoIIIE* mutant strain failed to produce any mature spores (Figure 5.1B). Thus, this phenotype almost completely abolishes spore development in the Δ*spoIIQ* Δ*spoIIIM* Δ*pbpG* triple mutant.

Collectively, these observations suggest that septum stability requires SpoIIQ, SpoIIIE, SpoIIIM and PbpG. Importantly, the septal retraction phenotype also suggests that the septal membranes are unfused during chromosome translocation into the forespore.

5.3.2 Compromising the activity of the A-Q complex does not lead to septal retraction

Since the AH-Q transenvelope interaction is an integral part of the A-Q complex and plays an important role in the localization and assembly of this complex (Doan *et al*., 2009; Rodrigues *et al*., 2016a; Morlot & Rodrigues, 2018), we wondered if the septal retraction phenotype happens as a result of disrupting the AH-Q interaction itself or due to a defective A-Q complex. To this end, we deleted *spoIIIAA*, that encodes for the cytoplasmic ATPase of the A-Q complex and is required for the activity of this complex (Meisner *et al*., 2008; Doan *et al*., 2009), in cells lacking *spoIIIM, pbpG* or both. We used fluorescence microscopy to examine septal retraction

in cells of Δ*spoIIIAA*, Δ*spoIIIAA* Δ*spoIIIM*, Δ*spoIIIAA* Δ*pbpG* and Δ*spoIIIAA* Δ*spoIIIM* Δ*pbpG* that harbour the CFP reporter expressed in the forespore (under P_{spoIIQ} control).

Interestingly, we observed that the absence of SpoIIIAA did not lead to septal retraction in any of the genetic backgrounds examined (Figure 5.2). Furthermore, the degree of miscompartmentalization when *spoIIIAA* was deleted in Δ*spoIIIM*, Δ*pbpG* or Δ*spoIIIM* Δ*pbpG* cells was comparable to the miscompartmentalization observed in the Δ*spoIIIM*, Δ*pbpG* or Δ*spoIIIM* Δ*pbpG* cells in an otherwise-WT background (compare Figure 5.2 with Figure 3.5, Chapter 3). This result suggests that septal retraction occurs due to disruption of the AH-Q ratchet interaction and not due to disruption of A-Q complex activity.

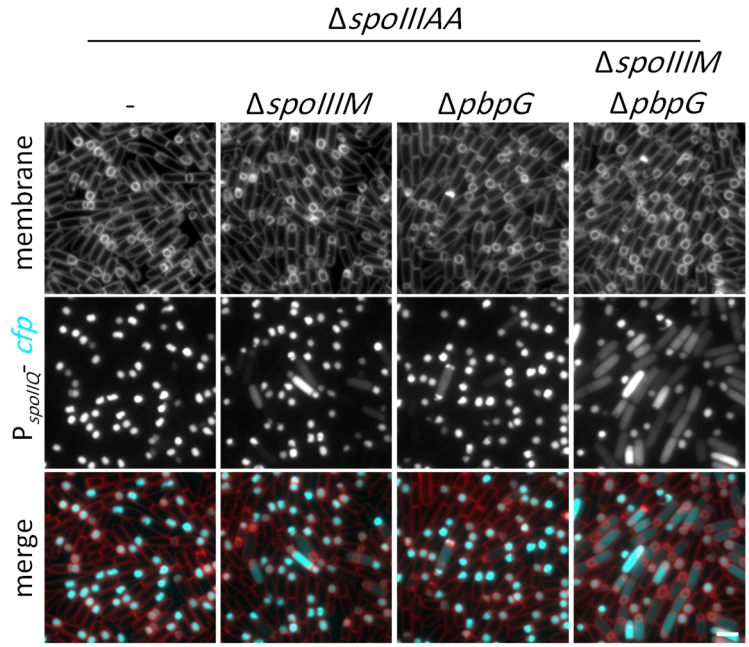

Figure 5.2: Septal retraction does not happen due to defective A-Q complex. Representative images of the effect of a defective A-Q complex on WT (bAT281), Δ*spoIIIM* (bAT283), Δ*pbpG* (bAT285) and Δ*spoIIIM* Δ*pbpG* (bAT287) strains in a Δ*spoIIIAA* background at T3. Scale bar is 2 µm.

5.3.3 Blocking PG hydrolysis suppresses the septal retraction defect

In the previous chapters, we showed that PG hydrolysis by the DMP complex results in a severe miscompartmentalization defect when both *spoIIIM* and *pbpG* are absent. This led us to wonder if PG hydrolysis by the DMP complex could also drive septal retraction. To investigate this hypothesis, we introduced a deletion of both *spoIIP* and *spoIID* in cells lacking *spoIIQ*, *spoIIQ spoIIIM*, *spoIIQ pbpG*, *spoIIQ spoIIIM pbpG* or *spoIIQ spoIIIE*. These strains were also engineered to express CFP under the control of a forespore promoter (P_{spoIIQ}). If PG hydrolysis drives septal retraction, we would expect that blocking PG hydrolysis would prevent this phenotype and restore compartmentalization of the CFP reporter.

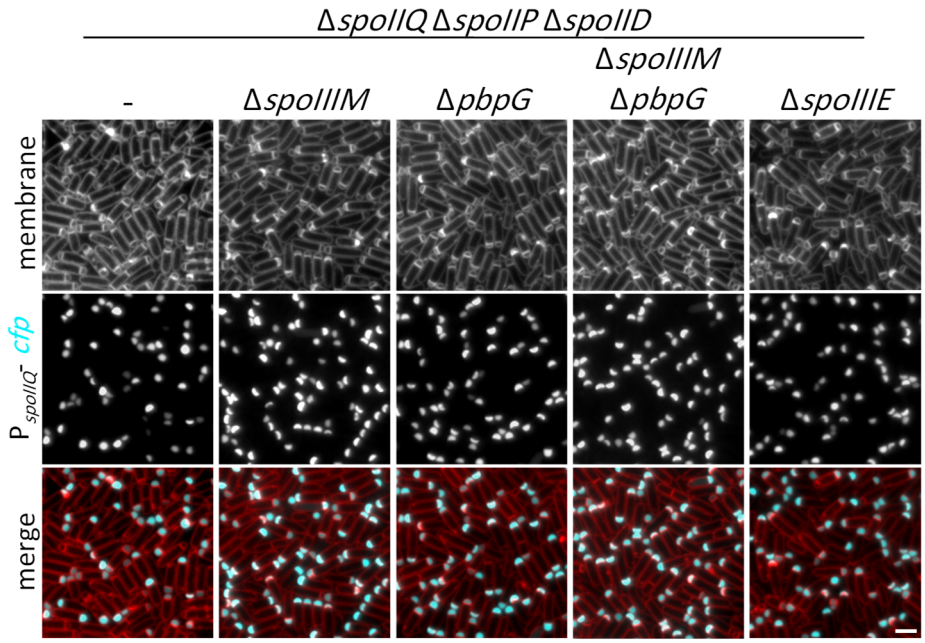

Figure 5.3: Blocking PG hydrolysis prevents septal retraction. Representative images of septal retraction suppression when PG is blocked in WT (bAT490), Δ*spoIIIM* (bAT491), Δ*pbpG* (bAT492), Δ*spoIIIM* Δ*pbpG* (bAT494) and Δ*spoIIIE* (bAT497) strains in a Δ*spoIIQ* Δ*spoIIP* Δ*spoIID* background at T3. Scale bar is 2 μm.

Consistent with the idea that septal retraction occurs due to the activity of the DMP complex PG hydrolases, SpoIID and SpoIIP, our fluorescence microscopy data showed that blocking PG hydrolysis completely supressed the septal retraction phenotype and restored CFP compartmentalization in the forespore compartment, in all the genetic backgrounds (Figure 5.3). This suggests that PG hydrolysis is what leads to septal retraction. Collectively, these results highlight the importance of the AH-Q interaction, SpoIIIE, SpoIIIM and PbpG in the stabilization of the unfused septal membrane during PG hydrolysis by the DMP complex.

5.3.4 SpoIIIE still resides in complexes in cells exhibiting septal retraction

The above data demonstrate that the Δ*spoIIQ* Δ*spoIIIM* Δ*pbpG* triple mutant cells phenocopy the Δ*spoIIQ* Δ*spoIIIE* double mutant cells with regards to septal retraction. This could suggest that SpoIIIE becomes unstable in the absence of SpoIIQ, SpoIIIM and PbpG, leading to septal retraction due to a lack of the proposed SpoIIIE membrane fusion function (Fleming *et al*., 2010). To test this idea, we examined the localization of the previously used SpoIIIE-GFP fluorescent fusion (Figure 4.2, Chapter 4) (Burton *et al*., 2007), expressed as the single source of SpoIIIE, in cells lacking *spoIIQ*, *spoIIQ spoIIIM*, *spoIIQ pbpG* and *spoIIQ spoIIIM pbpG*. If SpoIIIE stability depends on SpoIIQ, SpoIIIM and PbpG, we would expect that in their absence, the SpoIIIE-GFP focus would disappear. We used fluorescence microscopy to visualize the SpoIIIE-GFP focus throughout a sporulation time-course. Since cells exhibiting

septal retraction look quite similar to vegetative cells, we examined SpoIIIE-GFP localization in all cells, sporulating and non-sporulating.

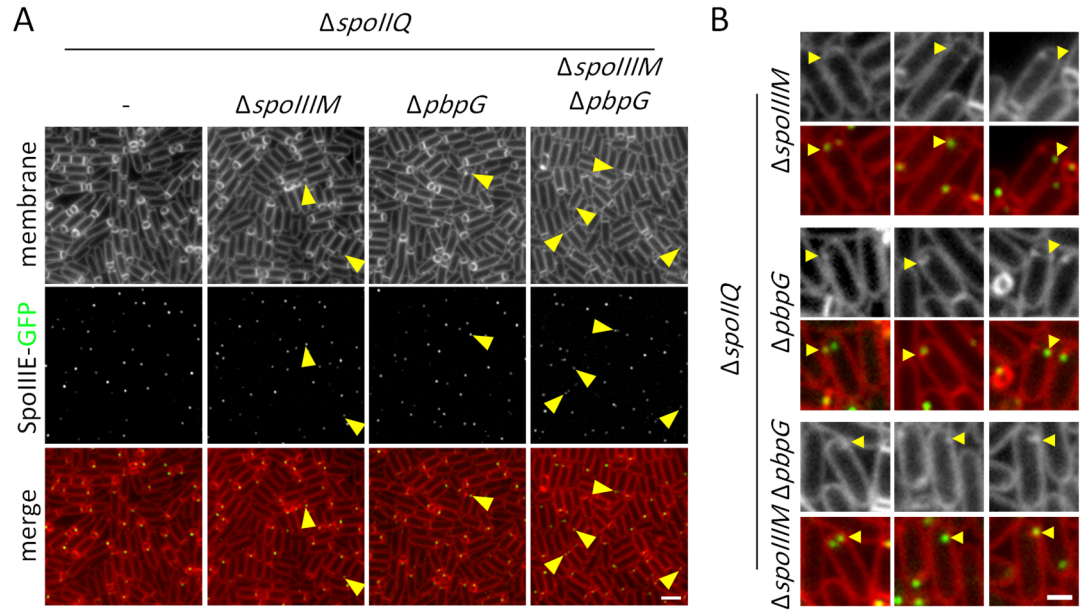

C

Time-point (hours)

SpoIIIE-GFP localization patterns		T2				T2.5				T3			
		ΔQ	ΔQ ΔM	ΔQ ΔG	ΔQ ΔM ΔG	ΔQ	ΔQ ΔM	ΔQ ΔG	ΔQ ΔM ΔG	ΔQ	ΔQ ΔM	ΔQ ΔG	ΔQ ΔM ΔG
vegetative		97.0 (± 1)	82.6 (± 12)	79.8 (± 12)	41.1 (± 6)	97.9 (± 1)	56.9 (± 4)	50.4 (± 8)	8.9 (± 3)	98.2 (± 1)	42.0 (± 7)	32.7 (± 5)	3.1 (± 2)
retraction		0.0 (± 0)	12.6 (± 11)	15.4 (± 11)	**44.7 (± 4)**	0.0 (± 0)	37.5 (± 3)	47.3 (± 9)	**80.8 (± 6)**	0.0 (± 0)	54.3 (± 7)	64.2 (± 6)	**87.3 (± 3)**
		0.0 (± 0)	1.7 (± 2)	0.8 (± 1)	**9.7 (± 3)**	0.0 (± 0)	2.6 (± 1)	0.9 (± 0.2)	**8.9 (± 2)**	0.8 (± 1)	2.8 (± 2)	2.4 (± 1)	**8.3 (± 2)**
vegetative		2.2 (± 1)	1.8 (± 1)	2.3 (± 0.3)	2.8 (± 1)	1.6 (± 0.4)	1.1 (± 0.5)	0.9 (± 1)	1.1 (± 2)	1.0 (± 0.3)	0.5 (± 0.2)	0.7 (± 1)	1.2 (± 1)
		0.8 (± 0.5)	1.3 (± 0.2)	1.7 (± 0.4)	1.7 (± 1.3)	0.5 (± 0.4)	1.8 (± 0.3)	0.5 (± 0.2)	0.3 (± 0.2)	0.0 (± 0)	0.4 (±1)	0.0 (± 0)	0.1 (± 0.2)

Figure 5.4: SpoIIIE still resides in complexes in cells with septal retraction. (A) Representative images of SpoIIIE-GFP localization in the Δ*spoIIQ* (bAT558), Δ*spoIIQ* Δ*spoIIIM* (bAT559), Δ*spoIIQ* Δ*pbpG* (bAT560) and Δ*spoIIQ* Δ*spoIIIM* Δ*pbpG* (bAT561) strains in a Δ*spoIIIE* mutant background at 2 hrs after the onset of sporulation (T2). Yellow arrowheads point to SpoIIIE-GFP localization in septal retracted cells. Scale bar is 2 µm. **(B)** Zoomed-in, representative examples of SpoIIIE-GFP localization as foci in retracted septa in the Δ*spoIIQ* mutant combined with Δ*spoIIIM* (bAT559), Δ*pbpG* (bAT560) and Δ*spoIIIM* Δ*pbpG* (bAT561) at 3 hrs after the onset of sporulation (T3). Yellow arrowheads point to retracting septa containing SpoIIIE-GFP. Scale bar is 1 µm. **(C)** Frequency of SpoIIIE-GFP localization patterns (average of 3 biological replicates, ± STDEV; *n*>150, per strain, per time-point, per biological replicate) at 2 (T2), 2.5 (T2.5) and 3 hrs (T3) after the onset of sporulation in the Δ*spoIIQ* mutant alone (bAT558), or combined with Δ*spoIIIM* (bAT559), Δ*pbpG* (bAT560) and Δ*spoIIIM* Δ*pbpG* (bAT561). The quantification groups include 1) SpoIIIE-GFP focus in the middle of the asymmetric septum, 2) SpoIIIE-GFP focus attached to one of the retracted septal membranes, 3) Split SpoIIIE-GFP foci separated upon septal retraction, and the last two groups include vegetative cells with 4) SpoIIIE-GFP focus at the septum between sister cells and 5) Dispersed SpoIIIE-GFP signal at the septum between sister cells.

Throughout the three timepoints, we observed that in the Δ*spoIIQ* (otherwise-WT) strain, SpoIIIE-GFP foci localized to the septum in most of the sporulating cells (Figure 5.4A), while the few vegetative cells present displayed either a bright focus or dispersed GFP signal at the septum between the sister cells. Similarly, many Δ*spoIIQ* Δ*spoIIIM* cells localized SpoIIIE-GFP to the mid-point of the asymmetric septum at early stages of sporulation (T2) (Figure 5.4A). Importantly, at T2.5 and T3, when the septal retraction phenotype becomes more obvious, many cells still had a SpoIIIE-GFP focus (Figure 5.4B). To better investigate this observation, we quantified the number of SpoIIIE-GFP foci at T2, T2.5 and T3 into five categories, as described in Figure 5.4C.

As with the Δ*spoIIQ* Δ*spoIIIM* cells, in the Δ*spoIIQ* Δ*pbpG* strain the majority of cells with retracted septa had a SpoIIIE-GFP focus (Figure 5.4A, B & C). Similarly, the Δ*spoIIQ* Δ*spoIIIM* Δ*pbpG* cells contained a SpoIIIE-GFP focus at early and late time-points (after retraction), in the vast majority of cells (Figure 5.4A, B & C). Interestingly, we observed that some cells with retracted septa contained two SpoIIIE-GFP foci (Figure 5.4A, B & C). These two SpoIIIE-GFP foci might represent the two complexes of SpoIIIE described previously using photoactivated-localization microscopy (PALM), where each complex is hypothesized to translocate an arm of the chromosome (Fiche *et al*., 2013; Shin *et al*., 2015). These findings suggest that SpoIIIE remains stable and resides in complexes when septal retraction occurs and that septal retraction in Δ*spoIIQ* Δ*spoIIIM* Δ*pbpG* cells does not happen as a result of SpoIIIE instability or degradation. Thus, SpoIIIM and PbpG play a more direct role in preventing septal retraction in cells lacking SpoIIQ.

Finally, to better assess the position of the SpoIIIE-GFP focus in Δ*spoIIQ* Δ*spoIIIM* Δ*pbpG* cells with retracted septa, we used 3-Dimensional Structured Illumination Microscopy (3D-SIM) at T2 to capture images of the cells before the septa fully retract. Based on the data in Figure 5.1E, >80% of the cells exhibit septal retraction in this strain background at T2. In this experiment, we stained the cells with FM4-64 to visualize the membranes. 3D sectioning and quantification of the signal intensity showed that SpoIIIE-GFP localized to the edges of the retracted septal membrane in the Δ*spoIIQ* Δ*spoIIIM* Δ*pbpG* triple mutant cells (Figure 5.5A & B). In contrast, quantification of the signal intensity of SpoIIIE-GFP and the membrane staining in the Δ*spoIIQ* cells showed that the SpoIIIE-GFP focus localized to the middle of the non-retracted septum (Figure 5.5A & B). Again, we observed some cells with retracted septa that contained two SpoIIIE-GFP foci, with each focus remaining localized to the periphery of

retracted septa (Figure 5.5A & B). These results demonstrate that SpoIIIE remains stable and localized at the edges of retracted septa, which represent an enlarged septal pore.

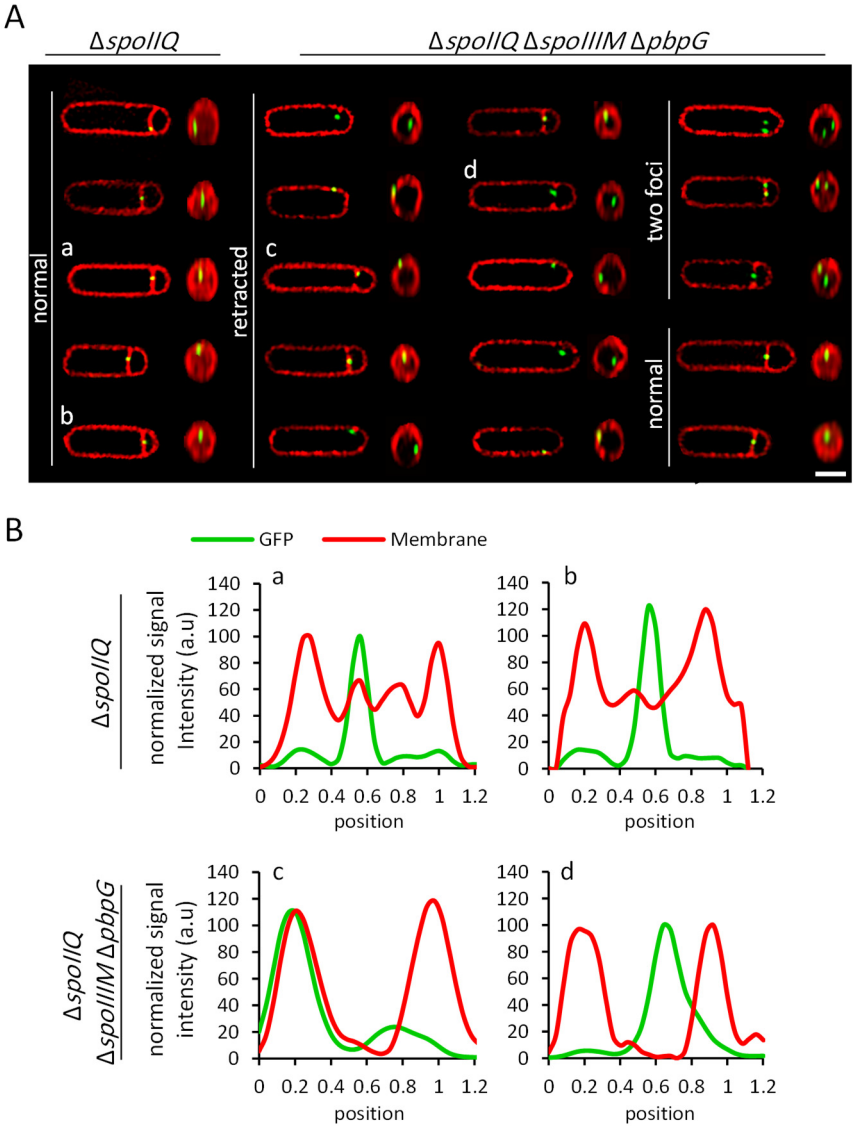

Figure 5.5: SpoIIIE is stable and localizes to the edges of retracted septa. (A) Representative images and 3D slicing of SpoIIIE-GFP localization at the septum using 3D-SIM in Δ*spoIIQ* mutant (bAT558) alone or combined with the Δ*spoIIIM* Δ*pbpG* double mutant (bAT561) at 2 hrs after the onset of sporulation (T2). Examples of normal septa with one SpoIIIE-GFP focus and retracted septa with one or two SpoIIIE-GFP foci are shown. Images are SpoIIIE-GFP (green) merged with membrane (red). Scale bar is 1 µm. **(B)** Normalized SpoIIIE-GFP and membrane signal intensity along the asymmetric septum in cells labelled in (A) with lowercase letter for Δ*spoIIQ* mutant (a & b) and Δ*spoIIQ* Δ*spoIIIM* Δ*pbpG* triple mutant (c & d).

5.3.5 SpoIIIM, PbpG and SpoIIIE are required for efficient septal pore closure in coordination with completion of chromosome translocation

The data presented thus far suggest that SpoIIIM and PbpG function with SpoIIIE to ensure successful chromosome translocation across a septal pore and maintenance of cytoplasmic compartmentalization between the mother cell and forespore at this pore. In the absence of

SpoIIIM and PbpG, and when septal PG hydrolysis occurs, our data suggest that the septal pore enlarges, resulting in chromosome efflux and forespore cytoplasmic miscompartmentalization. Furthermore, if these cells also lack SpoIIQ, the septal pore expands further, resulting in septal membrane retraction. These observations led us to hypothesize that SpoIIIM and PbpG also function to coordinate efficient and timely closure of the septal pore, with completion of chromosome translocation. According to this hypothesis, cells lacking SpoIIIM and/or PbpG are unable to coordinate septal pore closure with completion of chromosome translocation during septal PG hydrolysis, and if these cells also lack SpoIIQ, the membranes that line the pore retract. To investigate this hypothesis, and taking advantage of the septal retraction phenotype, we reasoned that if we hold back PG hydrolysis by the DMP complex in cells lacking SpoIIIM and PbpG, this would allow enough time for the septal pore to close after chromosome translocation. Consequently, once PG hydrolysis is allowed to resume, and if septal pore closure has occurred, there would be less septal retraction in cells lacking SpoIIIM and PbpG (Figure 5.6A). This is exactly what we found using the approach and results described below.

(a) Experimental approach

In our approach, the parental strain had the gene encoding σ^E (*sigE*) deleted. σ^E controls the expression of the DMP complex genes (*spoIID*, *spoIIP, spoIIM*), and its deletion results in cells with two forespore compartments (bi-septa). σ^E also controls the expression of *spoIIIM*, so effectively, the parental strain is a *spoIIIM* null mutant. In this parental strain, we reintroduced the DMP complex genes under the control of an IPTG-inducible promoter and engineered the strain to express CFP under the control of a σ^F-dependent promoter (P_{spoIIQ}). To this parental strain, we then introduced null mutations in *spoIIQ, spoIIQ pbpG,* and *spoIIQ spoIIIE* (Figure 5.6A).

As expected, without IPTG induction, PG hydrolysis was blocked and most of the sporulating cells developed two forespore compartments with flat septa, containing forespore-specific CFP signal (Figure 5.6A). Using the SYTOX Orange dye to stain the chromosomes, we quantified the number of cells that appeared to have completed chromosome translocation into one or both forespore compartments (Figure 5.6B). We then induced the expression of the PG hydrolases by addition of IPTG at T2 and T3. We chose these time-points because they exhibit different frequencies in the completion of chromosome translocation based on DNA staining: ~50% of all strains examined at T2, except the Δ*spoIIQ* Δ*spoIIIE* strain, had completed chromosome translocation into the two forespore compartments, whereas at T3, almost 80% of

these strains had completed chromosome translocation into the two forespore compartments (Figure 5.6B). Importantly, these data suggest that all the strains, apart from the Δ*spoIIQ* Δ*spoIIIE* strain, have a similar efficiency of chromosome translocation into their forespores at each time-point (T2 and T3). Thus, the induction of the PG hydrolases at T2 and T3 would allow us to examine how SpoIIIM and PbpG contribute to the timing of septal pore closure in relation to chromosome translocation completion. Furthermore, at T2, many cells (about 50%) were still undergoing chromosome translocation, indicating that the septal pore is still open in these cells; thus septal retraction would likely occur at a higher frequency at this time-point. On the other hand, because there is a higher number of cells that have completed chromosome translocation at T3, we would expect a lower frequency of septal retraction when the PG hydrolases are induced at T3 compared to T2, unless the septal pore remains open after chromosome translocation, as anticipated for cells lacking PbpG (and SpoIIIM) (Figure 5.6B). Indeed, this is what we found, as summarized in Figure 5.6C and detailed in the following figures.

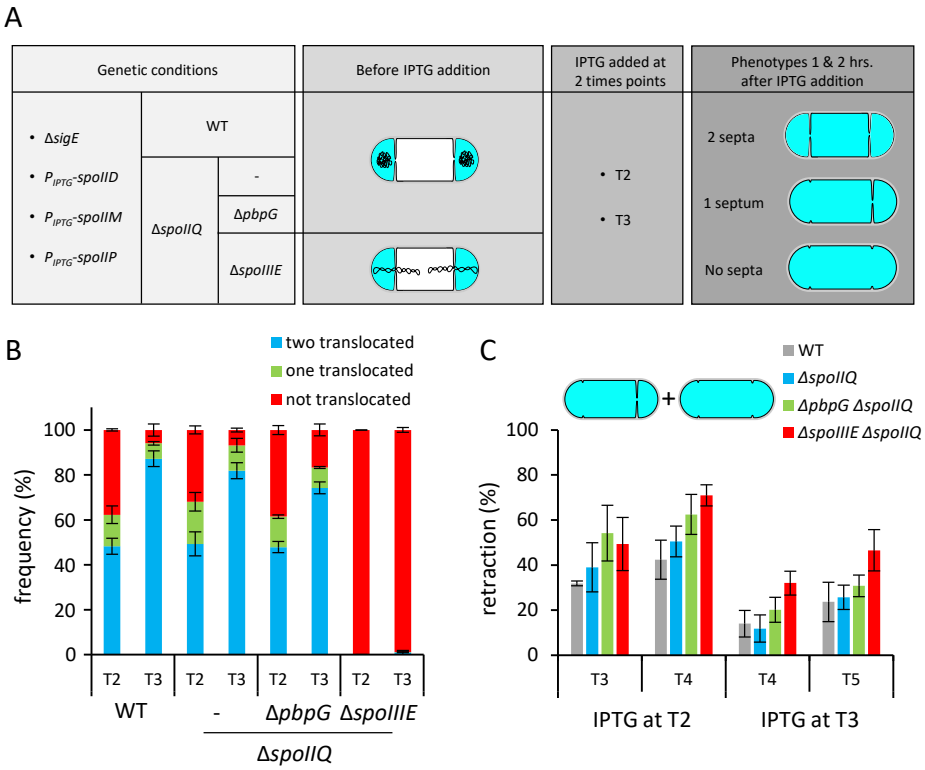

Figure 5.6: Experimental approach of septal retraction induction and quantification of chromosome translocation. (A) Schematic illustration of the experimental design, where all strains are harbouring Δ*sigE* with IPTG-inducible expression of *spoIID*, *spoIIM* and *spoIIP*. Strains tested include an otherwise-WT strain, Δ*spoIIQ*, Δ*spoIIQ* Δ*pbpG* and Δ*spoIIQ* Δ*spoIIIE*. Before IPTG addition, cells have two polar septa, with CFP fluorescence (cyan) expressed in both forespore compartments. Chromosomes are represented by black squiggles that are translocated to both forespores in WT, Δ*spoIIQ* and Δ*spoIIQ* Δ*pbpG* strains, but not in the Δ*spoIIQ* Δ*spoIIE* strain. Expression of *spoIID*, *spoIIM* and *spoIIP* was induced with the addition of IPTG at 2 hr (T2) or 3 hrs (T3) from the onset of starvation. Phenotypes were scored 1 hr and 2 hrs after IPTG addition, and were classified as cells

having 2 septa, 1 septum or no septa. CFP fluorescence leaks from the forespores as septa retract. **(B)** Average frequency of cells with two translocated (blue), one translocated (green) or no translocated (red) chromosomes in otherwise-WT (bAT538), Δ*spoIIQ* (bAT539), Δ*spoIIQ* Δ*pbpG* (bAT540) and Δ*spoIIQ* Δ*spoIIIE* (bAT557) strains during a sporulation time-course. Error bars are standard deviation of 3 biological replicates (n>600 per time-point, per strain). **(C)** Average frequency of cells with septal retraction in otherwise-WT (bAT538), Δ*spoIIQ* (bAT539), Δ*spoIIQ* Δ*pbpG* (bAT540) and Δ*spoIIQ* Δ*spoIIIE* (bAT557) strains imaged 1 hr and 2 hrs after IPTG addition at T2 and T3 to induce expression of *spoIID*, *spoIIM* and *spoIIP* in Δ*sigE* cells. Error bars are standard deviation of 3 biological replicates (n>600 per time-point, per strain, per replicate).

(b) Results

When the PG hydrolases were induced at T2 (Figures 5.6A & 5.7A) and the cells with CFP signal were examined one hr later (T3), we found that the majority of otherwise-WT and Δ*spoIIQ* cells still contained two septa, with only a minor increase in the number of cells with one septum and a small proportion of cells with no septa (Figure 5.7B). When the cells were examined two hrs after the induction of the hydrolases, at T4, we observed a slight increase in the number of cells with single or no septa (Figure 5.7A & B). This suggests that while most WT or Δ*spoIIQ* cells formed septa and then closed the septal pore, a subset of them had not completed pore closure, leading to retraction upon induction of the PG hydrolases. Interestingly, in the Δ*spoIIQ* Δ*pbpG* cells, when the cells were examined one hr after PG hydrolase induction (T3), we noticed a larger increase in the number of cells with one or no septa, relative to the WT or Δ*spoIIQ* cells (Figure 5.7A & B). A similar trend was observed when cells were examined two hrs after induction of the PG hydrolases (T4) (Figure 5.7A & B). Thus, although the Δ*spoIIQ* Δ*pbpG* cells had a similar frequency of chromosome translocation completion as otherwise-WT or Δ*spoIIQ* cells, they exhibited a higher degree of septal retraction (Figure 5.6A, Figure 5.7A & Figure 5.6B). This suggests that the timing of septal pore closure is not coordinated with completion of chromosome translocation in cells lacking SpoIIIM and PbpG.

In a second experiment, we induced the PG hydrolases at T3 and examined the CFP-producing sporangia at T4 and T5 (Figure 5.7C, D & Figure 5.6C). In the otherwise-WT and Δ*spoIIQ* cells at T4, we noticed that most of the cells remained with two septa (>85%), while fewer cells had one or no septa (Figure 5.7D). At T5, we observed that the otherwise-WT and Δ*spoIIQ* cells with two septa slightly decreased to >75% and this was coupled with a small increase in the cells with one or no septa (Figure 5.7C, D & Figure 5.6C). These results suggest that the majority of the otherwise-WT and Δ*spoIIQ* cells had completed septal pore closure at the onset of PG hydrolase induction at T3. In the Δ*spoIIQ* Δ*pbpG* cells, at T4, we found that although most of the cells had two septa (79%), the frequency was lower compared to otherwise-WT

and Δ*spoIIQ* cells (Figure 5.7D). A similar trend was observed after two hrs of PG hydrolysis induction (T5); the majority of cells still had two septa (69%), while the number of cells with one or no septa slightly increased (Figure 5.7C, D & Figure 5.6C). Our data here suggest that timing of septal pore closure in coordination with completion of chromosome translocation is mediated by PbpG (and SpoIIIM).

Next, we performed the above induction experiments in the Δ*spoIIQ* Δ*spoIIIE* sporulating cells that do not translocate the forespore chromosome (Figure 5.6A). Interestingly, we observed that the Δ*spoIIQ* Δ*spoIIIE* cells behaved similarly to the Δ*spoIIQ* Δ*pbpG* cells: the number of cells with septal retraction decreased when the PG hydrolases were induced at T3 versus T2 (Figure 5.7A, C & Figure 5.6C). This suggests that septal pore closure can happen over untranslocated chromosomes in the absence of SpoIIIE. Furthermore, these observations indicate that SpoIIIE is not absolutely required for septal membrane fission but plays an important role in clearing the septum of DNA during the final steps of cytokinesis. Consistent with this idea, we observed detached forespores containing DNA in all the genetic backgrounds tested (Appendix III, Figure S5.2). In the SpoIIIE mutant, this observation suggests that cytokinesis occurred over untranslocated DNA, bisecting it.

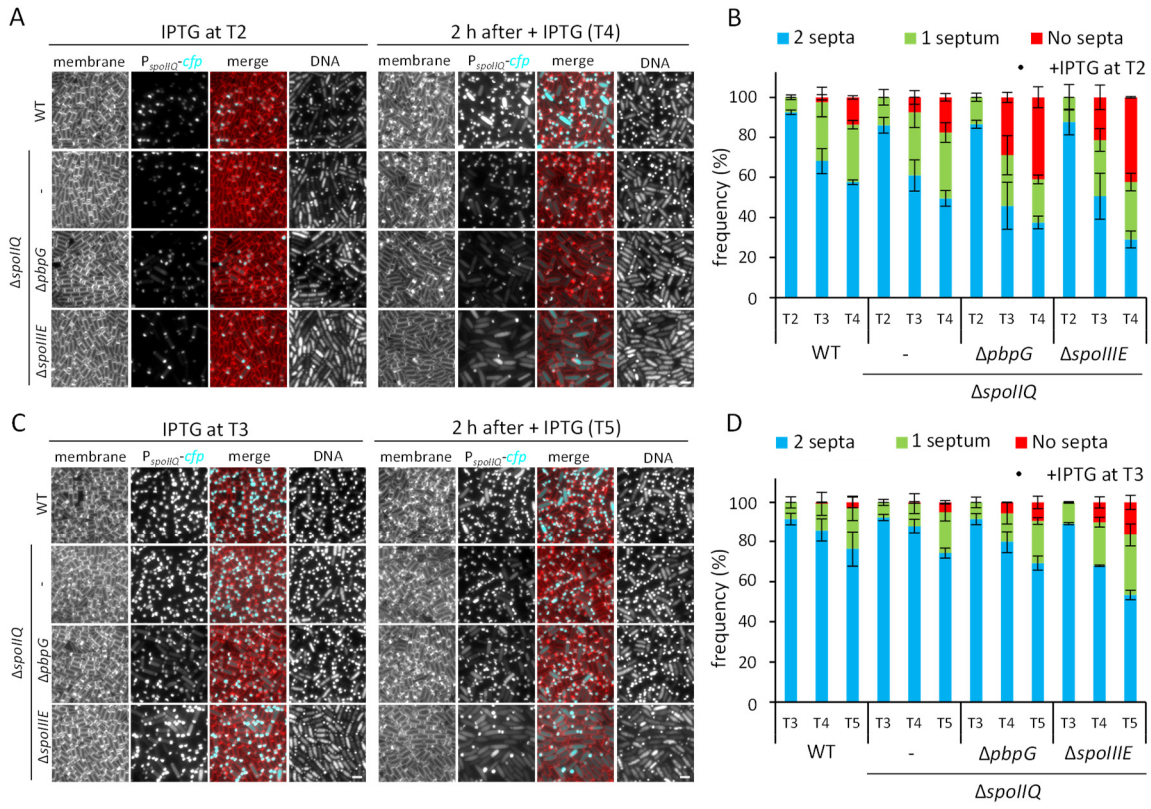

Figure 5.7: SpoIIIE, SpoIIIM and PbpG are required for septal pore closure. (A) Representative images of cells expressing CFP under P_{spoIIQ} in otherwise-WT (bAT538), Δ*spoIIQ* (bAT539), Δ*spoIIQ* Δ*pbpG* (bAT540)

and Δ*spoIIQ* Δ*spoIIIE* (bAT557) strains in a Δ*sigE* background at T2 (before IPTG induction) and T4 (2h after IPTG addition to induce the DMP complex). DNA is stained with SYTOX Orange. Scale bar is 2 μm. **(B)** Average frequency of cells with two septa (blue), one septum (green) or no septa (red) for strains shown in (A) at T2, T3 and T4, with addition of IPTG at T2. Error bars are standard deviation of 3 biological replicates (n>450 per time-point, per strain, per biological replicate). **(C)** Representative images of cells expressing CFP from a forespore-specific promoter (P_{spoIIQ}) in otherwise-WT (bAT538), Δ*spoIIQ* (bAT539), Δ*spoIIQ* Δ*pbpG* (bAT540) and Δ*spoIIQ* Δ*spoIIIE* (bAT557) strains in a Δ*sigE* background at T3 (before IPTG induction) and T5 (2h after IPTG addition to induce the DMP complex). DNA is stained with SYTOX Orange. Scale bar is 2 μm. **(D)** Average frequency of cells with two septa (blue), one septum (green) or no septa (red) for strains shown in (C) at T3, T4 and T5, with addition of IPTG at T3. Error bars are standard deviation of 3 biological replicates (n>600 per time-point, per strain, per biological replicate).

5.4 Discussion

In the previous chapters, we proposed that SpoIIIM and PbpG are required to maintain septal pore stability during chromosome translocation. Here, in this chapter, we provide further evidence of this septal pore. The evidence for this septal pore arose from analyzing compartmentalization in the absence of SpoIIQ, a component of the AH-Q zipper-like interaction across the septal membranes (Broder & Pogliano, 2006). In cells lacking SpoIIQ, SpoIIIM and PbpG, or SpoIIQ and SpoIIIE, we observed a new phenotype that we designated as septal retraction. Importantly, we also found that septal retraction happens due to the PG hydrolytic activity of the DMP complex. Thus, the results in this chapter suggest that septal pore stability, in the face of septal PG hydrolysis, is maintained by multiple factors, including SpoIIIM, PbpG, SpoIIIE and the AH-Q zipper.

Using the septal retraction phenotype, we then developed an approach that demonstrated that SpoIIIM and PbpG are also required for efficient septal pore closure in coordination with completion of chromosome translocation. Importantly, using this approach we also showed that SpoIIIE is not absolutely required for septal membrane fusion, as had been previously suggested (Fleming *et al*., 2010).

Collectively, our findings lead us to propose a model for chromosome translocation involving a highly-stabilized septal pore.

5.4.1 The AH-Q interaction stabilizes the septal pore during engulfment

A striking phenotype observed in this chapter is the retraction of septal membranes shortly after σ^F activation when the AH-Q interaction is abolished in cells lacking SpoIIIM and/or PbpG (Figure 5.1). In these experiments, our data showed that the septum had been formed and forespore specific σ^F-dependent CFP expression occurred, but the absence of *spoIIQ spoIIIM* and *pbpG* or *spoIIQ spoIIIE* caused the septum to retract. A similar pattern of septum disassembly after its formation was previously reported during early stages of sporulation, where the sporangia forms two septa, but the activity of the DMP complex degrades one of them, allowing the other to develop into the forespore (Eichenberger *et al*., 2001). However, under this condition, the forespore compartment of the septum undergoing dissociation does not activate σ^F (Eichenberger *et al*., 2001) and thus lacks other factors that are required for septal stability, such as SpoIIQ and PbpG.

Previously, it was suggested that the transenvelope interaction between SpoIIIAH and SpoIIQ acts as a ratchet that ensures forward movement of the membranes during engulfment

(Blaylock *et al*., 2004; Broder & Pogliano, 2006). In this chapter, we demonstrated another critical role for the AH-Q zipper-like interaction in the stabilization of the membranes that surround the septal pore during hydrolysis of septal PG. Our data show that disrupting the AH-Q interaction compromises pore stability and leads to pore retraction when SpoIIIM and PbpG are absent. Previous work demonstrated that in lysozyme-protoplasted cells, the AH-Q transenvelope interaction is sufficient to hold the mother cell and forespore membranes together and support membrane migration in the absence of the cell wall (Broder & Pogliano, 2006). Based on this finding, it seems possible that the AH-Q interaction functions in a similar capacity during septal PG remodelling and helps to maintain the septal membranes tightly connected, as the septal PG is thinned by the DMP complex and the membranes become less stable. As hypothesized in Chapter 4, the absence of SpoIIIM and PbpG likely compromises PG synthesis and disrupts the balance between PG synthesis and hydrolysis at the septum. The lack of PG synthesis, combined with the absence of SpoIIQ, likely causes destabilization of the septum, which is made worse when septal PG hydrolysis by the DMP complex occurs, thus leading to pore expansion and septal retraction. Indeed, and consistent with this idea, blocking PG hydrolysis by deleting *spoIIP* and *spoIID* completely suppressed the septal retraction defect (Figure 5.3).

Interestingly, we found that cells lacking SpoIIQ and SpoIIIE almost phenocopy cells lacking SpoIIQ, SpoIIIM and PbpG. One possible interpretation of this observation is that when SpoIIIE assembles at the septal pore to translocate the chromosome, it then interacts and recruits SpoIIIM and PbpG to synthesize PG around the pore. Therefore, when SpoIIIE is absent, these interactions are lost and there is no activation of septal PG synthesis around the pore, leading to its expansion due to PG hydrolysis.

5.4.2 A highly stabilized pore within the unfused septal membranes

The septal retraction phenotype reported here is inconsistent with the Membrane Channel Model, where the septal membranes are fused during chromosome translocation. In the Membrane Channel Model, it is suggested that SpoIIIE is required for septal membrane fusion (Fleming *et al*., 2010; Shin *et al*., 2015). One possibility that arose from the phenotypic similarity between Δ*spoIIQ* Δ*spoIIIM* Δ*pbpG* cells and the Δ*spoIIQ* Δ*spoIIIE* cells in terms of the degree of septal retraction (Figure 5.1B & E), was that in cells lacking SpoIIQ, PbpG and SpoIIIM, SpoIIIE becomes unstable, thereby compromising its putative septal membrane fusion role. However, we observed that SpoIIIE remains stable and forms a focus (i.e. complexes) in the Δ*spoIIQ* Δ*spoIIIM* Δ*pbpG* triple mutant cells (Figure 5.4), suggesting that

even when SpoIIIE is present, the septal membranes remain unfused and are susceptible to retraction. In these cells, SpoIIIE-GFP appeared as a bright focus, suggesting that it might still be bound to the DNA even after the pore collapses. As hypothesized in Chapter 4, this observation suggests that SpoIIIM and PbpG are required to release SpoIIIE from the DNA.

The Aqueous Pore Model was originally proposed by two separate groups, the Errington and Nöllmann laboratories (Wu & Errington, 1997; Errington *et al*., 2001; Fiche *et al*., 2013). One aspect that was lacking to support this model was genetic evidence that the pore could be somehow maintained by proteins in the septum. Our data provide support for this aspect of the model by identifying the factors that maintain pore stability. Since the septal pore is likely small enough to allow passage of the DNA strands and prevent cytoplasmic molecules from passing through, it would be technically challenging to visualize the actual pore. Future work using high-resolution imaging by cryo-correlative light and electron microscopy (cryoCLEM) could help to visualize SpoIIIE-GFP complexes assembled within the pore in WT cells or in mutant cells that are just beginning to undergo septal retraction.

Although we have yet to obtain physical evidence of this pore using these high-resolution imaging techniques, our observation of septal retraction in two genetic conditions (Δ*spoIIQ* Δ*spoIIIM* Δ*pbpG* and Δ*spoIIQ* Δ*spoIIIE*) provides strong evidence that this pore is stabilized by multiple factors: 1) PG synthesis, directly through PbpG, and possibly indirectly by SpoIIIM, to provide more rigidity to the pore; 2) SpoIIIE, that appears to organize PG synthesis around the pore by potentially recruiting PbpG and SpoIIIM to the pore, and 3) the AH-Q interaction, which ensures that septal membranes are tightly connected across septal PG at the onset of PG hydrolysis.

5.4.3 Coordinating septal closure with chromosome translocation

Using the septal retraction phenotype and its dependency on PG hydrolysis, we developed an approach to test the idea that PbpG, SpoIIIM and SpoIIIE coordinate septal pore closure with the completion of chromosome translocation (Figure 5.6 & 5.7). In this approach, we delayed septal PG hydrolysis in cells lacking SpoIIIM, PbpG and SpoIIIE and then monitored septal retraction upon PG hydrolysis at an early and later time point. We made three major observations, as discussed next.

First, we observed an inverse correlation between the number of cells that have completed chromosome translocation and the frequency of septal retraction. When we induced PG hydrolysis at T2, we observed a higher frequency of septal retraction, as many cells had yet to

complete chromosome translocation into the forespore (Figure 5.7A & B). While at T3, when most of the cells had completed chromosome translocation into the forespore, we noticed a reduction in septal retraction (Figure 5.7C & D). Thus, while the chromosome is translocating through the septal pore, the pore is more susceptible to retraction. This observation itself is evidence of a septal pore but also suggests that completion of chromosome translocation determines the timing of septal pore closure under normal conditions. We propose that SpoIIIE senses the completion of chromosome translocation into the forespore and then stimulates septal PG synthesis to close the pore. Consistent with this hypothesis, it was suggested that the SpoIIIE homolog in *E. coli*, FtsK, senses the completion of chromosome segregation and then stimulates PG synthesis to complete cytokinesis (Coltharp *et al*., 2016). This idea is supported by the interactions of FtsK with PG synthases and other proteins that appear to activate PG synthesis (Di Lallo *et al*., 2003; Berezuk *et al*., 2018). For instance, FtsK interacts with PBP1a, PBP3 (or FtsI) and SPOR domain-containing proteins including RlpA, FtsN and DamX that were found to stimulate PG synthesis during cell division (Di Lallo *et al*., 2003; Berezuk *et al*., 2018; Pazos *et al*., 2020). Similarly, it is possible that SpoIIIE could play an analogous role during sporulation, where it completes chromosome translocation and directly interacts with SpoIIIM and PbpG to initiate septal pore closure through PG synthesis. Such coordination between chromosome translocation and PG synthesis ensures that pore closure (cytokinesis) does not happen over untranslocated DNA.

Second, we observed that SpoIIIM and PbpG contribute of the efficiency of septal pore closure once chromosome translocation is complete; thus, as hypothesized above, it is likely that PG synthesis by PbpG and SpoIIIM contributes to completion of cytokinesis. Consistent with this idea, it has been proposed that cell wall synthesis in yeast and bacteria is what completes the final steps of cytokinesis during division (Proctor *et al*., 2012; Coltharp *et al*., 2016; Yang *et al*., 2017; Bisson-Filho *et al*., 2017). Interestingly in *E. coli*, PG synthesis is suggested to complete cytokinesis by generating the final constrictive force (Yang *et al*., 2017; Bisson-Filho *et al*., 2017). This observation is supported by the fact that FtsZ (the protein that orchestrates cytokinesis) dissociates before the completion of constriction (Söderström *et al*., 2014; Yang *et al*., 2017). Furthermore, previous work showed that compromising PG synthesis during cell division leads to delayed cytokinesis (Huls *et al*., 1999; Aarsman *et al*., 2005; Coltharp *et al*., 2016). Therefore, we suggest that septal PG synthesis mediated by SpoIIIM and PbpG achieves pore closure after chromosome translocation is completed. Thus, blocking/delaying PG

hydrolysis in the absence of SpoIIIM and PbpG allows more time to complete septal pore closure in cells that have completed chromosome translocation (Figure 5.7C & D).

Third, we observed that septal pore closure can occur, albeit at a slower rate, in the absence of SpoIIIM, PbpG and SpoIIIE, suggesting that other PG synthases contribute to this process (Figure 5.7C). Consistent with this idea, as our data suggest, in the absence of SpoIIIE or SpoIIIM and PbpG, cytokinesis can occur. In the absence of SpoIIIE, our data further show that cytokinesis can occur over the untranslocated chromosome, bisecting the DNA (Appendix III, Figure S5.2), revealing the importance of coordinating chromosome translocation with cytokinesis. We hypothesize that these yet-to-be-defined PG synthases are likely essential, or else they would have appeared in our Tn-seq with PbpG.

Chapter 6:

Molecular insight into how PG remodeling is coordinated with chromosome translocation

6.1 Disclaimer

This is to acknowledge that Dr Helena Chan has contributed to the work presented in this chapter. Dr. Chan generated the PbpG constructs and performed the BACTH and co-IP assays in sections 6.3.4 and 6.3.5.

6.2 Introduction

The data in the previous chapters suggest that chromosome translocation is coordinated with PG remodeling at a highly-stabilized septal pore to ensure its stability during chromosome translocation and its closure upon completion of chromosome translocation into the forespore. In this Chapter, we investigated if the catalytic activity of PbpG is required to ensure septal pore stability and closure. To this end, we performed site-directed mutagenesis on PbpG and generated a mutant that largely abolishes PbpG function. This mutant, PbpG*, produces sporulating cells that exhibit miscompartmentalization, chromosome efflux and septal retraction when SpoIIQ is absent, suggesting that PG synthesis by PbpG is required to ensure that the septal pore is stable and able to complete cytokinesis.

In addition, in this chapter, we explored the hypothesis that chromosome translocation is coordinated with PG remodeling through direct interactions between SpoIIIE, SpoIIIM and PbpG. Using fluorescence microscopy, we demonstrated that efficient and stable SpoIIIM localization to the septum requires SpoIIIE. Using bacterial two-hybrid (BACTH), we demonstrate that SpoIIIE interacts with SpoIIIM and PbpG. Furthermore, using co-immunoprecipitation (co-IP) assays, we demonstrate that SpoIIIE interacts with SpoIIIM *in vivo.* Overall, the data presented in this chapter suggest that the coordination between chromosome translocation and PG remodelling requires PG synthesis by PbpG and direct protein-protein interactions between SpoIIIE, SpoIIIM and PbpG.

6.3 Results

6.3.1 PbpG catalytic activity is required for proper spore development

In Chapters 4 and 5, we proposed that PbpG synthesizes septal PG to both stabilize the septal pore during chromosome translocation and to complete cytokinesis and pore closure after chromosome translocation into the forespore is finalized. To test this idea directly, we examined if the catalytic activity of PbpG is required for septal pore stability.

6.3.1.1 Generating the PbpG catalytic mutant - PbpG*

We generated an allele, referred to as *pbpG**, with alanine substitutions in predicted active site residues within the transpeptidase domain and transglycosylase domain of PbpG. To do so, we aligned the PbpG sequence against other well-characterized class A PBPs, mapped out the active site residues (Figure 6.1A) and mutated the residues implicated in transglycosylase (E94A) and transpeptidase activity (S365A) (Figure 6.1A) (Terrak *et al*., 1999). To facilitate the validation of protein levels in the mutant by immunoblot analysis using a His6 antibody

(Figure 6.1B), we planned to introduce the mutations into a PbpG-His6 construct. However, we found that the PbpG-His6 construct failed to fully complement the sporulation efficiency of the Δ*pbpG* Δ*pbpF* background to the level of Δ*pbpF* background. To bypass this technical problem, we generated PbpG* in the context of an N-terminal His6-PbpG fusion, referred to as PbpG^{WT}, that complemented the sporulation efficiency of the Δ*pbpG* Δ*pbpF* background (Figure 6.1C) to the levels of the *pbpF* mutant and was thus fully functional. Consistent with the idea that PbpG* harbours a defect in PG synthesis, it did not complement the *pbpG* deletion in the Δ*pbpG* Δ*pbpF* background (0.16%, Figure 6.1C) nor in the *pbpG spoIIIM* null double mutant (57%, Figure 6.1C). However, we note that PbpG* is not completely catalytically inactive and still retains some residual activity, since it did not generate the same sporulation defects as the *pbpG* null mutant in the abovementioned genetic background. For unknown reasons, we could not detect His6-PbpG^{WT} nor His6-PbpG* by immunoblotting with His6 antibodies. However, using the partially functional C-terminal fusions to PbpG mentioned earlier, we were able detect PbpG and PbpG* as C-terminal His6 fusions and demonstrate that mutations to the catalytic site residues do not impact protein levels (Figure 6.1B). Although we could not validate His6-PbpG* directly by immunoblotting, we decided to proceed with this N-terminal construct, since the parental His6-PbpG^{WT} is fully functional.

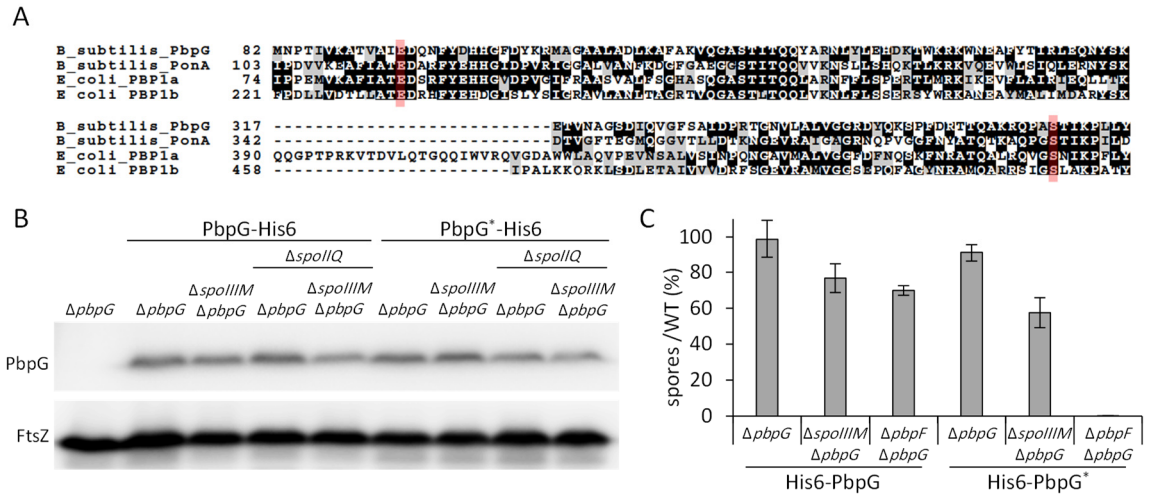

Figure 6.1: Generating a PG-synthesis defective *pbpG* allele (*pbpG). (A)** Sequence alignment of PbpG against other Class A PBPs: PonA from *Bacillus subtilis* (accession number: P39793), PBP1A and PBP1B from *Escherichia coli* (accession numbers: P02918 and P02919, respectively) to identify the catalytic residues involved in PG synthesis. Red shaded residues are the predicted catalytic site residues involved in transglycosylation (E94) and transpeptidation (S365). **(B)** Immunoblot analysis demonstrating levels of PbpG-His6 as a sole source in Δ*pbpG* (bHC036), Δ*spoIIIM* Δ*pbpG* (bHC035), Δ*spoIIQ* Δ*pbpG* (bHC051) and Δ*spoIIQ* Δ*spoIIIM* Δ*pbpG* (bHC050), and PbpG catalytic mutant (PbpG*) in Δ*pbpG* (bHC040), Δ*spoIIIM* Δ*pbpG* (bHC046), Δ*spoIIQ* Δ*pbpG* (bHC052) and Δ*spoIIQ* Δ*spoIIIM* Δ*pbpG* (bHC053). Cells were collected 2 hrs after the onset of sporulation (T2). Importantly, the immunoblot highlights that mutating the catalytic residues does not affect the levels of PbpG. FtsZ is used a loading control. **(C)** Sporulation efficiency of strains expressing His6-PbpG or

His6-PbpG catalytic mutant (His6-PbpG*) as the sole source of PbpG relative to WT (bAT087). Strains used were Δ*pbpG* (bAT855), Δ*spoIIIM* Δ*pbpG* (bAT856) and Δ*pbpG* Δ*pbpF* (bAT857) for His6-PbpG, and Δ*pbpG* (bAT858), Δ*spoIIIM* Δ*pbpG* (bAT859) and Δ*pbpG* Δ*pbpF* (bAT890) for His6-PbpG*. His6-PbpG complemented the sporulation defect of the Δ*spoIIIM* Δ*pbpG* and Δ*pbpG* Δ*pbpF* double mutants, while the His6-PbpG* catalytic mutant failed to do so, suggesting that catalytic activity was severely disrupted.

Next, we introduced His6-PbpG^{WT} (expressed ectopically from the *ycgO* locus as the sole source of PbpG) in Δ*pbpG* and Δ*pbpG* Δ*spoIIIM* backgrounds to generate an otherwise-WT and Δ*spoIIIM* strain expressing His6-PbpG^{WT}. Similarly, we introduced His6-PbpG* (expressed ectopically from the *ycgO* locus as sole source of PbpG) in Δ*pbpG* and Δ*pbpG* Δ*spoIIIM* backgrounds to generate the PbpG* and Δ*spoIIIM* PbpG* strains. To investigate the role of the catalytic activity of PbpG, we examined the different phenotypes described thus far: miscompartmentalization, chromosome translocation, SpoIIIE localization and septal retraction. In the miscompartmentalization and chromosome translocation experiments, we observed that the Δ*spoIIIM* PbpG* strain produced phenotypes that were less severe compared to the *spoIIIM pbpG* null mutant (Figure 6.2A, B & C). This further suggests that PbpG* might still retain some residual catalytic activity. Whereas, in the SpoIIIE localization and septal retraction experiments, the Δ*spoIIIM* PbpG* strain exhibited similar phenotypes to the null mutant of *spoIIIM pbpG*. These experiments are described in more detail next.

6.3.1.2 The catalytic activity of PbpG is required for compartmentalization

To examine if septal PG synthesis by PbpG contributes to compartmentalization, we engineered the WT, Δ*spoIIIM*, PbpG* and Δ*spoIIIM* PbpG* strains to express CFP in the forespore under P_{spoIIQ} control and quantified the number of miscompartmentalized cells over a sporulation time-course. At T3, the WT cells (Δ*pbpG* His6-PbpG^{WT}) produced compartmentalized oblong forespores similar to the WT, as shown in Chapter 3, section 3.3.3 (Figure 6.2A & B). As anticipated, the Δ*spoIIIM* cells showed a mild degree of miscompartmentalization (Figure 6.2A & B). These findings are consistent with the sporulation efficiency data showing that His6-PbpG^{WT} is fully functional.

Consistent with the *pbpG* null mutant, the PbpG* strain had the jellybean forespore morphology and a small number of cells exhibited miscompartmentalization (Figure 6.2A & B). Interestingly, we noticed that 52% of the Δ*spoIIIM* PbpG* cells were miscompartmentalized at T3.5 (Figure 6.2A & B) compared to ~90% of the *spoIIIM pbpG* null mutant (Figure 3.5C, Chapter 3). These results suggest that the catalytic activity of PbpG is required for maintaining forespore compartmentalization during engulfment.

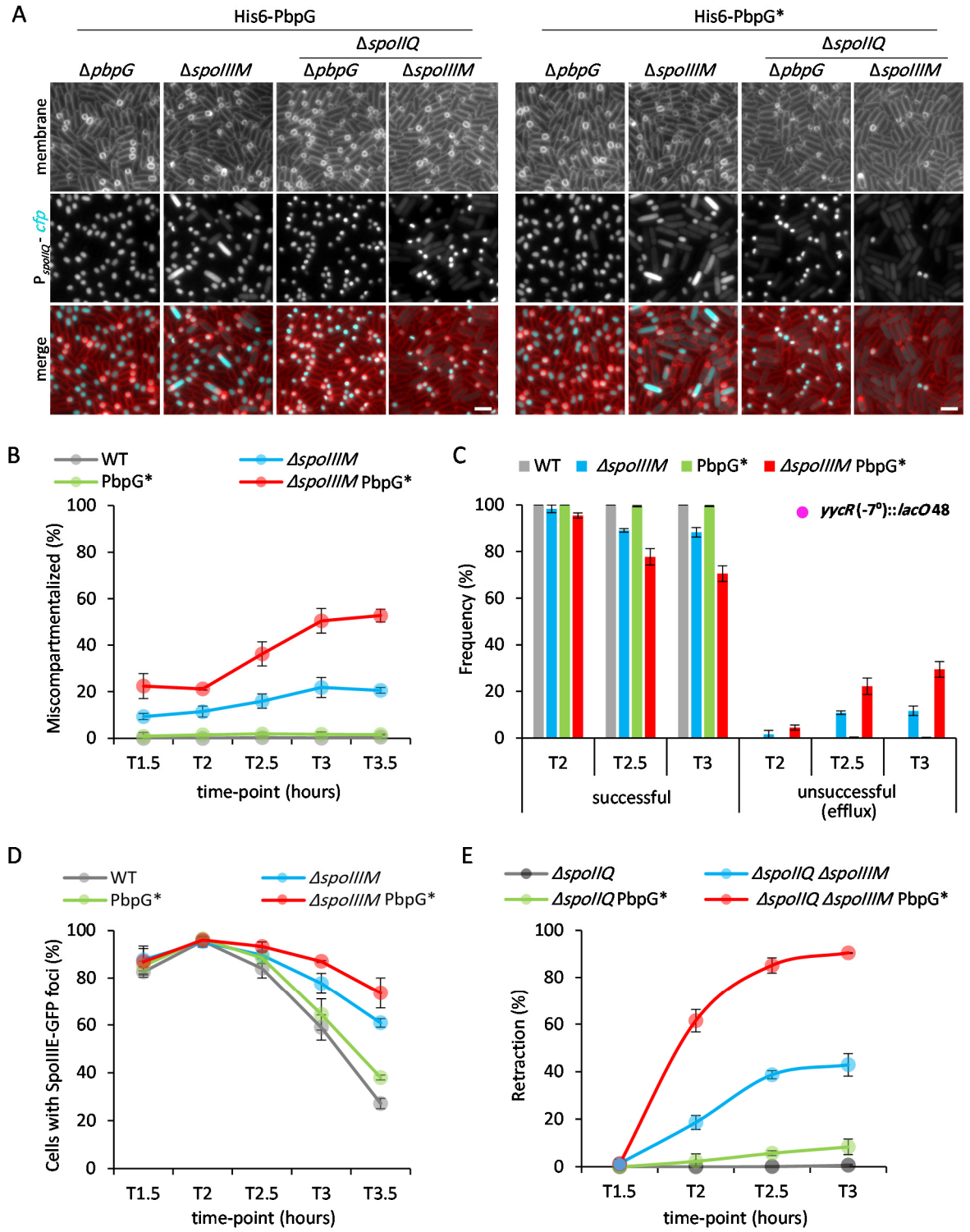

Figure 6.2: PbpG catalytic activity is required for septal pore stability and closure. (A) Representative images of the miscompartmentalization and septal retraction phenotypes in strains harboring PbpG^{WT} or PbpG* as the sole source of PbpG. PbpG^{WT} was inserted in the following strains: (otherwise-WT) Δ*pbpG* (bAT855), (Δ*spoIIIM*) Δ*spoIIIM* Δ*pbpG* (bAT856), (otherwise-Δ*spoIIQ*) Δ*spoIIQ* Δ*pbpG* (bAT861) and (Δ*spoIIQ* Δ*spoIIIM*) Δ*spoIIQ* Δ*spoIIIM* Δ*pbpG* (bAT862), while PbpG* was used in the strains: (PbpG*) Δ*pbpG* (bAT858), (Δ*spoIIIM* PbpG*) Δ*spoIIIM* Δ*pbpG* (bAT859), (Δ*spoIIQ* PbpG*) Δ*spoIIQ* Δ*pbpG* (bAT863) and (Δ*spoIIQ* Δ*spoIIIM* PbpG*) Δ*spoIIQ* Δ*spoIIIM* Δ*pbpG* (bAT864). Scale bar is 2 µm. **(B)** Average frequency of miscompartmentalized cells during a sporulation time-course in WT (bAT855, grey), Δ*spoIIIM* (bAT856, blue), *pbpG** (bAT858, green) and Δ*spoIIIM pbpG** (bAT859, red) strains. Error bars for each time-point are standard

deviation of 3 biological replicates (*n*>900 per time-course, per strain, per biological replicate). **(C)** Average frequency of cells with a LacI-GFP focus in the forespore (successful translocation) or two LacI-GFP foci in the mother cell (unsuccessful translocation, expulsion) during a sporulation time-course in WT (bAT865, grey), Δ*spoIIIM* (bAT866, blue), PbpG* (bAT867, green) and Δ*spoIIIM* PbpG* (bAT868, red) harbouring the *lacO*48 array at the *yycR* locus (-7°). Error bars for each time-point are standard deviation of 3 biological replicates (*n*>600 per time-course, per strain, per biological replicate). **(D)** Average frequency of cells with SpoIIIE-GFP foci in WT (bAT869, grey), Δ*spoIIIM* (bAT870, blue), PbpG* (bAT871, green) and Δ*spoIIIM* PbpG* (bAT872, red) strains during a sporulation time-course. Error bars for each time-point are standard deviation of 3 biological replicates (*n*>950 per time-course, per strain, per biological replicate). **(E)** Average frequency of cells exhibiting septal retraction during a sporulation time-course in WT (bAT861, grey), Δ*spoIIIM* (bAT862, blue), PbpG* (bAT863, green) and Δ*spoIIIM* PbpG* (bAT864, red) strains during a sporulation time-course. Error bars for each time-point are standard deviation of 3 biological replicates (*n*>700 per time-course, per strain, per biological replicate).

6.3.1.3 The catalytic activity of PbpG is required for chromosome retention in the forespore

Next, we tested if the catalytic activity of PbpG is required for retaining the chromosome in the forespore after translocation. To do so, we engineered cells with the *lacO*/LacI system, with the *lacO*48 array inserted at the *yycR* locus (-7°) and LacI-GFP at the *amyE* locus (27.9°) (as described in Chapter 4, section 4.3.4). Using fluorescence microscopy, we examined the cells of WT, Δ*spoIIIM*, PbpG* and Δ*spoIIIM* PbpG* strains and quantified the number of cells with one GFP focus in the forespore or two foci in the mother cell, over three time-points (T2, T2.5 and T3).

As predicted, the WT cells were able to retain the GFP focus in the forespore throughout the examined timepoints (Figure 6.2C). Whereas, in the Δ*spoIIIM* cells, we observed a decreasing trend of cells with the forespore having a GFP focus, coupled with an increase in cells with two mother cell foci (Figure 6.2C). This indicates that some Δ*spoIIIM* cells had lost the chromosome to the mother cell, as described in Chapter 4, section 4.3.4.

As expected, the vast majority of the PbpG* forespores contained the GFP focus (Figure 6.2C), with only a very small fraction of cells harbouring two mother cell foci (Figure 6.2C). Interestingly, we found that 29% of the Δ*spoIIIM* forespores expressing PbpG* failed to retain the GFP focus in the forespore at T3, and instead had two GFP foci in the mother cell (Figure 6.2C). For comparison, in the previous chapter we showed that 49% of the *spoIIIM pbpG* null mutant cells have two GFP foci inside the mother cell at T3 (Appendix II, Figure S4.1, Chapter 4). To summarize, these data suggest that PG synthesis by PbpG contributes to retention of the chromosome in the forespore.

6.3.1.4 The catalytic activity of PbpG is required for dispersal of the SpoIIIE focus

To investigate if the catalytic activity of PbpG is required for dispersal of the SpoIIIE-GFP focus, we employed fluorescence microscopy to examine SpoIIIE-GFP localization during a sporulation time-course, in WT, Δ*spoIIIM*, PbpG* and Δ*spoIIIM* PbpG* cells. Then, we quantified the number of cells with a SpoIIIE-GFP focus over this time-course. At T3.5, as expected, our quantification data showed that fewer WT (27%) cells had the SpoIIIE-GFP focus (Figure 6.2D) while many Δ*spoIIIM* cells (61%) still had the SpoIIIE-GFP focus at the same timepoint (Figure 6.2D). At T3.5, many of the PbpG* cells (38%) had the SpoIIIE-GFP focus dispersed (Figure 6.2D). Importantly, we observed that the majority of Δ*spoIIIM* PbpG* cells still had the SpoIIIE-GFP focus at T3.5 (73%) (Figure 6.2D), similar to the null mutant of *spoIIIM pbpG* at the same timepoint (48%) (Appendix II, Figure S4.1, Chapter 4). This indicates that PbpG-mediated PG synthesis is required for SpoIIIE dispersal.

6.3.1.5 PbpG catalytic activity is required for septal pore stability

Finally, we tested if the catalytic activity of PbpG is required for septal pore stability and prevention of septal retraction in cells lacking the AH-Q zipper-like interaction. To this end, we examined septal retraction in WT, Δ*spoIIIM*, PbpG* and Δ*spoIIIM* PbpG* cells that lack *spoIIQ*. These cells also expressed CFP under the control of a forespore promoter (P_{spoIIQ}) to monitor miscompartmentalization and septal retraction. As expected, Δ*spoIIQ* cells were compartmentalized and did not undergo septal retraction (Figure 6.2A & E). In the Δ*spoIIQ* Δ*spoIIIM* cells, we found that 42% of the cells underwent septal retraction at T3 (Figure 6.2A & E). As expected, a small number of the Δ*spoIIQ* PbpG* cells exhibited septal retraction at T3 (8%) (Figure 6.2A & E). The most significant observation of this experiment was that septal retraction happened in ~90% of the Δ*spoIIQ* Δ*spoIIIM* PbpG* cells at T3 (Figure 6.2A & E). This high frequency of septal retraction in the Δ*spoIIQ* Δ*spoIIIM* PbpG* cells is comparable to that of the triple mutant of *spoIIQ spoIIIM pbpG* (97%) (Figure 5.1C, Chapter 5). These data indicate that the catalytic activity of PbpG is required for septal pore stability.

Collectively, the observations made from the different phenotypes described above suggest that PG synthesis by PbpG is required for coordination between chromosome translocation and PG remodeling at a septal pore.

6.3.2 SpoIIIM localization and stability is dependent on SpoIIIE

In Chapter 4, we hypothesized that SpoIIIM could stimulate PG synthesis around the septal pore or bridge SpoIIIE to the septal PG through its LysM domain. Such roles would require

SpoIIIM localization at the septal pore and/or interaction with SpoIIIE. To test the idea that SpoIIIM localizes at the septal pore, we investigated SpoIIIM localization during spore development. To do so, we constructed a GFP-SpoIIIM fluorescent fusion that was ectopically introduced at the *ycgO* locus and expressed as the sole source of SpoIIIM. The GFP-SpoIIIM construct complemented the sporulation efficiency of the Δ*spoIIIM* strain, but only partially complemented in Δ*spoIIIM* Δ*pbpG* cells (Appendix IV, Figure S6.1A), suggesting that GFP-SpoIIIM is not fully functional in the absence of PbpG. With this limitation in mind, we examined the localization of GFP-SpoIIIM over a sporulation time-course using fluorescence microscopy.

Interestingly, we found that GFP-SpoIIIM formed a focus or band at the septum in WT cells at the beginning of engulfment (Fig. 6.3A). Importantly, as engulfment progressed, some cells had a GFP-SpoIIIM focus that was located in the forespore membranes. At later time-points, when most cells are completing engulfment, fewer cells had a GFP-SpoIIIM focus or band, suggesting that GFP-SpoIIIM disassembles or is degraded (Figure 6.3A). This pattern of GFP-SpoIIIM localization is similar to GFP-SpoIIIE localization during engulfment (see Figure 4.3.2, Chapter 4), suggesting that SpoIIIM localization might depend on SpoIIIE.

If SpoIIIM localization depends on SpoIIIE, then we would expect a different pattern of GFP-SpoIIIM localization in the absence of *spoIIIE*, compared to otherwise-WT cells. Indeed, when *spoIIIE* was deleted, we observed fewer cells with a GFP-SpoIIIM focus and instead, most cells contained a GFP-SpoIIIM septal band (Figure 6.3A). Furthermore, we noticed that the GFP-SpoIIIM signal (band and foci) disappeared earlier in the time-course in the absence of *spoIIIE* compared to WT cells (Figure 6.3A). Quantification of GFP-SpoIIIM signal (band or foci) confirmed our observation: at T3 only 6% of Δ*spoIIIE* cells contained GFP-SpoIIIM signal, while in contrast, 28% of the WT cells had GFP-SpoIIIM signal (Figure 6.3B). These findings suggest that SpoIIIM localization and stability depend on SpoIIIE.

To further validate the localization relationship between SpoIIIE and SpoIIIM, we took advantage of a SpoIIIE36 mutant, which fails to translocate the chromosome (Wu & Errington, 1994; Pogliano *et al*., 1997). Unlike GFP-SpoIIIE, GFP-SpoIIIE36 fails to disperse as engulfment nears completion, but instead persists as a stable focus (Pogliano *et al*., 1997; Besprozvannaya *et al*., 2014). If SpoIIIM localization depends on SpoIIIE, we would expect GFP-SpoIIIM to persist in *spoIIIE36* mutant cells. To test this idea, we examined GFP-SpoIIIM localization in cells expressing the *spoIIIE36* allele, over a sporulation time-course. We

observed that in *spoIIIE36* cells, GFP-SpoIIIM signal persisted in a larger fraction of cells compared to the WT *spoIIIE* (Figure 6.3A). Quantification of cells with GFP-SpoIIIM signal in the *spoIIIE36* mutant showed that at T3, 58% still contained signal, as opposed to 28% and 6% in the WT and *spoIIIE* null mutant, respectively (Figure 6.3B). This result further supports the idea SpoIIIM localization and stability depend on SpoIIIE.

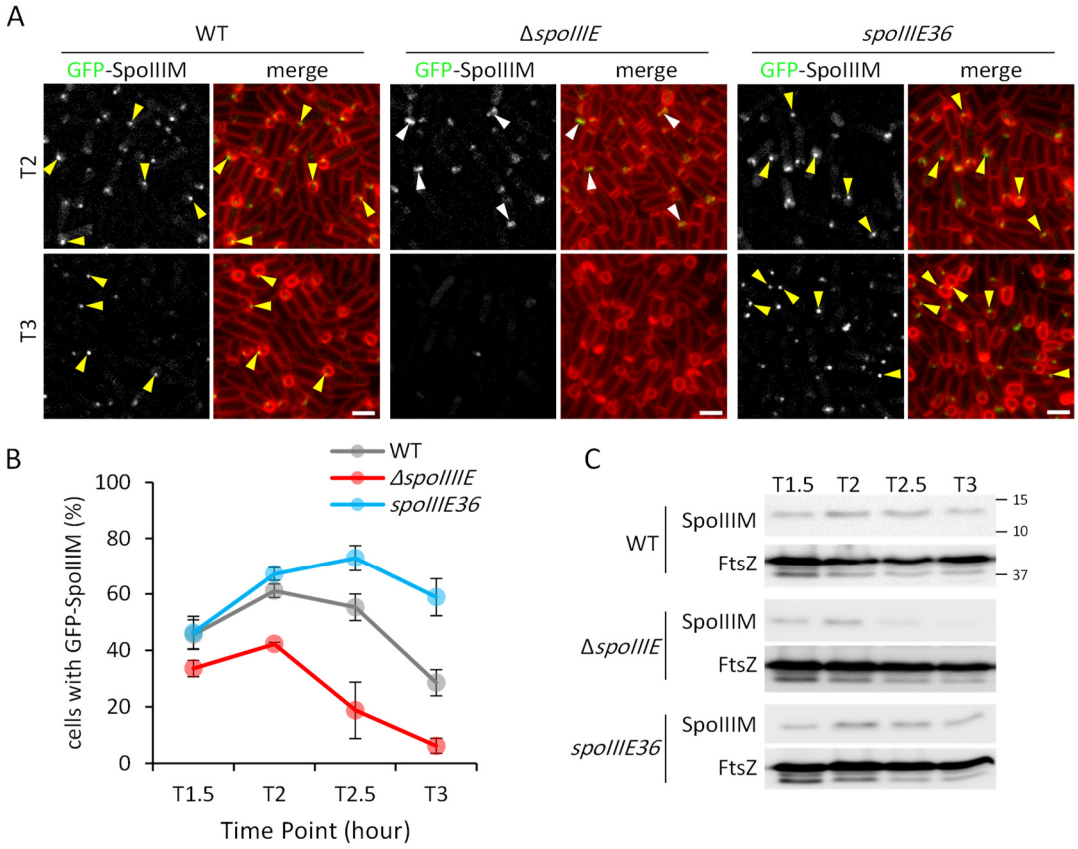

Figure 6.3: SpoIIIM localization and stability are dependent on SpoIIIE. (A) Representative images of GFP-SpoIIIM localization in WT (bAT023), Δ*spoIIIE* (bAT440) and *spoIIIE36* (bAT743) strains at T2 and T3. Yellow arrowheads refer to GFP-SpoIIIM foci that localized initially to the septum and then dispersed as engulfment neared completion in WT, and remained as a stable focus in the *spoIIIE36* strain. White arrowheads refer to GFP-SpoIIIM septal bands in Δ*spoIIIE* cells. Scale bar is 2 µm. **(B)** Average frequency of cells with GFP-SpoIIIM signal in WT (bAT023, grey), Δ*spoIIIE* (bAT440, red) and *spoIIIE36* (bAT743, blue) strains during a sporulation time-course. Error bars for each time-point are standard deviation of 3 biological replicates (n>750 per time-course, per strain, per biological replicate). **(C)** Immunoblot analysis of SpoIIIM-His6 using anti-His6 antibodies in WT (bAT121), Δ*spoIIIE* (bAT834) and SpoIIIE36 (bAT844) strains, suggesting that *spoIIIE* is required for SpoIIIM-His6 stability. FtsZ was used as a loading control.

Since the GFP-SpoIIIM construct was not fully functional in the Δ*spoIIIM* Δ*pbpG* background, we repeated the above localization experiments with GFP-SpoIIIM in merodiploid strains, with GFP-SpoIIIM expressed under the control of a stronger mother-cell promoter (P_{spoIID}) and inserted at the *ycgO* locus. Importantly, expression of GFP-SpoIIIM as a merodiploid did not cause negative effects on sporulation efficiency (Appendix IV, Figure S6.1A). In support of

the idea that SpoIIIM localization depends on SpoIIIE, GFP-SpoIIIM was not stable in the absence of *spoIIIE* and persisted in cells expressing the *spoIIIE36* allele, even in the merodiploid background (Appendix IV, Figure S6.1B). Thus, these observations support the above data that SpoIIIM localization is dependent on SpoIIIE.

Finally, based on the above microscopy data, it appears that SpoIIIM becomes unstable when *spoIIIE* is absent. To investigate this, we employed immunoblotting to analyze the stability of a fully functional SpoIIIM-His6 fusion (Appendix IV, Figure S6.1A) in WT cells, in the absence of *spoIIIE* and in the *spoIIIE36* mutant. Cell lysates were prepared from cells harvested during a sporulation time-course, from T1.5 to T3. In contrast to the WT cells, we found that there was less SpoIIIM-His6 in the Δ*spoIIIE* background, particularly at the later time-points (Figure 6.3C). Furthermore, consistent with the persistent localization of GFP-SpoIIIM in *spoIIIE36* cells, SpoIIIM-His6 could be detected in this strain at later time-points (Figure 6.3C). These data suggest SpoIIIM stability strongly depends on SpoIIIE.

Collectively, the above localization and immunoblot data suggest that the localization and stability of SpoIIIM depend on SpoIIIE, possibly through the formation of a complex *in vivo*.

6.3.3 The LysM domain of SpoIIIM is surface-exposed

Our bioinformatic analysis of SpoIIIM suggested that it has a single transmembrane segment at its N-terminus, followed by a C-terminal LysM domain (Bateman, 2019). Accordingly, we predicted that SpoIIIM would be anchored in the membrane through its transmembrane segment, while its LysM domain would be facing the septal PG in the space between the mother cell and forespore membranes (Figure 6.4A). To test these bioinformatic predictions, we investigated the topology of SpoIIIM using a protease accessibility assay (Besingi & Clark, 2015). In this assay, cells are protoplasted so that proteins displayed at the cell surface would be directly accessible to the protease and be digested. Whereas, if the protein exists in the cytoplasm, it would be inaccessible to protease digestion unless the membrane is solubilized by a detergent. To perform this assay, we expressed SpoIIIM-His6 as the sole source of SpoIIIM in Δ*spoIIQ* Δ*spoIIIM* sporulating cells to ensure that the membrane proteins present in the inner and outer forespore membranes, including SpoIIIM, would not be artificially inaccessible because of protoplast engulfment (Broder & Pogliano, 2006). The first reaction (control reaction) did not include any reagents added to protoplasted cells. In a second reaction, the protoplasted cells were treated with trypsin to digest the surface-exposed proteins. Finally,

in a third reaction, protoplasts were incubated in the presence of trypsin and Triton X-100, a detergent that solubilizes the membranes but does not interfere with trypsin proteolysis.

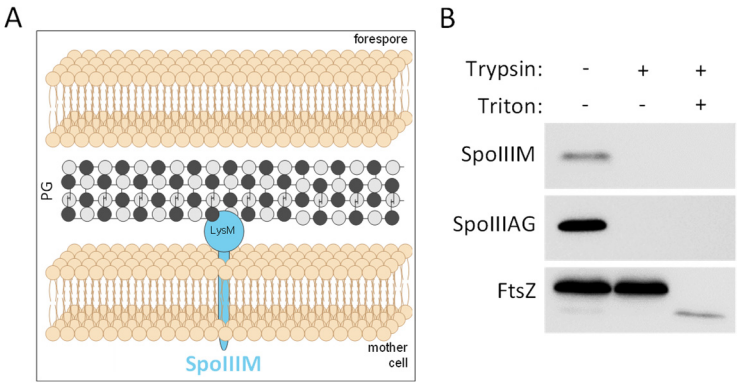

Figure 6.4: SpoIIIM has its LysM domain surface-exposed. (A) Schematic showing prediction of SpoIIIM topology. The LysM domain is predicted to be surface-exposed, facing the septal PG, while the transmembrane segment is embedded in the membrane. **(B)** SpoIIIM is surface-exposed and thus became accessible to digestion by trypsin. Immunoblot analysis of protoplasted sporulating cells using anti-His6 antibodies. Cells expressed SpoIIIM-His6 as the sole source of SpoIIIM in strain Δ*spoIIQ* Δ*spoIIIM* (bAT811). Cells were treated with trypsin in the presence and absence of the detergent Triton X-100. Consistent with the prediction that SpoIIIM is membrane-anchored, it remained cell-associated after the generation of protoplasts, and its LysM domain was susceptible to trypsin digestion in the absence of Triton X-100. As controls, the immunoblot was performed for a membrane protein with an extracellular domain (SpoIIIAG) and for a cytoplasmic protein (FtsZ).

In this experiment, we employed two control reactions using a cytoplasmic protein FtsZ and SpoIIIAG, a protein previously shown to have a surface-exposed domain (Rodrigues *et al*., 2016a). By immunoblotting with anti-FtsZ antibodies, we showed that FtsZ could only be digested by trypsin when Triton X-100 was added to the reaction (Figure 6.4B). Since SpoIIIAG is a membrane protein with an extracellular domain, immunoblot analysis using anti-AG antibodies to the SpoIIIAG extracellular domain showed that it was accessible to the trypsin and was digested in the reaction lacking Triton X-100 (Figure 6.4B). For SpoIIIM-His6 immunoblotting, we used anti-His6 antibodies. Consistent with bioinformatic predictions, SpoIIIM-His6 was digested by trypsin in the absence of Triton X-100 (Figure 6.4B), similar to SpoIIIAG. This indicates that SpoIIIM is a membrane-embedded protein with an extracellular LysM domain facing the septal PG.

6.3.4 SpoIIIM and PbpG directly interact with SpoIIIE in bacterial two-hybrid assays

In the previous chapter, we hypothesized that SpoIIIM, PbpG and SpoIIIE together coordinate chromosome translocation with PG remodeling at a septal pore. We hypothesized that this coordination mechanism could happen through direct protein-protein interactions between SpoIIIE, SpoIIIM and PbpG. To investigate this hypothesis, we conducted bacterial two-hybrid

assays (BACTH) in the *E. coli* BTH101 strain. We separately tested if SpoIIIE interacts with SpoIIIM or PbpG. To do so, SpoIIIE was fused to the T25 or T18 catalytic domains of the *Bordetella pertussis* adenylate cyclase (Karimova *et al*., 1998). Similarly, we fused SpoIIIM or PbpG separately to either of the T25 or T18 subunits. If an interaction exists, the interacting partners will reconstitute the catalytic activity of adenylate cyclase, and thus lead to cAMP synthesis that activates the expression of LacZ (β-galactosidase) (Ouellette *et al*., 2017). The β-galactosidase will give rise to blue coloured colonies when the cells are spotted on agar plates containing X-gal (Ouellette *et al*., 2017). As a control, we used SlmA that had been previously shown by BACTH to self-interact, resulting in blue coloured colonies (Figure 6.5A) (Cho *et al*., 2011).

Consistent with previous reports demonstrating that the C-terminal domain of SpoIIIE can oligomerize into hexameric rings (Cattoni *et al*., 2013, 2014), we found that SpoIIIE self-interacted and formed blue colonies (Figure 6.5A). Interestingly, SpoIIIE-T25 interacted with SpoIIIM-T18 and the reciprocal fusions showed the same result (Figure 6.5A). Similarly, we detected a positive interaction between SpoIIIE and PbpG (Figure 6.5A). These results indicate that the coordination of chromosome translocation with septal PG remodeling at the septal pore by SpoIIIE, SpoIIIM and PbpG happens through direct protein-protein interactions.

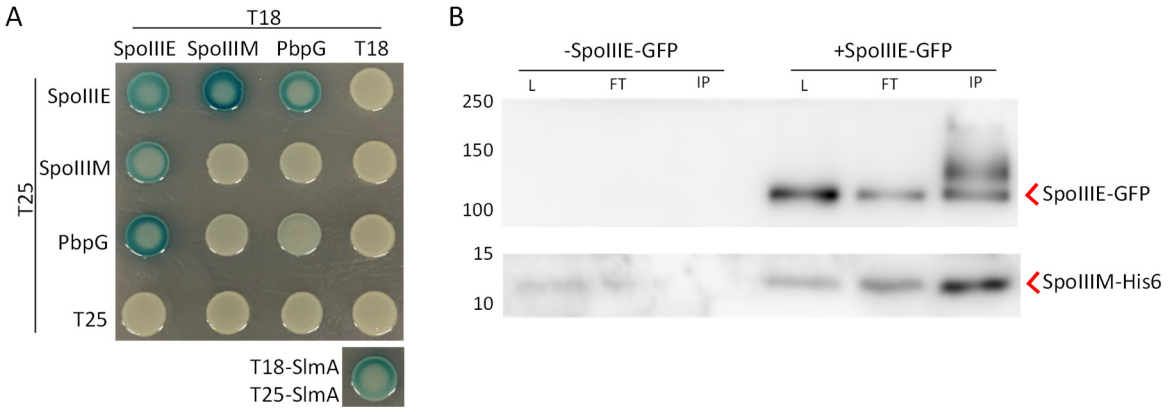

Figure 6.5: SpoIIIE, SpoIIIM and PbpG form a complex. (A) Bacterial two-hybrid assay of T18 and T25 fusions to SpoIIIE, SpoIIIM and PbpG. The blue colour represents positive interactions, while the yellowish/white colour indicates lack of interaction. As a positive control, T18-SlmA and T25-SlmA interaction was used (Cho *et al*., 2011). **(B)** Immunoblot analysis of immunoprecipitation of SpoIIIE-GFP from sporulating cells expressing SpoIIIM-His6 as the sole source of SpoIIIM in Δ*spoIIIE* (bAT834) or SpoIIIE-GFP (bAT835) strains. SpoIIIM-His6 was co-immunoprecipitated and detected only in SpoIIIE-GFP (bAT835) cells, but was not detected in the Δ*spoIIIE* (bAT834) mutant cells. This suggests specific interaction between SpoIIIM and SpoIIIE.

6.3.5 SpoIIIE forms a complex with SpoIIIM *in vivo*

To further investigate the interaction between SpoIIIE and SpoIIIM, we conducted co-immunoprecipitation experiments on detergent solubilized membrane fractions of *Bacillus subtilis* sporulating cells expressing SpoIIIE-GFP and SpoIIIM-His6 (see section 2.13, Materials and Methods). Sporulating cells were collected at T2 to allow better detection of the interaction before the SpoIIIE focus disperses as engulfment nears completion. After cell lysis, we incubated the solubilized membrane fraction with GFP-Trap beads to immobilize SpoIIIE-GFP and its interacting partner/s. Next, we eluted the samples from the beads and performed immunoblot analysis to examine if SpoIIIM-His6 co-immunoprecipitated with SpoIIIE-GFP. In support of the BACTH results, we detected SpoIIIM-His6 in the eluate fraction (IP) of cells expressing SpoIIIE-GFP (Figure 6.5B). As a control, we could not detect SpoIIIM-His6 in the eluate fraction of cells that lack SpoIIIE-GFP. Thus, consistent with the fluorescence microscopy experiments described earlier, these data indicate that SpoIIIE forms a complex with SpoIIIM *in vivo*.

6.4 Discussion

In this chapter, building upon our hypothesis that chromosome translocation is coordinated with PG remodeling at a septal pore, we found that the catalytic activity of PbpG is required to counterbalance the effect of PG hydrolysis to achieve balanced PG remodeling around the septal pore, through which the chromosome is translocated. Furthermore, we showed that SpoIIIM localization and stability depend on SpoIIIE, suggesting that SpoIIIE forms a complex with SpoIIIM *in vivo*. Importantly, using protein-protein interaction assays, we found that SpoIIIE interacts with SpoIIIM and PbpG, suggesting that the coordination between chromosome translocation and PG remodeling at the septal pore is orchestrated by protein-protein interactions between these proteins.

6.4.1 PG synthesis by PbpG plays an important role in septal pore stability and closure

The previous chapters led to our hypothesis that PG synthesis by PbpG plays an important role, together with SpoIIIM, in maintaining the septal pore. In this chapter, we tested this hypothesis by introducing mutations to predicted catalytic site residues of PbpG and then examined the capacity of the catalytic mutant to support compartmentalization, forespore chromosome retention, SpoIIIE localization and septal pore stability. Our data showed that disrupting the catalytic activity of PbpG led to miscompartmentalization, chromosome efflux, failure of SpoIIIE to disperse and septal retraction (Figure 6.2A & E).

One of the things that we learned from the characterization of this PbpG catalytic mutant (PbpG*) was that it was not completely catalytically inactive. Our sporulation efficiency assays indicated that the *pbpG** allele in a *pbpF* null background produces 10-fold more spores than the *pbpG pbpF* double null mutant. Thus, PbpG* still retains some residual activity. A previous report highlighted other residues that contribute to the catalytic activity of PBP1b, a homolog of PbpG, in *E. coli* (Terrak *et al*., 1999). In future work, we could mutate these additional residues and examine if this PbpG mutant completely phenocopies the *pbpG* null.

Although PbpG* in cells lacking SpoIIIM produced less severe miscompartmentalization and chromosome translocation phenotypes than the null mutant of *spoIIIM pbpG*, our results demonstrate that the full catalytic activity of PbpG is required for these processes (Figure 6.2). Interestingly, we observed that PbpG* in cells lacking SpoIIIM almost phenocopied the *spoIIIM pbpG* null mutant during the examination of SpoIIIE localization and septal retraction. This suggests that proper SpoIIIE localization and prevention of septal retraction requires PbpG

to be fully active and that the residually active allele we developed is not sufficient to ensure SpoIIIE dispersal and prevent septal retraction. Why the residual activity of PbpG* is sufficient to retain some compartmentalization and normal chromosome translocation but fails to support SpoIIIE dispersal and septal pore stability is unclear. Nonetheless, the data presented in this chapter suggest that PG synthesis by PbpG is an important element in the coordination between chromosome translocation and septal PG remodeling.

As a discussion point on the more technical side, as we detailed in the results (section 6.3.1.1), we could not detect the functional N-terminal His6-PbpG fusion by immunoblotting, and hence we could not use it for co-immunoprecipitation with SpoIIIE-GFP. It is unclear why His6-PbpG is undetectable, even though it is fully functional (Figure 6.1B). One possible reason is that the His6 tag becomes embedded within the denatured protein, thus preventing the anti-His6 antibody from binding to the tag. Alternatively, it may be cleaved off, leaving the C-terminal part of the protein intact. In future work, an alternative solution would be to generate a fully functional PbpG fusion using other tags like FLAG-tag or a fluorescent fusion such as GFP.

6.4.2 SpoIIIE, PbpG and SpoIIIM likely form a complex *in vivo*

Previously, we proposed that SpoIIIE could interact with PbpG to stimulate PG synthesis around the septal pore. Indeed, we detected an interaction between SpoIIIE and PbpG using bacterial two-hybrid assays (Figure 6.5A). Thus, it is formally possible that SpoIIIE stimulates PbpG, activating PG synthesis around the septal pore to restore the septal PG that is lost during septal thinning by the DMP complex. Interestingly, it appears that SpoIIIE and PbpG localization patterns could be different. In previous reports, PbpG was found to localize as a band at the septum that becomes enriched at the leading edge of the engulfing membranes (Scheffers, 2005; Ojkic *et al*., 2016), whereas SpoIIIE localizes as a focus in the septum that then disperses in the forespore membranes. Since SpoIIIE and PbpG appear to localize differently, it appears that their interaction could be transient. Future work examining the co-localization of SpoIIIE and PbpG could reveal the extent of the interaction, especially since previous studies examining the localization of PbpG utilized inducible or non-native promoters that could affect the amount of protein produced and hence affect PbpG localization (Scheffers, 2005; Ojkic *et al*., 2016).

In Chapter 4, we hypothesized that SpoIIIM could interact with SpoIIIE. Consistent with this hypothesis, in this chapter we found that SpoIIIM localization is similar to that of SpoIIIE. We

observed that SpoIIIM localizes to the septum as a focus in most WT cells, and is then observed as a focus in the forespore membranes before it disassembles upon engulfment completion (Figure 6.3A). Importantly, we showed that SpoIIIM localization and its stability are dependent on SpoIIIE, suggesting that SpoIIIM localizes to the septal pore in a SpoIIIE-dependent manner. When we deleted SpoIIIE, we noticed that cells produced GFP-SpoIIIM as a septal band and the overall GFP signal disappeared earlier compared to the WT cells (Figure 6.3A & B). Furthermore, immunoblot analysis using anti-His6 antibodies demonstrated that SpoIIIM-His6 becomes unstable and is likely degraded in cells lacking SpoIIIE (Figure 6.3C). In further support of SpoIIIM's dependency on SpoIIIE, we showed that cells expressing the *spoIIIE36* allele, which unlike the wild-type SpoIIIE protein persists as a focus, resulted in prolonged SpoIIIM localization and stability (Figure 6.3A, B & C). Importantly, we demonstrated that SpoIIIM and SpoIIIE interact in bacterial two-hybrid assays, (Figure 6.5A) and can be immunoprecipitated together from detergent solubilized membranes of sporulating cells (Figure 6.5B). Together, these results suggest that SpoIIIM forms a complex with SpoIIIE.

6.4.3 Speculating on the significance of the interactions between SpoIIIE, PbpG and SpoIIIM

Based on the interactions between SpoIIIE and SpoIIIM, it is possible that they form a complex *in vivo* during engulfment. The complex between SpoIIIE and SpoIIIM could function to ensure septal pore stability by bridging SpoIIIE to the PG. We propose that SpoIIIM^{LysM} could bind to the septal PG and its TM segment interacts with one of the SpoIIIE transmembrane segments, to possibly mediate SpoIIIE bridging to the PG around the pore. We envisage that this PG-bridging role for SpoIIIM may provide more stability to SpoIIIE and the septal pore membranes. In support of this idea, the protease accessibility assay of SpoIIIM showed that its LysM domain is facing the extracellular environment (i.e. septal PG) (Figure 6.4). Future work could be directed at examining whether SpoIIIM binds to PG *in vitro* through its LysM domain. If so, we would also expect that mutation of conserved PG-binding residues in the LysM domain of SpoIIIM would compromise its role in the complex.

Another possible role of SpoIIIM, through its interaction with SpoIIIE, is the activation of PG synthesis around the septal pore. Consistent with this suggested role, it was shown that the DNA translocase from *E. coli*, FtsK, interacts with small proteins such as DedD, DamX and FtsN, that contain another type of PG-binding domain (SPOR domain) (Di Lallo *et al*., 2003; Pazos *et al*., 2020). Interestingly, these proteins are able to activate the PG synthesis activity of PBPs *in vitro* (Pazos *et al*., 2020). Therefore, SpoIIIM might also activate septal PG

synthesis, possibly through its LysM domain. Some LysM domains have been recently shown to also mediate protein-protein interactions (e.g. in another sporulation protein SafA) (Pereira *et al*., 2019). To investigate this idea, it would be interesting to perform mass spectrometry analyses of proteins that co-immunoprecipitate with SpoIIIM to identify its interacting partners.

Although SpoIIIE and PbpG appear to localize differently, our BACTH data show that SpoIIIE interacts with PbpG (Figure 6.5A). It is possible that SpoIIIE stimulates or directs PbpG activity to generate new PG around the septal pore. This idea could be further investigated by incubating PbpG with lipid II precursors with and without SpoIIIE, to examine whether SpoIIIE influences PbpG's PG synthetic activity. These assays could also include DNA, since SpoIIIE binding to DNA may influence its capacity to acts as an activator of PbpG.

Chapter 7:

General Discussion

7.1 Overview

Bacterial spore development has been one of the main subjects for investigating morphogenesis in prokaryotes. Over the last five decades, many key players involved in spore formation have been characterized, including proteins that are required for the formation of the multilayered spore envelope. The GCW constitutes one of these layers and is synthesized by two functionally redundant class A PBPs known as PbpG and PbpF. At the beginning of this thesis, why the spore requires two class A PBPs for GCW synthesis was an outstanding question. This thesis has not only revealed a specialized role for PbpG during spore development but has also uncovered an essential coordination mechanism between two fundamental processes occurring at the onset of engulfment.

Using genetic screens, a poorly characterized gene renamed *spoIIIM* was identified as being required, together with PbpG, for maintaining important aspects of spore development, including cytoplasmic and genetic compartmentalization. Using a variety of approaches, this thesis compiles multiple lines of evidence suggesting that SpoIIIM and PbpG function, together with SpoIIIE, in a previously uncharacterized mechanism that coordinates PG remodeling with chromosome translocation during spore development. Importantly, this thesis also reveals that the coordination between these processes occurs at a septal pore, to achieve efficient chromosome translocation across the septal membranes, retention of the chromosome in the forespore, as well as cytoplasmic compartmentalization. Collectively, the data generated in this thesis have led to a more complete understanding of the early stages of spore development that can be summarized in a comprehensive model called the “Highly Stabilized Septal Pore Model” (Figure 7.2).

7.2 Coordination of PG remodeling and chromosome segregation at a septal pore

Prior to this thesis, chromosome translocation and PG remodeling at the onset of engulfment were thought to occur independently. This thesis revealed how these processes are coordinated with each other to maintain efficient spore development. A fundamental aspect of this coordination process lies in the necessity to maintain a precise balance between PG synthesis and PG hydrolysis during the early stages of engulfment (Figure 7.1A). This thesis suggests that SpoIIIE plays a central role in maintaining this balance by interacting with SpoIIIM and PbpG.

One of the most important results supporting the coordination between PG remodeling and chromosome translocation is the phenotypic similarities between forespores of cells lacking either SpoIIIM and PbpG or SpoIIIE. In Chapter 3, using fluorescence microcopy it was shown that cells lacking SpoIIIM and PbpG produce forespores of similar morphology and degree of forespore cytoplasmic miscompartmentalization as cells lacking SpoIIIE. Furthermore, it was also found that cytoplasmic miscompartmentalization of these forespores can be suppressed by abolishing or reducing the PG hydrolytic activity of the DMP complex. This was the first evidence that SpoIIIM and PbpG function to counterbalance the effect of the DMP complex during engulfment.

Another observation that emphasizes the importance of the coordination between PG remodeling and chromosome translocation was the chromosome retention defect exhibited by cells lacking SpoIIIM and PbpG. In Chapter 4, using a fluorescence microscopy-based assay that exploited the LacI/*lacO* system, it was found that most cells lacking SpoIIIM and PbpG initially translocated the entire chromosome into the forespore. However, the forespore chromosome was eventually lost back to the mother cell through a process likely involving passive efflux of the chromosome (Figure 7.1B). Importantly, as with the miscompartmentalization phenotype, this chromosome retention defect was also suppressed by abolishing or reducing DMP complex activity. These major phenotypes, the function of PbpG in PG synthesis and the fact that these phenotypes are driven by PG hydrolysis, all point to the necessity for maintaining a balance between PG remodeling and chromosome translocation (Figure 7.1A).

Interestingly, the quantitative analysis of SpoIIIE-GFP localization and SpoIIIE-GFP signal intensity in cells lacking SpoIIIM and PbpG, presented in Chapter 4, suggested that their miscompartmentalization and chromosome efflux defects cannot be explained by unstable SpoIIIE. In previous work, it had been suggested that in cells lacking SpoIIIE, a pore is left open in the septum, through which miscompartmentalization occurs (Hilbert *et al*., 2004). However, the SpoIIIE localization data obtained in cells lacking SpoIIIM and PbpG highlight that miscompartmentalization can occur in the presence of a functional and stable SpoIIIE, leading to the hypothesis that a pore must also exist in cells lacking SpoIIIM and PbpG. Given that the miscompartmentalization and chromosome efflux phenotypes could be suppressed by abolishing hydrolytic activity of the DMP complex, these results collectively suggested that the DMP complex drives enlargement of the septal pore if SpoIIIM and PbpG are missing (Figure 7.1B). Thus, SpoIIIM and PbpG function to counteract the hydrolytic activity of the

DMP complex and maintain balanced PG remodeling at the septal pore, restricting its size. Consistent with this idea, in Chapter 6, using a *pbpG* mutant that is defective in its catalytic activity, it was found that PG synthesis by PbpG is required for maintaining forespore compartmentalization and chromosome retention in the forespore, in the absence of SpoIIIM.

The need for balanced PG remodeling during chromosome translocation is in keeping with data suggesting that remodeling of the septum during engulfment requires a balance between PG synthesis and hydrolysis (Figure 7.1A) (Ojkic *et al*., 2016) and with cryo-electron tomography data demonstrating changes in septal PG thickness before and after PG hydrolysis (Tocheva *et al*., 2013). Collectively, the data presented in this thesis provide yet another important example in prokaryotic biology where the balance between PG synthesis and hydrolysis is critical for maintaining cell viability.

7.3 The AH-Q interaction stabilizes the septal pore

Prior to this work, conflicting data led to a debate surrounding how the chromosome is translocated across the septal membranes during spore development. This debate was centred on two models known as the Aqueous Pore Model and the Channel Model (Wu & Errington, 1997; Errington *et al*., 2001; Liu *et al*., 2006; Becker & Pogliano, 2007; Burton *et al*., 2007; Fleming *et al*., 2010; Fiche *et al*., 2013; Shin *et al*., 2015). One of the key differences between these models is the nature of septal membranes during chromosome translocation, unfused in the Aqueous Pore Model and fused in the Channel Model. A major contribution of this thesis is strong genetic evidence that the septal membranes are unfused during chromosome translocation and the identification of various players that stabilize the septal pore formed by the unfused septal membranes during spore development.

As pointed to in the previous section, balanced PG remodeling is critical for stabilizing the septal pore and preventing it from expanding. However, this thesis reveals yet another key player in the stabilization of the septal pore, the AH-Q interaction. In Chapter 5, exciting data showed that abolishing the AH-Q interaction in the absence of SpoIIIM, PbpG and SpoIIIE, results in complete expansion of the septal pore, leading to a phenotype designated as septal retraction (Figure 7.1C). This phenotype was observed using fluorescence microscopy and TEM, and implies that the septal membranes are unfused, and thereby susceptible to retraction, during chromosome translocation. Furthermore, it was demonstrated that the septal pore could remain stable in the absence of these proteins, as long as septal PG hydrolysis by the DMP complex is blocked (Figure 7.1C). Thus, septal PG synthesis mediated directly by PbpG, and

likely indirectly through SpoIIIM, as well as the AH-Q interaction across the septal membranes keeps the pore stable, once the DMP complex starts hydrolysing and thinning the septal PG.

The septal retraction phenotype reported in this thesis uncovers yet another critical role for the highly-conserved AH-Q interaction, as a stabilization factor of the septal membranes surrounding the septal pore. Several previous studies showed that the AH-Q interaction serves multiple functions including structure and assembly of the A-Q complex, localization of several sporulation proteins implicated in engulfment, activation of σ^K, spore coat formation, spore maturation and germination (Blaylock *et al*., 2004; Doan *et al*., 2005, 2009; Camp & Losick, 2008; McKenney & Eichenberger, 2012; Ojkic *et al*., 2014; Rodrigues *et al*., 2016b; Ramírez-Guadiana *et al*., 2017; Luhur *et al*., 2020). Thus, this thesis further emphasizes the central role of the AH-Q interaction in maintaining spore development.

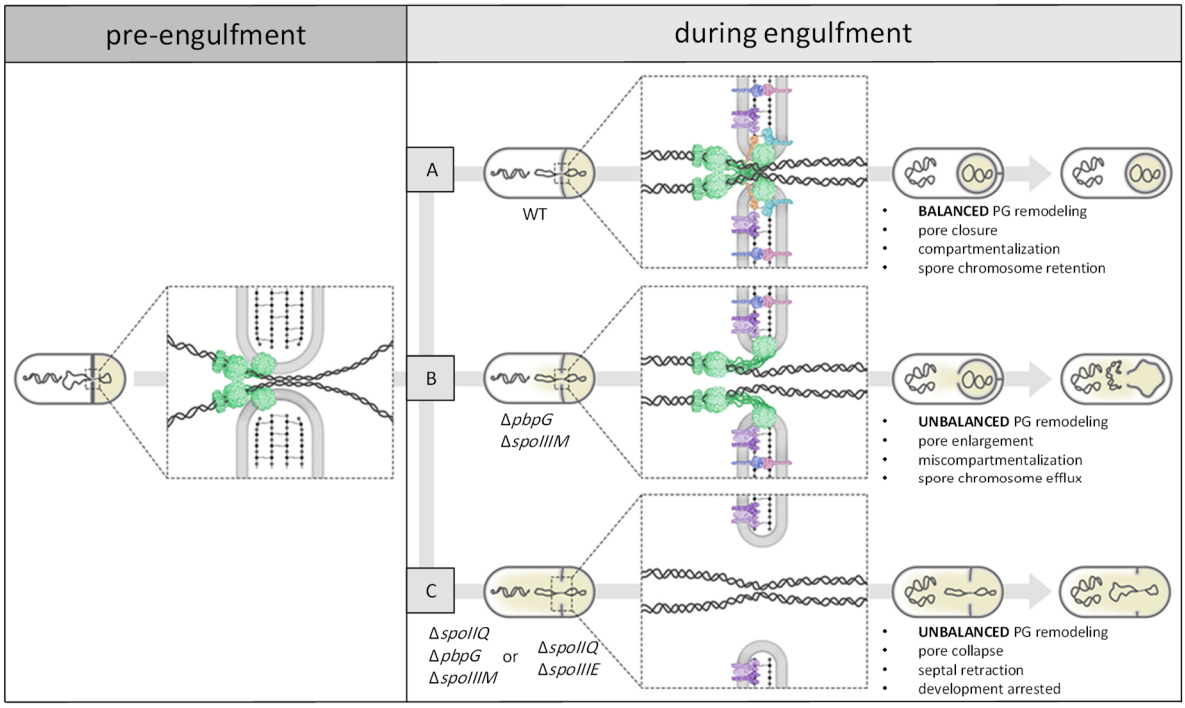

Figure 7.1: Schematic illustrations of the septal pore before and during engulfment in three different genetic backgrounds. Before engulfment, SpoIIIE (green) assembles to translocate the chromosome (black squiggles) through the septal pore, within a thick septum that undergoes thinning by the DMP complex at the onset of engulfment. **(A)** In WT cells, the septal pore is stabilized by PbpG (light teal), SpoIIIM (light orange) and the transenvelope AH-Q interaction (blue and purple). The presence of SpoIIIM and PbpG likely functions to maintain balanced PG remodeling in the face of DMP complex activity (violet complex), ensuring pore stability and efficient pore closure upon chromosome translocation, leading to maintenance of compartmentalization (yellow) and retention of the chromosome in the forespore. **(B)** The absence of SpoIIIM and PbpG leads to unbalanced PG remodeling, that drives pore enlargement through which miscompartmentalization and chromosome efflux occur. **(C)** In the absence of SpoIIQ and SpoIIIE or SpoIIQ, SpoIIIM and PbpG, septal pore stability is severely compromised, leading to pore collapse due to unbalanced PG remodeling that results in septal retraction and arresting of spore development.

7.4 Molecular interactions between SpoIIIE and SpoIIIM & PbpG

A major conclusion in Chapter 6 is that SpoIIIE likely forms a complex with SpoIIIM and PbpG during the early stages of engulfment and that this complex underlies the coordination between chromosome translocation and PG remodeling at the septal pore (Figure 7.2).

As described in Chapter 6, the interaction between SpoIIIM and SpoIIIE is supported by multiple lines of evidence. Using bacterial two-hybrid and co-immunoprecipitation assays, SpoIIIE was demonstrated to interact with SpoIIIM. Interestingly, fluorescence microscopy and immunoblotting analysis showed that SpoIIIM localization and stability depend on SpoIIIE. Furthermore, SpoIIIM appeared to have a localization pattern similar to that of SpoIIIE, suggesting that a SpoIIIE-SpoIIIM complex is assembled at the septal pore (Figure 7.2). Although this thesis provides evidence of the SpoIIIM-SpoIIIE interaction, it remains unclear how the interaction between SpoIIIE and SpoIIIM contributes to the coordination between chromosome translocation and PG remodeling, and hence the stability of the septal pore. One hypothesis is that SpoIIIM functions to bridge SpoIIIE to the septal PG around the pore and thereby provide more stability to the septal pore. Consistent with this hypothesis, it was found that SpoIIIM has a surface exposed LysM domain, which is generally thought to be implicated in PG binding (Buist *et al*., 2008). Another hypothesis is that SpoIIIM, through its LysM domain, interacts with another yet-unidentified PG synthase to stimulate its PG synthetic activity around the septal pore. In support of this role, recent reports showed that the LysM domain of the coat assembly protein, SafA, participates in protein-protein interactions (Pereira *et al*., 2019). Interestingly, other proteins such as DamX, DedD and FtsN, which harbour another type of PG binding domain (SPOR domain), stimulate the activity of some class A PBPs *in vitro* (Pazos *et al*., 2020). Therefore, it is possible that SpoIIIM could similarly stimulate another PG synthase from the mother cell side to synthesize PG. The nature of this PG synthase is currently unknown and could be the subject of future investigations (see Future Work, section 7.5)

Interestingly, bacterial two-hybrid assays also showed that SpoIIIE interacts with PbpG. Although previous reports showed that PbpG is enriched at the leading edges of the engulfing membranes (Scheffers, 2005; Ojkic *et al*., 2016), a localization that is different from SpoIIIE's localization, the interaction between SpoIIIE and PbpG could be transient. Therefore, it is possible that SpoIIIE interacts with PbpG to promote synthesis of PG around the septal pore (Figure 7.2), whereas the main site of PG synthesis by PbpG is ahead of the engulfing membranes (Tocheva *et al*., 2013; Ojkic *et al*., 2016). Nonetheless, despite the likely transient

nature of the interaction between SpoIIIE and PbpG, it is critical for coordinating chromosome translocation with PG synthesis at the septal pore.

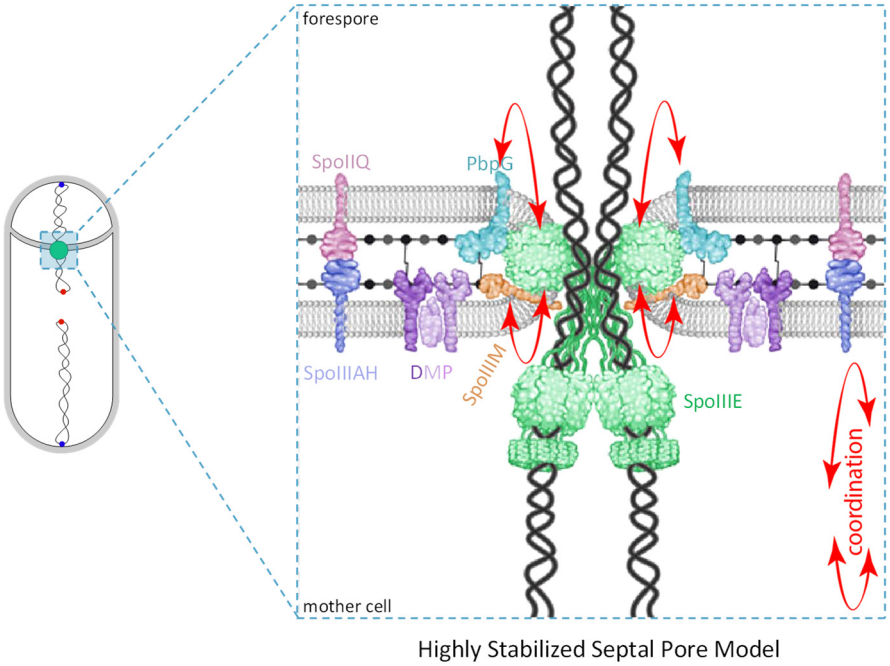

Figure 7.2: Schematic representation of the Highly Stabilized Septal Pore Model. The model suggests that SpoIIIE assembles at a septal pore within the asymmetric septum to translocate the forespore chromosome. At the septal pore, SpoIIIE, SpoIIIM and PbpG coordinate (red arrows) chromosome translocation and PG remodeling. The septal pore is stabilized by PG synthesis mediated by PbpG, direct interactions between SpoIIIE and SpoIIIM and the AH-Q transenvelope interaction. All of these stabilizing factors are required to counterbalance the effect of the DMP complex on the septal pore during chromosome translocation.

From a comparative molecular biology point of view, this thesis reveals some similarities between how SpoIIIE and FtsK function to coordinate the last steps of cytokinesis with chromosome segregation. During cell division in *E. coli*, FtsK has been shown to interact with proteins involved in PG synthesis, as a mean to coordinate the final steps of cytokinesis with chromosome segregation (Di Lallo *et al*., 2003; Errington *et al*., 2003; Grenga *et al*., 2008; Grainge, 2010; Berezuk *et al*., 2018). This thesis reveals that SpoIIIE engages directly with PbpG and SpoIIIM during sporulation to maintain coordination between PG remodeling and chromosome translocation, and complete cytokinesis once the chromosome is translocated into the forespore. Thus, it appears that *B. subtilis* and *E. coli* employ similar strategies to couple efficient chromosome segregation with septal PG remodelling during the final steps of cytokinesis.

7.5 Future work

This thesis is a step forward in our understanding of spore development and how PG remodeling is coordinated with chromosome translocation in bacteria. The Highly Stabilized Septal Pore Model raises several important questions that will require further investigation to reveal the finer details of how this coordination mechanism occurs.

One important question that remains unresolved is the significance of the SpoIIIE interaction with PbpG. It is possible that SpoIIIE activates PbpG to synthesize new septal PG during and after chromosome translocation. Using recently described *in vitro* PG synthesis assays (Qiao *et al*., 2014; Sjodt *et al*., 2018), it would be interesting to test if SpoIIIE influences the enzymatic activity of PbpG. For example, purified PbpG could be incubated with lipid II PG precursors with or without SpoIIIE, to examine if PbpG catalytic activity is stimulated in the presence of SpoIIIE.

Another important question relates to the function of the SpoIIIM LysM domain. To this end, it would be interesting to generate alanine substitution mutants at conserved residues within the LysM domain of SpoIIIM, that have been shown to be required for PG binding in the well-studied LysM domain of AtlA in *Enterococcus faecalis* (Mesnage *et al*., 2014). These SpoIIIM LysM mutants could be used as a single source of SpoIIIM to examine SpoIIIM localization, compartmentalization, and septal stability. If PG binding is essential for SpoIIIM function, cells harbouring SpoIIIM LysM mutations would be expected to phenocopy the *spoIIIM* null mutant cells with regards to, for example, defects in compartmentalization and septal stability.

In *E. coli*, FtsK interacts with many cell division proteins (Baldwin, 2004; Gundry *et al*., 2010; Louche *et al*., 2017), and thus it is possible that SpoIIIE could interact with many more proteins to maintain the coordination between chromosome translocation and cytokinesis at the septal pore. To identify SpoIIIE-interacting partners, detergent solubilized pull-down assays using SpoIIIE-GFP as the bait, followed by mass spectrometry, could reveal the SpoIIIE interaction network.

Although SpoIIIE appears to be predominantly localized on the mother cell side of the septal pore (Wu & Errington, 1997; Fleming *et al*., 2010; Fiche *et al*., 2013; Shin *et al*., 2015), it would be interesting to examine SpoIIIE localization within the septal pore using high-resolution approaches. One approach is cryo-CLEM, that utilizes fluorescence microscopy and cryo-electron microscopy on the same cells, to examine the subcellular localization and

organization of proteins and protein complexes (Schellenberger *et al*., 2014; Tuijtel *et al*., 2019).

Finally, considering that *B*. *subtilis* and the human pathogen *Clostridioides difficile* share many conserved sporulation proteins, undergo comparable spore development stages and have similar structures of the dormant spore (Fimlaid & Shen, 2015; Driks & Eichenberger, 2016; Ribis *et al*., 2018), it is intriguing to propose that chromosome translocation is also coordinated with PG remodeling at a stabilized septal pore during *C. difficile* sporulation. In support of this hypothesis, multiple studies showed that the AH-Q transenvelope interaction in *C. difficile* is critical for engulfment and other aspects of spore development (Crawshaw *et al*., 2014; Fimlaid *et al*., 2015; Serrano *et al*., 2016). Analogous to its role in *B. subtilis*, the DMP complex in *C. difficile* is required for PG degradation, and thus initiation of engulfment (Morlot *et al*., 2010; Nocadello *et al*., 2016; Dik *et al*., 2017; Dembek *et al*., 2018; Ribis *et al*., 2018; Kelly & Salgado, 2019). Furthermore, TEM imaging revealed that *C. difficile* spores have a similar thin layer of GCW (Paredes-Sabja *et al*., 2014; Rabi *et al*., 2017; Shen *et al*., 2019), however the proteins involved in GCW synthesis are yet to be characterized. Interestingly, using whole-genome sequencing, putative genes encoding SpoIIIE-like proteins have been identified in *C. difficile* (Dong *et al*., 2014; Pettit *et al*., 2014; Ramírez-Vargas *et al*., 2017; Shaw *et al*., 2019). Therefore, it is possible that *C. difficile* uses a similar mechanism to translocate the chromosome into the forespore through a highly-stabilized septal pore. Thus, future studies to investigate and target this process using antimicrobial agents could abolish sporulation in *C. difficile* and hence markedly reduce the recurrence and transmission of infections (Deakin *et al*., 2012).

7.6 Concluding remarks

Collectively, this thesis provides a more complete picture of how bacteria differentiate into spores, a morphological process that involves an asymmetric septum with a pore that must coordinate multiple developmental processes at once: the translocation of a chromosome across it, the maintenance of compartmentalization, and the dramatic remodeling of the forespore envelope. This thesis also provides a robust framework from which future studies could advance knowledge of the detailed molecular mechanisms of how PG remodeling is coordinated with chromosome translocation during spore development in model and pathogenic spore-forming bacteria.

Appendices

Appendix I

Tables

Table S3.1: Top hits of Δ*pbpG* screen (bCR1557). The Tn-seq data analysis shows *pbpF* as the top hit in the absence of *pbpG*. *spoIIIM* appears to be important in the absence of *pbpG*.

Gene	p-value	Count ratio	Predicted function
pbpF	0	0.003	Penicillin-binding protein 2C
yqfZ (spoIIIM)	0.00118	0.041	Unknown
tenA	0.00265	0.142	Thiaminase II
murAB	0.00318	0.652	UDP-N-acetylglucosamine 1-carboxyvinyltransferase
ykzE	0.00481	0.004	Unknown
yteV	0.03171	0.05	Unknown

Table S3.2: Top hits of Δ*pbpF* screen (bCR1558). *pbpG* is the top hit in the absence of *pbpF*.

Gene	p-value	Count ratio	Predicted function
pbpG	0	0.05	Penicillin-binding protein 2d
ykzE	0.00481	0.004	Unknown
ykpC	0.00639	0.005	Unknown
yoyF	0.03697	0.016	Unknown
ykzB	0.03799	0.003	Unknown
ykvS	0.01892	0.023	Unknown

Supplementary figures

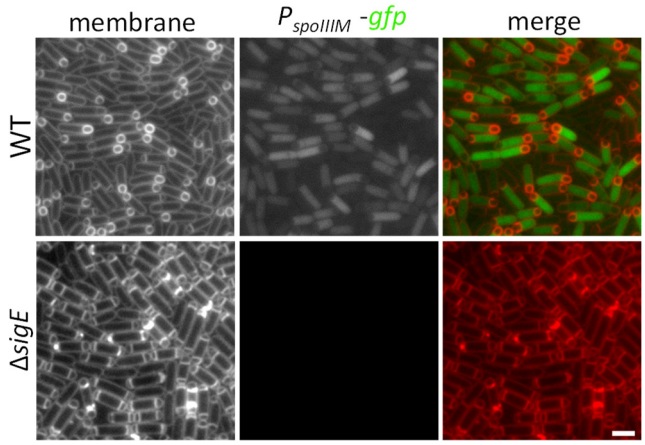

Figure S3.1: SigE controls the expression of *spoIIIM*. The top panel of images shows the expression of GFP under the control of $P_{spoIIIM}$ in WT cells (bAT57), while the lower panel has no GFP in Δ*sigE* cells (bAT58). Scale bar is 2 µm.

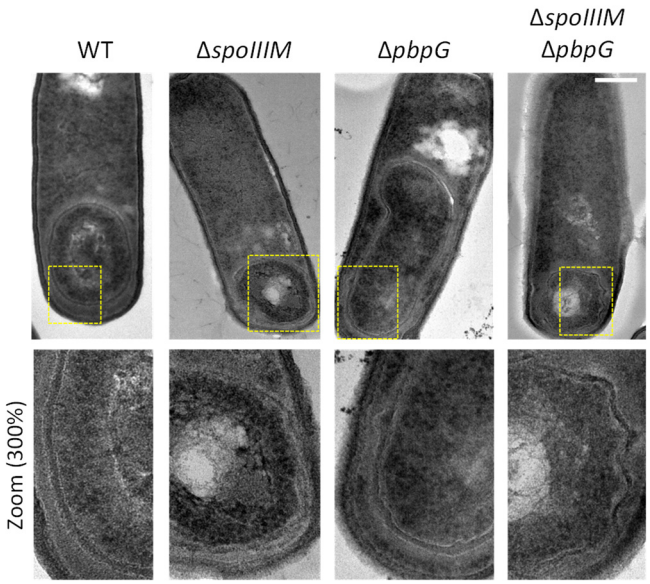

Figure S3.2: *spoIIIM* mutants have forespore morphological defects. Transmission electron microscopy images of WT (bAT087), Δ*spoIIIM* (bAT088), Δ*pbpG* (bAT089) and Δ*spoIIIM* Δ*pbpG* (bAT091) cells showing defective forespores in the absence of *spoIIIM*. Scale bar, 500 nm.

Appendix II

Supplementary figures

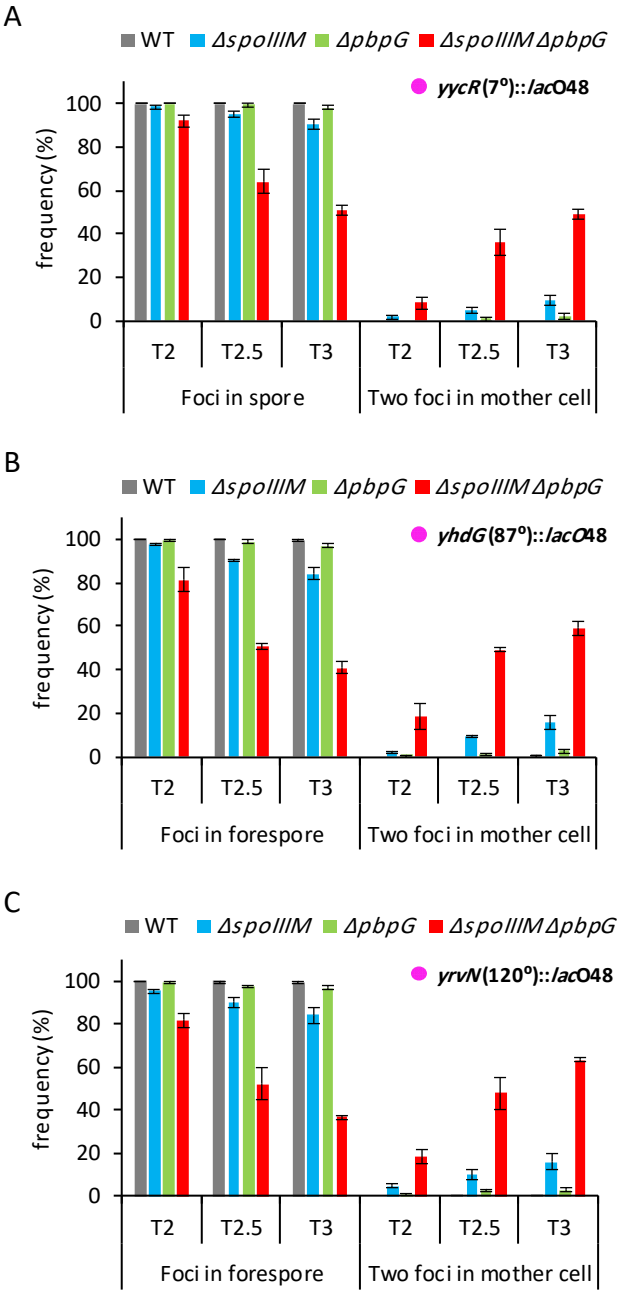

Figure S4.1: Successful chromosome translocation requires SpoIIIM and PbpG. Average frequency of cells with a LacI-GFP focus in the forespore (successful translocation) or with no or two LacI-GFP foci in the mother cell (unsuccessful translocation, efflux) during a sporulation time-course, with *lacO*48 integrated **(A)** at the *yycR* locus (-7°) in the strains of WT (bAT648, grey), Δ*spoIIIM* (bAT627, blue), Δ*pbpG* (bAT628, green) and Δ*spoIIIM* Δ*pbpG* (bAT629, red). Error bars for each time-point are standard deviation of 3 biological replicates (*n*>650 per time-course, per strain, per biological replicate), **(B)** at the *yhdG* locus (87°), in WT (bAT647, grey), Δ*spoIIIM* (bAT633, blue), Δ*pbpG* (bAT634, green) and Δ*spoIIIM* Δ*pbpG* (bAT635, red) strains. Error bars for each time-point are standard deviation of 3 biological replicates (*n*>600 per time-course, per strain) and **(C)** at the *yrvN* locus (120°), in WT (bAT649, grey), Δ*spoIIIM* (bAT643, blue), Δ*pbpG* (bAT644, green) and Δ*spoIIIM* Δ*pbpG* (bAT645, red) strains. Error bars for each time-point are standard deviation of 3 biological replicates (*n*>650 per time-course, per strain).

Appendix III

Supplementary figures

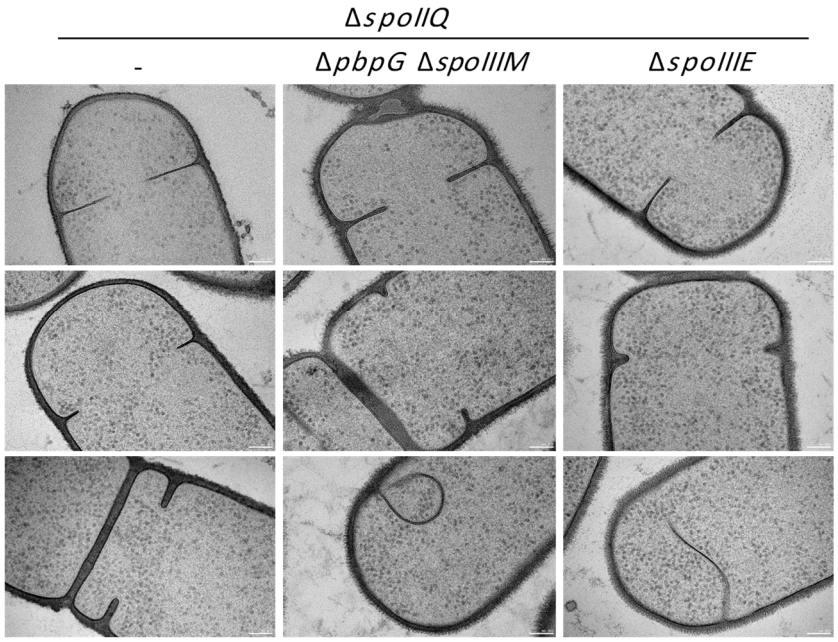

Figure S5.1: Septal retraction observed by transmission electron microscopy. Representative images of the retraction of asymmetric septa in the Δ*spoIIQ* mutant (bAT478) alone or combined with the Δ*spoIIIM* Δ*pbpG* double mutant (bAT481) and Δ*spoIIIE* mutant (bAT476) at 3 hrs after the onset of sporulation (T3). The septa in the Δ*spoIIIM* Δ*pbpG* double mutant and Δ*spoIIIE* mutant are thought to represent retracted septa since the data in Fig. 4B, D, show that almost all cells have retracted septa. Scale bar is 100 nm.

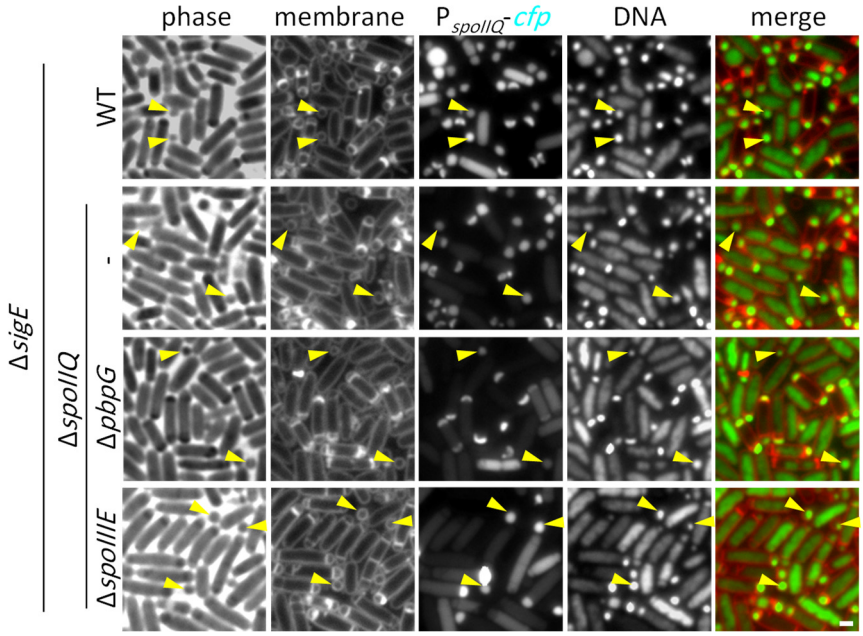

Figure S5.2: Excised spores containing DNA. Representative images of cells expressing CFP under P_{spoIIQ} in otherwise-WT (bAT538), Δ*spoIIQ* (bAT539), Δ*spoIIQ* Δ*pbpG* (bAT540) and Δ*spoIIQ* Δ*spoIIIE* (bAT557) strains in a Δ*sigE* background. DNA was stained with SYTOX Orange. Yellow arrows are pointing to detached forespores. Scale bar is 2 µm.

Appendix IV

Supplementary figures

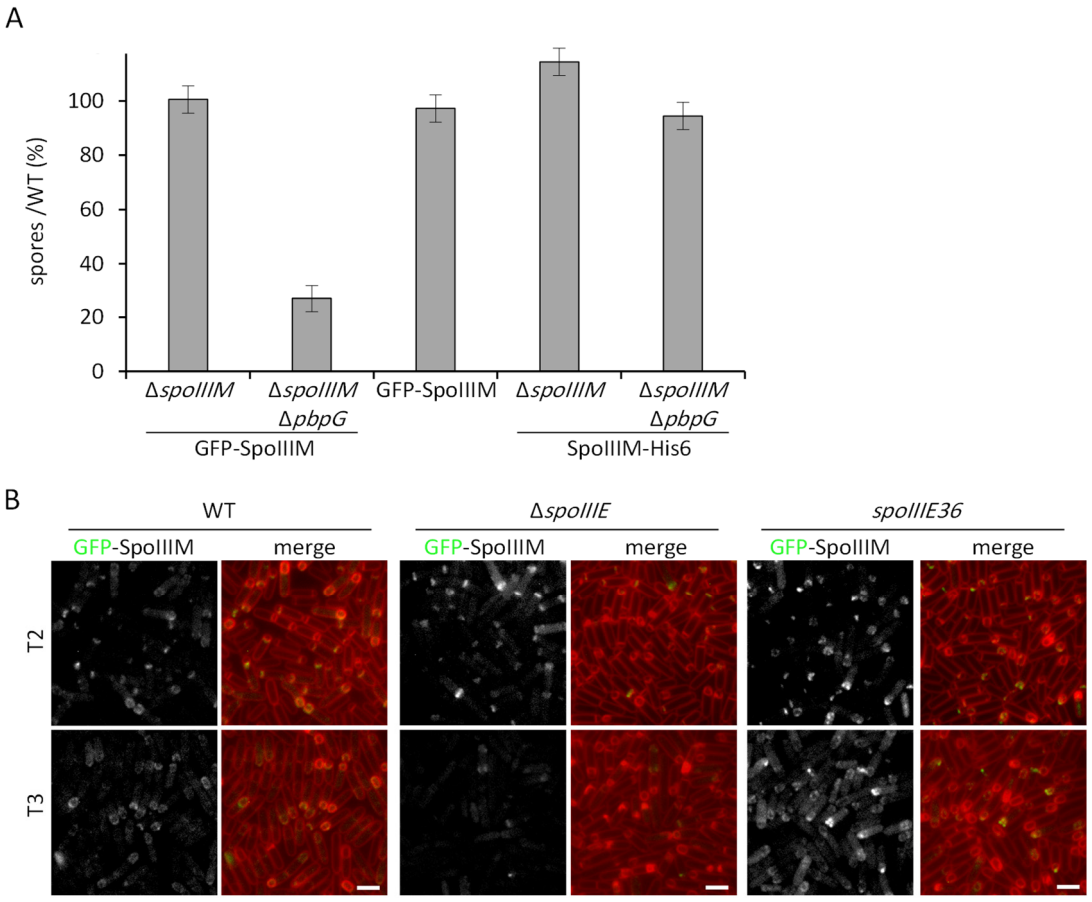

Figure S6.1: Sporulation efficiency of GFP-SpoIIIM and SpoIIIM-His6, and localization of GFP-SpoIIIM in merodiploid backgrounds. (A) Average sporulation efficiency relative to WT (bDR2413) of Δ*spoIIIM* (bCR1592) where $P_{spoIIIM}$-GFP-SpoIIIM complemented in Δ*spoIIIM* (bAT023) and partially complemented in Δ*spoIIIM* Δ*pbpG* (bAT024), and P_{spoIID}-GFP-SpoIIIM in merodiploid background. The histogram also shows the sporulation efficiency of the functional SpoIIIM-His6 in Δ*spoIIIM* (bAT121) and Δ*spoIIIM* Δ*pbpG* (bAT122) strains. Error bars are standard deviation of 3 biological replicates. **(B)** Representative images of GFP-SpoIIIM localization as a second source of SpoIIIM (merodiploid) in WT (bAT353), Δ*spoIIIE* (bAT442) and *spoIIIE36* (bAT837) strains at T2 and T3. Scale bar is 2 µm.

References

Aarsman, M. E. G., Piette, A., Fraipont, C., Vinkenvleugel, T. M. F., Nguyen-Distèche, M., & Den Blaauwen, T. (2005). Maturation of the *Escherichia coli* divisome occurs in two steps. *Molecular Microbiology*, *55*(6), 1631–1645.

Abanes-De Mello, A., Sun, Y., Aung, S., & Pogliano, K. (2002). A cytoskeleton-like role for the bacterial cell wall during engulfment of the *Bacillus subtilis* forespore. *Genes and Development*, *16*(24), 3253–3264.

Anagnostopoulos, C., & Spizizen, J. (1961). Requirements for Transformation in *Bacillus subtilis*. *Journal of Bacteriology*, *81*(5), 741–746.

Angeles, D. M., & Scheffers, D.-J. (2020). The cell wall of *Bacillus subtilis*. *Current Issues in Molecular Biology*, *41*, 539–596.

Arigoni, F., Duncan, L., Alper, S., Losick, R., & Stragier, P. (1996). SpoIIE governs the phosphorylation state of a protein regulating transcription factor σ^F during sporulation in *Bacillus subtilis*. *Proceedings of the National Academy of Sciences*, *93*(8), 3238–3242.

Asare, P. T., Bandara, N., Jeong, T. Y., Ryu, S., Klumpp, J., & Kim, K. P. (2015). Complete genome sequence analysis and identification of putative metallo-beta-lactamase and SpoIIIE homologs in *Bacillus cereus* group phage BCP8-2, a new member of the proposed Bastille-like group. *Archives of Virology*, *160*(10), 2647–2650.

Atrih, A., Williamson, M. P., Bacher, G., & Foster, S. J. (1999). Analysis of Peptidoglycan Structure from Vegetative Cells of *Bacillus subtilis* 168 and Role of PBP 5 in Peptidoglycan Maturation. *Journal of Bacteriology*, *181*(13), 3956–3966.

Aung, S., Shum, J., Abanes-De Mello, A., Broder, D. H., Fredlund-Gutierrez, J., Chiba, S., & Pogliano, K. (2007). Dual localization pathways for the engulfment proteins during *Bacillus subtilis* sporulation. *Molecular Microbiology*, *65*(6), 1534–1546.

Baldwin, M. A. (2004). Protein identification by mass spectrometry: Issues to be considered. *Molecular and Cellular Proteomics*, *3*(1), 1–9.

Banzhaf, M., van den Berg van Saparoea, B., Terrak, M., Fraipont, C., Egan, A., Philippe, J., Zapun, A., Breukink, E., Nguyen-Distèche, M., den Blaauwen, T., & Vollmer, W. (2012). Cooperativity of peptidoglycan synthases active in bacterial cell elongation. *Molecular Microbiology*, *85*(1), 179–194.

Barák, I., & Muchová, K. (2018). The positioning of the asymmetric septum during sporulation

in *Bacillus subtilis*. *PLoS ONE*, *13*(8):e0201979.

Barák, I., Muchová, K., & Labajová, N. (2019). Asymmetric cell division during *Bacillus subtilis* sporulation. *Future Microbiology*, *14*(4), 353–363.

Barák, I., & Youngman, P. (1996). SpoIIE mutants of *Bacillus subtilis* comprise two distinct phenotypic classes consistent with a dual functional role for the SpoIIE protein. *Journal of Bacteriology*, *178*(16), 4984–4989.

Barre, F.-X. (2007). FtsK and SpoIIIE: The tale of the conserved tails. *Molecular Microbiology*, *66*(5), 1051–1055.

Barreteau, H., Kovač, A., Boniface, A., Sova, M., Gobec, S., & Blanot, D. (2008). Cytoplasmic steps of peptidoglycan biosynthesis. *FEMS Microbiology Reviews*, *32*(2), 168–207.

Bateman, A. (2019). UniProt: A worldwide hub of protein knowledge. *Nucleic Acids Research*, *47*(D1), D506–D515.

Bath, J., Ling Juan Wu, Errington, J., & Wang, J. C. (2000). Role of *Bacillus subtilis* SpoIIIE in DNA transport across the mother cell-prespore division septum. *Science*, *290*(5493), 995–997.

Bauer, M. P., Notermans, D. W., van Benthem, B. H. B., Brazier, J. S., Wilcox, M. H., Rupnik, M., Monnet, D. L., van Dissel, J. T., & Kuijper, E. J. (2011). *Clostridium difficile* infection in Europe: a hospital-based survey. *The Lancet*, *377*(9759), 63–73.

Becker, E. C., & Pogliano, K. (2007). Cell-specific SpoIIIE assembly and DNA translocation polarity are dictated by chromosome orientation. *Molecular Microbiology*, *66*(5), 1066–1079.

Ben-Yehuda, S., Fujita, M., Liu, X. S., Gorbatyuk, B., Skoko, D., Yan, J., Marko, J. F., Liu, J. S., Eichenberger, P., Rudner, D. Z., & Losick, R. (2005). Defining a centromere-like element in *Bacillus subtilis* by identifying the binding sites for the chromosome-anchoring protein RacA. *Molecular Cell*, *17*(6), 773–782.

Ben-Yehuda, S., & Losick, R. (2002). Asymmetric cell division in *Bacillus subtilis* involves a spiral-like intermediate of the cytokinetic protein FtsZ. *Cell*, *109*(2), 257–266.

Ben-Yehuda, S., Rudner, D. Z., & Losick, R. (2003a). Assembly of the SpoIIIE DNA Translocase Depends on Chromosome Trapping in *Bacillus subtilis*. *Current Biology*,

13(24), 2196–2200.

Ben-Yehuda, S., Rudner, D. Z., & Losick, R. (2003b). RacA, a bacterial protein that anchors chromosomes to the cell poles. *Science*, *299*(5606), 532–536.

Berezuk, A. M., Glavota, S., Roach, E. J., Goodyear, M. C., Krieger, J. R., & Khursigara, C. M. (2018). Outer membrane lipoprotein RlpA is a novel periplasmic interaction partner of the cell division protein FtsK in *Escherichia coli*. *Scientific Reports*, 8, 12933 (2018).

Berezuk, A. M., Goodyear, M., & Khursigara, C. M. (2014). Site-directed fluorescence labeling reveals a revised N-terminal membrane topology and functional periplasmic residues in the *Escherichia coli* cell division protein FtsK. *Journal of Biological Chemistry*, *289*(34), 23287–23301.

Bertsche, U., Kast, T., Wolf, B., Fraipont, C., Aarsman, M. E. G., Kannenberg, K., Von Rechenberg, M., Nguyen-Distèche, M., Den Blaauwen, T., Höltje, J. V., & Vollmer, W. (2006). Interaction between two murein (peptidoglycan) synthases, PBP3 and PBP1B, in *Escherichia coli*. *Molecular Microbiology*, *61*(3), 675–690.

Besingi, R. N., & Clark, P. L. (2015). Extracellular protease digestion to evaluate membrane protein cell surface localization. *Nature Protocols*, *10*(12), 2074–2080.

Besprozvannaya, M., & Burton, B. M. (2014). Do the same traffic rules apply? Directional chromosome segregation by SpoIIIE and FtsK. *Molecular Microbiology*, *93*(4), 599–608.

Besprozvannaya, M., Pivorunas, V. L., & Burton, B. M. (2014). Mechanistic study of classical translocation-dead SpoIIIE36 reveals the functional importance of the hinge within the SpoIIIE motor. *Journal of Bacteriology*, *196*(13), 2481–2490.

Besprozvannaya, M., Pivorunas, V. L., Feldman, Z., & Burton, B. M. (2013). SpoIIIE protein achieves directional DNA translocation through allosteric regulation of ATPase activity by an accessory domain. *Journal of Biological Chemistry*, *288*(40), 28962–28974.

Bhavsar, A. P., & Brown, E. D. (2006). Cell wall assembly in *Bacillus subtilis*: How spirals and spaces challenge paradigms. *Molecular Microbiology*, *60*(5), 1077–1090.

Bigot, S., Sivanathan, V., Possoz, C., Barre, F.-X., & Cornet, F. (2007). FtsK, a literate chromosome segregation machine. *Molecular Microbiology*, *64*(6), 1434–1441.

Biller, S. J., & Burkholder, W. F. (2009). The *Bacillus subtilis* SftA (YtpS) and spoIIIe DNA

translocases play distinct roles in growing cells to ensure faithful chromosome partitioning. *Molecular Microbiology*, *74*(4), 790–809.

Bisicchia, P., Steel, B., Mariam Debela, M. H., Löwe, J., & Sherratt, D. (2013). The N-terminal membrane-spanning domain of the *Escherichia coli* DNA translocase FtsK hexamerizes at midcell. *mBio,* 4(6):e00800-13.

Bisson-Filho, A. W., Hsu, Y. P., Squyres, G. R., Kuru, E., Wu, F., Jukes, C., Sun, Y., Dekker, C., Holden, S., VanNieuwenhze, M. S., Brun, Y. V., & Garner, E. C. (2017). Treadmilling by FtsZ filaments drives peptidoglycan synthesis and bacterial cell division. *Science*, *355*(6326), 739–743.

Blaylock, B., Jiang, X., Rubio, A., Moran, C. P., & Pogliano, K. (2004). Zipper-like interaction between proteins in adjacent daughter cells mediates protein localization. *Genes and Development*, *18*(23), 2916–2928.

Bobrovskyy, M., Willing, S. E., Schneewind, O., & Missiakas, D. (2018). EssH peptidoglycan hydrolase enables staphylococcus aureus type VII secretion across the bacterial cell wall envelope. *Journal of Bacteriology*, 200:e00268-18.

Bodi, K. L., Camilli, A., & van Opijnen, T. (2009). Tn-seq: high-throughput parallel sequencing for fitness and genetic interaction studies in microorganisms. *Nature Methods*, *6*(10), 767–772.

Bogush, M., Xenopoulos, P., & Piggot, P. J. (2007). Separation of chromosome termini during sporulation of *Bacillus subtilis* depends on SpoIIIE. *Journal of Bacteriology*, *189*(9), 3564–3572.

Bose, B., Reed, S. E., Besprozvannaya, M., & Burton, B. M. (2016). Missense mutations allow a sequence-blind mutant of spoIIIE to successfully translocate chromosomes during sporulation. *PLoS ONE*, 11(2): e0148365.

Broder, D. H., & Pogliano, K. (2006). Forespore Engulfment Mediated by a Ratchet-Like Mechanism. *Cell*, *126*(5), 917–928.

Browne, H. P., Forster, S. C., Anonye, B. O., Kumar, N., Neville, B. A., Stares, M. D., Goulding, D., & Lawley, T. D. (2016). Culturing of "unculturable" human microbiota reveals novel taxa and extensive sporulation. *Nature*, *533*(7604), 543–546.

Buist, G., Steen, A., Kok, J., & Kuipers, O. P. (2008). LysM, a widely distributed protein motif

for binding to (peptido)glycans. *Molecular Microbiology*, *68*(4), 838–847.

Burton, B. M., & Dubnau, D. (2010). Membrane-associated DNA transport machines. *Cold Spring Harbor Perspectives in Biology*, *2*:a000406

Burton, B. M., Marquis, K. A., Sullivan, N. L., Rapoport, T. A., & Rudner, D. Z. (2007). The ATPase SpoIIIE Transports DNA across Fused Septal Membranes during Sporulation in *Bacillus subtilis*. *Cell*, *131*(7), 1301–1312.

Caccamo, P. D., & Brun, Y. V. (2017). The Molecular Basis of Noncanonical Bacterial Morphology. *Trends in Microbiology*, *26*(3), 191-208.

Camp, A. H., & Losick, R. (2008). A novel pathway of intercellular signalling in *Bacillus subtilis* involves a protein with similarity to a component of type III secretion channels. *Molecular Microbiology*, *69*(2), 402–417.

Camp, A. H., & Losick, R. (2009). A feeding tube model for activation of a cell-specific transcription factor during sporulation in *Bacillus subtilis*. *Genes and Development*, *23*(8), 1014–1024.

Camp, A. H., Wang, A. F., & Losick, R. (2011). A small protein required for the switch from σ^F to σG during sporulation in *Bacillus subtilis*. *Journal of Bacteriology*, *193*(1), 116–124.

Carballido-López, R., Formstone, A., Li, Y., Ehrlich, S. D., Noirot, P., & Errington, J. (2006). Actin Homolog MreBH Governs Cell Morphogenesis by Localization of the Cell Wall Hydrolase LytE. *Developmental Cell*, *11*(3), 399–409.

Carniol, K., Kim, T. J., Price, C. W., & Losick, R. (2004). Insulation of the σ^F regulatory system in *Bacillus subtilis*. *Journal of Bacteriology*, *186*(13), 4390–4394.

Cattoni, D. I., Chara, O., Godefroy, C., Margeat, E., Trigueros, S., Milhiet, P. E., & Nöllmann, M. (2013). SpoIIIE mechanism of directional translocation involves target search coupled to sequence-dependent motor stimulation. *EMBO Reports*, *14*(5), 473–479.

Cattoni, D. I., Thakur, S., Godefroy, C., Le Gall, A., Lai-Kee-Him, J., Milhiet, P. E., Bron, P., & Nöllmann, M. (2014). Structure and DNA-binding properties of the *Bacillus subtilis* SpoIIIE DNA translocase revealed by single-molecule and electron microscopies. *Nucleic Acids Research*, *42*(4), 2624–2636.

Cava, F., Kuru, E., Brun, Y. V., & de Pedro, M. A. (2013). Modes of cell wall growth differentiation in rod-shaped bacteria. *Current Opinion in Microbiology*, *16*(6), 731–737.

Caveney, N. A., Caballero, G., Voedts, H., Niciforovic, A., Worrall, L. J., Vuckovic, M., Fonvielle, M., Hugonnet, J. E., Arthur, M., & Strynadka, N. C. J. (2019). Structural insight into YcbB-mediated beta-lactam resistance in *Escherichia coli*. *Nature Communications*, *10*(1), 1–11.

Chara, O., Borges, A., Milhiet, P. E., Nöllmann, M., & Cattoni, D. I. (2018). Sequence-dependent catalytic regulation of the SpoIIIE motor activity ensures directionality of DNA translocation. *Scientific Reports*, *8*(1), 1–10.

Chary, V. K., Xenopoulos, P., & Piggot, P. J. (2006). Blocking chromosome translocation during sporulation of *Bacillus subtilis* can result in prespore-specific activation of σ^G that is independent of σ^E and of engulfment. *Journal of Bacteriology*, *188*(20), 7267–7273.

Chastanet, A., & Losick, R. (2007). Engulfment during sporulation in *Bacillus subtilis* is governed by a multi-protein complex containing tandemly acting autolysins. *Molecular Microbiology*, *64*(1), 139–152.

Cho, H., McManus, H. R., Dove, S. L., & Bernhardt, T. G. (2011). Nucleoid occlusion factor SlmA is a DNA-activated FtsZ polymerization antagonist. *Proceedings of the National Academy of Sciences*, *108*(9), 3773–3778.

Cho, H., Uehara, T., & Bernhardt, T. G. (2014). Beta-lactam antibiotics induce a lethal malfunctioning of the bacterial cell wall synthesis machinery. *Cell*, *159*(6), 1310–1311.

Cho, H., Wivagg, C. N., Kapoor, M., Barry, Z., Rohs, P. D. A., Suh, H., Marto, J. A., Garner, E. C., & Bernhardt, T. G. (2016). Bacterial cell wall biogenesis is mediated by SEDS and PBP polymerase families functioning semi-Autonomously. *Nature Microbiology*, *1*, 16172.

Coltharp, C., Buss, J., Plumer, T. M., & Xiao, J. (2016). Defining the rate-limiting processes of bacterial cytokinesis. *Proceedings of the National Academy of Sciences*, *113*(8), E1044–E1053.

Coppolecchia, R., DeGrazia, H., & Moran, C. P. (1991). Deletion of *spoIIAB* blocks endospore formation in *Bacillus subtilis* at an early stage. *Journal of Bacteriology*, *173*(21), 6678–6685.

Cortesão, M., Fuchs, F. M., Commichau, F. M., Eichenberger, P., Schuerger, A. C., Nicholson, W. L., Setlow, P., & Moeller, R. (2019). *Bacillus subtilis* spore resistance to simulated mars surface conditions. *Frontiers in Microbiology*, *10*(2), 1–16.

Crawshaw, A. D., Serrano, M., Stanley, W. A., Henriques, A. O., & Salgado, P. S. (2014). A mother cell-to-forespore channel: Current understanding and future challenges. *FEMS Microbiology Letters*, *358*(2), 129–136.

Crozat, E., & Grainge, I. (2010). FtsK DNA Translocase: The Fast Motor That Knows Where It's Going. *ChemBioChem*, *11*(16), 2232–2243.

Crozat, E., Rousseau, P., Fournes, F., & Cornet, F. (2014). The FtsK Family of DNA translocases finds the ends of circles. *Journal of Molecular Microbiology and Biotechnology*, *24*(5–6), 396–408.

D'Ulisse, V., Fagioli, M., Ghelardini, P., & Paolozzi, L. (2007). Three functional subdomains of the *Escherichia coli* FtsQ protein are involved in its interaction with the other division proteins. *Microbiology*, *153*(1), 124–138.

Dajkovic, A., Tesson, B., Chauhan, S., Courtin, P., Keary, R., Flores, P., Marlière, C., Filipe, S. R., Chapot-Chartier, M. P., & Carballido-Lopez, R. (2017). Hydrolysis of peptidoglycan is modulated by amidation of meso-diaminopimelic acid and Mg2+ in *Bacillus subtilis*. *Molecular Microbiology*, *104*(6), 972–988.

De Jong, I. G., Veening, J. W., & Kuipers, O. P. (2010). Heterochronic phosphorelay gene expression as a source of heterogeneity in *Bacillus subtilis* spore formation. *Journal of Bacteriology*, *192*(8), 2053–2067.

Deakin, L. J., Clare, S., Fagan, R. P., Dawson, L. F., Pickard, D. J., West, M. R., Wren, B. W., Fairweather, N. F., Dougan, G., & Lawley, T. D. (2012). The *Clostridium difficile spo0A* gene is a persistence and transmission factor. *Infection and Immunity*, *80*(8), 2704–2711.

Decker, A. R., & Ramamurthi, K. S. (2017). Cell Death Pathway That Monitors Spore Morphogenesis. *Trends in Microbiology*, *25*(8), 637–647.

Demarre, G., Galli, E., & Barre, F.-X. (2013). The FtsK family of DNA pumps. *Advances in Experimental Medicine and Biology*, *767*, 245–262.

Dembek, M., Kelly, A., Barwinska-Sendra, A., Tarrant, E., Stanley, W. A., Vollmer, D., Biboy, J., Gray, J., Vollmer, W., & Salgado, P. S. (2018). Peptidoglycan degradation machinery

in *Clostridium difficile* forespore engulfment. *Molecular Microbiology*, *110*(3), 390–410.

Di Lallo, G., Fagioli, M., Barionovi, D., Ghelardini, P., & Paolozzi, L. (2003). Use of a two-hybrid assay to study the assembly of a complex multicomponent protein machinery: bacterial septosome differentiation. *Microbiology*, *149*(12), 3353–3359.

Diez, V., Schujman, G. E., Gueiros-Filho, F. J., & de Mendoza, D. (2012). Vectorial signalling mechanism required for cell-cell communication during sporulation in *Bacillus subtilis*. *Molecular Microbiology*, *83*(2), 261–274.

Dik, D. A., Marous, D. R., Fisher, J. F., & Mobashery, S. (2017). Lytic transglycosylases: concinnity in concision of the bacterial cell wall. *Critical Reviews in Biochemistry and Molecular Biology*, *52*(5), 503–542.

Doan, T., Coleman, J., Marquis, K. A., Meeske, A. J., Burton, B. M., Karatekin, E., & Rudner, D. Z. (2013). FisB mediates membrane fission during sporulation in *Bacillus subtilis*. *Genes and Development*, *27*(3), 322–334.

Doan, T., Marquis, K. A., & Rudner, D. Z. (2005). Subcellular localization of a sporulation membrane protein is achieved through a network of interactions along and across the septum. *Molecular Microbiology*, *55*(6), 1767–1781.

Doan, T., Morlot, C., Meisner, J., Serrano, M., Henriques, A. O., Moran, C. P., & Rudner, D. Z. (2009). Novel secretion apparatus maintains spore integrity and developmental gene expression in *Bacillus subtilis*. *PLoS Genetics*, *5*(7): e1000566.

Doan, T., & Rudner, D. Z. (2007). Perturbations to engulfment trigger a degradative response that prevents cell-cell signalling during sporulation in *Bacillus subtilis. Molecular Microbiology*, *64*(2), 500–511.

Domínguez-Cuevas, P., Porcelli, I., Daniel, R. A., & Errington, J. (2013). Differentiated roles for MreB-actin isologues and autolytic enzymes in *Bacillus subtilis* morphogenesis. *Molecular Microbiology*, *89*(6), 1084–1098.

Domínguez-Escobar, J., Chastanet, A., Crevenna, A. H., Fromion, V., Wedlich-Söldner, R., Carballido-López, R., Domínguez-Escobar, J., Chastanet, A., Crevenna, A. H., Fromion, V., Wedlich-Söldner, R., & Carballido-López, R. (2011). Processive Movement of MreB-Associated Cell Wall Biosynthetic Complexes in Bacteria. *Science*, *333*(7), 225–228.

Dong, D., Chen, X., Jiang, C., Zhang, L., Cai, G., Han, L., Wang, X., Mao, E., & Peng, Y.

(2014). Genetic analysis of Tn916-like elements conferring tetracycline resistance in clinical isolates of *Clostridium difficile*. *International Journal of Antimicrobial Agents*, *43*(1), 73–77.

Driks, A., & Eichenberger, P. (2016). The Spore Coat. *Microbiology Spectrum*, *4*(2):TBS-0023.

Du, S., & Lutkenhaus, J. (2017). Assembly and activation of the *Escherichia coli* divisome. *Molecular Microbiology*, *105*(2), 177–187.

Dubarry, N., & Barre, F.-X. (2010). Fully efficient chromosome dimer resolution in *Escherichia coli* cells lacking the integral membrane domain of FtsK. *EMBO Journal*, *29*(3), 597–605.

Dubarry, N., Possoz, C., & Barre, F.-X. (2010). Multiple regions along the *Escherichia coli* FtsK protein are implicated in cell division. *Molecular Microbiology*, *78*(5), 1088–1100.

Ducret, A., Quardokus, E. M., & Brun, Y. V. (2016). MicrobeJ, a tool for high throughput bacterial cell detection and quantitative analysis. *Nature Microbiology*, *1*(7), 16077.

Dworkin, J. (2014). *Protein Targeting during Bacillus subtilis Sporulation*, *2*(1):TBS-0006.

Dworkin, J., & Losick, R. (2005). Developmental commitment in a bacterium. *Cell*, *121*(3), 401–409.

Dworkin J. 2014. Protein targeting during *Bacillus subtilis* sporulation. *Microbiology Spectrum* 2(1):TBS-0006-2012.

Egan, A. J. F., Biboy, J., van't Veer, I., Breukink, E., & Vollmer, W. (2015). Activities and regulation of peptidoglycan synthases. *Philosophical Transactions of the Royal Society B: Biological Sciences*, *370*(1679).

Egan, A. J. F., Cleverley, R. M., Peters, K., Lewis, R. J., & Vollmer, W. (2017). Regulation of bacterial cell wall growth. *The FEBS Journal*, *284*(6), 851–867.

Egan, A. J. F., Errington, J., & Vollmer, W. (2020). Regulation of peptidoglycan synthesis and remodelling. *Nature Reviews Microbiology*, *18*(8), 446–460.

Egan, A. J. F., Jean, N. L., Koumoutsi, A., Bougault, C. M., Biboy, J., Sassine, J., Solovyova, A. S., Breukink, E., Typas, A., Vollmer, W., & Simorre, J. P. (2014). Outer-membrane lipoprotein LpoB spans the periplasm to stimulate the peptidoglycan synthase PBP1B.

Proceedings of the National Academy of Sciences, *111*(22), 8197–8202.

Egan, A. J. F., Maya-Martinez, R., Ayala, I., Bougault, C. M., Banzhaf, M., Breukink, E., Vollmer, W., & Simorre, J. P. (2018). Induced conformational changes activate the peptidoglycan synthase PBP1B. *Molecular Microbiology*, *110*(3), 335–356.

Eichenberger, P. (2010). The red-ox status of a penicillin-binding protein is an on/off switch for spore peptidoglycan synthesis in *Bacillus subtilis*. *Molecular Microbiology*, *75*(1), 10–12.

Eichenberger, P., Fawcett, P., & Losick, R. (2001). A three-protein inhibitor of polar septation during sporulation in *Bacillus subtilis*. *Molecular Microbiology*, *42*(5), 1147–1162.

Eichenberger, P., Jensen, S. T., Conlon, E. M., Van Ooij, C., Silvaggi, J., González-Pastor, J. E., Fujita, M., Ben-Yehuda, S., Stragier, P., Liu, J. S., & Losick, R. (2003). The σ^E regulon and the identification of additional sporulation genes in *Bacillus subtilis*. *Journal of Molecular Biology*, *327*(5), 945–972.

El Najjar, N., El Andari, J., Kaimer, C., Fritz, G., Rösch, T. C., & Graumann, P. L. (2018). Single-molecule tracking of DNA translocases in *Bacillus subtilis* reveals strikingly different dynamics of SftA, SpoIIIE, and FtsA. *Applied and Environmental Microbiology*, *84*(8):e02610-17.

El Najjar, N., Kaimer, C., Rösch, T., & Graumann, P. L. (2017). Requirements for Septal Localization and Chromosome Segregation Activity of the DNA Translocase SftA from *Bacillus subtilis*. *Journal of Molecular Microbiology and Biotechnology*, *27*(1), 29–42.

Emami, K., Guyet, A., Kawai, Y., Devi, J., Wu, L. J., Allenby, N., Daniel, R. A., & Errington, J. (2017). RodA as the missing glycosyltransferase in *Bacillus subtilis* and antibiotic discovery for the peptidoglycan polymerase pathway. *Nature Microbiology*, *2*, 16253.

Ent, F. Van Den, Amos, L. A., & Löwe, J. (2001). Prokaryotic origin of the actin cytoskeleton. *Nature*, *413*(9), 39–44.

Erickson, H. P., & Osawa, M. (2017). FtsZ constriction force – curved protofilaments bending membranes. *Sub-Cellular Biochemistry*, *84*, 139–160.

Errington, J. (2003). Regulation of endospore formation in *Bacillus subtilis*. *Nature Reviews Microbiology*, *1*(2), 117–126.

Errington,J. (2010). From spores to antibiotics via the cell cycle. *Microbiology*, *156*(1), 1–13.

Errington, J., Bath, J., & Wu, L. J. (2001). DNA transport in bacteria. *Nature Reviews Molecular Cell Biology*, *2*(7), 538–544.

Errington, J., & Wu, L. J. (2017). Cell cycle machinery in *Bacillus subtilis*. *Sub-Cellular Biochemistry*, *84*, 67–101.

Errington, J., Daniel, R. A., & Scheffers, D.-J. (2003). Cytokinesis in Bacteria. *Microbiology and Molecular Biology Reviews*, *67*(1), 52–65.

Fawcett, P., Eichenberger, P., Losick, R., & Youngman, P. (2000). The transcriptional profile of early to middle sporulation in *Bacillus subtilis*. *Proceedings of the National Academy of Sciences*, *97*(14), 8063–8068.

Fay, A., Meyer, P., & Dworkin, J. (2010). Interactions between late-acting proteins required for peptidoglycan synthesis during sporulation. *Journal of Molecular Biology*, *399*(4), 547–561.

Feucht, A., Abbotts, L., & Errington, J. (2002). The cell differentiation protein SpoIIE contains a regulatory site that controls its phosphatase activity in response to asymmetric septation. *Molecular Microbiology*, *45*(4), 1119–1130.

Fiche, J. B., Cattoni, D. I., Diekmann, N., Langerak, J. M., Clerte, C., Royer, C. A., Margeat, E., Doan, T., & Nöllmann, M. (2013). Recruitment, Assembly, and Molecular Architecture of the SpoIIIE DNA Pump Revealed by Superresolution Microscopy. *PLoS Biology*, *11*(5): e1001557.

Fimlaid, K. A., Jensen, O., Donnelly, M. L., Siegrist, M. S., & Shen, A. (2015). Regulation of *Clostridium difficile* Spore Formation by the SpoIIQ and SpoIIIA Proteins. *PLoS Genetics*, *11*(10): e1005562.

Fimlaid, K. A., & Shen, A. (2015). Diverse mechanisms regulate sporulation sigma factor activity in the Firmicutes. *Current Opinion in Microbiology*, *24*, 88–95.

Fleming, T. C., Shin, J. Y., Lee, S. H., Becker, E., Huang, K. C., Bustamante, C., & Pogliano, K. (2010). Dynamic SpoIIIE assembly mediates septal membrane fission during *Bacillus subtilis* sporulation. *Genes and Development*, *24*(11), 1160–1172.

Foulger, D., & Errington, J. (1989). The role of the sporulation gene *spollIE* in the regulation

of prespore-specific gene expression in *Bacillus subtilis*. *Molecular Microbiology*, *3*(9), 1247–1255.

Frankel, M. B., & Schneewind, O. (2012). Determinants of murein hydrolase targeting to cross-wall of *Staphylococcus aureus* peptidoglycan. *Journal of Biological Chemistry*, *287*(13), 10460–10471.

Fujita, M., & Losick, R. (2003). The master regulator for entry into sporulation in *Bacillus subtilis* becomes a cell-specific transcription factor after asymmetric division. *Genes and Development*, *17*(9), 1166–1174.

Fujita, M., & Losick, R. (2005). Evidence that entry into sporulation in *Bacillus subtilis* is governed by a gradual increase in the level and activity of the master regulator Spo0A. *Genes and Development*, *19*(18), 2236–2244.

Garner, E. C., Bernard, R., Wang, W., Zhuang, X., Rudner, D. Z., & Mitchison, T. (2011). Coupled, circumferential motions of the cell wall synthesis machinery and MreB filaments in *B. subtilis*. *Science*, *333*(6039), 222–225.

Gautam, A., Vyas, R., & Tewari, R. (2011). Peptidoglycan biosynthesis machinery: A rich source of drug targets. *Critical Reviews in Biotechnology*, *31*(4), 295–336.

Gibson, D. G., Young, L., Chuang, R. Y., Venter, J. C., Hutchison, C. A., & Smith, H. O. (2009). Enzymatic assembly of DNA molecules up to several hundred kilobases. *Nature Methods*, *6*(5), 343–345.

Graham, T. G. W., Wang, X., Song, D., Etson, C. M., van Oijen, A. M., Rudner, D. Z., & Loparo, J. J. (2014). ParB spreading requires DNA bridging. *Genes and Development*, *28*(11), 1228–1238.

Grainge, I. (2010). FtsK - a bacterial cell division checkpoint? *Molecular Microbiology*, *78*(5), 1055–1057.

Grainge, I. (2013). Simple topology: FtsK-directed recombination at the dif site. *Biochemical Society Transactions*, *41*(2), 595–600.

Grenga, L., Luzi, G., Paolozzi, L., & Ghelardini, P. (2008). The *Escherichia coli* FtsK functional domains involved in its interaction with its divisome protein partners. *FEMS Microbiology Letters*, *287*(2), 163–167.

Gundry, R. L., White, M. Y., Murray, C. I., Kane, L. A., Fu, Q., Stanley, B. A., & Van Eyk, J. E. (2010). Preparation of Proteins and Peptides for Mass Spectrometry Analysis in a Bottom-Up Proteomics Workflow. *Current Protocols in Molecular Biology*, 90: 10.25.1-10.25.23.

Gutierrez, J., Smith, R., & Pogliano, K. (2010). SpoIID-mediated peptidoglycan degradation is required throughout engulfment during *Bacillus subtilis* sporulation. *Journal of Bacteriology*, *192*(12), 3174–3186.

Hajduk, I. V., Mann, R., Rodrigues, C. D. A., & Harry, E. J. (2019). The ParB homologs, Spo0J and Noc, together prevent premature midcell Z ring assembly when the early stages of replication are blocked in *Bacillus subtilis*. *Molecular Microbiology*, *112*(3), 766–784.

Haldenwang, W. G. (1995). The sigma factors of *Bacillus subtilis*. *Microbiological Reviews*, *59*(1), 1–30.

Harry, E. J., Pogliano, K., & Losick, R. (1995). Use of immunofluorescence to visualize cell-specific gene expression during sporulation in *Bacillus subtilis*. *Journal of Bacteriology*, *177*(12), 3386–3393.

Harwood, C. R., & Cutting, S. M. (1990). *Molecular biological methods for Bacillus*. Wiley.

Hashimoto, M., Ooiwa, S., & Sekiguchi, J. (2012). Synthetic lethality of the *lytE cwlO* genotype in *Bacillus subtilis* is caused by lack of D, L-endopeptidase activity at the lateral cell wall. *Journal of Bacteriology*, *194*(4), 796–803.

Higgins, D., & Dworkin, J. (2012). Recent progress in *Bacillus subtilis* sporulation. *FEMS Microbiology Reviews*, *36*(1), 131–148.

Hilbert, D. W., Chary, V. K., & Piggot, P. J. (2004). Contrasting Effects of σ^E on Compartmentalization of σ^F Activity during Sporulation of *Bacillus subtilis*. *Journal of Bacteriology*, *186*(7), 1983–1990.

Hilbert, D. W., & Piggot, P. J. (2003). Novel *spoIIE* mutation that causes uncompartmentalized σ^F Activation in *Bacillus subtilis*. *Journal of Bacteriology*, *185*(5), 1590–1598.

Hilbert, D. W., & Piggot, P. J. (2004). Compartmentalization of Gene Expression during *Bacillus subtilis* Spore Formation. *Microbiology and Molecular Biology Reviews*, *68*(2), 234–262.

Hoch, J. A. (1993). The phosphorelay signal transduction pathway in the initiation of *Bacillus subtilis* sporulation. *Journal of Cellular Biochemistry*, *51*(1), 55–61.

Horneck, G, Bucker, H., & Reitz, G. (1994). Long-term survival of bacterial spores in space. *Advances in Space Research : The Official Journal of the Committee on Space Research (COSPAR)*, *14*(10), 41–45.

Horneck, Gerda, Moeller, R., Cadet, J., Douki, T., Mancinelli, R. L., Nicholson, W. L., Panitz, C., Rabbow, E., Rettberg, P., Spry, A., Stackebrandt, E., Vaishampayan, P., & Venkateswaran, K. J. (2012). Resistance of bacterial endospores to outer space for planetary protection purposes-experiment PROTECT of the EXPOSE-E Mission. *Astrobiology*, *12*(5), 445–456.

Hoskins, J. A., Matsushima, P., Mullen, D. L., Tang, J., Zhao, G., Meier, T. I., Nicas, T. I., & Jaskunas, S. R. (1999). Gene disruption studies of penicillin-binding proteins 1a, 1b, and 2a in Streptococcus pneumoniae. *Journal of Bacteriology*, *181*(20), 6552–6555.

Huls, P. G., Vischer, N. O. E., & Woldringh, C. L. (1999). Delayed nucleoid segregation in *Escherichia coli*. *Molecular Microbiology*, *33*(5), 959–970.

Hussain, S., Wivagg, C. N., Szwedziak, P., Wong, F., Schaefer, K., Izoré, T., Renner, L. D., Holmes, M. J., Sun, Y., Bisson-Filho, A. W., Walker, S., Amir, A., Löwe, J., & Garner, E. C. (2018). MreB filaments align along greatest principal membrane curvature to orient cell wall synthesis. *eLife*, *7*, e32471.

Imamura, D., Zhou, R., Feig, M., & Kroos, L. (2008). Evidence that the *Bacillus subtilis* SpoIIGA protein is a novel type of signal-transducing aspartic protease. *Journal of Biological Chemistry*, *283*(22), 15287–15299.

Jean, N. L., Rutherford, T. J., & Löwe, J. (2020). FtsK in motion reveals its mechanism for double-stranded DNA translocation. *Proceedings of the National Academy of Sciences*, *117*(25), 14202–14208.

Johnson, C. M., & Grossman, A. D. (2014). Identification of host genes that affect acquisition of an integrative and conjugative element in *Bacillus subtilis*. *Molecular Microbiology*, *93*(6), 1284–1301.

Jones, L. J. F., Carballido-López, R., & Errington, J. (2001). Control of cell shape in bacteria: Helical, actin-like filaments in *Bacillus subtilis*. *Cell*, *104*(6), 913–922.

Kaimer, C., González-Pastor, J. E., & Graumann, P. L. (2009). SpoIIIE and a novel type of DNA translocase, SftA, couple chromosome segregation with cell division in *Bacillus subtilis*. *Molecular Microbiology*, *74*(4), 810–825.

Kaimer, C., Schenk, K., & Graumann, P. L. (2011). Two DNA translocases synergistically affect chromosome dimer resolution in *Bacillus subtilis*. *Journal of Bacteriology*, *193*(6), 1334–1340.

Karimova, G., Pidoux, J., Ullmann, A., & Ladant, D. (1998). A bacterial two-hybrid system based on a reconstituted signal transduction pathway. *Proceedings of the National Academy of Sciences*, *95*(10), 5752–5756.

Kelly, A., & Salgado, P. S. (2019). The engulfasome in *C. difficile*: Variations on protein machineries. *Anaerobe*, *60*, 102091.

Kennedy, S. P., Chevalier, F., & Barre, F.-X. (2008). Delayed activation of Xer recombination at dif by FtsK during septum assembly in *Escherichia coli*. *Molecular Microbiology*, *68*(4), 1018–1028.

Khanna, K., Lopez-Garrido, J., & Pogliano, K. (2020). Shaping an Endospore: Architectural Transformations during *Bacillus subtilis* Sporulation. *Annual Review of Microbiology*, *74*, 361–386.

Khanna, K., Lopez-Garrido, J., Zhao, Z., Watanabe, R., Yuan, Y., Sugie, J., Pogliano, K., & Villa, E. (2019). The molecular architecture of engulfment during *Bacillus subtilis* sporulation. *eLife*, *8*, e45257.

Khvorova, A., Chary, V. K., Hilbert, D. W., & Piggot, P. J. (2000). The chromosomal location of the *Bacillus subtilis* sporulation gene *spoIIR* is important for its function. *Journal of Bacteriology*, *182*(16), 4425–4429.

Kim, H., Hahn, M., Grabowski, P., McPherson, D. C., Otte, M. M., Wang, R., Ferguson, C. C., Eichenberger, P., & Driks, A. (2006). The *Bacillus subtilis* spore coat protein interaction network. *Molecular Microbiology*, *59*(2), 487–502.

Kloosterman, T. G., Lenarcic, R., Willis, C. R., Roberts, D. M., Hamoen, L. W., Errington, J., & Wu, L. J. (2016). Complex polar machinery required for proper chromosome segregation in vegetative and sporulating cells of *Bacillus subtilis*. *Molecular Microbiology*, *101*(2), 333–350.

Koch, A. L. (2000). The Exoskeleton of Bacterial Cells (the Sacculus): Still a Highly Attractive Target for Antibacterial Agents That Will Last For a Long Time. *Critical Reviews in Microbiology*, *26*(1), 1–35.

Konkol, M. A., Blair, K. M., & Kearns, D. B. (2013). Plasmid-encoded comi inhibits competence in the ancestral 3610 strain of *Bacillus subtilis*. *Journal of Bacteriology*, *195*(18), 4085–4093.

Koo, B. M., Kritikos, G., Farelli, J. D., Todor, H., Tong, K., Kimsey, H., Wapinski, I., Galardini, M., Cabal, A., Peters, J. M., Hachmann, A. B., Rudner, D. Z., Allen, K. N., Typas, A., & Gross, C. A. (2017). Construction and Analysis of Two Genome-Scale Deletion Libraries for *Bacillus subtilis*. *Cell Systems*, *4*(3), 291-305.e7.

Kovács, Á. T. (2016). Bacterial differentiation via gradual activation of global regulators. *Current Genetics*, *62*(1), 125–128.

Kovács, Á. T. (2019). *Bacillus subtilis*. *Trends in Microbiology*, *27*(8), 724–725.

Leclercq, S., Derouaux, A., Olatunji, S., Fraipont, C., Egan, A. J. F., Vollmer, W., Breukink, E., & Terrak, M. (2017). Interplay between Penicillin-binding proteins and SEDS proteins promotes bacterial cell wall synthesis. *Scientific Reports*, *7*, 43306.

Lee, T. K., & Huang, K. C. (2013). The role of hydrolases in bacterial cell-wall growth. *Current Opinion in Microbiology*, *16*(6), 760–766.

Leggett, M. J., Mcdonnell, G., Denyer, S. P., Setlow, P., & Maillard, J. Y. (2012). Bacterial spore structures and their protective role in biocide resistance. *Journal of Applied Microbiology*, *113*(3), 485–498.

Levdikov, V. M., Blagova, E. V., McFeat, A., Fogg, M. J., Wilson, K. S., & Wilkinson, A. J. (2012). Structure of components of an intercellular channel complex in sporulating *Bacillus subtilis*. *Proceedings of the National Academy of Sciences*, *109*(14), 5441–5445.

Levin, P. A., & Losick, R. (1996). Transcription factor SpoOA switches the localization of the cell division protein FtsZ from a medial to a bipolar pattern in *Bacillus subtilis*. *Genes and Development*, *10*(4), 478–488.

Levine, J. H., Fontes, M. E., Dworkin, J., & Elowitz, M. B. (2012). Pulsed feedback defers cellular differentiation. *PLoS Biology*, *10*(1), 1001252.

Li, Z., & Piggot, P. J. (2001). Development of a two-part transcription probe to determine the completeness of temporal and spatial compartmentalization of gene expression during bacterial development. *Proceedings of the National Academy of Sciences*, *98*(22), 12538–12543.

Lin, D. C. H., & Grossman, A. D. (1998). Identification and characterization of a bacterial chromosome partitioning site. *Cell*, *92*(5), 675–685.

Liu, N.-J.L., Dutton, R. J., & Pogliano, K. (2006). Evidence that the SpoIIIE DNA translocase participates in membrane fusion during cytokinesis and engulfment. *Molecular Microbiology*, *59*(4), 1097–1113.

Liu, N., Chistol, G., & Bustamante, C. (2015). Two-subunit DNA escort mechanism and inactive subunit bypass in an ultra-fast ring ATPase. *eLife*, *4*:e09224.

Lopez-Garrido, J., Ojkic, N., Khanna, K., Wagner, F. R., Villa, E., Endres, R. G., & Pogliano, K. (2018). Chromosome Translocation Inflates *Bacillus* Forespores and Impacts Cellular Morphology. *Cell*, *172*(4), 758-770.e14.

Louche, A., Salcedo, S. P., & Bigot, S. (2017). Protein–Protein Interactions: Pull-Down Assays. Methods in Molecular Biology, vol 1615, 247–255.

Loyo, C. L., & Burton, B. M. (2018). Quantitative Transformation Efficiency Assay for *Bacillus subtilis*. *Bio-Protocol*, *8*(23), e3109.

Luhur, J., Chan, H., Kachappilly, B., Mohamed, A., Morlot, C., Awad, M., Lyras, D., Taib, N., Gribaldo, S., Rudner, D. Z., & Rodrigues, C. D. A. (2020). A dynamic, ring-forming MucB / RseB-like protein influences spore shape in *Bacillus subtilis*. *PLoS Genetics*, *16*(12): e1009246.

MacDonald, L., Baldini, G., & Storrie, B. (2015). Does super-resolution fluorescence microscopy obsolete previous microscopic approaches to protein co-localization? *Methods in Molecular Biology*, *1270*, 255–275.

Männik, J., & Bailey, M. W. (2015). Spatial coordination between chromosomes and cell division proteins in *Escherichia coli*. *Frontiers in Microbiology*, 6:306.

Männik, J., Bailey, M. W., O'Neill, J. C., & Männik, J. (2017). Kinetics of large-scale chromosomal movement during asymmetric cell division in *Escherichia coli*. *PLoS Genetics*, *13*(2): e1006638.

Margolin, W. (2009). Sculpting the Bacterial Cell. *Current Biology*, *19*(17), R812–R822.

Margolis, P. S., Driks, A., & Losick, R. (1993). Sporulation gene *spoIIB* from *Bacillus subtilis*. *Journal of Bacteriology*, *175*(2), 528–540.

Marquis, K. A., Burton, B. M., Nöllmann, M., Ptacin, J. L., Bustamante, C., Ben-Yehuda, S., & Rudner, D. Z. (2008). SpoIIIE strips proteins off the DNA during chromosome translocation. *Genes and Development*, *22*(13), 1786–1795.

Martínez-Lumbreras, S., Alfano, C., Evans, N. J., Collins, K. M., Flanagan, K. A., Atkinson, R. A., Krysztofinska, E. M., Vydyanath, A., Jackter, J., Fixon-Owoo, S., Camp, A. H., & Isaacson, R. L. (2018). Structural and Functional Insights into *Bacillus subtilis* Sigma Factor Inhibitor, CsfB. *Structure*, *26*(4), 640-648.e5.

Massey, T. H., Mercogliano, C. P., Yates, J., Sherratt, D. J., & Löwe, J. (2006). Double-Stranded DNA Translocation: Structure and Mechanism of Hexameric FtsK. *Molecular Cell*, *23*(4), 457–469.

May, P. F. J., Zawadzki, P., Sherratt, D. J., Kapanidis, A. N., & Arciszewska, L. K. (2015). Assembly, translocation, and activation of XerCD-dif recombination by FtsK translocase analyzed in real-time by FRET and two-color tethered fluorophore motion. *Proceedings of the National Academy of Sciences*, *112*(37), E5133–E5141.

McCausland, J. W., Yang, X., Lyu, Z., Soderstrom, B., Xiao, J., & Liu, J. (2019). Treadmilling FtsZ polymers drive the directional movement of sPGsynthesis enzymes via a Brownian ratchet mechanism. *Nature Communications*, *12*(1), 609.

Mckenney, P. T., Driks, A., & Eichenberger, P. (2013). The *Bacillus subtilis* endospore: Assembly and functions of the multilayered coat. *Nature Reviews Microbiology*, *11*(1), 33–44.

McKenney, P. T., & Eichenberger, P. (2012). Dynamics of spore coat morphogenesis in *Bacillus subtilis*. *Molecular Microbiology*, *83*(2), 245–260.

McPherson, D. C., Driks, A., & Popham, D. L. (2001). Two Class A High-Molecular-Weight Penicillin-Binding Proteins of. *Journal of Bacteriology*, *183*(20), 6046–6053.

Meador-Parton, J., & Popham, D. L. (2000). Structural analysis of *Bacillus subtilis* spore peptidoglycan during sporulation. *Journal of Bacteriology*, *182*(16), 4491–4499.

Mearls, E. B., Jackter, J., Colquhoun, J. M., Farmer, V., Matthews, A. J., Murphy, L. S., Fenton, C., & Camp, A. H. (2018). Transcription and translation of the *sigG* gene is tuned for proper execution of the switch from early to late gene expression in the developing *Bacillus subtilis* spore. *PLoS Genetics*, *14*(4): e1007350.

Meeske, A. J., Riley, E. P., Robins, W. P., Uehara, T., Mekalanos, J. J., Kahne, D., Walker, S., Kruse, A. C., Bernhardt, T. G., & Rudner, D. Z. (2016). SEDS proteins are a widespread family of bacterial cell wall polymerases. *Nature*, *537*(7622), 634–638.

Meeske, A. J., Rodrigues, C. D. A., Brady, J., Lim, H. C., Bernhardt, T. G., & Rudner, D. Z. (2016). High-Throughput Genetic Screens Identify a Large and Diverse Collection of New Sporulation Genes in *Bacillus subtilis*. *PLoS Biology*, *14*(1): e1002341.

Meeske, A. J., Sham, L.-T., Kimsey, H., Koo, B.-M., Gross, C. A., Bernhardt, T. G., & Rudner, D. Z. (2015). MurJ and a novel lipid II flippase are required for cell wall biogenesis in *Bacillus subtilis*. *Proceedings of the National Academy of Sciences*, *112*(20), 6437–6442.

Meisner, J., Maehigashi, T., Andre, I., Dunham, C. M., & Moran, C. P. (2012). Structure of the basal components of a bacterial transporter. *Proceedings of the National Academy of Sciences*, *109*(14), 5446–5451.

Meisner, J., Wang, X., Serrano, M., Henriques, A. O., & Moran, C. P. (2008). A channel connecting the mother cell and forespore during bacterial endospore formation. *Proceedings of the National Academy of Sciences*, *105*(39), 15100–15105.

Meisner, J., Montero Llopis, P., Sham, L. T., Garner, E., Bernhardt, T. G., & Rudner, D. Z. (2013). FtsEX is required for CwlO peptidoglycan hydrolase activity during cell wall elongation in *Bacillus subtilis*. *Molecular Microbiology*, *89*(6), 1069–1083.

Mesnage, S., Dellarole, M., Baxter, N. J., Rouget, J. B., Dimitrov, J. D., Wang, N., Fujimoto, Y., Hounslow, A. M., Lacroix-Desmazes, S., Fukase, K., Foster, S. J., & Williamson, M. P. (2014). Molecular basis for bacterial peptidoglycan recognition by LysM domains. *Nature Communications*, *5*:4269.

Meyer, P., Gutierrez, J., Pogliano, K., & Dworkin, J. (2010). Cell wall synthesis is necessary for membrane dynamics during sporulation of *Bacillus subtilis*. *Molecular Microbiology*, *76*(4), 956–970.

Miller, A. K., Brown, E. E., Mercado, B. T., & Herman, J. K. (2016). A DNA-binding protein

defines the precise region of chromosome capture during *Bacillus* sporulation. *Molecular Microbiology*, *99*(1), 111–122.

Mitosch, K., & Bollenbach, T. (2014). Bacterial responses to antibiotics and their combinations. *Environmental Microbiology Reports*, *6*(6), 545–557.

Moeller, R., Setlow, P., Reitz, G., & Nicholson, W. L. (2009). Roles of small, acid-soluble spore proteins and core water content in survival of *Bacillus subtilis* spores exposed to environmental solar UV radiation. *Applied and Environmental Microbiology*, *75*(16), 5202–5208.

Morales Angeles, D., Liu, Y., Hartman, A. M., Borisova, M., de Sousa Borges, A., de Kok, N., Beilharz, K., Veening, J. W., Mayer, C., Hirsch, A. K. H., & Scheffers, D.-J. (2017). Pentapeptide-rich peptidoglycan at the *Bacillus subtilis* cell-division site. *Molecular Microbiology*, *104*(2), 319–333.

Morlot, C., & Rodrigues, C. D. A. (2018). The New Kid on the Block: A Specialized Secretion System during Bacterial Sporulation. *Trends in Microbiology*, *26*(8), 663–676.

Morlot, C., Uehara, T., Marquis, K. A., Bernhardt, T. G., & Rudner, D. Z. (2010). A highly coordinated cell wall degradation machine governs spore morphogenesis in *Bacillus subtilis*. *Genes and Development*, *24*(4), 411–422.

Mueller, E. A., Egan, A. J., Breukink, E., Vollmer, W., & Levin, P. A. (2019). Plasticity of *Escherichia coli* cell wall metabolism promotes fitness and antibiotic resistance across environmental conditions. *eLife*, *8*, e40754.

Nelson, D. E., & Young, K. D. (2001). Contributions of PBP 5 and DD-carboxypeptidase penicillin binding proteins to maintenance of cell shape in *Escherichia coli*. *Journal of Bacteriology*, *183*(10), 3055–3064.

Nicholson, W. L., & Setlow, P. (1990). (Sporulation, germination, and outgrowth) *Molecular biological methods for Bacillus*. Wiley.

Nikolaidis, I., Favini-Stabile, S., & Dessen, A. (2014). Resistance to antibiotics targeted to the bacterial cell wall. *Protein Science*, *23*(3), 243–259.

Nocadello, S., Minasov, G., Shuvalova, L. S., Dubrovska, I., Sabini, E., & Anderson, W. F. (2016). Crystal Structures of the SpoIID Lytic Transglycosylases Essential for Bacterial Sporulation. *Journal of Biological Chemistry*, *291*(29), 14915–14926.

Nugroho, F. A., Yamamoto, H., Kobayashi, Y., & Sekiguchi, J. (1999). Characterization of a new sigma-K-dependent peptidoglycan hydrolase gene that plays a role in *Bacillus subtilis* mother cell lysis. *Journal of Bacteriology*, *181*(20), 6230–6237.

Ojkic, N., López-Garrido, J., Pogliano, K., & Endres, R. G. (2014). Bistable Forespore Engulfment in *Bacillus subtilis* by a Zipper Mechanism in Absence of the Cell Wall. *PLoS Computational Biology*, *10*(10): e1003912.

Ojkic, N., López-Garrido, J., Pogliano, K., & Endres, R. G. (2016). Cell-wall remodeling drives engulfment during *Bacillus subtilis* sporulation. *eLife*, *5*, 1–30.

Ortiz, C., Natale, P., Cueto, L., & Vicente, M. (2015). The keepers of the ring: Regulators of FtsZ assembly. *FEMS Microbiology Reviews*, *40*(1), 57–67.

Ouellette, S. P., Karimova, G., Davi, M., & Ladant, D. (2017). Analysis of membrane protein interactions with a bacterial adenylate cyclase-based two-hybrid (BACTH) technique. *Current Protocols in Molecular Biology*, *2017*(April), 20.12.1-20.12.24.

Paradis-Bleau, C., Markovski, M., Uehara, T., Lupoli, T. J., Walker, S., Kahne, D. E., & Bernhardt, T. G. (2010). Lipoprotein cofactors located in the outer membrane activate bacterial cell wall polymerases. *Cell*, *143*(7), 1110–1120.

Paredes-Sabja, D., Setlow, P., & Sarker, M. R. (2011). Germination of spores of *Bacillales* and *Clostridiales* species: Mechanisms and proteins involved. *Trends in Microbiology*, *19*(2), 85–94.

Paredes-Sabja, D., Shen, A., & Sorg, J. A. (2014). *Clostridium difficile* spore biology: Sporulation, germination, and spore structural proteins. *Trends in Microbiology*, *22*(7), 406–416.

Pazos, M., Peters, K., Boes, A., Safaei, Y., Kenward, C., Caveney, N. A., Laguri, C., Breukink, E., Strynadka, N. C. J., Simorre, J. P., Terrak, M., & Vollmer, W. (2020). SPOR proteins are required for functionality of class a penicillin-binding proteins in *Escherichia coli*. *MBio*, *11*(6), 1–16.

Pease, P. J., Levy, O., Cost, G. J., Gore, J., Ptacin, J. L., Sherratt, D., Bustamante, C., & Cozzarelli, N. R. (2005). Sequence-Directed DNA Translocation by Purified FtsK. *Science*, *307*(5709), 586 LP – 590.

Pedersen, L. B., Ragkousi, K., Cammett, T. J., Melly, E., Sekowska, A., Schopick, E., Murray,

T., & Setlow, P. (2000). Characterization of ywhE, which encodes a putative high-molecular-weight class A penicillin-binding protein in *Bacillus subtilis*. *Gene*, *246*(1–2), 187–196.

Pereira, F. C., Nunes, F., Cruz, F., Fernandes, C., Isidro, A. L., Lousa, D., Soares, C. M., Moran, C. P., Henriques, A. O., & Serrano, M. (2019). A LysM Domain intervenes in sequential protein-protein and protein-peptidoglycan interactions important for spore coat assembly in *Bacillus subtilis*. *Journal of Bacteriology*, *201*(4):e00642-18.

Perez, A. R., Abanes-De Mello, A., & Pogliano, K. (2000). SpoIIB localizes to active sites of septal biogenesis and spatially regulates septal thinning during engulfment in *Bacillus subtilis*. *Journal of Bacteriology*, *182*(4), 1096–1108.

Pettit, L. J., Browne, H. P., Yu, L., Smits, W. K., Fagan, R. P., Barquist, L., Martin, M. J., Goulding, D., Duncan, S. H., Flint, H. J., Dougan, G., Choudhary, J. S., & Lawley, T. D. (2014). Functional genomics reveals that *Clostridium difficile* Spo0A coordinates sporulation, virulence and metabolism. *BMC Genomics*, *15*(1), 1–15.

Piggot, P. J., & Hilbert, D. W. (2004). Sporulation of *Bacillus subtilis*. *Current Opinion in Microbiology*, *7*(6), 579–586.

Pinho, M. G., Kjos, M., & Veening, J. W. (2013). How to get (a)round: Mechanisms controlling growth and division of coccoid bacteria. *Nature Reviews Microbiology*, *11*(9), 601–614.

Pogliano, J., Osborne, N., Sharp, M. D., Mello, A. A. De, Perez, A., Sun, Y. L., & Pogliano, K. (1999). A vital stain for studying membrane dynamics in bacteria: A novel mechanism controlling septation during *Bacillus subtilis* sporulation. *Molecular Microbiology*, *31*(4), 1149–1159.

Pogliano, K., Hofmeister, A. E. M., & Losick, R. (1997). Disappearance of the σ^E transcription factor from the forespore and the SpoIIE phosphatase from the mother cell contributes to establishment of cell-specific gene expression during sporulation in *Bacillus subtilis*. *Journal of Bacteriology*, *179*(10), 3331–3341.

Pogliano, K., Pogliano, J., & Becker, E. (2003). Chromosome segregation in Eubacteria. *Current Opinion in Microbiology*, *6*(6), 586–593.

Popham, D. L. (2002). Specialized peptidoglycan of the bacterial endospore: The inner wall of the lockbox. *Cellular and Molecular Life Sciences*, *59*(3), 426–433.

Popham, D. L., & Bernhards, C. B. (2015). Spore Peptidoglycan. *Microbiology Spectrum*, *3*(6), 1–21.

Popham, D. L., & Setlow, P. (1993). Cloning, nucleotide sequence, mutagenesis, and mapping of the *Bacillus subtilis* pbpD gene, which codes for penicillin-binding protein 4. *Journal of Bacteriology*, *176*(15), 7197–7205.

Proctor, S. A., Minc, N., Boudaoud, A., & Chang, F. (2012). Contributions of turgor pressure, the contractile ring, and septum assembly to forces in cytokinesis in fission yeast. *Current Biology*, *22*(17), 1601–1608.

Ptacin, J. L., Nöllmann, M., Becker, E. C., Cozzarelli, N. R., Pogliano, K., & Bustamante, C. (2008). Sequence-directed DNA export guides chromosome translocation during sporulation in *Bacillus subtilis*. *Nature Structural and Molecular Biology*, *15*(5), 485–493.

Qiao, Y., Lebar, M. D., Schirner, K., Schaefer, K., Tsukamoto, H., Kahne, D., & Walker, S. (2014). Detection of Lipid-Linked Peptidoglycan Precursors by Exploiting an Unexpected Transpeptidase Reaction. *Journal of the American Chemical Society*, *136*(42), 14678–14681.

Rabi, R., Turnbull, L., Whitchurch, C. B., Awad, M., & Lyras, D. (2017). Structural Characterization of *Clostridium sordellii* Spores of Diverse Human, Animal, and Environmental Origin and Comparison to Clostridium difficile Spores. *mSphere*, *2*(5), e00343-17.

Ramírez-Guadiana, F. H., Meeske, A. J., Rodrigues, C. D. A., Barajas-Ornelas, R. del C., Kruse, A. C., & Rudner, D. Z. (2017). A two-step transport pathway allows the mother cell to nurture the developing spore in *Bacillus subtilis*. *PLoS Genetics*, *13*(9): e1007015.

Ramírez-Guadiana, F. H., Rodrigues, C. D. A., Marquis, K. A., Campo, N., Barajas-Ornelas, R. del C., Brock, K., Marks, D. S., Kruse, A. C., & Rudner, D. Z. (2018). Evidence that regulation of intramembrane proteolysis is mediated by substrate gating during sporulation in *Bacillus subtilis*. *PLoS Genetics*, *14*(11): e1007753.

Ramírez-Vargas, G., Quesada-Gómez, C., Acuña-Amador, L., López-Ureña, D., Murillo, T., Del Mar Gamboa-Coronado, M., Chaves-Olarte, E., Thomson, N., Rodríguez-Cavallini, E., & Rodríguez, C. (2017). A *Clostridium difficile* lineage endemic to Costa Rican

hospitals is multidrug resistant by acquisition of chromosomal mutations and novel mobile genetic elements. *Antimicrobial Agents and Chemotherapy*, *61*(4), e02054-16.

Ramos-Silva, P., Serrano, M., & Henriques, A. O. (2019). From Root to Tips: Sporulation Evolution and Specialization in *Bacillus subtilis* and the Intestinal Pathogen *Clostridioides difficile*. *Molecular Biology and Evolution*, *36*(12), 2714–2736.

Randich, A. M., & Brun, Y. V. (2015). Molecular mechanisms for the evolution of bacterial morphologies and growth modes. *Frontiers in Microbiology*, *6*:580.

Ranjit, D. K., Jorgenson, M. A., & Young, K. D. (2017). PBP1B glycosyltransferase and transpeptidase activities play different essential roles during the de novo regeneration of rod morphology in *Escherichia coli*. *Journal of Bacteriology*, *199*(7), 1–17.

Reyes-Lamothe, R., Nicolas, E., & Sherratt, D. J. (2012). Chromosome replication and segregation in bacteria. *Annual Review of Genetics*, *46*(1), 121–143.

Ribis, J. W., Fimlaid, K. A., & Shen, A. (2018). Differential requirements for conserved peptidoglycan remodeling enzymes during *Clostridioides difficile* spore formation. *Molecular Microbiology*, *110*(3), 370–389.

Riley, E. P., Schwarz, C., Derman, A. I., & Lopez-Garrido, J. (2021). Milestones in *Bacillus subtilis* sporulation research. *Microbial Cell*, *8*(1), 1–16.

Rodrigues, C. D. A., Marquis, K. A., Meisner, J., & Rudner, D. Z. (2013). Peptidoglycan hydrolysis is required for assembly and activity of the transenvelope secretion complex during sporulation in *Bacillus subtilis*. *Molecular Microbiology*, *89*(6), 1039–1052.

Rodrigues, C. D. A., Henry, X., Neumann, E., Kurauskas, V., Bellard, L., Fichou, Y., Schanda, P., Schoehn, G., Rudner, D. Z., & Morlot, C. (2016a). A ring-shaped conduit connects the mother cell and forespore during sporulation in *Bacillus subtilis*. *Proceedings of the National Academy of Sciences*, *113*(41), 11585–11590.

Rodrigues, C. D. A., Ramírez-Guadiana, F. H., Meeske, A. J., Wang, X., & Rudner, D. Z. (2016b). GerM is required to assemble the basal platform of the SpoIIIA–SpoIIQ transenvelope complex during sporulation in *Bacillus subtilis*. *Molecular Microbiology*, *102*(2), 260–273.

Rohs, P. D. A., Buss, J., Sim, S. I., Squyres, G. R., Srisuknimit, V., Smith, M., Cho, H., Sjodt, M., Kruse, A. C., Garner, E. C., Walker, S., Kahne, D. E., & Bernhardt, T. G. (2018). A

central role for PBP2 in the activation of peptidoglycan polymerization by the bacterial cell elongation machinery. *PLoS Genetics*, *14*(10): e1007726.

Sassine, J., Sousa, J., Lalk, M., Daniel, R. A., & Vollmer, W. (2020). Cell morphology maintenance in *Bacillus subtilis* through balanced peptidoglycan synthesis and hydrolysis. *Scientific Reports*, *10*(1), 17910.

Sassine, J., Xu, M., Sidiq, K. R., Emmins, R., Errington, J., & Daniel, R. A. (2017). Functional redundancy of division specific penicillin-binding proteins in *Bacillus subtilis*. *Molecular Microbiology*, *106*(2), 304–318.

Sauvage, E., Kerff, F., Terrak, M., Ayala, J. A., & Charlier, P. (2008). The penicillin-binding proteins: Structure and role in peptidoglycan biosynthesis. *FEMS Microbiology Reviews*, *32*(2), 234–258.

Sauvage, E., & Terrak, M. (2016). Glycosyltransferases and transpeptidases/penicillin-binding proteins: Valuable targets for new antibacterials. *Antibiotics*, *5*(1):12.

Schaeffer, P., Millet, J., & Aubert, J. P. (1965). Catabolic repression of bacterial sporulation. *Proceedings of the National Academy of Sciences*, *54*(3), 704–711.

Schanda, P., Triboulet, S., Laguri, C., Bougault, C. M., Ayala, I., Callon, M., Arthur, M., & Simorre, J. P. (2014). Atomic model of a cell-wall cross-linking enzyme in complex with an intact bacterial peptidoglycan. *Journal of the American Chemical Society*, *136*(51), 17852–17860.

Scheffers, D.-J. (2005). Dynamic localization of penicillin-binding proteins during spore development in *Bacillus subtilis*. *Microbiology*, *151*(3), 999–1012.

Scheffers, D.-J., & Pinho, M. G. (2005). Bacterial Cell Wall Synthesis: New Insights from Localization Studies. *FEMS Microbiology Reviews*, *30*(2), 565–569.

Schellenberger, P., Kaufmann, R., Siebert, C. A., Hagen, C., Wodrich, H., & Grünewald, K. (2014). High-precision correlative fluorescence and electron cryo microscopy using two independent alignment markers. *Ultramicroscopy*, *143*, 41–51.

Scheurwater, E., Reid, C. W., & Clarke, A. J. (2008). Lytic transglycosylases: Bacterial space-making autolysins. *International Journal of Biochemistry and Cell Biology*, *40*(4), 586–591.

Schindelin, J., Arganda-Carreras, I., Frise, E., Kaynig, V., Longair, M., Pietzsch, T., Preibisch, S., Rueden, C., Saalfeld, S., Schmid, B., Tinevez, J.-Y., White, D. J., Hartenstein, V., Eliceiri, K., Tomancak, P., & Cardona, A. (2012). Fiji: an open-source platform for biological-image analysis. *Nature Methods*, *9*(7), 676–682.

Schumacher, M. A., Lee, J., & Zeng, W. (2016). Molecular insights into DNA binding and anchoring by the *Bacillus subtilis* sporulation kinetochore-like RacA protein. *Nucleic Acids Research*, *44*(11), 5438–5449.

Sciochetti, S. A., & Piggot, P. J. (2000). A tale of two genomes: Resolution of dimeric chromosomes in *Escherichia coli* and *Bacillus subtilis*. *Research in Microbiology*, *151*(7), 503–511.

Serrano, M., Crawshaw, A. D., Dembek, M., Monteiro, J. M., Pereira, F. C., Pinho, M. G., Fairweather, N. F., Salgado, P. S., & Henriques, A. O. (2016). The SpoIIQ-SpoIIIAH complex of *Clostridium difficile* controls forespore engulfment and late stages of gene expression and spore morphogenesis. *Molecular Microbiology*, *100*(1), 204–228.

Serrano, M., Gao, J. X., Bota, J., Bate, A. R., Meisner, J., Eichenberger, P., Moran, C. P., & Henriques, A. O. (2015). Dual-Specificity Anti-sigma Factor Reinforces Control of Cell-Type Specific Gene Expression in *Bacillus subtilis*. *PLoS Genetics*, *11*(4): e1005104.

Setlow, P. (2006). Spores of *Bacillus subtilis*: Their resistance to and killing by radiation, heat and chemicals. *Journal of Applied Microbiology*, *101*(3), 514–525.

Setlow, P. (2007). I will survive: DNA protection in bacterial spores. *Trends in Microbiology*, *15*(4), 172–180.

Sharp, M. D., & Pogliano, K. (1999). An in vivo membrane fusion assay implicates SpoIIIE in the final stages of engulfment during *Bacillus subtilis* sporulation. *Proceedings of the National Academy of Sciences*, *96*(25), 14553–14558.

Sharp, M. D., & Pogliano, K. (2002). Role of cell-specific SpoIIIE assembly in polarity of DNA transfer. *Science*, *295*(5552), 137–139.

Sharp, M. D., & Pogliano, K. (2003). The membrane domain of SpoIIIE is required for membrane fusion during *Bacillus subtilis* sporulation. *Journal of Bacteriology*, *185*(6), 2005–2008.

Sharpe, M. E., & Errington, J. (1995). Postseptational chromosome partitioning in bacteria.

Proceedings of the National Academy of Sciences, *92*(19), 8630–8634.

Sharpe, M. E., & Errington, J. (1996). The *Bacillus subtilis soj-spoOJ* locus is required for a centromere- like function involved in prespore chromosome partitioning. *Molecular Microbiology*, *21*(3), 501–509.

Shaw, H. A., Khodadoost, L., Preston, M. D., Corver, J., Mullany, P., & Wren, B. W. (2019). *Clostridium difficile* clade 3 (RT023) have a modified cell surface and contain a large transposable island with novel cargo. *Scientific Reports*, *9*(1): 15330.

Shen, A., Edwards, A. N., Sarker, M. R., & Paredes-Sabja, D. (2019). Sporulation and Germination in Clostridial Pathogens. *Microbiology Spectrum*, *7*(6):GPP3-0017-2018.

Sherratt, D. J., Arciszewska, L. K., Crozat, E., Graham, J. E., & Grainge, I. (2010). The *Escherichia coli* DNA translocase FtsK. *Biochemical Society Transactions*, *38*(2), 395–398.

Shin, J. Y., Lopez-Garrido, J., Lee, S. H., Diaz-Celis, C., Fleming, T., Bustamante, C., & Pogliano, K. (2015). Visualization and functional dissection of coaxial paired SpoIIIE channels across the sporulation septum. *eLife*, *4*, e06474.

Shuster, B., Khemmani, M., Abe, K., Huang, X., Nakaya, Y., Maryn, N., Buttar, S., Gonzalez, A. N., Driks, A., Sato, T., & Eichenberger, P. (2019). Contributions of crust proteins to spore surface properties in *Bacillus subtilis*. *Molecular Microbiology*, *111*(3), 825–843.

Sjodt, M., Brock, K., Dobihal, G., Rohs, P. D. A., Green, A. G., Hopf, T. A., Meeske, A. J., Srisuknimit, V., Kahne, D., Walker, S., Marks, D. S., Bernhardt, T. G., Rudner, D. Z., & Kruse, A. C. (2018). Structure of the peptidoglycan polymerase RodA resolved by evolutionary coupling analysis. *Nature*, *556*(7699), 118–121.

Sjodt, M., Rohs, P. D. A., Gilman, M. S. A., Erlandson, S. C., Zheng, S., Green, A. G., Brock, K. P., Taguchi, A., Kahne, D., Walker, S., Marks, D. S., Rudner, D. Z., Bernhardt, T. G., & Kruse, A. C. (2020). Structural coordination of polymerization and crosslinking by a SEDS–bPBP peptidoglycan synthase complex. *Nature Microbiology*, *5*(6), 813–820.

Smith, M. C. M. (1991). Molecular biological methods for *Bacillus*. (New York: John Wiley & Sons).

Smith, T. J., & Foster, S. J. (1995). Characterization of the involvement of two compensatory autolysins in mother cell lysis during sporulation of *Bacillus subtilis* 168. *Journal of*

Bacteriology, *177*(13), 3855–3862.

Söderström, B., Skoog, K., Blom, H., Weiss, D. S., von Heijne, G., & Daley, D. O. (2014). Disassembly of the divisome in *Escherichia coli*: Evidence that FtsZ dissociates before compartmentalization. *Molecular Microbiology*, *92*(1), 1–9.

Stouf, M., Meile, J. C., & Cornet, F. (2013). FtsK actively segregates sister chromosomes in *Escherichia coli*. *Proceedings of the National Academy of Sciences*, *110*(27), 11157–11162.

Sullivan, N. L., Marquis, K. A., & Rudner, D. Z. (2009). Recruitment of SMC by ParB-parS Organizes the Origin Region and Promotes Efficient Chromosome Segregation. *Cell*, *137*(4), 697–707.

Sun, G., Yang, M., Jiang, L., & Huang, M. (2021). Regulation of pro-σ^K activation : a key checkpoint in *Bacillus subtilis* sporulation. *BioRxiv*, 0–2.

Sun, Y. L., Sharp, M. D., & Pogliano, K. (2000). A dispensable role for forespore-specific gene expression in engulfment of the forespore during sporulation of *Bacillus subtilis*. *Journal of Bacteriology*, *182*(10), 2919–2927.

Swick, M. C., Koehler, T. M., & Driks, A. (2016). Surviving Between Hosts: Sporulation and Transmission. *Microbiology Spectrum*, *4*(4), 1–18.

Taguchi, A., Welsh, M. A., Marmont, L. S., Lee, W., Sjodt, M., Kruse, A. C., Kahne, D., Bernhardt, T. G., & Walker, S. (2019). FtsW is a peptidoglycan polymerase that is functional only in complex with its cognate penicillin-binding protein. *Nature Microbiology*, *4*(4), 587–594.

Takahashi, N., Gruber, C. C., Yang, J. H., Liu, X., Braff, D., Yashaswini, C. N., Bhubhanil, S., Furuta, Y., Andreescu, S., Collins, J. J., & Walker, G. C. (2017). Lethality of MalE-LacZ hybrid protein shares mechanistic attributes with oxidative component of antibiotic lethality. *Proceedings of the National Academy of Sciences*, *114*(34), 9164–9169.

Tan, I. S., & Ramamurthi, K. S. (2013). Membrane remodeling: FisB will do in a pinch. *Current Biology*, *23*(6), R251–R253.

Tan, I. S., & Ramamurthi, K. S. (2014). Spore formation in *Bacillus subtilis*. *Environmental Microbiology Reports*, *6*(3), 212–225.

Terrak, M., Ghosh, T. K., Van Heijenoort, J., Van Beeumen, J., Lampilas, M., Aszodi, J., Ayala, J. A., Ghuysen, J. M., & Nguyen-Distèche, M. (1999). The catalytic, glycosyl transferase and acyl transferase modules of the cell wall peptidoglycan-polymerizing penicillin-binding protein 1b of *Escherichia coli*. *Molecular Microbiology*, *34*(2), 350–364.

Tocheva, E. I., López-Garrido, J., Hughes, H. V., Fredlund, J., Kuru, E., Vannieuwenhze, M. S., Brun, Y. V., Pogliano, K., & Jensen, G. J. (2013). Peptidoglycan transformations during *Bacillus subtilis* sporulation. *Molecular Microbiology*, *88*(4), 673–686.

Tuijtel, M. W., Koster, A. J., Jakobs, S., Faas, F. G. A., & Sharp, T. H. (2019). Correlative cryo super-resolution light and electron microscopy on mammalian cells using fluorescent proteins. *Scientific Reports*, *9*(1), 1369.

Typas, A., Banzhaf, M., Gross, C. A., & Vollmer, W. (2012). From the regulation of peptidoglycan synthesis to bacterial growth and morphology. *Nature Reviews Microbiology*, *10*(2), 123–136.

Typas, A., Banzhaf, M., van den Berg van Saparoea, B., Verheul, J., Biboy, J., Nichols, R. J., Zietek, M., Beilharz, K., Kannenberg, K., Von Rechenberg, M., Breukink, E., Den Blaauwen, T., Gross, C. A., & Vollmer, W. (2010). Regulation of peptidoglycan synthesis by outer membrane proteins. *Cell*, *143*(7), 1097–1109.

Uehara, T., & Bernhardt, T. G. (2011). More than just lysins: Peptidoglycan hydrolases tailor the cell wall. *Current Opinion in Microbiology*, *14*(6), 698–703.

Uehara, T., Dinh, T., & Bernhardt, T. G. (2009). LytM-domain factors are required for daughter cell separation and rapid ampicillin-induced lysis in *Escherichia coli*. *Journal of Bacteriology*, *191*(16), 5094–5107.

Uehara, T., & Park, J. T. (2008). Growth of *Escherichia coli*: Significance of peptidoglycan degradation during elongation and septation. *Journal of Bacteriology*, *190*(11), 3914–3922.

Uehara, T., Parzych, K. R., Dinh, T., & Bernhardt, T. G. (2010). Daughter cell separation is controlled by cytokinetic ring-activated cell wall hydrolysis. *EMBO Journal*, *29*(8), 1412–1422.

Vasudevan, P., Weaver, A., Reichert, E. D., Linnstaedt, S. D., & Popham, D. L. (2007). Spore

cortex formation in *Bacillus subtilis* is regulated by accumulation of peptidoglycan precursors under the control of sigma K. *Molecular Microbiology*, *65*(6), 1582–1594.

Vermassen, A., Leroy, S., Talon, R., Provot, C., Popowska, M., & Desvaux, M. (2019, February 28). Cell wall hydrolases in bacteria: Insight on the diversity of cell wall amidases, glycosidases and peptidases toward peptidoglycan. *Frontiers in Microbiology*, *10*(2), 331.

Vigouroux, A., Cordier, B., Aristov, A., Alvarez, L., Özbaykal, G., Chaze, T., Oldewurtel, E. R., Matondo, M., Cava, F., Bikard, D., & van Teeffelen, S. (2020). Class-A penicillin binding proteins do not contribute to cell shape but repair cellwall defects. *eLife*, *9*:e51998.

Vollmer, W., Joris, B., Charlier, P., & Foster, S. (2008). Bacterial peptidoglycan (murein) hydrolases. *FEMS Microbiology Reviews*, *32*(2), 259–286.

Wagner-Herman, J. K., Bernard, R., Dunne, R., Bisson-Filho, A. W., Kumar, K., Nguyen, T., Mulcahy, L., Koullias, J., Gueiros-Filho, F. J., & Rudnera, D. Z. (2012). RefZ facilitates the switch from medial to polar division during spore formation in *Bacillus subtilis*. *Journal of Bacteriology*, *194*(17), 4608–4618.

Wang E., A. F., Deighan, P., Chen, S., Barrasso, K., Garcia, C. P., Martínez-Lumbreras, S., Alfano, C., Krysztofinska, E. M., Thapaliya, A., Camp, A. H., Isaacson, R. L., Hochschild, A., & Losick, R. (2017). A novel RNA polymerase-binding protein that interacts with a sigma-factor docking site. *Molecular Microbiology*, *105*(4), 652–662.

Wang, X., Montero Llopis, P., Rudner, D. Z., Llopis, P. M., & Rudner, D. Z. (2014). *Bacillus subtilis* chromosome organization oscillates between two distinct patterns. *Proceedings of the National Academy of Sciences*, *111*(35), 12877–12882.

Webb, C. D., Teleman, A., Gordon, S., Straight, A., Belmont, A., Lin, D. C. H., Grossman, A. D., Wright, A., & Losick, R. (1997). Bipolar localization of the replication origin regions of chromosomes in vegetative and sporulating cells of *B. subtilis*. *Cell*, *88*(5), 667–674.

Willis, C., Errington, J., & Wu, L. J. (2020). Cohesion of sister chromosome termini during the early stages of sporulation in *Bacillus subtilis*. *Journal of Bacteriology*, *202*(20).

Wu, L. J. (2009). It takes two DNA translocases to untangle chromosomes from the division septum: MicroCommentary. *Molecular Microbiology*, *74*(4), 773–776.

Wu, L. J., & Errington, J. (1994). *Bacillus subtilis* SpoIIIE Protein required for DNA Segregation during Asymmetric Cell Division. *Science*, *264*(5158), 572–575.

Wu, L. J., & Errington, J. (1997). Septal localization of the SpoIIIE chromosome partitioning protein in *Bacillus subtilis*. *EMBO Journal*, *16*(8), 2161–2169.

Wu, L. J., & Errington, J. (1998). Use of asymmetric cell division and *spoIIIE* mutants to probe chromosome orientation and organization in *Bacillus subtilis*. *Molecular Microbiology*, *27*(4), 777–786.

Wu, L. J., Lewis, P. J., Allmansberger, R., Hauser, P. M., & Errington, J. (1995). A conjugation-like mechanism for prespore chromosome partitioning during sporulation in *Bacillus subtilis*. *Genes and Development*, *9*(11), 1316–1326.

Wyckoff, T. J., Taylor, J. A., & Salama, N. R. (2012). Beyond growth: Novel functions for bacterial cell wall hydrolases. *Trends in Microbiology*, *20*(11), 540–547.

Yan, X., Yu, H. J., Hong, Q., & Li, S. P. (2008). Cre/lox system and PCR-based genome engineering in *Bacillus subtilis*. *Applied and Environmental Microbiology*, *74*(17), 5556–5562.

Yang, D. C., Peters, N. T., Parzych, K. R., Uehara, T., Markovski, M., & Bernhardt, T. G. (2011). An ATP-binding cassette transporter-like complex governs cell-wall hydrolysis at the bacterial cytokinetic ring. *Proceedings of the National Academy of Sciences*, *108*(45), E1052-60.

Yang, X., Lyu, Z., Miguel, A., McQuillen, R., Huang, K. C., & Xiao, J. (2017). GTPase activity-coupled treadmilling of the bacterial tubulin FtsZ organizes septal cell wall synthesis. *Science*, *355*(6326), 744–747.

Zeigler, D. R., Prágai, Z., Rodriguez, S., Chevreux, B., Muffler, A., Albert, T., Bai, R., Wyss, M., & Perkins, J. B. (2008). The origins of 168, W23, and other *Bacillus subtilis* legacy strains. *Journal of Bacteriology*, *190*(21), 6983–6995.

Zhao, H., Patel, V., Helmann, J. D., & Dörr, T. (2017). Don’t let sleeping dogmas lie: new views of peptidoglycan synthesis and its regulation. *Molecular Microbiology*, *106*(6), 847–860